Domain-Wall Brane Phenomenology in Five and Six Dimensions

Benjamin David Callen

Submitted in total fulfilment
of the requirements of the degree of
Doctor of Philosophy

June 2014

School of Physics
University of Melbourne
Principal Supervisor: Professor Raymond R. Volkas

Abstract

This thesis explores the construction and phenomenology of models based on domain-wall branes in five and six dimensions. In these models, the extra dimensions are infinite. In 5D, we explore how a model with a single domain-wall brane can account for the fermion mass spectra. In 6D, we construct a model with intersecting domain-wall branes and show how we can localize scalars, fermions and gauge bosons.

We first analyze the fermion mass hierarchy problem as well as the problems of generating quark and lepton mixing in the context of the 4+1-dimensional $SU(5)$ domain-wall brane model first proposed by Davies, George and Volkas. We exploit the split-fermion mechanism which naturally arises in the model to show that the fermion mass hierarchy as well as the Cabibbo-Kobayashi-Maskawa (CKM) mixing angles can be accounted for naturally. We later suggest that the same mechanism cannot be used to generate acceptable lepton mixing.

We then modify the original $SU(5)$ model by including a discrete A_4 flavor symmetry. The SM fermions and scalars are then assigned to appropriate $SU(5) \times A_4$ representations and we give an example parameter choice for which the fermion mass hierarchy and the CKM mixing angles are generated by the split fermion mechanism while realistic, large lepton mixing angles are produced from the special properties of A_4. We show that the splitting of scalars in the extra dimension can solve the vacuum alignment problem inherent to most models with discrete flavor symmetries.

In the second half of the thesis, we deal with models in six dimensions. We show that a $\mathbb{Z}_2 \times \mathbb{Z}_2$-invariant scalar field theory with four scalar fields can generate two intersecting domain walls, with two of the fields condensing in the interiors of the walls to form 'lumps'. We show that for a special parameter choice, one can obtain analytic solutions. We also discuss how the same mechanisms used to localize fermions and scalars in five-dimensional models can be used to localize these fields to the domain-wall intersection.

Lastly, we deal with how to trap gauge fields to the domain-wall intersection in the previous six-dimensional model. We achieve this by giving

the fields that form 'lumps' gauge charges, so that a confining, non-Abelian gauge group G is spontaneously broken to subgroups H_1 and H_2, localizing the associated gauge fields to the respective walls by the Dvali-Shifman mechanism. On the intersection there is a further breaking to $H_1 \cap H_2$ and we then outline the conditions under which gauge fields are then localized to the intersection. We show that this mechanism can localize the Standard Model gauge fields starting from an $SU(7)$ theory.

We thus find that the domain-wall brane model-building framework represents an interesting approach to reproducing the essential components of the Standard Model. We also find that this framework is very flexible, with the possibility to extend it with additional extra dimensions, as well as with larger gauge groups as previously shown.

Declaration

This is to certify that:

(a) the thesis comprises of my original work towards the PhD except where indicated in the Preface,

(b) due acknowledgement has been made in the text to all other material used,

(c) the thesis is less that 100,000 words in length, exclusive of tables, maps, bibliographies, appendices and footnotes.

Benjamin David Callen

Date:

Preface

Chapter 2 is based on the publication [1] by Callen and Volkas which appeared in Physical Review D. The contributions from the author include all the calculations. Some of the work in Chapter 2 contributed to the author's Honours thesis; this includes the mass fitting for the one-generation case, the general way to split the fermion profiles to get hierarchical fermion masses, and the generation of Majorana masses for the neutrinos in the model. The analysis for the three-generation case without mixing as well as the analysis for fitting the Cabibbo angle in the two-generation case is new work. Please note that the analysis in which it is shown that the profiles for the Higgs boson and its Kaluza-Klein modes satisfy Schrödinger's equation with a hyperbolic Scarf potential is original work and initially appeared in [1], but in this thesis we give that analysis in the introduction for the convenience of the reader and to avoid repetition.

Chapter 3 is based on the publication [2] which appeared in Physical Review D. The idea of adding a discrete A_4 flavor symmetry was initially proposed by Volkas and the author chose the $SU(5) \times A_4$ representations and completed all the subsequent calculations.

Chapter 4 is based on the publication [3] which appeared in Physical Review D. Although somewhat similar and inspired from the work in Nadine Pesor's Honours thesis [4], the model with four fields that the author constructed and treated in the above paper is different and the nature of the intersecting domain-wall solution is different. The author constructed an analytic, intersecting domain-wall solution, showed that scalars and fermions could be localized to the particular solution and calculated their profiles. Volkas suggested the importance of checking whether solutions for which the angle of intersection between the domain walls is less than ninety degrees are energy degenerate with the desired perpendicular solution, and we address this in Chapter 4.

Chapter 5 is based on the publication [5] which appeared in Physical Review D. It is a completely original idea proposed by the author and the author also constructed the various toy models based on the gauge group $SU(7)$, some of which lead to a Standard Model gauge group localized to the domain-wall intersection.

Acknowledgements

Firstly, I would like to thank Raymond Volkas for his excellent supervision and for showing faith in me. I very much appreciate how he has encouraged me to pursue new ideas, to develop my taste for creative problem solving, and to explore new avenues of research and to take risks. Volkas has given me financial assistance after the completion of my Australian Postgraduate Award scholarship, without which the completion of my PhD would have been much more difficult. I would also like to thank him and the department for funding my overseas research trips to Taiwan in 2010 for the inaugural APCosPA winter school, and to Italy and Greece in 2011, in particular for the Corfu summer school and to visit the University of Padova.

Secondly, I would also like to thank the other members of my supervisory panel, Tony Gherghetta and Andrew Melatos, for giving me much good advice and making sure I made progress in my PhD studies.

Thirdly, I would like to thank my friends and colleagues within the Centre of Excellence for Particle Physics at the Terascale (CoEPP). I feel very privileged to have been part of this research group, particularly during such an exciting time in particle physics with the discovery of the Higgs boson at the LHC and the hosting of the ICHEP conference in Melbourne in 2012. In particular I would like to thank those who I interacted with at the Melbourne node of CoEPP.

I would also like to thank the School of Physics and everybody I have met through it. It has always provided an engaging atmosphere in which to research. I have always enjoyed going to GOSS seminars and socializing with my peers afterwards.

Many thanks also to Ferruccio Feruglio for some fruitful discussions in Padova, particularly in regards to the work of Chapter 3 and Ref. [2].

I would like to also thank Damien George for some useful discussions with regards to the work in Chapter 4 and Ref. [3].

Much thanks also go to Graeme Smithies for the grammatical corrections and suggestions that he made after proofreading the entire thesis. I am very grateful for the time and effort that he spent.

Lastly, I would like to thank my family, Shirley, David and Rory, for the support they have given me over all the years of my education at the University of Melbourne.

List of Figures

List of Tables

Abbreviations

ADD - the model of Arkani-Hamed, Dimopoulos and Dvali
AdS - Anti de Sitter
CoS - Clash-of-Symmetries
DS - Dvali-Shifman
ED - Extra dimensions
QCD - Quantum Chromodynamics
KK - Kaluza-Klein
n+1D - n+1-dimensional spacetime (for some integer n)
RS1 - Randall-Sundrum Type I
RS2 - Randall-Sundrum Type II
SM - Standard Model
eV - electron volt
VEV - Vacuum expectation value
UV - Ultraviolet

Contents

Chapter 1

Introduction

Extra dimensions of spacetime have been of interest to physics since the original models of Kaluza [6] and Klein[7]. These models proposed that at short distances, there existed a tiny, circular fifth dimension at each point of four-dimensional spacetime in which gravity propagates. Upon dimensional reduction, five-dimensional (5D) general relativity then reduces to ordinary 4D general relativity together with electromagnetism, yielding an early example of unification of these two important theories. Furthermore, adding additional dimensions with non-trivial compact topologies can yield 4D general relativity along with a non-Abelian Yang-Mills gauge theory [8, 9]; for example, adding three extra dimensions with the topology of a 3-sphere yields an $SU(2)$ gauge group in the dimensionally reduced theory.

String theory has extensively used the Kaluza-Klein idea to achieve compactification of the extra dimensions. In string theory, particles are proposed to be extended one-dimensional objects called strings at high energies. Generally, there exist anomalies in such a theory and to cancel them out requires the addition of six new dimensions compactified into a Calabi-Yau manifold [10]. Strings can be closed, where they form closed loops, or open where two ends of a string are detached. In 1989, Dai, Leigh and Polchinski [11] discovered that ends of open strings in general had to end on dynamical objects called D-branes, which can be thought of as special types of p-branes which are extended p-dimensional objects. Polchinski further elaborated that D-branes were in fact fundamental objects in string theory [12].

D-branes present an alternative method of compactification to the Kaluza-Klein idea. This idea of having our visible universe confined to such an object (in many cases, a 3-brane) is known as the 'braneworld' scenario. Embedding the Standard Model in higher dimensions in this way can solve many problems. In the original large extra dimensional model of Arkani-Hamed, Dimopoulos and Dvali [13], the Standard Model fields are confined to a 3-

brane embedded in a spacetime with a number of compact extra dimensions of radius R while gravity is allowed to propagate in all the dimensions. They found that for two or more extra dimensions that the ordinary four-dimensional Planck scale of order 10^{19} GeV could be reproduced even with an extra-dimensional Planck scale as low as 1 TeV provided $R \leq 1$mm, solving the Hierarchy problem.

Later, Randall and Sundrum showed that a model, the Randall-Sundrum type 1 model (RS1), with two branes situated at the two ends of a slice of five-dimensional Anti-de Sitter space (AdS_5) could also solve the Hierarchy problem [14]. In this scenario a positive tension brane, the UV brane, localizes gravity while the Standard Model fields are confined to a negative tension brane, the IR brane, at the other end where gravity is exponentially suppressed by a warp factor. Later, it was shown that if the IR brane was taken to infinity and the SM fields localized to the UV brane that one obtains a new model, the Randall-Sundrum type 2 model (RS2) [15], for which the extra-dimension is in fact infinite!

Large extra-dimensional models as well as the Randall-Sundrum models can solve some problems in the quark and lepton sectors. It was found that by allowing fermions to propagate into the bulk that the masses of the SM fermions, which spans twelve orders of magnitude, could be generated naturally [16, 17, 18]. Arkani-Hamed and Schmaltz proposed the split fermion mechanism [19] as a way to solve the fermion mass hierarchy problem in the ADD and RS2 models. In this scenario, fermions are given different 5D bulk masses which shift their localization centers and lead to them being split. Upon dimensional reduction, Yukawa coupling constants depend on overlap integrals of the fermion profiles which are exponentially sensitive to the bulk masses and so in this way, not only can the fermion mass hierarchy be solved, but proton decay in Grand Unified Theories (GUTs) can be suppressed naturally.

At this point, it is worth considering what types of branes we can use in the braneworld scenario. In all the above mentioned braneworld models, the branes used are introduced into the theory fundamentally by hand, breaking translational invariance along the extra dimension explicitly. This motivates the question of whether a brane may be generated *dynamically* instead, breaking translational invariance spontaneously. A natural candidate for a dynamically generated brane is a topological soliton.

There are many different kinds of topological solitons. They are stable solitary wave solutions to non-linear equations of scalar field theories which belong to non-trivial homotopy classes of mappings between a subspace (usually a boundary) of spacetime to the moduli space of vacua of the theory. The simplest type is a domain wall which maps the endpoints of spatial in-

finity along one dimension to two distinct, degenerate vacua of a scalar field. Strings are non-trivial mappings of the subset of spacetime with the topology of a circle to the moduli space; that is they belong to non-trivial homotopy classes of $\pi_1(M)$, where M denotes the moduli space. Further, monopoles and instantons belong to non-trivial classes of $\pi_2(M)$ and $\pi_3(M)$ respectively.

Naturally, one wishes to first consider domain walls; as prototype branes they are the simplest type of topological defect. Using a domain wall in this way is in fact a very old idea first proposed by Rubakov and Shaposhnikov [20]. To reproduce a 3+1D theory on the domain wall it is necessary to localize scalars, fermions, gauge fields and gravity onto the wall dynamically. Fermions are localized by Yukawa coupling them to the background scalar field forming the domain wall [21]. Scalars are similarly localized through quartic interactions. Gravity can also be successfully localized [22]. Localizing gauge bosons is notoriously difficult; the only plausible way conjectured to work is the Dvali-Shifman mechanism, whereby a non-Abelian gauge group G which is respected and confining in the bulk is broken to a subgroup H on the domain wall by another scalar field, thereby localizing the gauge fields of H by a dual Meissner effect.

Davies, George and Volkas put forward a model combining all of the physics described in the above paragraph based on the grand unification group $SU(5)$ in 4+1D spacetime [23]. In this model, a singlet scalar field generates the domain-wall kink while the component proportional to hypercharge of an adjoint scalar field attains a lump-like profile to break $SU(5)$ to the Standard Model, thus localizing SM gauge fields by the Dvali-Shifman mechanism. Quarks and leptons are embedded in $SU(5)$ multiplets in the usual way and when coupled to both background scalar fields one finds that a split fermion mechanism arises naturally in the model. A Higgs doublet (embedded in an $SU(5)$ quintet) is localized to the wall and a tachyonic mass generated for it so that electroweak symmetry is broken on the wall. Fermions are then Yukawa coupled to the Higgs in the usual way.

In this thesis, we examine the phenomenology and construction of several domain-wall brane models in five and six dimensions. In Chapter 2, we first analyze the problem of generating the fermion mass hierarchy, quark mixing and lepton mixing naturally via the split fermion mechanism in the model proposed in Ref. [23]. We show that the fermion mass hierarchy problem can be solved along with generation of the Cabibbo angle, while sufficient lepton mixing cannot be generated by this mechanism (while maintaining the other desirable phenomenology). In Chapter 3, we analyze a modified version of the $SU(5)$ model in which a discrete A_4 flavor symmetry is added and scalars and fermions are assigned appropriate A_4 representations. We show that lepton mixing can be generated in this model while also generating the fermion

mass hierarchy and quark mixing. We show that a splitting mechanism for scalars can also resolve the vacuum alignment problem so common in models with discrete flavor symmetries. In Chapter 4, we look at constructing a general model in six-dimensional flat spacetime in which a 3+1D-universe is constructed on the intersection of two perpendicular domain walls. We find analytic solutions for a very special parameter choice and we calculate the profiles of the Kaluza-Klein spectrum for fermions and scalars localized to the wall. In Chapter 5, we propose a realization of the Clash-of-Symmetries mechanism [24, 25] whereby a gauge group G is broken to two different subgroups H and H' on each wall, which in turn induces a further breaking to $H \cap H'$ on the intersection of the domain walls. Chapter 6 is our conclusion.

Before we initiate our discussion of the works of this thesis we shall discuss the necessary background knowledge in greater detail in this introductory chapter. In Section 1.1, we elaborate our discussion of Kaluza-Klein theory, extra dimensions, string theory and branes. In Section 1.2 we discuss the ADD model. Section 1.3 discusses further the Randall-Sundrum models. We then discuss topological defects in Section 1.4. In Section 1.5, we introduce domain-wall brane models of a single, infinite extra dimension, discussing all the mechanisms for the localization of fermions, scalars, gauge bosons as well as gravity, and in Section 1.6 we discuss how all the essential components of the framework are put together to yield the 4+1-dimensional $SU(5)$ domain-wall brane model proposed by Davies, George and Volkas. In Section 1.7, we discuss the fermion mass hierarchy problem. In Section 1.8, we give an overview of neutrino masses and the see-saw mechanism and, in Section 1.9, we review quark and lepton mixing. In Section 1.10 gives a review of discrete flavor symmetries. Section 1.11 gives a review of extra-dimensional approaches generating the fermion mass hierarchy as well as quark and lepton mixing, including approaches which combine extra dimensions with discrete flavor symmetries. Section 1.12 discusses some models generating two perpendicular domain walls, some with nested domain walls and others with intersecting domain walls. In Section 1.13, we give a full, detailed outline for the arguments of this thesis.

1.1 Extra Dimensions and Branes

1.1.1 Kaluza-Klein Theory

Unification of the fundamental forces of nature has always been an ideal that has motivated theoretical physicists. By 1915, with Einstein's construction of general relativity, there were two theories which seemed to describe all that

was known about the laws of physics. Einstein's theory described gravitation as a curvature of spacetime. Maxwell's equations described the behavior of electric and magnetic fields in the presence of electric charges and currents. As Maxwell's equations had led to a unified description of electricity and magnetism, it was only natural to speculate on a possible description unifying electromagnetism and general relativity.

Nordström was the first to notice that the electromagnetic field strength tensor of electromagnetism in its formulation in special relativity and the four-vector representing gravity in *scalar* gravity could be embedded into the field strength tensor of a five-dimensional electromagnetic theory [26, 27, 28]. Ordinary four-dimensional electromagnetism along with gravity as represented by Poisson's equation are reproduced when the constraint that the derivative of all components of the five-component gauge field with respect to the fifth coordinate vanish. Kaluza and Klein did a similar embedding within the context of 5D general relativity [6, 7]. The two of them independently proposed that the fifth dimension was compactified on a circle so that the underlying spacetime manifold was $M_4 \times S^1$, where M_4 denotes 4D Minkowski space. They recognized that the 5D metric would contain a field transforming as a vector under 4D Lorentz transformations as well as an additional scalar called the dilaton. In quoting the basic results of Kaluza-Klein theory, we follow closely the treatise given by Bailin and Love [8]. Another useful overview is given by Duff [9].

In five dimensions, we may write the metric in the form

$$G_{MN}(x,\theta) = \begin{pmatrix} g_{\mu\nu}(x,\theta) - \frac{\kappa^2}{R^2} A_\mu(x,\theta) A_\nu(x,\theta) \Phi(x,\theta) & \frac{\kappa}{R} A_\mu(x,\theta)\Phi(x,\theta) \\ \frac{\kappa}{R} A_\nu(x,\theta)\Phi(x,\theta) & -\Phi(x,\theta) \end{pmatrix}. \tag{1.1}$$

Here, x denotes the usual coordinates of M_4 and $0 \leq \theta = y/R \leq 2\pi$, where y is the fifth coordinate and R is the compactification radius of the fifth dimension. Also, $\kappa^2 = 16\pi G$ with G being Newton's constant of gravitation. Local transformations of the θ coordinate of the form

$$\theta \to \theta' = \theta + \frac{\kappa}{R}\epsilon(x), \tag{1.2}$$

yield, working from the standard general coordinate transformations

$$G_{MN} = G_{PQ} \frac{\partial x'^P}{\partial x^M} \frac{\partial x'^Q}{\partial x^N}, \tag{1.3}$$

the following transformation for the field A_μ,

$$A_\mu \to A'_\mu = A_\mu + \partial_\mu \epsilon. \tag{1.4}$$

This transformation is the usual gauge transformation of an Abelian gauge field. Hence, gauge invariance is realized as a spacetime symmetry in this theory as one might suspect, as a subset of general coordinate invariance.

We start from the five-dimensional Einstein action

$$S_{5D} = -\frac{1}{16\pi G_5}\int d^5x|det(G_{MN})|^{1/2}R_5 \tag{1.5}$$

where we denote G_5 as the five-dimensional Newton's constant and R_5 as the five-dimensional Ricci scalar. Noting that in this coordinate system, the ground state metric is just the flat metric

$$ds^2 = \eta_{\mu\nu}dx^\mu dx^\nu - R^2 d\theta^2, \tag{1.6}$$

if we suppress the dynamics of the dilaton field by using its ground state value $\Phi = R^2$, we can show that the effective action describing solely the gravitational and vector sectors yields 4D general relativity and electromagnetism. This effective action is

$$-\frac{2\pi R}{16\pi G_5}\int d^4x|det(g)|^{1/2}R_4 - \frac{16\pi G}{4}\frac{2\pi R}{16\pi G_5}\int d^4x|det(g)|^{1/2}F_{\mu\nu}F^{\mu\nu}. \tag{1.7}$$

This yields the correct actions for 4D general relativity and electromagnetism if we identify the usual 4D Newton constant G with the 5D one G_5 as

$$G = \frac{G_5}{2\pi R}. \tag{1.8}$$

If we consider a 5D massless scalar field $\Psi(x,\theta)$, given that the modes of this field propagating through the circular extra dimension must satisfy periodic boundary conditions, one can try expanding Ψ as

$$\Psi(x,\theta) = \sum_{n\in\mathbb{Z}} e^{in\theta}\psi_m(x) = \sum_{n\in\mathbb{Z}} e^{2ny\pi i/R}\psi_m(x), \tag{1.9}$$

where n is an index running over the set of integers $\mathbb{Z}$. Substituting this into the 5D Klein-Gordon equation

$$\Box_{5D}\Psi(x,y) = \big[\Box_{4D} - \frac{d^2}{dy^2}\big]\Psi(x,y) = \big[\Box_{4D} - \frac{1}{R^2}\frac{d^2}{d\theta^2}\big]\Psi(x,\theta), \tag{1.10}$$

one finds that the above equation reduces to a set of 4D Klein-Gordon equations for the 4D modes $\psi_m(x)$

$$\big[\Box + m_n^2\big]\psi_n(x) = 0, \tag{1.11}$$

where

$$m_n^2 = \frac{n^2}{R^2}. \tag{1.12}$$

Finally, one notes by inspection that the general coordinate transformation in Eq. 1.2, which corresponds to the usual Abelian gauge transformation, requires that the charges q_n of the 4D modes $\psi_n(x)$ are given as

$$q_n = -\frac{n\kappa}{R}. \tag{1.13}$$

The above two results regarding the masses and electric charges of the resultant 4D modes derived from the massless 5D scalar field present some obvious problems for the Kaluza-Klein theory for unifying electromagnetism and general relativity. Firstly, the modes with electric charges are the modes with $n \neq 0$. This means that we cannot have the zero mode as a particle with the same charge as an electron, and if we included a fermionic field we could not use the analogous mode as our candidate electron. Secondly, if we suppose that the quantized charges of the massive modes are separated by gaps of order the electron charge e, then this implies due to Eq. 1.13 that the square of the radius of the extra dimension is of order

$$R^2 = \frac{\kappa^2}{e^2} = \frac{256\pi^2 G^2}{e^2}, \tag{1.14}$$

from which one can deduce that R is of order the Planck scale. So not only are all charged particles massive, if they have charges of order the electron charge they have masses of order the Planck mass. This is obviously phenomenologically disallowed.

The above treatment of a 5D massless scalar field in the presence of gravity in the spacetime with the topology proposed by Kaluza and Klein, as well as the reduction of the original 5D Einstein-Hilbert action to the 4D Einstein-Hilbert action plus the 4D action for the free electromagnetic field are important examples of dimensional reduction. In most extra-dimensional theories, we are ultimately interested in the physics at low energies and long distances. In such an approach based on effective field theory, one normally describes 5D fields as a tower of 4D modes, each with a characteristic *profile* depending solely on the extra-dimensional coordinate(s). The phase factors dependent on θ (or y) in the expansion of Ψ are examples of extra-dimensional profiles. These profiles are rather like wavefunctions in that they tell you where a particle belonging to a particular mode is likely to be found in the extra dimension if you could measure the extra-dimensional coordinate. Furthermore, the effective coupling constants of non-trivial interactions amongst modes of different fields resulting from an initial interaction of the 5D fields

will depend on overlap integrals of the products of these profiles. In effect, what we are doing when we do this is *averaging* the physics in the hidden dimension(s) to give the relevant, effective quantities (coupling constants, masses, etc...) in the 4D low energy effective field theory.

1.1.2 String Theory and Branes

String theory is currently the most popular approach to an acceptable, renormalizable unification of general relativity with quantum theory and the strong and electroweak interactions of the Standard Model. It traces its origins to work by Veneziano and was considered as an alternative approach to Quantum Chromodynamics (QCD) for explaining the particle zoo of hadrons and mesons that appeared at particle colliders in the 1960's, an application of string theory known as the *dual resonance model*. In string theory, at short distances fundamental particles are really not the point particles they are treated as in quantum field theory but rather tiny, vibrating, one-dimensional extended objects known as strings. Strings can be either closed, like circular elastic bands, or open, where there are two ends which are not connected, like a string on a guitar.

Eventually, it was realized in the mid-1970's that QCD was the correct theory describing the strong interaction and that string theory had a number of theoretical and phenomenological problems. The first was that the dual resonance model first proposed by Veneziano contained a tachyon. Secondly, the theory was generally anomalous. In the original bosonic string theory, it was found that the theory was anomaly free and consistent only when spacetime had the *critical number* of dimensions, which turned out to be 26.

To introduce fermions in string theory, it is necessary to introduce supersymmetry and formulate the theory in terms of *superstrings* rather than bosonic strings. For any supersymmetric theory containing more than 32 supercharges, any supersymmetric multiplet is guaranteed to contain particles with spins higher than two, whose actions are very difficult to formulate consistently. Supersymmetry with 32 supercharges corresponds to $N = 8$ supersymmetry in four dimensions and to minimal $N = 1$ supersymmetry in eleven dimensions. Since the dimensionality of a Dirac spinor has more than 32 components in any spacetime with more than eleven dimensions, the maximum dimensionality that could be considered for a supersymmetric string theory was eleven. In 1984, Michael Green and John Schwarz showed that the set of gauge and gravitational anomalies exactly cancelled in a particular string theory known as Type I superstring theory in ten dimensions with either an $SO(32)$ or $E_8 \times E_8$ gauge group [10]. They not only showed that the critical dimension for a theory based on superstrings was ten, but that

the choice of gauge group was restricted to the two previously mentioned groups.

It was initially thought that strings were the only fundamental objects in string theory. However, when one looks a bit more carefully at the Nambu-Goto action for open strings, one finds that for the action to be consistent there must be some boundary conditions imposed on the ends of the open strings. For instance, let's look at the action for an open bosonic string. The action, following [29, 30], in conformal gauge is given by

$$S = -\frac{T}{2}\int_M d\sigma d\tau \partial_a X^\mu \partial_a X_\mu, \tag{1.15}$$

where M denotes the manifold of the string parametrized by a temporal coordinate τ and spatial coordinate $0 \leq \sigma \leq \pi$, T is the string tension, the lower case Roman index a denotes world-sheet indices representing τ and σ, the lower case Greek index μ denotes spacetime indices and $X^\mu(\tau, \sigma)$ represents the spacetime coordinate of the point of the string parametrized by (τ, σ). By performing the variation $X^\mu \to X^\mu + \delta X^\mu$, one finds that the variation in the action after integrating by parts is

$$\delta S = -T\int_M d\sigma d\tau \delta X^\mu \Box X_\mu + T\int_{\partial M} d\sigma \delta X^\mu \partial_n X_\mu, \tag{1.16}$$

where the ∂_n denotes the derivative normal to the boundary of the string ∂M. Both terms in the above variation must vanish. The first term vanishing yields the wave equation for a string. For the second term, which represents a term on the boundary of the open string, to vanish it must be necessary that

$$\partial_n X^\mu = 0. \tag{1.17}$$

This is a Neumann boundary condition, and it is the only condition which preserves Poincaré invariance. Since the Dirichlet condition where the string coordinate X^μ is constant on the boundary also satisfies the above condition, one could also consider imposing Dirichlet boundary conditions instead. Unlike the Neumann boundary condition, X^μ = constant explicitly breaks Poincaré invariance. Hence, for much of String Theory's history, before 1989, Dirichlet boundary conditions were not considered.

However, there is an alternative interpretation. One could interpret the spaces defined by the Dirichlet condition X^μ = constant as extended objects on which open strings end. In 1989, Dai, Leigh and Polchinski [11] found that under a T-duality transformation, a theory containing open oriented strings satisfying the Neumann condition plus closed oriented strings was actually

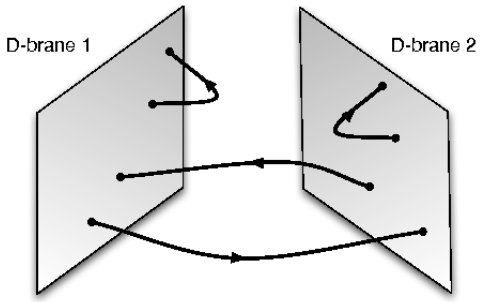

Figure 1.1: Open strings beginning and ending on D-branes. Strings beginning on one D-brane and ending on another will always be massive if the branes are separated by a non-zero distance. (This figure was originally used in the review article "Gauge/String Duality, Hot QCD and Heavy Ion Collisions" by Jorge Casalderrey-Solana, Hong Liu, David Mateos, Krishna Rajagopal, and Urs Achim Wiedemann (Reference: CERN-PH-TH-2010-316, MIT-CTP-4198, ICCUB-10-202).)

dual to another theory with open strings satisfying *Dirichlet* boundary conditions. Furthermore, they showed that the hyperplane on which these open strings ended coupled to closed strings in the dual theory. This showed, since T-duality is an essential feature of string theory, that the existence of these hyperplanes suggested by imposing Dirichlet boundary conditions on open strings was unavoidable and furthermore that these hyperplanes were in fact dynamical objects. This new type of object was termed a Dirichlet-brane or *D-brane*.

D-branes belong to a general class of objects called p-branes. A p-brane is a higher dimensional generalization of a string which extends in p dimensions and a p-brane which is also a D-brane is also known as a Dp-brane. A D0-brane is just a point particle, a D1-brane is a string, a D2-brane is a two-dimensional membrane and one can have D3-branes, D4-branes and so on up to $p = 9$ in 10-dimensional string theory. The dynamics of open strings which begin and end on D-branes are localized to those same D-branes. A graph of this is shown in Fig. 1.1. Furthermore [11, 30], it turns out that on a single D-brane there always exists a massless state corresponding to a string with both ends terminating on the same D-brane and this massless mode corresponds to a photon of a $U(1)$ gauge theory localized on the D-brane. Hence, a D-brane is a natural candidate for the localization of fields

and gauge dynamics.

1.2 Large Extra Dimensions and The ADD Model

Supersymmetry is a necessary part of string theory since it is needed to introduce fermions into the theory. However, for supersymmetry to be a part of nature it is necessary that it is broken at some energy scale. A big problem with string theory was the breaking mechanism for space-time supersymmetry (that is, supersymmetry of the full higher dimensional space in which strings and branes propagate). Naturally, with the extra-dimensions compactified at the Planck scale, the scale of supersymmetry breaking is typically of the order the Planck scale, which is a problem if one insists that supersymmetry solves the Hierarchy problem since to do this the supersymmetry breaking must happen at the electroweak scale. In Ref. [31], Antoniadis proposed a solution to this problem. He considered a model with a large, compact extra dimension of the order of a few inverse TeV (or TeV^{-1}) and argued that it was consistent with perturbative string theory.

With D-branes now considered to be interesting dynamical objects propagating in a higher dimensional space on which gauge fields and matter can be localized, it was natural to consider whether the physics of our 3+1-dimensional universe could be reproduced on a D3-brane. When one introduces extra dimensions, gravity must necessarily propagate in all dimensions. In light of the result of Ref. [31], where the scale of supersymmetry breaking was reduced from the Planck scale by making an extra dimension of order TeV^{-1}, one can naturally wonder if the Standard Model fields could be localized to a D3-brane propagating in a higher dimensional space in which the compact extra dimensions are *large*, rather than of the order the Planck scale, so that gravity is diluted in these extra dimensions to the extent that it becomes naturally as weak as it appears in comparison to the other fundamental forces of nature. This is precisely what Arkani-Hamed, Dimopoulos and Dvali proposed and they showed that this was an alternative solution to the Hierarchy problem [32]. This model is known as the ADD model (after the authors).

In the ADD model [32], spacetime is taken to be (4+n)-dimensional with the topology of $M_4 \times T_n$ where M_4 is the usual 3+1-dimensional Minkowskian manifold and T_n is some compact manifold of dimension n of typical length R and volume R^n. The SM fields are taken to be localized to 3+1D submanifold while gravity propagates in all dimensions. In this model, the 4D Planck mass

M_{Pl}, is not the fundamental scale of gravity in the theory but rather that role is played by the (4+n)-dimensional Planck mass $M_{Pl(4+n)}$. The authors argued that for two test masses m_1 and m_2 placed within a radius $r < R$ that the effective gravitational potential between the masses is

$$V(r) \sim \frac{m_1 m_2}{M^{n+2}_{Pl(4+n)}} \frac{1}{r^{n+1}}, (r \ll R), \tag{1.18}$$

since by Gauss's law the volume containing these masses will be some (4+n)-dimensional subspace of radius r. However, if the masses are placed at a distance much larger than R, then the volume enclosing the volume of m_1, for example, will have fully enclosed the portion of T_n between m_1 and m_2 and thus can only extend further along the non-compact dimensions, leading to a gravitational potential of the form

$$V(r) \sim \frac{m_1 m_2}{M^{n+2}_{Pl(4+n)} R^n} \frac{1}{r}, (r \gg R). \tag{1.19}$$

Arkani-Hamed, Dimopoulos and Dvali used the gravitational potential in these two limits to argue that the effective 4D Planck mass reproduced on the 4D-submanifold where the Standard Model fields reside is related to the extra-dimensional Planck mass and the extra-dimensional scale R as

$$M^2_{Pl} \sim M^{2+n}_{Pl(4+n)} R^n. \tag{1.20}$$

If one wishes to use the model to solve the Hierarchy problem, then one requires that the extra-dimensional Planck mass is of the order the electroweak scale m_{EW}. If we demand that this is so, then R must be of order

$$R \sim 10^{\frac{30}{n}-17}\text{cm} \times (\frac{1\text{TeV}}{\text{m}_{\text{EW}}})^{1+\frac{2}{\text{n}}}. \tag{1.21}$$

For a single extra dimension, R is of the order 10^{13}cm, and thus the extra dimension is roughly the size of the solar system and clearly in conflict with experiment. However, for the case $n = 2$, one finds that R is of the order of 1mm! At the time, this did not conflict with experiment. This implied that models with a brane-localized Standard Model embedded in a higher dimensional universe, which not only evaded the current experimental limits but could also be feasibly tested in the future, could be constructed. This is not the case in String Theory for which the extra-dimensional behaviour is only apparent at Planckian energies. This naturally led to other approaches for which the extra-dimensional physics could become apparent at low energy scales. The Randall-Sundrum Type I model (RS1) also resolves the Hierarchy problem as well as containing a KK spectrum for which the typical mass gap between the modes is of the order of a TeV. We discuss this model as well as the RS2 model in the next section.

1.3 The Randall-Sundrum Models

Randall and Sundrum proposed an alternative to the ADD model which employed a higher dimensional spacetime with non-factorizable geometry [14]. The ADD model resolved the hierarchy between the Planck scale and the electroweak scale at the cost of introducing a new one, namely that between the electroweak scale and the compactification scale. Furthermore, generically there would be Kaluza-Klein modes that would be excited at very low energies, since the compactification scale is much lower than the electroweak scale. Randall and Sundrum were able to get around these issues with the construction of a five-dimensional model in a slice of Anti-de Sitter space.

In the Randall-Sundrum type I model (RS1), the fifth dimension parametrized by the coordinate ϕ is actually taken to have the geometry of the orbifold $S^1/\mathbb{Z}_2$ where $(x, -\phi)$ is identified with (x, ϕ), where x denotes the ordinary 3+1D coordinates x^μ. This orbifold has two fixed points at $\phi = 0$ and $\phi = \pi$. These fixed points are identified with the positions of two 3-branes: the UV brane at $\phi = 0$ and the IR brane at $\phi = \pi$. In the RS1 model, the Standard Model is taken to be localized on one of these branes, namely the IR brane. Hence, the action may be written a priori as

$$S = S_{grav} + S_{vis} + S_{hid}, \tag{1.22}$$

where S_{grav} is just the ordinary 4+1D Einstein-Hilbert action

$$S_{grav} = \int d^4x \int_{-\pi}^{\pi} d\phi \sqrt{-G}(-\Lambda + 2M^3 R), \tag{1.23}$$

and S_{vis} and S_{hid} are the brane-localized actions to the IR and UV branes respectively,

$$\begin{aligned} S_{vis} &= \int d^4x d\phi \sqrt{-g_{vis}} \delta(\phi - \pi)(\mathcal{L}_{vis} - V_{vis}), \\ S_{hid} &= \int d^4x d\phi \sqrt{-g_{hid}} \delta(\phi)(\mathcal{L}_{hid} - V_{hid}). \end{aligned} \tag{1.24}$$

Here, V_{vis} and V_{hid} are the vacuum energies of the respective branes.

To construct a solution which respects 3+1D Pioncaré invariance, Randall and Sundrum assumed that the background solution to the 5D Einstein equations took the form

$$ds^2 = e^{-2\sigma(\phi)} \eta_{\mu\nu} dx^\mu dx^\nu + r_c^2 d\phi^2, \tag{1.25}$$

where r_c is the compactification length scale, and σ is some function depending on the extra-dimensional coordinate ϕ.

Upon substituting the ansatz metric into the 5D Einstein field equations, one finds that the resultant equations for σ are

$$\frac{6\sigma'^2}{r_c^2} = \frac{-\Lambda}{4M^3}, \frac{3\sigma''}{r_c^2} = \frac{V_{hid}}{4M^3 r_c}\delta(\phi) + \frac{V_{vis}}{4M^3 r_c}\delta(\phi - \pi). \tag{1.26}$$

The solution to the former which respects the orbifold symmetry $\phi \to -\phi$ is

$$\sigma = r_c|\phi|\sqrt{\frac{-\Lambda}{24M^3}}. \tag{1.27}$$

Immediately, we see from the above equation that for there to be a consistent solution, the cosmological constant must be negative. This implies that the 5D bulk encased by the branes is a slice of five-dimensional Anti-de Sitter spacetime (AdS_5).

For the solution to be consistent over the whole orbifold $S_1/\mathbb{Z}_2$, σ must be periodic in ϕ. Differentiating twice the solution in Eq. 1.27, we obtain

$$\sigma'' = 2r_c\sqrt{\frac{-\Lambda}{24M^3}}\big[\delta(\phi) - \delta(\phi - \pi)\big]. \tag{1.28}$$

Thus, to be consistent with the latter equation in Eq. 1.26, the following condition must be imposed for some energy scale k,

$$V_{hid} = -V_{vis} = 24M^3 k,\ \Lambda = -24M^3 k^2. \tag{1.29}$$

This is the famous Randall-Sundrum fine-tuning condition. This condition is required to ensure that not only do we have a solution to the 5D Einstein field equations but also that the solution respects 4D Poincaré invariance.

The resultant metric may be thus written

$$ds^2 = e^{-2kr_c|\phi|}\eta_{\mu\nu}dx^\mu dx^\nu + r_c^2 d\phi^2. \tag{1.30}$$

To work out the physical consequences of this warped geometry, we need to perturb about this background solution and work out the effective 4D gravitational action. Hence, we need to promote the 5D metric to

$$ds^2 = e^{-2kT(x)|\phi|}[\eta_{\mu\nu} + \overline{h}_{\mu\nu}]dx^\mu dx^\nu - T^2(x)d\phi^2. \tag{1.31}$$

Here, $T(x)$ represents a scalar field whose vacuum expectation value is r_c and thus also contains perturbations about this compactification radius scale. The field $\overline{h}_{\mu\nu}$ represents perturbations to the background 4D Minkowskian

metric. Upon dimensional reduction, one can determine the effective 4D Planck scale by inspection of the effective action under the 4D background metric. When one does this, one finds that the 4D Planck scale is related to the 5D Planck scale M, compactification radius r_c and k as

$$M_{Pl}^2 = \frac{M^3}{k}(1 - e^{-2kr_c\pi}). \tag{1.32}$$

This equation tells us that the compactification radius has little effect on the effective Planck scale due to the exponential sensitivity in the limit that $kr_c >> 1$. This is rather unlike the ADD scenario where the extra-dimensional radius had a very demonstrable effect.

Now let's analyze the action for a Higgs field localized on the IR brane. On the UV brane, one can see that the localized 4D metric is precisely $g_{hid,\mu\nu} = \overline{g}_{\mu\nu}$. On the IR brane the the metric picks up a warp factor with $g_{vis,\mu\nu} = e^{-2kr_c\pi}\overline{g}_{\mu\nu}$. Thus, if we have a Higgs field H localized to the IR brane, then the action on the IR brane S_{vis} contains a piece

$$S_{vis} \supset \int dx^4\sqrt{-g_{vis}}\big(g_{vis}^{\mu\nu}D_\mu H^\dagger D_\nu H - \lambda(|H|^2 - v_0^2)^2\big), \tag{1.33}$$

which upon substituting g_{vis} for $e^{-2kr_c\pi}\overline{g}_{\mu\nu}$ and performing the wave-function renormalization $H \to e^{kr_c\pi}H$ may be rewritten

$$S_{vis} \supset \int dx^4\sqrt{-\overline{g}}\big(\overline{g}^{\mu\nu}D_\mu H^\dagger D_\nu H - \lambda(|H|^2 - e^{-2kr_c\pi}v_0^2)^2\big). \tag{1.34}$$

From the above equation, we determine that the bare vacuum expectation value v_0 on the IR brane from the fundamental higher dimensional theory corresponds to a scale

$$v = e^{-kr_c\pi}v_0, \tag{1.35}$$

in the low energy 4D effective field theory. It turns out that it is only necessary to take $kr_c \sim 12.5$ to yield a warp factor of $e^{-2kr_c\pi} \sim 10^{-17}$ so that in taking $v_0 \sim M \sim k \sim M_{Pl} = 10^{19}\,\text{GeV}$ we get a resultant effective electroweak scale of $v \sim 10^2\,\text{GeV}$, which is the correct order-of-magnitude result. Thus, RS1 solves the Hierarchy problem, and we can naturally produce the correct electroweak scale physics with a small dimension of roughly ten times the Planck length.

A remarkable thing that Randall and Sundrum noticed about the physics of this warped background geometry was that it could lead to a second type of model, known as the Randall-Sundrum type II model (RS2), where the extra dimension is in fact infinite [15]. Notice that in taking the limit $r_c \to \infty$, we are taking the IR brane out to infinity and effectively removing it

so that all the Standard Model fields must now reside on the UV brane, an important corollary from which is that this model no longer solves the Hierarchy problem.

If one looks at the relationship between the 5D Planck mass, the compactification radius, k and the effective 4D Planck mass given in Eq. 1.32, one notes that the piece proportional to the warp factor goes to zero in the limit that the compactification radius goes to infinity. Thus, the Planck scale does not blow up or go to infinity in the infinite radius limit but rather gives a finite result that can be meaningful. Randall and Sundrum provided this as a first clue that a meaningful 4D gravitational theory could still be reproduced in the infinite radius limit.

To show that 4D gravity is reproduced, we must show that there exists a graviton zero mode localized to the brane as well as the excited modes. All of these modes will contribute to fluctuations about the background so to calculate their profiles we perturb the background metric by promoting the background metric $ds^2 = e^{-2k|y|}\eta_{\mu\nu} - dy^2$ to $ds^2 = e^{-2k|y|}[\eta_{\mu\nu} + h_{\mu\nu}(x,y)] - dy^2$, determine the resulting dynamical equation for $h_{\mu\nu}(x,y)$ and then expand it as a tower of solutions. Before we perform the expansion and solve for the modes, we fix the gauge by choosing the traceless transverse condition $\partial^\mu h_{\mu\nu} = 0$ and $h^\mu_\mu = 0$. This choice of gauge makes all the components of $h_{\mu\nu}(x,y)$ equal so that we may drop the indices and simply write $h(x,y)$. We then expand $h(x,y)$ as

$$h(x,y) = \sum_m \psi_m(y) e^{ipx}, \tag{1.36}$$

where obviously $p^2 = m^2$ and m denotes the masses of the modes. The resulting equation as determined from the Einstein field equations is

$$\big[-\frac{m^2}{2} e^{2k|y|} - \frac{1}{2}\partial_y^2 - 2k\delta(y) + 2k^2 \big] \psi_m(y) = 0. \tag{1.37}$$

By making a change of variables to $z = sgn(y)(e^{k|y|} - 1)/k$, $\hat{\psi}_m(z) = \psi_m(y) e^{k|y|/2}$, $\hat{h}(x,z)$, the above equation may be rewritten as

$$\big[-\frac{1}{2}\partial_z^2 + V(z) \big] \hat{\psi}_m(z) = m^2 \hat{\psi}_m(z), \tag{1.38}$$

where the potential $V(z)$ is given by

$$V(z) = \frac{15k^2}{8(k|z|+1)^2} - \frac{3k}{2}\delta(z). \tag{1.39}$$

The above potential is sometimes referred to as a 'volcano' potential since there is an infinitely deep, point-source potential well at $z = 0$ generated by

the Dirac delta function and the potential decreases to zero on either side of the well after attaining a maximum. There is just a single bound, localized mode for which $m = 0$ and thus this mode is interpreted precisely as the 4D graviton! Since the potential decays to zero at infinity, the KK spectrum forms a continuum and there is a mode for all $m > 0$. The KK modes also asymptote to plane waves at infinity and to enter the region around the potential well, these plane waves need to overcome the potential barriers around the maxima of this volcano potential. Therefore, the KK modes contribute very minimally to the effective theory of gravity localized to the brane.

One can calculate the resultant modified gravitational force law between masses m_1 and m_2 separated by a distance r by integrating all the contributions from the modes

$$V_{grav}(r) = G_N \frac{m_1 m_2}{r} + \int_0^\infty \frac{G_N}{k} \frac{m_1 m_2 e^{-mr}}{r} \frac{m}{k}. \tag{1.40}$$

The first term is the usual Newtonian gravitation potential and it comes from the bound zero mode graviton. The second term with the integral is a sum of the contributions of the KK modes, which have a suppression factor of e^{-mr} due to Yukawa's law for forces mediated by massive bosons. There is also an additional suppression factor of m/k due to the fact that the KK modes are suppressed by the potential barriers around the well at $y = 0$. When one performs the integration, one finds that the gravitational potential is precisely

$$V_{grav}(r) = G_N \frac{m_1 m_2}{r}(1 + \frac{1}{r^2 k^2}). \tag{1.41}$$

Hence, we have reproduced an effective 3+1D gravity theory from a 4+1D one. At distances $r >> \frac{1}{k}$ the correction contained inside the parentheses of Eq. 1.41, $1/r^2k^2$, is much smaller than one and therefore at large distances the usual Newtonian law of gravitation is reproduced. For distances roughly equal to or smaller than $r \sim 1/k$, the correction obviously becomes important and in this limit the correction dominates, yielding an inverse cubic law for the gravitational potential. In the Randall-Sundrum models, particularly in RS2 in which gravity is localized to one brane and thus its scale must be Planckian, k is expected to be of order the Planck scale so in this way experimental limits due to the correction term are easily avoided.

The RS2 model is a fascinating one since all extra-dimensional models up to its inception contained only compact extra dimensions. For the first time, it was shown that this need not be the case and a realistic effective 3+1D theory could be reproduced from a 4+1D one in which the extra dimension is in fact infinite. Arkani-Hamed, Dimopoulos, Dvali and Kaloper showed later

that the number of infinite extra dimensions can be arbitrary by extending the RS2 framework to 3+n+1D spacetime with an effective 3+1D gravity theory reproduced on the intersection of n fundamental branes [33]. One could also think of using a thick brane or domain wall instead of a fundamental brane to reproduce the same physics. As we will see later, the RS2 model provides a model for how to trap gravity on domain-wall branes.

1.4 Topological Defects

In this section we will discuss topological defects. Topological defects are solutions to non-linear differential equations which map a subset of spacetime (usually a boundary) to a moduli space under a non-trivial homotopy class. The simplest type of topological soliton is a domain wall.

Domain walls appear naturally in quartic scalar field theories. They are mappings between two energy degenerate, stable minima of a scalar potential. Let η be a real scalar field in $1+1D$ spacetime, where the spatial coordinate is y, with the potential

$$V(\eta) = \frac{1}{4}\lambda(\eta^2 - v^2)^2. \tag{1.42}$$

This potential has minima at the values $\eta = \pm v$. To find a domain wall solution, we require a solution to the Euler-Lagrange equations for η subject to the boundary conditions

$$\eta(\pm\infty) = \pm v. \tag{1.43}$$

Proposing that η solely depends on the spatial coordinate y, the Euler-Lagrange equation is thus

$$-\frac{d^2\eta}{dy^2} + \lambda(\eta^2 - v^2)\eta = 0. \tag{1.44}$$

One can then easily show that the desired solution for η is

$$\eta(y) = v\tanh(ky), \tag{1.45}$$

where $k^2 = \lambda v^2/2$. A graph of the domain wall is shown in Fig. 1.2.

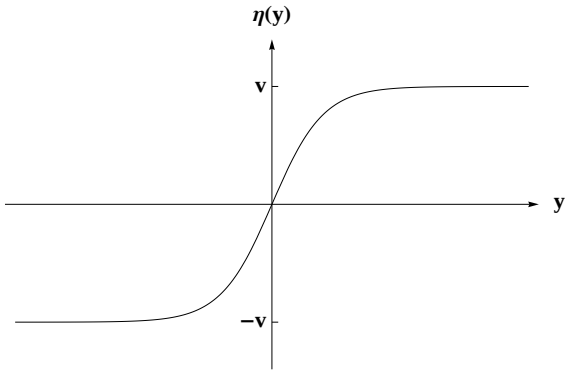

Figure 1.2: A graph of the domain-wall solution given in Eq. 1.45.

The trivial solution where η is constant and settles into one of the minima has a lower energy density than the above configuration in which η is a map associating the different ends at spatial infinity along y. However, to deform the latter into the former, one would have to take η along one entire domain and have its values in that domain switch over from the corresponding vacuum to that of the other domain. Since there are infinitely many points, this transformation requires an infinite amount of energy, and thus the solitonic solution is stable. This stability is ultimately due to the fact that the homotopy group π_0 of the vacuum manifold is non-trivial: it is precisely a set of two discrete, disconnected vacua related by the $\mathbb{Z}_2$ symmetry. For π_0, there exists two homotopy classes: one which maps both $y = -\infty$ and $y = +\infty$ to one point, which describes the situation when η settles homogeneously and isotropically to one vacuum, and one which maps $y = -\infty$ and $y = +\infty$ to the two different points, which describes the domain wall situation. Mappings belonging to different homotopy classes cannot be continuously deformed into each other. Hence, domain walls of the form given in Eq. 1.45 are said to be *topologically* stable.

Another way to see this topological stability is by noticing that there is a corresponding conserved topological charge [34]. One can define the topological current to be

$$J^\mu = \epsilon^{\mu\nu}\partial_\nu\eta. \tag{1.46}$$

Due to the anti-symmetric properties of the alternating tensor, it is obvious that this current satisfies the continuity equation and is conserved. The corresponding topological charge is

$$Q = \int dy J^0 = \eta(y = +\infty) - \eta(y = -\infty). \tag{1.47}$$

For the solution where η settles into a constant vacuum Q vanishes but for the domain wall $Q = 2v$. Hence, due to the conservation of this charge, the domain wall cannot evolve to the constant vacuum solution.

The energy of the domain wall solution is given by

$$T = \int dy \frac{1}{2}(\frac{d\eta}{dy})^2 + V(\eta(y)) = \frac{2}{3}kv^2. \tag{1.48}$$

Domain walls are based on non-trivial mappings under the homotopy group $\pi_0(M)$, where here M denotes the moduli space of the theory. One can also form topologically stable solitons based on higher homotopy groups and more complicated moduli spaces. The next most simplest example is that of strings. Strings, also known as vortices, are based on mapping a boundary of spacetime with the topology of the circle S^1 to M which belong to non-trivial homotopy classes of the fundamental group $\pi_1(M)$. If we write down a 2+1D theory with a complex scalar Φ with the potential

$$V(\Phi) = \frac{1}{2}\lambda(\Phi^\dagger\Phi - v^2)^2, \tag{1.49}$$

one can easily see that for this theory that any element of M must take the form $\Phi = e^{i\phi}v$ and thus $M \simeq S^1$. Hence, the fundamental group in this case will be $\pi_1(M) \simeq \pi_1(S^1) \simeq \mathbb{Z}$. The integers of this $\mathbb{Z}$ group are called winding numbers. One can now look for solutions in terms polar coordinates (r, θ) for which $\Phi \to ve^{i\theta}$ as $r \to \infty$. This boundary condition is an example of a mapping from the circle at infinity to the vacuum manifold with a winding number of 1, and a solution satisfying this boundary condition cannot decay into the trivial vacuum since the topological charge associated with the winding number is conserved. Similarly, solutions for which $\Phi \to ve^{ni\theta}$ as $r \to \infty$ have a winding number of n, and these solutions cannot decay or morph into either the vacuum solution or any solution with a different winding number.

Yet another example in 3+1D spacetime is that of a monopole. Monopoles are based on the second homotopy group $\pi_2(M)$, and the most famous, simple example where they occur is a Higgs model with an $SO(3)$ gauge group, with a Higgs field in the fundamental representation. Here, the vacuum manifold $M \simeq S^2$, breaking $SO(3)$ to $SO(2) \simeq U(1)$, and thus $\pi_2(M) \simeq \pi_2(S^2) \simeq \mathbb{Z}$. This case is particularly interesting, given that under the remaining $U(1)$ theory, one can calculate the magnetic flux of the resulting solitonic solutions and one finds that it is non-zero and related to the winding numbers coming from $\pi_2(M)$, hence the name monopoles.

One can still go further in constructing topological solitons. Generically, whenever the nth homotopy group of the moduli space of a theory, $\pi_n(M)$,

is non-trivial we can construct stable, solitonic solutions which non-trivially map an n-sphere at infinity to M. In the special case when $M \simeq S^n$, this means that the boundary conditions satisfied by solitonic solutions need to at least be a sphere of dimensions n since $\pi_m(S^n)$ is trivial for all $m < 0$ and $\pi_n(S^n) \simeq \mathbb{Z}$.

1.5 Domain-Wall Braneworlds

Having laid out the basics of domain walls and of the Randall-Sundrum models, we are now ready to outline the domain-wall braneworld construction in 4+1D spacetime. In domain-wall braneworld models, one must reproduce an effective 3+1D field theory on the world volume of the domain wall. This involves localizing the Standard Model field content as well as gravity. Therefore, one must have at the very least a mechanism for the localization of scalar fields, fermions, gauge bosons and gravitons. The cases for the first two are relatively straightforward and we will attend to those first. Localization of fermions is simply achieved by Yukawa coupling them to the background scalar fields [21]. Scalars are localized through quartic scalar interactions with the background fields.

The localization of gauge bosons is highly non-trivial and in our framework we invoke the Dvali-Shifman mechanism, which is quite different from the mechanisms used to localize scalars and fermions. This mechanism relies on confinement dynamics to localize the gauge bosons of a subgroup H of a non-Abelian group G which is unbroken and in confinement phase in the bulk.

When one couples the background scalar fields to 4+1D gravity by writing down the appropriate 4+1D Einstein-Hilbert action with a cosmological constant, one finds that there still exists a localized graviton zero mode on the wall, reproducing a 3+1D gravitational theory. A fine-tuning condition analogous to the Randall-Sundrum fine-tuning condition must be imposed, and the background geometry is thus very similar to the RS2 model. There is a continuum of KK graviton modes and their contribution yields an inverse cubic correction at high energies to the ordinary 3+1D Newtonian Law for gravitational force.

1.5.1 Fermion Localization

The localization of chiral fermionic zero modes to a domain wall was first shown by Jackiw and Rebbi [21]. In the full analysis of fermion localization, we also follow closely Ref. [35]. Consider the domain wall solution in Eq. 1.45

of the previous section in 4+1D flat Minkowskian spacetime. Note that in 4+1D spacetime, the Clifford algebra consists of five Gamma matrices, with the first four being simply the same ones as for 3+1D $\Gamma^\mu = \gamma^\mu$ for $\mu = 0, 1, 2, 3$ and the fifth gamma matrix being $\Gamma^5 = -i\gamma_5$ where γ_5 is the 3+1D chirality operator. Dirac spinors in 4+1D still have four components but all fermions are now Dirac: there exist no Weyl or Majorana representations. Noting this, we may write down the Yukawa interaction coupling a 4+1D fermionic field Ψ to the scalar field η generating the domain walls

$$-h\overline{\Psi}\Psi\eta. \tag{1.50}$$

Including this Yukawa interaction in the full 4+1D action, the resultant 4+1D Dirac equation for the fermion field Ψ is

$$i\Gamma^M\partial_M\Psi - h\eta\Psi = 0. \tag{1.51}$$

Let's first look for a solution of the form $\Psi(x, y) = f(y)\psi(x)$, where ψ satisfies the massless 3+1D Dirac equation $i\gamma^\mu\partial_\mu\psi = 0$. Making this ansatz and multiplying from the left by γ_5 reduces Eq. 1.51 to

$$[f'(y) - h\eta(y)f(y)\gamma_5]\psi = 0. \tag{1.52}$$

If we now assume ψ is a Weyl spinor without assuming left or right chirality for the moment, denoting the γ_5 eigenvalue of ψ as $C_\psi = \pm 1$, we find that the solution for the profile $f(y)$ is

$$\begin{aligned} f(y) &= Ne^{+hC_\psi \int_0^y \eta(y')\,dy'}, \\ &= Ne^{+hC_\psi \int_0^y v\tanh(ky')\,dy'}, \\ &= N\,\mathrm{sech}\,(ky)^{-hvC_\psi/k}, \end{aligned} \tag{1.53}$$

where N is just a normalization factor. From this, we see that if $h > 0$, then if $C_\psi = +1$ and ψ is right-chiral, $f(y)$ is proportional to some positive power of $\cosh(ky)$ and thus diverges at infinity, whereas if $C_\psi = -1$ and ψ is left-chiral, $f(y)$ is some positive power of $\mathrm{sech}\,(ky)$ and decays to zero at infinity. This means that the right-chiral solution is non-normalizable and thus unphysical whereas the left-chiral solution is normalizable and thus a physical solution. If $h < 0$, then the right-chiral solution becomes the physical one and the left-chiral solution is unphysical. Furthermore, in both cases the physical solution has $f(y)$ being maximized about $y = 0$ in the center of the domain wall.

Thus, if we Yukawa couple the 4+1 fermion field Ψ to the domain wall, a single 3+1D chiral zero mode is produced and localized to the domain wall.

This is very important since one must worry about reproducing chirality in the effective field theory since the original 4+1D theory is vector-like and the Standard Model which we ultimately wish to localize to the wall is a chiral theory. These chiral zero modes will be our candidates for the Standard Model fermions. It is also important that we have produced a *massless* chiral zero mode since we wish that the Standard Model particles originally be massless prior to electroweak symmetry breaking which we achieve later through localizing a scalar field corresponding to the Higgs doublet.

Having described the chiral zero modes, one may wonder what other physical modes exist. After all, we are dealing with an extra-dimensional theory for which Kaluza-Klein modes are common, and naturally if we embed an electron inside a 4+1D field, we expect there to be KK electrons with higher masses. This is indeed the case and to do the required analysis we need to make a full expansion of Ψ of the form

$$\Psi = \sum_m f_L^m \psi_L^m + f_R^m \psi_R^m, \tag{1.54}$$

where the 3+1D chiral modes $\psi_{L,R}^m$ satisfy the 3+1D Dirac equation $i\gamma^\mu \partial_\mu \psi_{L,R} = m\psi_{R,L}$. We assume, without loss of generality, that for the analysis below $\tilde{h} > 0$. Substituting this expansion into Eq. 1.51 yields the respective equations for the profiles of the chiral modes

$$\begin{aligned} \frac{df_L^m}{dy} &= m f_R^m(y) - h\eta(y) f_L^m(y), \\ \frac{df_R^m}{dy} &= -m f_L^m(y) + h\eta(y) f_R^m(y). \end{aligned} \tag{1.55}$$

Doing some algebra by using the first of these equations to substitute for f_R^m in the second and vice versa for f_L^m in the first, as well as substituting $\eta(y) = \eta_{cl}(y) = v \tanh(ky)$, we obtain the following Schrödinger equations for the left-chiral and right-chiral profiles respectively

$$\begin{aligned} \big[-\frac{d^2}{d\tilde{y}^2} + \tilde{h}(\tilde{h}+1)\tanh^2(\tilde{y}) - \tilde{h} \big] f_L^m(\tilde{y}) &= \tilde{m}^2 f_L^m(\tilde{y}), \\ \big[-\frac{d^2}{d\tilde{y}^2} + \tilde{h}(\tilde{h}-1)\tanh^2(\tilde{y}) + \tilde{h} \big] f_R^m(\tilde{y}) &= \tilde{m}^2 f_R^m(\tilde{y}), \end{aligned} \tag{1.56}$$

where the tilded quantities are the dimensionless quantities $\tilde{y} = ky$, $\tilde{h} = hv/k$ and $\tilde{m} = m/k$.

The potentials in Eq. 1.56 are Pöshl-Teller potentials. The eigenvalues, which are exactly equal to the dimensionless squared masses in this case,

are well known [36, 37, 38, 39, 40]. The resultant squared masses for the left-chiral modes are

$$m^2 = (2n\tilde{h} - n^2)k^2, \quad = 2nhk - n^2k^2, \tag{1.57}$$

for $n = 0, 1, ..., \lfloor \tilde{h} \rfloor$.

The masses for the right-chiral modes are the same as in Eq. 1.57 except that n is in the range $n = 1, 2, ..., \lfloor \tilde{h} \rfloor$ with the $n = 0$ mode absent (since there is no right-chiral zero mode). Given that the respective Pöshl-Teller potentials in Eq. 1.56 are examples of shape-invariant potentials which can be generated by a superpotential [39, 40], we can easily compute the profiles for all the localized modes once we know the ground states for both potentials by applying the appropriate ladder operator. Figure 1.3 shows plots of the first few localized left-chiral and right-chiral modes including the zero mode. If change $\tilde{h}$ so that it is negative rather than positive, it is the right-chiral modes which have a localized KK tower starting from a zero mode and all the left-chiral modes are massive.

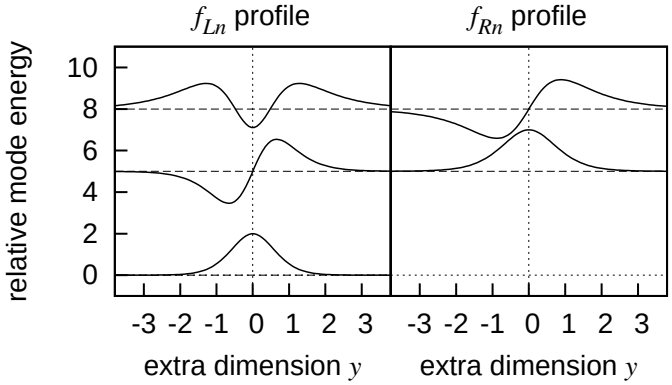

Figure 1.3: A plot of the tower of the first few localized left-chiral and right-chiral modes. (This plot is originally from Damien George's PhD thesis [41].)

Beyond the localized modes, there are also delocalized continuum modes which have energies above the highest mass localized mode. They behave like 4+1D fermions and are able to propagate through the entire bulk.

1.5.2 Scalar Localization

In describing scalar localization, we again follow closely Ref. [35]. To localize a scalar field to the domain wall, we need to introduce quartic interactions

between the background scalar field η and a scalar field Φ which is to contain our candidate localized scalar. The interaction potential containing the coupling Φ to the background as well as the self-interactions for Φ is

$$V_\Phi = \frac{1}{2}\lambda_{\Phi\eta}\eta^2\Phi^2 + \frac{1}{4}\lambda_\Phi\Phi^4 + \frac{1}{2}\mu_\phi^2. \tag{1.58}$$

Assuming that any vacuum expectation values for the modes of Φ are negligible in comparison to the vacua of the background field η, we can ignore the self-interaction term for Φ in determining the modes. We therefore compute the profiles for the modes by considering the 4+1D Klein-Gordon equation

$$\Box\Phi + \lambda_{\Phi\eta}\eta^2\Phi + \mu_\Phi^2\Phi = 0. \tag{1.59}$$

We expand Φ as a series of modes,

$$\Phi(x,y) = \sum p_m(y)\phi_m(x), \tag{1.60}$$

where the fields ϕ_m satisfy 3+1D Klein-Gordon equations with mass m, $\Box_{3+1}\phi_m = -m^2\phi_m$. Substituting this expansion and ansatz as well as the classical solution for η into Eq. 1.59, we find that, like the chiral fermion modes before, the profiles for the scalar modes satisfy Pöshl-Teller equations

$$\big[-\frac{d^2}{d\tilde{y}^2} + d(d+1)\tanh^2(\tilde{y}) - d\big]p_m(\tilde{y}) = \lambda_m p_m(\tilde{y}), \tag{1.61}$$

where here $d = \sqrt{\tilde{\lambda}_{\Phi\eta} + 1/4} - 1/2$, $\tilde{\lambda}_{\Phi\eta} = \lambda_{\Phi\eta}v^2/k^2$ and the eigenvalues $\lambda_m p_m$ given in terms of d, $\tilde{\lambda}_{\Phi\eta}$ and the masses m are

$$\lambda_m = -\frac{\mu_\Phi^2}{k^2} + \frac{m^2}{k^2} - d. \tag{1.62}$$

There are $\lceil d \rceil$ localized modes indexed by an integer $n = 0, 1, 2, ..., \lfloor d \rfloor$, and their eigenvalues are

$$\lambda_m^n = 2nd - n^2. \tag{1.63}$$

Thus, the squared masses for the localized modes are given by

$$m_n^2 = \mu_\Phi^2 + \big[(2n+1)d - n^2\big]k^2. \tag{1.64}$$

The squared mass for the lowest energy mode, the $n = 0$ mode, is $m_0^2 = \mu_\Phi^2 + d$. Hence the lowest energy localized mode for a scalar field has a non-zero squared mass unlike the chiral zero mode for a fermionic field which was massless. We also have the freedom to make $m_0^2 = \mu_\Phi^2 + d$ tachyonic so that

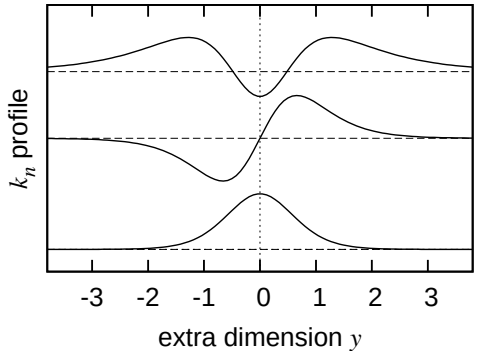

Figure 1.4: A plot of the $n = 0$, $n = 1$ and $n = 2$ modes for the discrete spectrum embedded in Φ. In the plot above, $d = 3$. (This plot is originally from Damien George's PhD thesis [41].)

this mode, ϕ_0, acquires a non-zero vacuum expectation value. If the VEV is small enough, we can ignore backreactions on the background fields and can just simply treat ϕ_0 as a Higgs field localized to the domain wall. Thus it is possible to localize the electroweak Higgs sector of the Standard Model if we attempt to construct a realistic model.

For the scalars, there is a single tower of localized modes and we can utilize the relevant ladder operator for the given Pöshl-Teller potential, just as we did with the fermions. One finds that the (non-dimensionalized) profile for the lowest energy mode is

$$\tilde{p}_0(\tilde{y}) = \tilde{C}_0 \operatorname{sech}^d(\tilde{y}). \tag{1.65}$$

A plot of this zero mode profile as well as the profiles for the $n = 1$ and $n = 2$ excited modes is given in Fig. 1.4.

1.5.3 The Split Fermion Mechanism

Before we move on to all the other localization mechanisms, let us mention the split fermion mechanism first proposed by Arkani-Hamed and Schmaltz [19]. Let's consider the same 4+1D fermionic field Ψ Yukawa coupled to the scalar field η generating the domain wall, but this time with a 4+1D bulk mass M. Although this bulk mass breaks the discrete $\mathbb{Z}_2$ symmetry, it is possible in principle to choose parameters such that the domain wall is meta-stable with a very long lifetime. The 4+1D Dirac equation then becomes

$$i\Gamma^M \partial_M \Psi - h\eta\Psi - M\Psi = 0. \tag{1.66}$$

Let us just analyze the chiral zero mode. Without loss of generality, let us choose h positive so that the zero mode is left-chiral. We find the profile by simply looking for a solution to the above equation of the form $f(y)\psi(x)$ where $\gamma_5\psi = -\psi$ and $i\gamma^\mu\partial_\mu\psi = 0$. In doing this we find that the equation for the profile of the zero mode becomes

$$[f'(y) + h\eta(y)f(y) + Mf(y)]\psi = 0. \tag{1.67}$$

Therefore, the new solution for $f(y)$ with the addition of the bulk mass may be written

$$f(y) = N\,\mathrm{sech}\,(ky)^{hv/k}e^{-My}. \tag{1.68}$$

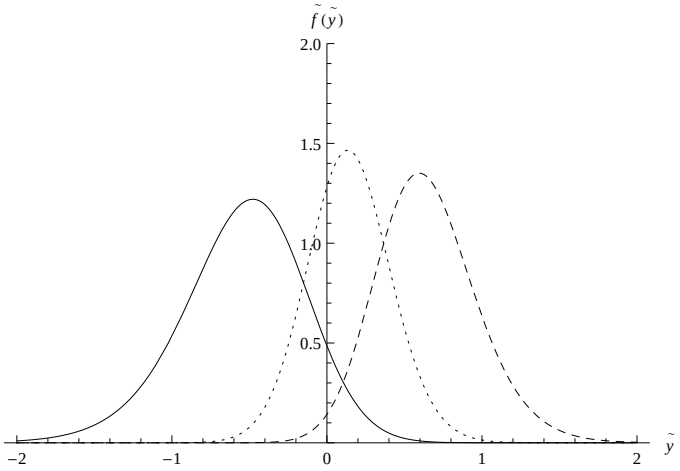

Figure 1.5: A plot of the non-dimensionalized profile $\tilde{f}(\tilde{y}) = k^{1/2}f(y)$ in terms of $\tilde{y} = ky$ for some example parameter choices. Here, the solid black line represents the choice with $\tilde{h} = hv/k = 9$ and $\tilde{M} = M/k = 4$, the dotted line is for $\tilde{h} = 15$, $\tilde{M} = -2$ and the dashed line is for $\tilde{h} = 15$, $\tilde{M} = -8$.

A plot of the profile for some example parameter choices is given in Fig. 1.5. The effect of the bulk mass term is to shift the localization center of the chiral zero mode away from $y = 0$. Instead, the chiral fermion is now localized around $y = -(M/hv)/k$, or in dimensionless units $\tilde{y} = -(\tilde{M}/\tilde{h})$ ($\tilde{M} = M/k$). This is important since in this scenario different fermions will not in general share the same bulk mass and thus will not share the same localization centers.

Let ψ be a 3+1D fermion in which the left and right-chiral components are embedded as chiral zero modes in the 4+1D fermionic fields Ψ_{ψ_L} and Ψ_{ψ_R} respectively and let a 3+1D Higgs field ϕ be embedded in the 4+1D

scalar Φ. Upon dimensional reduction of a Yukawa interaction of the form $Y_\psi \Psi_{\psi_L} \Psi_{\psi_R} \Phi$, where Y_ψ denotes the bulk Yukawa coupling, the effective 3+1D Yukawa coupling y_ψ for ψ will take the form

$$y_\psi = Y_\psi \int f_{\psi_L}(y) f_{\psi_R}(y) p_\phi(y)\, dy. \tag{1.69}$$

Not only does the 3+1D Yukawa coupling depend on a bulk Yukawa coupling constant but it also depends crucially on an overlap integral of the product of the profiles of the three particle species involved in the interaction. Thus, different fermions will have different masses. The more closely bunched the localization centers of f_{ψ_L}, f_{ψ_R} and p_ϕ are and the more they overlap, the higher the effective Yukawa coupling constant and thus fermion mass will be. Given that the profiles f_{ψ_L} and f_{ψ_R} depend exponentially on the couplings to the domain wall and the bulk masses, there is the potential to solve problems like the fermion mass hierarchy problem. In particular, one could explain why the quarks in each generation are more massive then the leptons by splitting them so that the quarks are closer to the localization center of the Higgs. If one goes to multiple generations of fermions, one can also promote M to a more general mass matrix and if it is taken to not commute with the analogous matrix for the couplings to η (which we can assume to be diagonal by choice of basis) then the different zero modes corresponding to each generation will mix, and once dimensional reduction is done, an average mixing is produced. This latter scenario is called the twisted split fermion scenario [42, 43].

1.5.4 Adding Gravity

The localization of gravity obviously involves successfully coupling the background scalar field configuration to 4+1D gravity. This problem has been solved many times already [44, 45, 46, 47, 48, 49, 50]. For a simple example, we will closely follow Ref. [50], under the unit and parameter conventions given in the overview of the same model by Ref. [22]. Let us write down the action for a single scalar field η coupled to gravity with a cosmological constant as

$$S = \int d^4x \int dy \sqrt{G} \big[-2M^3 R - \Lambda + \frac{1}{2} G^{MN} \partial_M \eta \partial_N \eta - V(\eta) \big]. \tag{1.70}$$

We wish to solve the resultant dynamical equations by making the usual Randall-Sundrum ansatz for a warped metric, $ds^5 = e^{-2\sigma(y)} \eta_{\mu\nu} dx^\mu dx^\nu - dy^2$ and making sure that for such a solution $\sigma(y)$ decays to zero at infinity.

Let the potential, $V(\eta)$, be defined by

$$V(\eta) = 3ak^2 M_{5D}^3 (1 + 4a) \cos^2(\frac{\phi}{D}), \tag{1.71}$$

where $D = 6aM_{5D}^3$, M_{5D} is the 4+1D Planck mass, a is a dimensionless free parameter and k is a free parameter with the dimension of an inverse length. This potential has a countably infinite set of vacua as well as a $\mathbb{Z}_2$ symmetry.

One can show that

$$\begin{aligned} \sigma(y) &= a \log\big[\cosh(ky)\big], \\ \eta(y) &= D \arctan\big[\sinh(ky)\big], \end{aligned} \tag{1.72}$$

is a solution to the Einstein and Einstein-Klein-Gordon equations with the cosmological constant set to $\Lambda = -6a^2k^2$ (which is the usual Randall-Sundrum fine-tuning condition). The effective 4D Planck scale reproduced on the wall is

$$M_{Pl}^2 = \frac{M_{5D}^3}{k} \frac{\sqrt{\pi}\Lambda(a)}{\Lambda(a + \frac{1}{2})}. \tag{1.73}$$

In the limit that a tends to zero, M_{Pl}^2 behaves asymptotically as $M_{Pl}^2 \sim M_{5D}^3/ka$ while in the limit $a \to \infty$, the asymptotic behaviour is $M_{Pl}^2 \sim M_{5D}^3\sqrt{\pi}/k\sqrt{a}$. Thus the weak gravity limit corresponds to the limit where a is small.

The above solution requires that the cosmological constant Λ be set to

$$\Lambda = -24M_{5D}^3 a^2 l^2. \tag{1.74}$$

Taking the thin brane limit $a \to 0$, $l \to \infty$ while keeping al finite reduces the model to the original RS2 model. From the above formula for the cosmological constant, one can identify $k = al$, where k is the parameter from the RS2 model.

To show that gravity is localized, we show that there is a localized graviton zero mode and that the physics of these modes reduces to 4D gravity at low energies. One can solve the relevant dynamical equations analytically in the special case that $a = 1$. To solve the equations it is easiest to shift to conformal coordinates with extra-dimensional coordinate $z = f(y)$ defined such that $dy^2 = e^{-2\sigma(y)}dz^2$. In this case the volcano potential is simply

$$V(z) = \frac{l^2}{\big(1 + (lz)^2\big)^2}\left(\frac{15}{4}(lz)^2 - \frac{3}{2}\right). \tag{1.75}$$

One can show that the normalized profile $\psi_0(z)$ for the graviton zero mode is

$$\psi_0(z) = \sqrt{\frac{l}{2}}(1 + (lz)^2)^{-3/4}, \tag{1.76}$$

which is square integrable and decays to zero as $z \to \pm\infty$ as required, implying that the massless graviton is localized to the wall. Like the volcano potential of the RS2 model, $V(z)$ also decays to zero out at infinity, which implies that the KK spectrum is continuous and is analogous to that of the RS2 model. This implies that we obtain a 3+1D gravitational theory on the domain wall with a small correction at high energies, which is the same result as for the RS2 model.

We have now shown that fermions, scalars and gravity can be localized on a domain wall. We next turn to the localization of gauge bosons.

1.5.5 The Dvali-Shifman Mechanism

Having described the localization mechanisms for scalars, fermions and gravitons above, we now turn to the localization of gauge bosons. This turns out to be a highly non-trivial task. In localizing gauge bosons from a higher dimensional theory, obviously the higher dimensional theory should contain a 4+1D Yang-Mills gauge theory containing these gauge fields.

One might first consider a similar approach as for fermions, scalars and gravity by directly coupling the gauge fields to the domain wall. This approach does not lead to a phenomenologically acceptable localization for massless gauge bosons [51]. The easiest way to see why this is not acceptable is to analyze the effective 3+1D couplings to the gauge bosons for the different fermion species. Consider a 4+1D gauge interaction for a fermion, $g_5\Psi\Gamma^M A_M\Psi$, where A_M is the gauge field and g_5 the bulk coupling constant. If ψ is the chiral zero mode of Ψ and A_M contains a zero mode corresponding to a 3+1D gauge boson a_μ, then after performing dimensional reduction on this gauge interaction one can see that the effective gauge coupling constant, g_4, for ψ is given by

$$g_4 = g_5 \int dy\ f_\psi^2(y) p_{a_\mu}(y), \tag{1.77}$$

where as usual $f_\psi(y)$ denotes the profile for the chiral zero mode ψ and $p_{a_\mu}(y)$ is the profile of the gauge boson. We have seen in previous sections that different species of fermion will in general couple differently to the domain wall and will have different bulk masses if we include them, leading them to have different profiles. This means that they will have different effective gauge couplings to a_μ, which is disastrous if a_μ is to be a non-Abelian gauge boson, since this means we lose gauge charge universality.

The mechanism that Dvali and Shifman proposed [52] to get around this problem, and the one which we invoke in our domain-wall braneworld models, relies on the non-perturbative physics of confinement. They originally

considered a simple model with an $SU(2)$ gauge theory, a real scalar field η and an $SU(2)$-adjoint scalar field χ with the potential

$$V(\eta,\chi) = \frac{1}{4}\lambda_\eta(\eta^2 - v^2)^2 + \lambda_{\eta\chi}(\eta^2 - v^2)Tr[\chi^2] + \mu_\chi^2 Tr[\chi^2] + \lambda_\chi Tr[\chi^2]^2. \tag{1.78}$$

The parameter conditions

$$\lambda_\eta > 0, \qquad \lambda_\chi > 0, \qquad \lambda_{\eta\chi} v^2 > \mu_\chi^2, \tag{1.79}$$

are imposed so that the potential is bounded from below and so that χ attains a tachyonic mass in the center of the defect. Thus, we expect a component of χ to condense on the wall and so we take this component to be that proportional to the isospin generator σ_z and we will label this component χ_1. After choosing the boundary conditions

$$\begin{aligned} \eta(y = \pm\infty) &= \pm v, \\ \chi_1(y = \pm\infty) &= 0, \end{aligned} \tag{1.80}$$

one can show that under the special parameter choice

$$2\mu_\chi^2(\lambda_{\eta\chi} - \lambda_\chi) + (\lambda_\eta\lambda_\chi - \lambda_{\eta\chi}^2)v^2 = 0, \tag{1.81}$$

the solution to the Euler-Lagrange equations is

$$\begin{aligned} \eta(y) &= v\tanh(ky), \\ \chi_1(y) &= A\,\mathrm{sech}\,(ky), \end{aligned} \tag{1.82}$$

where $k^2 = \mu_\chi^2$ and $A^2 = \frac{\lambda_{\eta\chi}v^2 - 2\mu_\chi^2}{\lambda_\chi}$. A plot of this solution is shown in Fig. 1.6.

We can see that the $SU(2)$ gauge theory is left unbroken towards both positive and negative infinity and it is spontaneously broken to $U(1)$ on the wall by χ. In this original 3+1D toy model, Dvali and Shifman took the $SU(2)$ theory to be in confinement phase. Therefore, in the bulk, all the gauge bosons, including the $U(1)$ photon which is left massless on the wall, must coexist in a massive $SU(2)$-glueball state. For the $U(1)$ photon, this means that there is an energy cost to propagating in the bulk since it is massless on the domain wall. The Dvali-Shifman proposal seeks to generalize this mass gap to the case where the $SU(2)$ group is replaced by a larger non-Abelian gauge group G and the $U(1)$ is replaced by a subgroup of G, H, which is in general semi-simple and can be non-Abelian or contain non-Abelian factors. The extension of the mass gap argument is then that

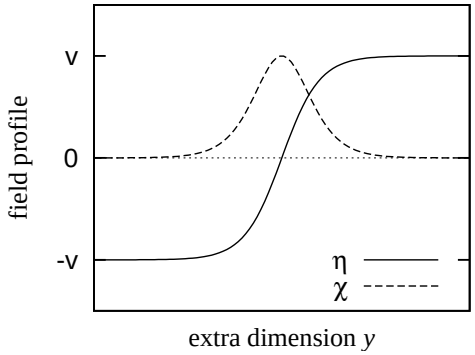

Figure 1.6: A plot of the profiles for η and χ_1. (This plot is originally from Damien George's PhD thesis [41].)

the confinement scale of G in the bulk is larger than the confinement scale of H (or any of the confinement scales of its non-Abelian factors) on the wall.

The Dvali-Shifman proposal is also augmented by the dual superconductor model of confinement first proposed by 't Hooft and Mandelstam [53, 54]. Under this picture, confinement arises due to a condensate being formed from magnetic monopoles. These magnetic monopoles can be constructed as solitons arising in a spontaneously broken non-Abelian gauge theory. This condensate is analogous to the condensates formed by Cooper pairs inside a superconductor, and given that its components are magnetically charged, it should under electromagnetic duality expel *electric* fields by a dual Meissner effect, hence the name dual superconductor. If we now place quarks inside this dual superconducting condensate, they will form flux strings whose potential grows linearly with distance, leading to quarks being confined in colorless mesons and baryons. One can now understand the Dvali-Shifman mechanism in terms of this picture, since if the bulk is confining it should under duality behave as a dual superconductor under this picture. Hence, if we go back to the case with $G = SU(2)$ and $H = U(1)$, the electric field lines of the Abelian group on the wall will be repelled by the dual superconducting bulk and will be forced to diverge out solely parallel to the world volume of the wall. Even if we place a test charge in the bulk, the lines of its electric field will form a flux string on to the wall and then diverge out, behaving as if the test charge was actually on the wall [51, 55]! Again, under the general Dvali-Shifman conjecture this is thought to extend to the case for general G and H. Given that the properties of the field lines of a test charge do not behave significantly differently when put in the bulk rather than on the wall, the way the test charge couples to other charged particles as well as

the localized gauge bosons is independent of the position of the test charge. Therefore, regardless of their localization profiles, all quarks will couple to gluons with equal strength if we localize the $SU(3)$ subgroup and therefore the Dvali-Shifman mechanism protects gauge charge universality if it works.

There are a couple of caveats we should take before proceeding with the assumption that the Dvali-Shifman mechanism traps gauge bosons to the domain wall. The first is that it has not been proven even in the original model in 3+1D spacetime. To this, we note that there is at least some numerical evidence from lattice gauge theory [56] that this mechanism works in 2+1D. The second point is that we ultimately wish to localize 3+1D gauge fields initially belonging to a higher dimensional Yang-Mills gauge theory. It is not strictly known whether 5D field theories are confining and furthermore 5D Yang-Mills gauge theories are known to be non-renormalizable. Given the non-renormalizability, we have to impose a cut-off λ_{UV} and be content that there is a confining phase at energies below this cut-off if it exists. Creutz showed in Ref. [57] using lattice simulations that a confining phase does in fact exist in an $SU(2)$ gauge theory in 4+1D spacetime. A similar analysis was done for $SU(5)$ in Ref. [41] with the same result.

Having given some details as to why the two aforementioned difficulties can be overcome, we will proceed assuming the Dvali-Shifman mechanism successfully traps gauge bosons on to the interior of a domain wall. We are now ready to delve into model building and we give an overview of the 4+1D domain-wall brane model proposed by Davies, George and Volkas for which $G = SU(5)$ and $H = SU(3) \times SU(2) \times U(1)$.

1.6 Putting it all together: The 4+1D SU(5) Domain-Wall Brane Model

Now that we have covered the essential components for constructing a domain-wall brane model, we will give an overview of the simplest such model, the 4+1D $SU(5)$ domain-wall brane model first proposed by Davies, George and Volkas, as it was described with one generation of SM fermions in the original paper [23]. Here, $SU(5)$ will be broken to $SU(3) \times SU(2) \times U(1)$ by an adjoint scalar χ attaining a lump-like VEV profile in the usual hypercharge component. We will also find that the profiles for the fermions and scalars are split in general.

The scalar fields in the model are

$$\eta \sim 1, \tag{1.83}$$
$$\chi \sim 24, \tag{1.84}$$
$$\Phi \sim 5^*. \tag{1.85}$$

Here, η is the field that will generate the domain-wall, χ will be the field condensing in the interior to break $SU(5)$ to the Standard Model and Φ will contain the electroweak Higgs doublet which is to be dynamically localized to the wall.

The fermion content of the theory consists of one generation of the SM fermions. The SM fermions are placed into the following $SU(5)$ representations,

$$\Psi_5 \sim 5^*, \tag{1.86}$$
$$\Psi_{10} \sim 10, \tag{1.87}$$

The field Ψ_5 contains the charge conjugate of the right-chiral down quark and the left-chiral lepton doublet, and Ψ^i_{10} contains the left-chiral quark doublet and the charge conjugates of the right-chiral up quark and the right-chiral electron.

The background domain wall configuration is formed from a self-consistent classical solution for the coupled fields η and χ. The relevant part of the action for describing the dynamics of the background is [23],

$$S = \int d^5x (T - V_{\eta\chi}), \tag{1.88}$$

where T contains all the $SU(5)$ gauge-covariant kinetic terms for all the fields. $V_{\eta\chi}$ is the part of Higgs potential containing the quartic potentials for η and χ, with

$$V_{\eta\chi} = (c\eta^2 - \mu_\chi^2)Tr(\chi^2) + a\eta Tr(\chi^3) + \lambda_1[Tr(\chi^2)]^2 + \lambda_2 Tr(\chi^4) + l(\eta^2 - v^2)^2. \tag{1.89}$$

We want χ to break $SU(5)$ to the SM on the domain wall, while having the bulk respect the original gauge symmetry. We do this in the standard way by giving the component χ_1 associated with the hypercharge generator Y a non zero value on the brane, and having all the other components vanish. Thus the potential reduces to

$$V_{\eta\chi} = \frac{\tilde{\lambda}}{4}\chi_1^4 + l(\eta^2 - v^2)^2 - \frac{1}{4}\sqrt{\frac{1}{15}}a\eta\chi_1^3 + \frac{1}{2}(c\eta^2 - \mu_\chi^2)\chi_1^2, \tag{1.90}$$

where $\tilde{\lambda} = \lambda_1 + \frac{7\lambda_2}{30}$.

To find the background configuration, we need to solve the Euler-Lagrange equations for η and χ_1 subject to the boundary conditions

$$\eta(y = \pm\infty) = \pm v, \tag{1.91}$$
$$\chi_1(y = \pm\infty) = 0, \tag{1.92}$$

which are degenerate global minima of $V_{\eta\chi}$. For the sake of simplicity, we choose to impose the constraints

$$2\mu_\chi^2(c - \tilde{\lambda}) + (2c\tilde{\lambda} - 4l\tilde{\lambda} - c^2)v^2 = 0, \tag{1.93}$$
$$a = 0, \tag{1.94}$$

yielding the analytic solutions,

$$\begin{aligned} \eta(y) &= v \tanh(ky), \\ \chi_1(y) &= A\,\mathrm{sech}(ky), \end{aligned} \tag{1.95}$$

where $k^2 = cv^2 - \mu_\chi^2$, and $A^2 = \frac{2\mu_\chi^2 - cv^2}{\tilde{\lambda}}$. We should stress that the above conditions are not fine-tuning conditions, and they are chosen simply so that the background fields obtain analytic forms. To find solutions, these conditions need not be imposed, and for a finite range of parameters we can always find numerical solutions which are kink-like for η and lump-like for χ [23]. The graphs of these solutions for η and χ_1 are shown in Figures 1.7(a) and 1.7(b) respectively.

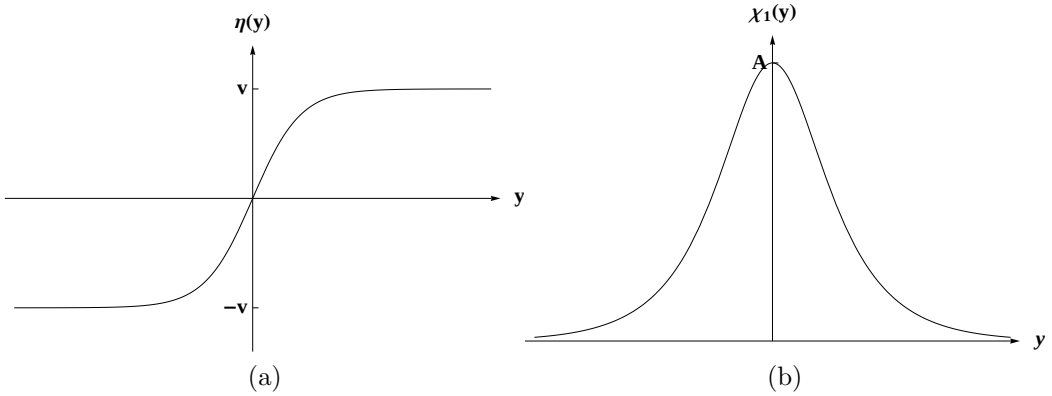

(a) (b)

Figure 1.7: (a) The kink η and (b) χ_1 as functions of the extra-dimensional coordinate y

To preserve the topological stability of the domain wall, a spontaneously broken $\mathbb{Z}_2$ reflection symmetry must be introduced. Under this discrete symmetry transformation,

$$\begin{aligned} y &\to -y, \\ \eta &\to -\eta, \\ \chi &\to -\chi, \\ \Psi_{5,10} &\to i\Gamma^5\Psi_{5,10}. \end{aligned} \tag{1.96}$$

The SM fermions now also couple to the field χ as well as η. Hence the background Yukawa potential, for one generation becomes,

$$Y_{DW} = h_{5\eta}\overline{\Psi}_5\Psi_5\eta + h_{5\chi}\overline{\Psi}_5\chi\Psi_5 + h_{10\eta}Tr(\overline{\Psi}_{10}\Psi_{10})\eta - 2h_{10\chi}Tr(\overline{\Psi}_{10}\chi\Psi_{10}). \tag{1.97}$$

The resulting 5D Dirac equation, for the charged fermions, is

$$i\Gamma^M\partial_M\Psi_{nY}(x,y) - h_{n\eta}\eta(y)\Psi_{nY}(x,y) - \sqrt{\frac{3}{5}}\frac{Y}{2}\chi_1(y)\Psi_{nY}(x,y) = 0,\ n = 5, 10. \tag{1.98}$$

Just as before, to find the zero modes, it is enough to look for solutions for each charged fermion of the form $\Psi_{nY}(x,y) = f_{nY}(y)\psi_{nY}(x)$ where the $\psi_{nY}(x)$ are 3+1D massless, left-chiral spinor fields. Substituting this into the above Dirac equations yields the solutions for the profiles,

$$f_{nY}(y) = C_{nY}e^{-b_{nY}(y)},\ \text{for n} = 1, 5, 10, \tag{1.99}$$

where the C_{nY} are normalization constants, and

$$\begin{aligned} b_{nY}(y) &= \tilde{h}_{n\eta}\log\left(\cosh\left(ky\right)\right) + Y\sqrt{\frac{3}{5}}\tilde{h}_{n\chi}\arctan\left(\tanh\left(\frac{ky}{2}\right)\right), \\ \tilde{h}_{n\eta} &= \frac{h_{n\eta}v}{k}, \\ \tilde{h}_{n\chi} &= \frac{h_{n\chi}A}{k}. \end{aligned} \tag{1.100}$$

To meaningfully describe the localization of the fermions in terms of numbers, we need to describe them in terms of dimensionless variables. The non-dimensionalized domain-wall Yukawa couplings $\tilde{h}_{n\eta}$ $\tilde{h}_{n\chi}$ have already been defined in Eq. 1.100 and so we just need to non-dimensionalize the profiles. Defining the non-dimensionalized extra-dimensional coordinate, $\tilde{y}$, as

$$\tilde{y} = ky, \tag{1.101}$$

and changing variables, we see that the normalization condition for the profiles becomes

$$\int f_{nY}(\tilde{y})^{\dagger} f_{ny}(\tilde{y})\, d\tilde{y} = k. \tag{1.102}$$

Hence, in order to use functions which are normalized to one over $\tilde{y}$, we define the non-dimensionalized profiles, $\tilde{f}_{nY}(\tilde{y})$, as

$$\tilde{f}_{nY}(\tilde{y}) = k^{-\frac{1}{2}} f_{nY}(\tilde{y}). \tag{1.103}$$

We can see from above that the couplings to the lump generated by χ depend on the hypercharge. Firstly, the coupling to this lump shifts the minima of the localization potentials away from $y = 0$, which means that the localization centers of the fermions are also shifted from $y = 0$. Secondly, since the different SM components embedded in the $SU(5)$ multiplets have different hypercharges, the localization centers of different SM components embedded in the same $SU(5)$ multiplet have different localization centers. In other words, the split fermion mechanism is naturally realized in this model. We give example profiles for the right-chiral down quark and lepton doublet, which are embedded in the quintet, in Fig. 1.8 and for the right-chiral up quark, right-chiral electron and quark doublet, which are embedded in the decuplet, in Fig. 1.9. We will describe more details of fermion localization, in particular the case with multiple generations and the localization of right-chiral neutrinos, in the subsequent chapters.

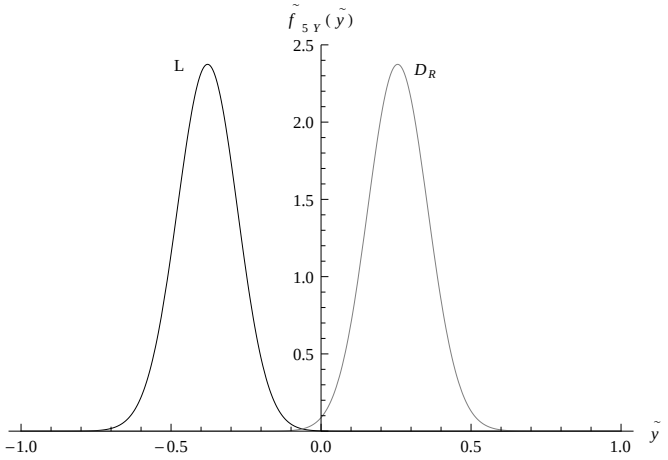

Figure 1.8: The profiles for the localized lepton doublet L and right-chiral down-type quark D_R arising from an arbitrary fermion quintet Ψ_5 for the parameter choice $\tilde{h}_{5\eta} = 100$ and $\tilde{h}_{5\chi} = -100$.

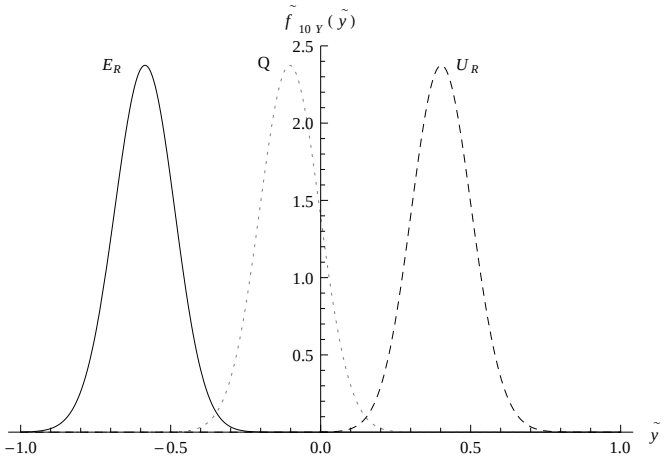

Figure 1.9: Profiles for a right-chiral electron-type lepton E_R, quark doublet Q and a right-chiral up-type quark U_R arising from an arbitrary fermion decuplet Ψ_{10} for the parameter choice $\tilde{h}_{10\eta} = 100$ and $\tilde{h}_{10\chi} = 100$.

The electroweak Higgs doublet is also embedded in a quintet and thus also couples to χ. Just like the fermions, there also turns out to be a 'split scalar' mechanism since the couplings to χ depend on the hypercharges of the different $SU(3)_c \times SU(2)_I \times U(1)_Y$-invariant components. The localization potential for Φ, which contains the electroweak Higgs, simply becomes

$$V_\Phi = \mu_\Phi^2 \Phi^\dagger \Phi + \lambda_3 (\Phi^\dagger \Phi)^2 + \lambda_4 \Phi^\dagger \Phi \eta^2 + 2\lambda_5 \Phi^\dagger \Phi Tr[\chi^2] + \lambda_6 \Phi^\dagger (\chi^T)^2 \Phi + \lambda_7 \Phi^\dagger \chi^T \Phi \eta. \tag{1.104}$$

To find the profiles of the electroweak Higgs doublet, Φ_w, and the colored Higgs triplet, Φ_c, embedded in the quintet Φ, we search for solutions of the form,

$$\Phi_{w,c}(x, y) = p_{w,c}(y)\phi_{w,c}(x), \tag{1.105}$$

where the $p_{w,c}$ are the respective profiles, and $\phi_{w,c}$ satisfy the Klein-Gordon equations,

$$\Box_{3+1d}\phi_{w,c} = m_{w,c}^2 \phi_{w,c} + \dots \tag{1.106}$$

where $m_{w,c}$ are the masses of the lowest energy modes for $\Phi_{w,c}$. Substituting this ansatz into the 4+1d KG equation with the potential V_Φ, one obtains the equations for the profiles

$$-\frac{d^2 p_{w,c}}{dy^2} + W_Y(y) p_{w,c}(y) = m_{w,c}^2 p_{w,c}(y), \tag{1.107}$$

where

$$W_Y(y) = \mu_\Phi^2 + \lambda_4\eta^2 + \lambda_5\chi_1^2 + \frac{3Y^2}{20}\lambda_6\chi_1^2 + \sqrt{\frac{3}{5}}\frac{Y}{2}\lambda_7\eta\chi_1. \tag{1.108}$$

Changing variables to the dimensionless coordinate $\tilde{y}$ defined in Eq. 1.101, the potentials of the above Schrödinger equations can be rewritten as shifted hyperbolic Scarf potentials, that is we can write them in the form

$$\begin{aligned}\Big[&- \tfrac{d^2}{d\tilde{y}^2} + A_Y^2 + (B_Y^2 - A_Y^2 - A_Y)\,\mathrm{sech}\,(\tilde{y})^2 \\ &+ B_Y(2A_Y+1)\,\mathrm{sech}\,(\tilde{y})\tanh(\tilde{y})\Big] p_{w,c}(\tilde{y}) = \lambda_{w,c}p_{w,c}(\tilde{y})\end{aligned} \tag{1.109}$$

where

$$\begin{aligned}A_Y &= \frac{-1+\sqrt{2((\tilde{\lambda}_5+\frac{3Y^2}{20}\tilde{\lambda}_6-\tilde{\lambda}_4-\frac{1}{4})^2+\frac{3Y^2}{20}\tilde{\lambda}_7^2)^{\frac{1}{2}}-2\tilde{\lambda}_5-\frac{3Y^2}{10}\tilde{\lambda}_6+2\tilde{\lambda}_4+\frac{1}{2}}}{2}, \\ B_Y &= \frac{\sqrt{\frac{3}{5}}\frac{Y}{2}\tilde{\lambda}_7}{\sqrt{2((\tilde{\lambda}_5+\frac{3Y^2}{20}\tilde{\lambda}_6-\tilde{\lambda}_4-\frac{1}{4})^2+\frac{3Y^2}{20}\tilde{\lambda}_7^2)^{\frac{1}{2}}-2\tilde{\lambda}_5-\frac{3Y^2}{10}\tilde{\lambda}_6+2\tilde{\lambda}_4+\frac{1}{2}}},\end{aligned} \tag{1.110}$$

and the non-dimensionalized Higgs parameters and masses are defined as

$$\begin{aligned}\tilde{\lambda}_4 &= \frac{\lambda_4 v^2}{k^2}, \\ \tilde{\lambda}_5 &= \frac{\lambda_5 A^2}{k^2}, \\ \tilde{\lambda}_6 &= \frac{\lambda_6 A^2}{k^2}, \\ \tilde{\lambda}_7 &= \frac{\lambda_7 vA}{k^2}, \\ \tilde{\mu}_\Phi^2 &= \frac{\mu_\Phi^2}{k^2}, \\ \tilde{m}_{w,c}^2 &= \frac{m_{w,c}^2}{k^2},\end{aligned} \tag{1.111}$$

and $\lambda_{w,c} = \tilde{m}_{w,c}^2 - \tilde{\mu}_\phi^2 - \tilde{\lambda}_4 + A_Y^2$ are the eigenvalues of the equations for the electroweak Higgs and the colored Higgs hyperbolic Scarf potentials.

The hyperbolic Scarf potential has been well studied [58] as it is a member of a class of potentials satisfying the shape-invariance condition in supersymmetric quantum mechanics (for more on shape-invariant potentials see

[40, 39]). For $A_Y > 0$, it is known to have a set of discrete bound modes for $n = 0, 1, ..., \lfloor A_Y \rfloor$, with eigenvalues

$$\lambda^n_{w,c} = 2nA_Y - n^2. \tag{1.112}$$

Combining this with the previous equations for $\lambda_{w,c}$, we see that the potentials have a discrete set of bound modes with masses given by

$$\tilde{m}^2_{n,w,c} = \tilde{\mu}^2_\Phi + \tilde{\lambda}_4 - (A_Y - n)^2. \tag{1.113}$$

The physical electroweak Higgs and colored Higgs fields in the effective 4D theory on the brane correspond to the $n = 0$ modes, and they thus exist in the 4D theory if $A_Y > 0$. Assuming this, the profiles for these Higgs particles, $p_w(y)$ and $p_c(y)$ respectively, have the same form as those of the zero mode profiles for the charged fermions,

$$\begin{aligned} p_{w,c}(y) &= C_{w,c} e^{-b_{w,c}(y)}, \\ b_{w,c}(y) &= A_Y \log\left(\cosh\left(ky\right)\right) + 2B_Y \arctan\left(\tanh\left(\frac{ky}{2}\right)\right). \end{aligned} \tag{1.114}$$

Hence, we can interpret A_Y and B_Y to be effective couplings of the Higgs fields to the kink and the lump respectively.

The effective couplings A_Y and B_Y depend on the hypercharges, and thus they are in general different for the two Higgs components. This has a number of consequences. Firstly, the localization centers of the different components of Φ are split according to the hypercharges. We give an example plot of the profiles for the electroweak and colored Higgs scalars in Fig. 1.10.

Secondly, since the masses of the electroweak and colored Higgs depend on their respective A_Y, the masses of the two components are split. There exists a parameter region where the electroweak Higgs has a tachyonic mass, $m^2_w < 0$, while that for the colored Higgs (if a bound state exists) is non-tachyonic, thus inducing electroweak symmetry breaking on the brane while preserving $SU(3)_c$, as is desired. Since we know the exact form of the masses, a straightforward analysis shows that this parameter region is

$$A^2_{+2/3} < \tilde{\mu}^2_\Phi + \tilde{\lambda}_4 < A^2_{-1}. \tag{1.115}$$

Thirdly, as there only exist discrete bound modes for a species if $A_Y > 0$, there exist parameter regions where the electroweak Higgs component will have discrete bound modes localized to the domain wall while at the same time the colored Higgs will have only unbound continuum modes in its spectrum. This suggests that an alternate approach to suppressing colored Higgs

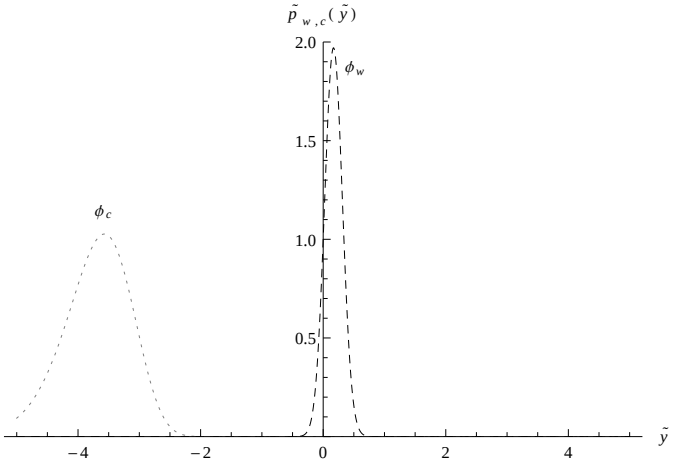

Figure 1.10: The profiles of the localized electroweak Higgs ϕ_w and colored Higgs scalar ϕ_c for an arbitrary quintet scalar Φ for parameters such that $\tilde{\lambda}_4 = -7500$, $\tilde{\lambda}_5 = 1500$, $\tilde{\lambda}_6 = -75000$, and $\tilde{\lambda}_7 = 2000$.

induced proton decay may be possible, as the continuum modes propagate in the full 4+1D spacetime so that the partial width contributed to proton decay from these modes may be suppressed by further powers of M_{GUT}. The analysis of this situation is beyond the scope of this thesis.

Lastly, gravity can still be localized and in this case, with a lump as well as a kink, we can choose parameters such that we obtain an analytic solution for η and χ as well as the warp factor. When we include gravity, the full action of the model becomes

$$S = \int d^5x\sqrt{G}(-2M^3 - \Lambda + T - Y_{DW} - Y_5 - V_{\eta\chi} - V_\Phi), \tag{1.116}$$

where T contains the kinetic terms, Λ is the cosmological constant and M is the 5D Planck mass. Writing the metric in the form

$$ds_5^2 = e^{-\rho(y)/6M^3}\eta_{\mu\nu}dx^\mu dx^\nu - dy^2, \tag{1.117}$$

and imposing the special parameter conditions

$$\begin{gathered} 2c - 4l - \tilde{\lambda},\ a = 0, \\ \mu_\chi^2 = lv^2\left(\frac{6M^3}{6M^3 + v^2}\right) + \frac{\tilde{\lambda}v^2}{2}\left(\frac{9M^3 + 2v^2}{6M^3 + v^2}\right), \end{gathered} \tag{1.118}$$

we find that there exists the analytical solution

$$\begin{aligned} \eta(y) &= v \tanh(ky), \\ \chi(y) &= v \,\mathrm{sech}\,(ky), \\ \rho(y) &= v^2 \log[\cosh(ky)], \end{aligned} \tag{1.119}$$

where $k^2 = 3M^3(cv^2 - \mu_\chi^2)/(3M^3 + v^2)$, if we also impose the usual Randall-Sundrum fine-tuning condition $\Lambda = -24M^3k^2$.

This warped background solution has essentially the same properties as the smooth domain-wall solution discussed in Sec. 1.5.4. As is generic in RS2-like models [59], the gravitons still experience a volcano potential and form a continuous KK spectrum, with a zero mode graviton localized to the domain wall. For the fermions, it was shown in [60] that once a fermionic field is coupled to the background fields that there still exists a chiral zero mode, but the warp factor causes the effective potential to decay to zero out at infinity; this means that like the gravitons, there is a continuous KK spectrum starting with the zero mode. For scalars, it was shown in [22] that in the case where the lowest energy mode of a scalar field is tachyonic, the spectrum consists of the lowest energy mode localized to the wall and then a continuous KK spectrum with positive definite masses starting infinitesimally close to zero.

The massive continuum modes are quasi-delocalized and propagate into the bulk. They then have to tunnel through the maxima of the volcano potential to enter the interior of the domain wall.

1.7 The Fermion Mass Hierarchy Problem

The Standard Model is a success in that it has given an very accurate description of the strong and electroweak interactions in terms of Yang-Mills gauge theory, as well as explaining why the W and Z bosons have mass by employing spontaneous symmetry breaking via the Higgs mechanism. With the addition of the three generations of Standard Model fermions, there are many Yukawa interactions with the Higgs field which are gauge invariant, leading to a plethora of dimensionless coupling constants. The electroweak Yukawa sector for the three generations of charged fermions is

$$\mathscr{L}_{Yukawa} = \lambda_1^{ij}\overline{L^i}\Phi e_R^j + \lambda_2^{ij}\overline{Q_L^i}\Phi^c U_R^j + \lambda_3^{ij}\overline{Q_L^i}\Phi D_R^j + h.c. \tag{1.120}$$

where $\Phi \sim (1, 2, -1)$ is the Higgs doublet and $\Phi^c = i\sigma_2\Phi^*$. After the Higgs attains a vacuum expectation value

$$\langle\Phi\rangle = \begin{pmatrix} 0 \\ v \end{pmatrix}, \tag{1.121}$$

one simply finds that the resultant components of the electron, up and down quark mass matrices are

$$m^{ij}_{E,U,D} = \lambda^{ij}_{1,2,3} v. \tag{1.122}$$

The Yukawa coupling constants are $\lambda^{ij}_{1,2,3}$ are dimensionless numbers. If the Standard Model were to be a natural theory, we would expect all of these constants to be of order 1. Evidently, given the measured masses for the fermions, this is not the case. If we ignore quark and lepton mixing for a moment and pretend the mass matrices are diagonal, then the component $m^{33}_U = \lambda^{33}_2 v$ of the up quark mass matrix will correspond to the top quark mass whereas $m^{11}_E = \lambda^{11}_1 v$ will correspond to the electron mass. Given that the top mass is approximately $m_t = 173$ GeV and given that we know that the Higgs vacuum expectation value must be equal to $v = 174$ GeV to yield the correct W and Z masses, λ^{33}_2 is roughly one and is thus natural. However, given the value for v and given that the electron mass is $m_e = 0.511$ MeV, this means that λ^{11}_1 is of order 10^{-6} and is thus unnaturally small. Similar hierarchies follow amongst the constants associated with the other fermion masses and given that the quark mixing angles are small, this situation does not change when we account for quark mixing.

Compounding the fermion mass hierarchy problem is the addition of neutrino masses. It is now known that the sum of the neutrino masses is less than about 0.3 eV [61, 62]. Hence there is an extra six orders of magnitude difference between the electron mass and the neutrino masses, compounding the problem. Furthermore, to generate neutrino masses we need to extend the Standard Model as there is no right-chiral neutrino. If we introduce right-chiral neutrinos along with the relevant Yukawa couplings to the Higgs which generate Dirac masses for the neutrino, the fermion mass spectrum now covers at least 12 orders of magnitude. We discuss neutrino masses and the see-saw mechanism in the next section.

1.8 Neutrino Masses and the See-Saw Mechanism

As alluded to at the end of the last section, the discovery of neutrino mass not only requires physics beyond the Standard Model but it also exacerbates the fermion mass hierarchy problem. We now know that at least two flavors of neutrino have mass via neutrino oscillations. From neutrino oscillations, it is not possible to directly measure the masses m_1, m_2 and m_3 of the neutrinos but it is possible to measure the difference between the squares of the masses of the neutrino mass eigenstates. From solar neutrino oscillations,

we have been able to determine the squared mass difference between the first and second generation neutrino mass eigenstates $\Delta m^2_{21} = m^2_2 - m^2_1 = 7.50^{+0.19}_{-0.20} \times 10^{-5}\,\mathrm{eV}^2$ [63]. We know from atmospheric neutrino oscillations that the modulus of the squared mass difference between the second and third eigenstates is $|\Delta m^2_{32}| = |m^2_3 - m^2_2| = 2.32^{0.12}_{-0.08} \times 10^{-3}\,\mathrm{eV}^2$ [63].

Note that because we do not know the sign of Δm^2_{32}, m_2 could be either less than or greater than m_3. This means that we can have two types of hierarchies for the neutrino mass eigenstates: we can have either the normal hierarchy, where $m_3 > m_2 > m_1$, or the inverted hierarchy $m_2 > m_3 > m_1$. It can also be the case that the neutrino masses are quasi-degenerate ($m_1 \sim m_2 \sim m_3$).

The easiest and most common way to give neutrinos mass is to include three generations of right-chiral neutrinos which are singlets under the Standard Model gauge group. The simplest way to make the neutrino masses is to simply add the Yukawa interactions

$$\mathscr{L}_{\nu,Yukawa} = \lambda_4^{ij} \bar{L}^i \Phi^c \nu_R^j + h.c. \tag{1.123}$$

This term simply yields a Dirac neutrino mass matrix, m_D after electroweak symmetry breaking,

$$m_\nu^{ij} = \lambda_4^{ij} v. \tag{1.124}$$

There is however a unique possibility for the neutrino given that it is chargeless and the right-chiral component is a Standard Model singlet, which is that we can also add a Majorana mass term. This term is written simply as

$$\frac{1}{2} M^{ij} \overline{(\nu_R^i)^c} \nu_R^j + h.c. \tag{1.125}$$

Hence, a key question with regards to neutrino mass and neutrinos in general is whether the neutrino is a Dirac or a Majorana fermion. If for some reason it turns out that $M = 0$, the neutrino is Dirac. Otherwise, the neutrino is Majorana.

Adding a combination of Dirac and Majorana masses also yields a viable mechanism for explaining the lightness of the neutrinos, called the seesaw mechanism. The simplest and easiest version of it to understand is called the Type I seesaw mechanism. Here, we simply add a combination of the Dirac and Majorana mass terms as given above. This leads to a total 6×6 mass matrix of the form

$$\frac{1}{2} (\overline{\nu_L}, \overline{\nu_R^c}) \begin{pmatrix} 0 & m_D \\ m_D^T & M \end{pmatrix} \begin{pmatrix} \nu_L^c \\ \nu_R \end{pmatrix} + h.c, \tag{1.126}$$

where here we have suppressed the flavor indices and where ν_L really stands for $(\nu_L^1, \nu_L^2, \nu_L^3)$ and likewise for ν_R. After diagonalization, one finds that in the mass eigenstate basis the resultant mass matrix is

$$\frac{1}{2}(\overline{\nu'_L}, \overline{\nu'^c_R}) \begin{pmatrix} M_L & 0 \\ 0 & M_R \end{pmatrix} \begin{pmatrix} \nu'^c_L \\ \nu'_R \end{pmatrix} + h.c, \tag{1.127}$$

where M_L is the mass matrix for the mass eigenstates which turn out to be predominantly composed of the left-chiral neutrinos and M_R is the mass matrix for the mass eigenstates which are predominantly composed of ν_R. One finds, in the limit that the Majorana mass terms are much larger than the Dirac mass terms, that the left mass matrix is approximately

$$M_L \approx -m_D M^{-1} m_D^T, \tag{1.128}$$

and the right mass matrix is approximately

$$M_R \approx M, \tag{1.129}$$

with the eigenstates being approximately $\nu'_L \simeq \nu_L - m_D^*(M^*)^{-1}(\nu_R)^c$ and $\nu'_R \simeq \nu_R + M^{-1}m_D^T(\nu L)^c$. If we take m_D and M to be real and deal with the case with just one generation of SM fermions, the mass eigenvalues and eigenstates simply reduce to $m_L = -\frac{m_D^2}{M}$ for $\nu'_L = \nu_L - \frac{m_D}{M}(\nu_R)^c$ and $m_R = M$ for $\nu'_R = \nu_R + \frac{m_D}{M}(\nu_L)^c$. Thus, the mass of ν'_L is suppressed with respect to the Dirac mass by a factor of m/M. If this factor is small enough, it can account for the smallness of the neutrino mass. For instance, if we take $M \simeq 3 \times 10^{14}$ GeV and $m_D = m_t = 173$ GeV, we find that the mass for the left Majorana mass eigenstate is around $m_L \sim 0.1$ eV.

We have in the last two sections outlined the basic problem with regards to the fine-tuning required for the fermion mass hierarchy in the Standard Model as well as the origin and smallness of the neutrino masses. In the next section, we will delve into the problems of quark and lepton mixing.

1.9 Quark and Lepton Mixing

Quark and lepton mixing arises due to the fact that the mass eigenstates of the various particle species are not the same as weak interaction eigenstates, thus leading to charged currents involving different flavors when we shift to the mass eigenbasis. Firstly, let's look at quark mixing, which is described by the Cabibbo-Kobayashi-Maskawa (CKM) matrix. After electroweak symmetry breaking, as discussed before, we obtain mass matrices for the up

and down quarks. The corresponding mass terms in the Lagrangian may be written as

$$\bar{U_R} M_U U_L + h.c, \tag{1.130}$$

and

$$\bar{D_R} M_D D_L + h.c, \tag{1.131}$$

where here $U_{L,R} = (u_{L,R}, c_{L,R}, t_{L,R})$ and $D_{L,R} = (d_{L,R}, s_{L,R}, b_{L,R})$ are tuples containing the three generations of up and down quarks.

These mass matrices are bidiagonalizable, which means that they are diagonalized by

$$\begin{aligned} \overline{M}_U &= V_{UR}^\dagger M_U V_{UL}, \\ \overline{M}_D &= V_{DR}^\dagger M_D V_{DL}, \end{aligned} \tag{1.132}$$

where $\overline{M}_{U,D}$ are the diagonalized mass matrices and the unitary matrices $V_{U,DL}$ and $V_{U,DR}$ are the left and right diagonalization matrices, defined by

$$\begin{aligned} U_L &= V_{UL} U'_L, \\ D_L &= V_{DL} D'_L, \end{aligned} \tag{1.133}$$

and

$$\begin{aligned} U_R &= V_{UR} U'_R, \\ D_L &= V_{DR} D'_R, \end{aligned} \tag{1.134}$$

where $U'_{L,R}$ and $D'_{L,R}$ contain the mass eigenstates. To determine the CKM matrix, we just need to know the left diagonalization matrices. Obviously these can't be determined from the diagonalization of $M_{U,D}$ but the matrices $M_{U,D}^\dagger M_{U,D}$ are

$$\begin{aligned} \bar{M}_U^\dagger \bar{M}_U &= V_{UL}^\dagger M_U^\dagger V_{UR} V_{UR}^\dagger M_U V_{UL} = V_{UL}^\dagger M_U^\dagger M_U V_{UL}, \\ \bar{M}_D^\dagger \bar{M}_D &= V_{DL}^\dagger M_D^\dagger V_{DR} V_{DR}^\dagger M_D V_{DL} = V_{DL}^\dagger M_D^\dagger M_D V_{DL}. \end{aligned} \tag{1.135}$$

Hence, we can determine V_{UL} and V_{DL} by calculating the eigenvectors of $M_U^\dagger M_U$ and $M_D^\dagger M_D$.

Now let's look at the charged current interactions in the quark sector of the Standard Model. These appear in the Standard Model Lagrangian as

$$\begin{aligned} \mathcal{L}_{cc} &= -\frac{g}{\sqrt{2}} \bar{U}_L \gamma_\mu D_L W_+^\mu + h.c, \\ &= -\frac{g}{\sqrt{2}} \bar{U'}_L \gamma_\mu V_{UL}^\dagger V_{DL} D'_L W_+^\mu + h.c, \\ &= -\frac{g}{\sqrt{2}} \bar{U'}_L \gamma_\mu V_{CKM} D'_L W_+^\mu + h.c. \end{aligned} \tag{1.136}$$

The matrix derived just above is the famous Cabibbo-Kobayashi-Maskawa matrix

$$V_{CKM} = V_{UL}^{\dagger} V_{DL}. \tag{1.137}$$

Given that V_{UL} and V_{DL} are not the same in general, it is obvious that the CKM matrix will have non-zero off-diagonal elements coupling the different generations of SM quarks through the charge current interactions. In the case of two generations, which was the case Cabibbo first considered before there was experimental evidence for a third generation, all the complex phases of V_{CKM} can be absorbed by redefinitions of the fields. In the realistic three generation case, first treated by Kobayashi and Maskawa, there is always one complex phase left over and this complex phase is a source of charge-parity (CP) violation in the Standard Model.

The standard way to parametrize the CKM matrix is through three Euler angles θ_{12}^{CKM}, θ_{13}^{CKM} and θ_{23}^{CKM} as well as the CP violating phase δ, which we represent as

$$\begin{aligned} V_{CKM} &= \begin{pmatrix} 1 & 0 & 0 \\ 0 & c_{23} & s_{23} \\ 0 & -s_{23} & c_{23} \end{pmatrix} \begin{pmatrix} c_{13} & 0 & s_{13}e^{-i\delta} \\ 0 & 1 & 0 \\ -s_{13}e^{i\delta} & 0 & c_{13} \end{pmatrix} \begin{pmatrix} c_{12} & s_{12} & 0 \\ -s_{12} & c_{12} & 0 \\ 0 & 0 & 1 \end{pmatrix}. \\ &= \begin{pmatrix} c_{12}c_{13} & s_{12}c_{13} & s_{13}e^{-i\delta} \\ -s_{12}c_{23} - c_{12}s_{23}s_{13}e^{i\delta} & c_{12}c_{23} - s_{12}s_{23}s_{13}e^{i\delta} & s_{23}c_{13} \\ s_{12}s_{23} - c_{12}c_{23}s_{13}e^{i\delta} & -c_{12}s_{23} - s_{12}c_{23}s_{13}e^{i\delta} & c_{23}c_{13} \end{pmatrix}, \end{aligned} \tag{1.138}$$

where here $c_{ij} = \cos(\theta_{ij}^{CKM})$ and $s_{ij} = \sin(\theta_{ij}^{CKM})$.

The quark mixing angles parametrizing the CKM matrix as well as the CP-violating phase turn out to be small. Given it is also known that $s_{13} < s_{23} < s_{12}$, the alternative and popular way to parametrize the CKM matrix is through the Wolfenstein form. Here, we expand the CKM matrix in terms of the Wolfenstein parameters λ, A, ρ and η, and to third order in λ the CKM matrix is approximately

$$V_{CKM} = \begin{pmatrix} 1 - \frac{\lambda^2}{2} & \lambda & A\lambda^3(\rho - i\eta) \\ -\lambda & 1 - \frac{\lambda^2}{2} & A\lambda^2 \\ A\lambda^3(1 - \rho - i\eta) & -A\lambda^2 & 1 \end{pmatrix} + O(\lambda^4). \tag{1.139}$$

According to the the PDG [63], the best fit for the Wolfenstein parameters are $\lambda = 0.2253 \pm 0.0007$, $A = 0.808^{+0.022}_{-0.015}$, $\rho = 0.132^{+0.022}_{-0.014}$ and $\eta = 0.341 \pm 0.013$, giving the most up to date data on the *magnitudes* of the CKM matrix

elements as

$$|V_{CKM}| = \begin{pmatrix} |V_{ud}| & |V_{us}| & |V_{ub}| \\ |V_{cd}| & |V_{cs}| & |V_{cb}| \\ |V_{td}| & |V_{ts}| & |V_{tb}| \end{pmatrix}, \\ = \begin{pmatrix} 0.97427 \pm 0.00015 & 0.22534 \pm 0.0006 & 0.00351^{+0.00015}_{-0.00014} \\ 0.22520 \pm 0.00065 & 0.97344 \pm 0.0001 & 0.0412^{+0.0011}_{-0.0005} \\ 0.00867^{+0.00029}_{-0.00031} & 0.0404^{+0.0011}_{-0.0005} & 0.999146^{+0.000021}_{-0.000046} \end{pmatrix}. \tag{1.140}$$

The corresponding Euler angles (in degrees) are $\theta_{12}^{CKM} = \arctan(V_{us}/V_{ud}) = 13.02^{+0.04}_{-0.03}$, $\theta_{12}^{CKM} = \arctan(V_{cb}/V_{tb}) = 2.36^{+0.06}_{-0.03}$, $\theta_{13}^{CKM} = \arcsin|V_{ub}| = 0.201^{+0.009}_{-0.008}$ and the CP violating phase (in radians) is $\delta = \arctan(\eta/\rho) = 1.20^{+0.05}_{-0.07}$.

Given that the lepton doublet couples to the $SU(2)$ weak isospin subgroup of the Standard Model in the same way as the quark doublet and given that we now know that neutrinos have mass, there is a matrix analogous to V_{CKM} describing the mixing of the various leptonic generations under charged currents, which can be written

$$\begin{aligned} \mathcal{L}_{cc} &= -\frac{g}{\sqrt{2}} \bar{E}_L \gamma_\mu N_L W_+^\mu + h.c, \\ &= -\frac{g}{\sqrt{2}} \bar{E'}_L \gamma_\mu V_{EL}^\dagger V_{NL} N'_L W_+^\mu + h.c, \\ &= -\frac{g}{\sqrt{2}} \bar{E'}_L \gamma_\mu V_{PMNS} N'_L W_+^\mu + h.c, \end{aligned} \tag{1.141}$$

where here E_L and N_L are tuples containing the weak interaction eigenstates for all the flavors of electrons and neutrinos respectively and E'_L and N'_L contain the mass eigenstates. From the above, we have derived the definition of the Pontecorvo-Maki-Nakagawa-Sakata (PMNS) matrix

$$V_{PMNS} = V_{EL}^\dagger V_{NL}. \tag{1.142}$$

where V_{EL} is the left diagonalization matrix for the electron-type leptons and V_{NL} is the left diagonalization matrix for the neutrinos.

The PMNS matrix is unitary and like the CKM matrix may be parametrized with Euler angles θ_{12}^{PMNS}, θ_{13}^{PMNS} and θ_{23}^{PMNS} and a Dirac CP phase δ', along with two additional Majorana CP phases α and β which can be non-zero only if the neutrinos are Majorana. Unlike the quark mixing angles, two of the angles associated with the PMNS matrix are large so Wolfenstein parametrization is inappropriate in this case. The most general PMNS matrix can be written

$$V_{PMNS} = \begin{pmatrix} 1 & 0 & 0 \\ 0 & c'_{23} & s'_{23} \\ 0 & -s'_{23} & c'_{23} \end{pmatrix} \begin{pmatrix} c'_{13} & 0 & s'_{13}e^{-i\delta'} \\ 0 & 1 & 0 \\ -s'_{13}e^{i\delta'} & 0 & c'_{13} \end{pmatrix} \begin{pmatrix} c'_{12}e^{i\alpha} & s'_{12}e^{i\beta} & 0 \\ -s'_{12}e^{i\alpha} & c'_{12}e^{i\beta} & 0 \\ 0 & 0 & 1 \end{pmatrix},$$

$$= \begin{pmatrix} c'_{12}c'_{13}e^{i\alpha} & s'_{12}c'_{13}e^{i\beta} & s'_{13}e^{-i\delta'} \\ -s'_{12}c'_{23}e^{i\alpha} - c'_{12}s'_{23}s'_{13}e^{i(\delta'+\alpha)} & c'_{12}c'_{23}e^{i\beta} - s'_{12}s'_{23}s'_{13}e^{i(\delta'+\beta)} & s'_{23}c'_{13} \\ s'_{12}s'_{23}e^{i\alpha} - c'_{12}c'_{23}s'_{13}e^{i(\delta'+\alpha)} & -c'_{12}s'_{23}e^{i\beta} - s'_{12}c'_{23}s'_{13}e^{i(\delta'+\beta)} & c'_{23}c'_{13} \end{pmatrix}, \tag{1.143}$$

where here $c'_{ij} = \cos(\theta_{ij}^{PMNS})$ and $s'_{ij} = \sin(\theta_{ij}^{PMNS})$.

The best fits for the Euler angles and Dirac CP phase for the PMNS matrix according to current data depend on whether the neutrino mass hierarchy is normal or inverted. According to [64], for a normal hierarchy the angles (in degrees) are $\theta_{12}^{PMNS} = 33.6^{+0.90}_{-1.0}$, $\theta_{13}^{PMNS} = 8.93^{+0.46}_{-0.48}$, $\theta_{23}^{PMNS} = 38.4^{+1.4}_{-1.3}$ and the Dirac CP phase (in radians) is $\delta'/\pi = 1.08^{+0.28}_{-0.31}$. For an inverted hierarchy, from the same reference, the mixing angles are $\theta_{12}^{PMNS} = 33.6^{+0.90}_{-1.0}$, $\theta_{13}^{PMNS} = 8.99^{+0.41}_{-0.48}$, $\theta_{23}^{PMNS} = 38.8^{+2.2}_{-1.3}$ and the Dirac CP phase is $\delta'/\pi = 1.09^{+0.38}_{-0.26}$. There is no data with regards to the Majorana CP phases since we are yet to determine if the neutrino is Dirac or Majorana and the form of the neutrino mass hierarchy.

The problems of quark and lepton mixing are to do with the fact that the Standard Model has nothing to say about the ultimate origin of these types of mixing and why the angles and phases parametrizing these mixing take on the values that they do. All the electroweak Yukawa coupling constants of the Standard Model have to be put in by hand, and if we did not know any of the experimental data on the CKM and PMNS mixing angles, we could potentially choose the constants such that mixing was absent. Furthermore, we would like to understand why the quark and lepton mixing patterns are so different, with the quark sector experiencing small mixing angles and the lepton sector large mixing angles.

Before the outcomes of the experiments at Daya Bay [65], RENO [66], Double Chooze [67] and T2K [68] it was not known whether θ_{13} for the lepton mixing matrix was non-zero. Prior to this, the experimental data were consistent with $\theta_{12} \simeq 34^\circ$, $\theta_{23} \simeq 45^\circ$ and $\theta_{13} \simeq 0^\circ$, leading to the proposal that the PMNS matrix was approximately equal to the tribimaximal matrix

V_{TB}

$$V_{TB} = \begin{pmatrix} \frac{2}{\sqrt{6}} & \frac{1}{\sqrt{3}} & 0 \\ -\frac{1}{\sqrt{6}} & \frac{1}{\sqrt{3}} & \frac{1}{\sqrt{2}} \\ -\frac{1}{\sqrt{6}} & \frac{1}{\sqrt{3}} & -\frac{1}{\sqrt{2}} \end{pmatrix}. \tag{1.144}$$

This led to much speculation as to whether there existed some discrete flavor symmetry like A_4 or T' that could be imposed on the Standard Model field content, such that the above pattern was generated naturally. There are some flavor symmetry models which also account for small quark mixing and with minor adjustments we can generate the relevant deviations from tribimaximal mixing in the lepton sector with the small θ_{13}. We discuss discrete flavor symmetry models in the next section.

1.10 Discrete Flavour Symmetries

As alluded to at the end of the last section, the approximately tribimaximal structure of lepton mixing strongly motivated models with discrete flavor symmetries. The first such model was based on the group A_4 and was proposed by Ma and Rajasekaran [69]. Other models based on A_4 can be found in References [70, 71, 72, 73]. Later models were also proposed based on more complicated discrete groups like T' (which is the double cover of A_4) [74, 75, 76], $\Delta(27)$ [77, 78], S_4 [79, 80, 81] and $PSL_2(7)$ [82, 83]. A nice review on discrete flavor symmetries can be found in Ref. [84]. For the purposes of this section, we are going to give a brief overview the model proposed by He, Keum and Volkas in Ref. [73] based on A_4. For the basic group theoretic properties of A_4, please read Appendix A.

In this A_4 model, the full symmetry group is $SU(3)_c \times SU(2)_I \times U(1)_Y \times A_4 \times U(1)_X$, where $U(1)_X$ is an auxiliary and non-gauged symmetry, which is usually taken to be a global $U(1)$ symmetry, which forbids unwanted operators, as we will discuss later. In this model, an A_4 triplet Higgs field Φ which couples to the charged fermions induces the breaking $A_4 \to C_3$, ensuring that the CKM matrix is equal to the identity at tree-level, while another A_4 Higgs triplet χ couples to neutrinos and performs the breaking $A_4 \to \mathbb{Z}_2$, leading to a tribimaximal form for the PMNS matrix. Small angles for the CKM matrix are then generated radiatively through cross-talk of the two sectors, although the coupling of Φ and χ leads to a vacuum alignment problem which we will discuss in due course. The SM fermions are assigned

to the following $SU(3)_c \times SU(2)_I \times U(1)_Y \times A_4$ representations,

$$\begin{aligned} &u_R \oplus u'_R \oplus u''_R \sim (3,1,\frac{4}{3})(1 \oplus 1' \oplus 1''), && Q \sim (3,2,\frac{1}{3})(3), \\ &d_R \oplus d'_R \oplus d''_R \sim (3,1,-\frac{2}{3})(1 \oplus 1' \oplus 1''), && L \sim (1,2,-1)(3), \\ &e_R \oplus e'_R \oplus e''_R \sim (1,1,-2)(1 \oplus 1' \oplus 1''), && \nu_R \sim (1,1,0)(3), \end{aligned} \tag{1.145}$$

and the scalar content of the theory is taken to be

$$\Phi \sim (1,2,-1)(3), \qquad \phi \sim (1,2,-1)(1), \qquad \chi \sim (1,1,0)(3). \tag{1.146}$$

The $G \otimes X$ invariant Yukawa Lagrangian is then

$$\begin{aligned} \mathcal{L}_{Yuk} =& \lambda_u(\overline{Q}\Phi)_1 u_R + \lambda'_u(\overline{Q}\Phi)_{1'} u''_R + \lambda''_u(\overline{Q}\Phi)_{1''} u'_R \\ &+ \lambda_d(\overline{Q}\tilde{\Phi})_1 d_R + \lambda'_d(\overline{Q}\tilde{\Phi})_{1'} d''_R + \lambda''_d(\overline{Q}\tilde{\Phi})_{1''} d'_R \\ &+ \lambda_e(\overline{L}\tilde{\Phi})_1 e_R + \lambda'_e(\overline{L}\tilde{\Phi})_{1'} e''_R + \lambda''_e(\overline{L}\tilde{\Phi})_{1''} e'_R \\ &+ \lambda_\nu(\overline{L}\nu_R)_1 \phi + M\left[\overline{\nu_R}(\nu_R)^c\right]_1 + \lambda_\chi\left[\overline{\nu_R}(\nu_R)^c\right]_{3_s}.\chi + h.c, \end{aligned} \tag{1.147}$$

where $\tilde{\Phi} = i\sigma_2\Phi^*$.

The aforementioned $U(1)_X$ symmetry is present in the Yukawa Lagrangian above and under this symmetry, L, e_R, e'_R, e''_R and ϕ have a charge $X = +1$ while all other fields have $X = 0$. This forbids $\overline{L}\nu_R\Phi$, which is a term we do not want so that we can get the desired structure for the neutrino mass matrix. This Abelian symmetry is anomalous and cannot be gauged, meaning that this symmetry must be broken explicitly to a discrete group that still prevents the unwanted term in order to get rid of the phenomenologically disallowed Nambu-Goldstone boson.

Let us first analyze the charged fermion sector. Let f index all three types of charged fermion, that is $f = u, d, e$. The resultant mass matrix for the fermion f is

$$(\overline{f_{1L}}, \overline{f_{2L}}, \overline{f_{3L}}) \begin{pmatrix} \lambda_f v_1 & \lambda'_f v_1 & \lambda''_f v_1 \\ \lambda_f v_2 & \omega\lambda'_f v_2 & \omega^2\lambda''_f v_2 \\ \lambda_f v_3 & \omega^2\lambda'_f v_3 & \omega\lambda''_f v_3 \end{pmatrix} \begin{pmatrix} f_R \\ f''_R \\ f'_R \end{pmatrix} + h.c, \tag{1.148}$$

where here $\omega = e^{2\pi i/3}$ as noted in Appendix A and $\langle\Phi\rangle = (v_1, v_2, v_3)$ is the VEV for Φ. Here, 1, 2 and 3 denote the components of the A_4 triplet fermions. For a certain parameter choice, one can show that the VEV pattern

$$v_1 = v_2 = v_3 = v, \tag{1.149}$$

which induces the breaking $A_4 \to C_3$ is a global minimum of the self-interaction potential for Φ (for the moment assume the cross-talk between the different Higgs fields are switched off). In this special case, the mass matrices for the charged fermions M_f can be shown to be of the form

$$M_f = U(\omega).\begin{pmatrix} \sqrt{3}\lambda_f v & 0 & 0 \\ 0 & \sqrt{3}\lambda'_f v & 0 \\ 0 & 0 & \sqrt{3}\lambda''_f v \end{pmatrix}, \tag{1.150}$$

which in turn implies that the left-diagonalization matrices V_{EL}, V_{UL} and V_{DL} are all equal to the unitary matrix

$$U(\omega) = \frac{1}{\sqrt{3}}\begin{pmatrix} 1 & 1 & 1 \\ 1 & \omega & \omega^2 \\ 1 & \omega^2 & \omega \end{pmatrix}. \tag{1.151}$$

Immediately, one sees that the CKM matrix is precisely the identity matrix at tree level

$$V_{CKM} = V_{UL}^\dagger V_{DL} = U(\omega)^\dagger U(\omega) = 1. \tag{1.152}$$

For the model to work, we assume that Φ does indeed take the VEV pattern of Eq. 1.149.

The neutrino sector is totally different since it couples to ϕ and χ and we will assume χ to attain a rather different VEV pattern to that of Φ. The Dirac mass matrix is generated by the term $(\overline{L}.\nu_R)_1\phi$ and after ϕ attains a VEV $\langle\phi\rangle = v_\phi$, the Dirac mass matrix generated is simply proportional to the identity matrix

$$M_\nu^D = \lambda_\nu v_\phi 1 = m_\nu^D 1. \tag{1.153}$$

There are two contributions to the Majorana mass matrix for the neutrinos: the bare Majorana mass term $M[\overline{\nu_R}(\nu_R)^c]_1$ and the contribution coming from the Yukawa interaction with χ, $\lambda_\chi[\overline{\nu_R}(\nu_R)^c]_{3_s}.\chi$. In contrast to the VEV pattern for Φ, we give χ the pattern

$$\langle\chi_1\rangle = \langle\chi_3\rangle = 0, \qquad \langle\chi_2\rangle = v_\chi \neq 0. \tag{1.154}$$

After breaking with the above VEV pattern, the Yukawa interaction $\lambda_\chi[\overline{\nu_R}(\nu_R)^c]_{3_s}.\chi$ generates non-zero $1-3$ and $3-1$ components in the Majorana mass matrix equal to $M_\chi = \lambda_\chi v_\chi$. Thus the full 6×6 neutrino mass matrix in the $(\nu_{1L}, \nu_{2L}, \nu_{3L}, (\nu_{1R})^c, (\nu_{2R})^c, (\nu_{3R})^c)$ basis is

$$\begin{pmatrix} 0 & 0 & 0 & m_\nu^D & 0 & 0 \\ 0 & 0 & 0 & 0 & m_\nu^D & 0 \\ 0 & 0 & 0 & 0 & 0 & m_\nu^D \\ m_\nu^D & 0 & 0 & M & 0 & M_\chi \\ 0 & m_\nu^D & 0 & 0 & M & 0 \\ 0 & 0 & m_\nu^D & M_\chi & 0 & M \end{pmatrix}. \tag{1.155}$$

Thus the effective left Majorana mass matrix is

$$M_L = -M_\nu^D M_R^{-1} (M_\nu^D)^T = -\frac{(m_\nu^D)}{M} \begin{pmatrix} \frac{M^2}{M^2-M_\chi^2} & 0 & -\frac{MM_\chi}{M^2-M_\chi^2} \\ 0 & 1 & 0 \\ -\frac{MM_\chi}{M^2-M_\chi^2} & 0 & \frac{M^2}{M^2-M_\chi^2} \end{pmatrix}. \quad (1.156)$$

The left diagonalization matrix is simply the orthogonal matrix

$$V_{NL} = \frac{1}{\sqrt{2}} \begin{pmatrix} 1 & 0 & -1 \\ 0 & \sqrt{2} & 0 \\ 1 & 0 & 1 \end{pmatrix}, \quad (1.157)$$

and thus the resultant PMNS matrix is

$$V_{PMNS} = V_{EL}^\dagger V_{NL} = U(\omega)^\dagger V_{NL} = \begin{pmatrix} \frac{2}{\sqrt{6}} & \frac{1}{\sqrt{3}} & 0 \\ -\frac{\omega}{\sqrt{6}} & \frac{\omega}{\sqrt{6}} & -\frac{e^{i\pi/6}}{\sqrt{2}} \\ -\frac{\omega^2}{\sqrt{6}} & \frac{\omega^2}{\sqrt{6}} & \frac{e^{-i\pi/6}}{\sqrt{2}} \end{pmatrix}. \quad (1.158)$$

Thus we have successfully reproduced a tribimaximal form for the PMNS matrix at tree level.

With the combinations of VEV patterns for Φ, A_4 is completely broken since Φ breaks the S generator and χ breaks the T generator. Hence, once we turn on interactions between Φ and χ, effects that break the C_3 group left unbroken by Φ will be communicated to the charged fermion sector, while effects that break the $\mathbb{Z}_2$ group left unbroken by χ will be communicated to the neutrino sector. This means that in the quark sector, there will be corrections to the tree-level result of Eq. 1.152 and thus small mixing angles will be generated as required. Further, in the neutrino sector, there will be corrections to the tree-level PMNS matrix in Eq. 1.158 and thus deviations from tribimaximal mixing. In particular, there will be a non-zero θ_{13} generated for the PMNS matrix.

Unfortunately, the cross-talk between two different symmetry breaking sectors also has the unwanted consequence of introducing a vacuum alignment problem. With interactions between the two triplets turned off, one can easily choose parameters such that the VEVs that we have chosen for Φ and χ are indeed global minima of their respective self-interaction potentials. However, when we turn on interactions this is no longer guaranteed [73, 71]. When we included terms such as $(\Phi^\dagger\Phi)_{1'}(\chi\chi)_{1''}$, after χ condenses, Φ attains a soft C_3-breaking mass term of the form $m^2(\Phi^\dagger\Phi)_{1''}$ which, if significant, potentially renders the C_3-preserving VEV unstable. Likewise there are other interactions involving non-trivial A_4 products of Φ and χ which will generate soft $\mathbb{Z}_2$-breaking terms for χ. Furthermore, minimization

of the potential yields a larger number of independent equations than known vacuum expectation values for the triplets. This means that to get the desired vacuum alignment we have described above, we must fine-tune the theory. This usually means setting the coupling constants of the most of the troubling cross-talking interactions to zero.

There are several ways to resolve the vacuum alignment problem. The first approach is the one made at the end of Ref. [73]: to make the theory supersymmetric so that the undesired terms are forbidden by holomorphy and renormalization constraints on the superpotential. Another is to use additional discrete symmetries forbidding the interactions [85]. Yet another is to exploit the physics of extra dimensions, by localizing the flavons on different branes or by splitting their extra-dimensional profiles with very little overlap so that the interactions are naturally eliminated or very suppressed [86, 87, 88]. It is this last possibility that we will discuss and implement later in this thesis, in a domain-wall brane model based on $SU(5) \times A_4$.

1.11 Models of Flavor in Extra Dimensions

As we observed in the previous sections on extra-dimensional models including domain-wall braneworld models, coupling constants such as those involved in the Yukawa sector of the Standard Model are dependent on overlap integrals of the profiles of the particles involved in the interaction. For Yukawa interactions, the relevant overlap integral is one for which the integrand is the product of the profile for the Higgs and of the profiles for the left and right-chiral fermions involved. It is often the case that these profiles depend exponentially on the relevant parameters of the underlying extra-dimensional theory, such as the 5D bulk masses of the fermions as we have seen from the split fermion mechanism [19]. Thus, with models based on large extra dimensions and warped RS models proposed it was natural to wonder whether the fermion mass spectra could be accommodated naturally in these models.

The RS1 model provides a natural framework for approaching the fermion mass hierarchy problem. In the original RS1 model, the SM fermions were simply placed fundamentally on the IR brane. This means that one would have to essentially perform the same fine-tunings in the theory localized to the IR brane. However, Grossman and Neubert [17] as well as Gherghetta and Pomarol [16] suggested the possibility of allowing the fermions to propagate in the bulk. It can be shown that the bulk Dirac masses for the 5D fields containing the SM fermions can be parametrized by a dimensionless number, which is usually denoted by c, multiplied by the AdS curvature scale k. It

turns out that for $c < 1/2$, the fermion zero mode is localized near the IR brane, for $c > 1/2$ it is localized near the UV brane and for $c = 1/2$ the mode is delocalized and evenly distributed throughout the bulk. It was shown in [18] that the fermion mass hierarchy and quark mixing could be generated by choosing a set of these dimensionless numbers which are all of order one and thus allowing the fermions to propagate differently in the bulk and be localized to different branes.

As we have mentioned in the above section, the split fermion mechanism can be utilized to generate hierarchical fermion masses. A simple application of this mechanism was shown to be sufficient to account for the fermion mass hierarchy in Ref. [89], for CP violation in 6D in Ref. [90] and for neutrino masses in Ref. [91].

It is also quite natural to consider combining the physics of extra dimensions with those of discrete flavor symmetries to not only resolve the problems of quark and lepton mixing as well as the fermion masses but also to resolve problems associated with each approach. Altarelli and Feruglio first proposed an RS1 model with a discrete A_4 flavor symmetry and an SM gauge group, and they resolved the vacuum alignment problem by putting the A_4 triplet flavons on different branes [86]. It was further shown by Kaddosh and Pallante that this problem could still be solved even when one allows the fermions and scalars to propagate through the bulk: in fact, they suppress the unwanted operators while still allowing enough cross-talk between the two sectors coupling to the different A_4-triplets to generate small quark mixing angles and a CP phase [88]. Some other models combining extra dimensions and discrete flavor symmetries are given in Refs. [87, 92, 93, 94].

In Chapters 2 and 3, we will exploit the split fermion and split scalar mechanisms to show that the $SU(5)$ domain-wall brane model given in Ref. [23] and its extension to include an A_4 flavor symmetry are viable models with respect to fitting the fermion mass spectra, including quark and lepton mixing. We will now give some of the background needed for understanding intersecting domain-wall brane models in the next section, which constitutes the second half of the thesis.

1.12 Models with Multiple Domain Walls

If we are to consider extending the domain-wall brane framework to more than one additional dimension, we need to consider either higher dimensional solitons (like strings) or we need to consider introducing more than one domain wall. For the former, we refer the reader to Refs. [95, 96] which discuss the localization of gravity on strings in 5+1D spacetime. In this section, we

consider the latter option.

In first motivating models with multiple domain-wall branes, it is encouraging to note that realistic models with multiple fundamental branes have been constructed. In particular, Arkani-Hamed, Dimopoulos, Dvali and Kaloper showed in Ref. [33] that the RS2 model could be extended to $4+n$ dimensional spacetime by localizing gravity to the intersection of n fundamental $4+n-1$-D branes. Some higher dimensional generalizations of the RS1 scenario were also considered in Refs. [97, 98]. In Ref. [99], fermion localization was discussed. Thus, the fact that there are some realistic models with fundamental branes in 5+1D and higher encourages us to consider the same for domain-wall brane models.

If one wants to introduce a second domain wall, there are two possibilities. The first is that of nested domain walls, which was first considered by Morris [100] and also treated in Ref. [101]. Morris considered a $\mathbb{Z}_2 \times \mathbb{Z}_2$ model with two scalar fields, η and χ, with the potential

$$V(\eta,\chi) = \frac{1}{4}\lambda_\eta(\eta^2-v^2)^2 + \frac{1}{2}\lambda_{\eta\chi}(\eta^2-v^2)\chi^2 + \frac{1}{2}\mu_\chi^2\chi^2 + \frac{1}{4}\lambda_\chi\chi^4. \quad (1.159)$$

One can show that for a certain parameter choice, a solution to the resultant Euler-Lagrange equations is of the form

$$\eta(y) = v\tanh(ky), \chi(y) = A\,\mathrm{sech}\,(ky), \quad (1.160)$$

which is just a kink-lump solution like those discussed previously. In Ref. [100], Morris showed that, given the second $\mathbb{Z}_2$ symmetry implies that there are two discrete vacua $\chi = \pm A$ at $y = 0$, there existed solutions in which χ interpolated between these vacua along $y = 0$. Furthermore, for the same parameter choice yielding the kink-lump solution in Eq. 1.160, these solutions satisfy the boundary conditions

$$\begin{aligned} \eta(y, z=\pm\infty) &= v\tanh(ky), \\ \chi(y, z=\pm\infty) &= \pm A\,\mathrm{sech}\,(ky), \\ \eta(y=\pm\infty, z) &= \pm v, \\ \chi(y=\pm\infty, z) &= 0, \end{aligned} \quad (1.161)$$

so along the lines $y = y_0$ where y_0 is a constant, χ interpolates between $\chi = -A\,\mathrm{sech}\,(ky_0)$ at $z = -\infty$ and $\chi = +A\,\mathrm{sech}\,(ky_0)$ at $z = +\infty$. Thus, along a line $y = y_0$, χ forms a domain wall. The height of the vacua of this domain wall is maximized in the center of the domain wall generated by η (ie. $y = 0$) and decreases to zero as $y \to \pm\infty$, where the η approaches its mimima. Hence, χ generates a nested domain wall which is localized to

the defect formed by η, and the entire system of defects formed by η and χ is known as a domain ribbon. One can then consider localizing fields as well as gravity on a domain ribbon. A generic treatment on the problem of localizing gravity on a domain ribbon was given in Ref. [102].

An alternative approach, and the one we will deal with in the later chapters of this thesis, is that of intersecting domain walls. Let's now take what is essentially the same potential as before but now let's choose the region which corresponds to χ being tachyonic and rewrite the potential as

$$V(\eta,\chi)=\frac{1}{4}\lambda_\eta(\eta^2-v_1^2)^2+\frac{1}{2}\lambda_{\eta\chi}(\eta^2-v_1^2)(\chi^2-v_2^2)+\frac{1}{4}\lambda_\chi(\chi^2-v_2^2)^2, \quad (1.162)$$

with all of the quartic couplings chosen to be positive. Now there will be four vacua of the theory, $\eta=\pm v_1$, $\chi=\pm v_2$. One can imagine forming a defect for which the solution interpolates between these four vacua along the corners of a quadrangle at the boundary at infinity. For example, we could take this quadrangle to be the square shown in Fig. 1.11 and demand that the boundary conditions of the solution along the square at infinity are

$$\begin{aligned}\eta(y,z=\pm\infty)&=v_1\tanh(ky),\\ \chi(y,z=\pm\infty)&=\pm v_2,\\ \eta(y=\pm\infty,z)&=\pm v_1,\\ \chi(y=\pm\infty,z)&=v_2\tanh(lz).\end{aligned} \quad (1.163)$$

When one solves for η and χ, one naturally will obtain a solution for η which interpolates between $\pm v_1$ along the y-axis and a solution for χ which interpolates between $\pm v_2$ along the z-axis. Thus, such a solution consists of two domain walls which intersect. One can now consider localizing fields to the intersection of the two domain walls.

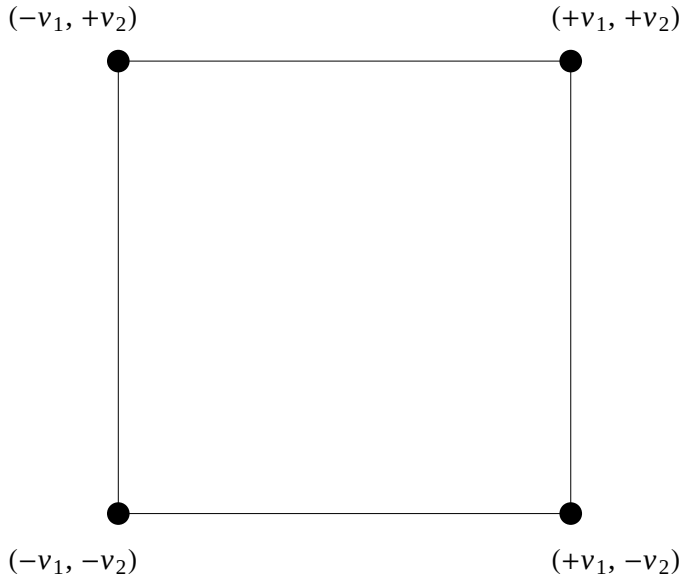

Figure 1.11: A graph of the boundary conditions satisfied by the fields generating the intersecting domain walls along a rectangle at infinity in the x-y plane. The solution for the fields converges to the four vacua of the theory at each corner.

This situation described above can be generalized to a system with n vacua being mapped to the n corners of an n-gon at infinity. In this case there are n walls interpolating between these distinct vacua along the edges of the polygon at infinity and the solution can be thought of as n half-walls extending from the core of the defect to each of the vacua at infinity. Such a string-like defect is known as a domain-wall junction. An analytic solution for a domain-wall junction was first given in [103]. A rare exact solution for two intersecting walls similar to the situation described above was found in the context of an $N = 2$ supersymmetric non-linear sigma model [104]. An intersecting wall solution found numerically was also given in Ref. [105].

We will deal with a model involving intersecting domain walls later in this thesis.

1.13 Outline of the Thesis

Starting from the original ideas of Kaluza and Klein, we have discussed the origins as well as the formulations of the main ideas and elements involved in the construction of domain-wall brane models. This discussion described the

construction of a domain wall as well as the localization of scalars, fermions, gauge bosons and gravity, and culminated with the formulation of the $SU(5)$ domain-wall brane model of Davies, George and Volkas [23]. This domain-wall brane framework has shown a lot of promise given that the desired particle content is present in the 3+1D effective field theory on the wall, but to construct a realistic model we must be able to reproduce the parameters of the Standard Model as determined by experiment. Hence, the first half of the thesis explores how to generate the fermion mass hierarchy as well as the CKM and PMNS mixing angles in the context of domain-wall brane models. Secondly, we would like to know if the 4+1D domain-wall framework can be extended and generalized. The latter half of the thesis seeks to extend the framework by adding another dimension and reducing a 5+1D theory to a 3+1D one by localizing fields to the intersection of two domain-wall branes.

In Chapter 2, which is based on the work in Ref. [1], we investigate whether the can naturally account for the fermion mass hierarchy as well as quark and lepton mixing. Exploiting the split fermion mechanism which was discussed previously and which arises naturally in the $SU(5)$ domain-wall brane model, we show that the fermion mass hierarchy can be resolved and that a realistic Cabibbo angle can be reproduced, suggesting that the CKM angles can also be accounted for. However, we find that the same parameter region which yields realistic fermion masses and quark mixing cannot yield realistic lepton mixing and we give reasons why this is the case.

The failure to obtain lepton mixing in the ordinary $SU(5)$ model in the desired parameter region motivates us to extend the model to include a discrete flavor symmetry. In Chapter 3, which is based on Ref. [2], we extend the basic $SU(5)$ model to one based on $SU(5) \times A_4$. In doing so, we assign the fermions and Higgs scalars to appropriate representations of $SU(5) \times A_4$ and we show that, with two of the Higgs scalars in the triplet representation of A_4 inducing the breaking patterns $A_4 \to C_3$ and $A_4 \to \mathbb{Z}_2$, one can generate a realistic PMNS matrix from the properties of A_4 whilst still utilizing the split fermion mechanism to yield the fermion mass hierarchy and the CKM mixing angles. Furthermore, we can also exploit the splitting of the A_4-triplet scalars to resolve the vacuum alignment problem which plagues many models based on discrete flavor symmetries in 3+1D.

Chapter 4 is the start of the second half of the thesis and it is based on Ref. [3]. In this chapter, we deal with a basic scalar field theory with four real scalar fields transforming under $\mathbb{Z}_2 \times \mathbb{Z}_2$ symmetry in 5+1D flat Minkowskian spacetime which can generate two intersecting domain walls along with fields which condense in the form of a lump parallel to each wall. We find that there exists an analytic solution for a special region of parameter space in which the walls are perpendicular. We also find that in the same region of

parameter space that there exists a whole set of energy degenerate solutions in which the walls intersect at an angle less than ninety degrees and a solution in which the walls are parallel. Although this seems troubling, we find that there exists a conserved topological charge which implies that none of the solutions in which the walls intersect can evolve to the solution where the walls are parallel, and we also suggest how the perpendicular solution may be made energetically favorable to the solutions for which the intersection angle is less than ninety degrees by perturbing to a nearby region of parameter space. After assuming that the perpendicular solution is stable, we show how chiral fermion zero modes and scalars can be localized to the intersection and we calculate the profiles of the localized modes.

Having constructed an intersecting domain-wall solution and localized fermions and scalars, we are then motivated to consider how to localize gauge bosons. Chapter 5, based on Ref. [5], extends the work in Chapter 4 by considering an application of the Dvali-Shifman mechanism, called the intersecting Clash-of-Symmetries mechanism, which can be naturally implemented in that particular model. In this mechanism, we give gauge charges to the fields which form lumps in the interior of the domain walls, breaking a non-Abelian gauge group G to two different subgroups H_1 and H_2 on each wall. This leads to H_1 and H_2 being localized to the respective walls by the Dvali-Shifman mechanism. On the intersection of the domain walls there is then further breaking to $H_1 \cap H_2$ and we conjecture that subgroups of this remaining group are localized if they belong inside larger non-Abelian, confining subgroups of both H_1 and H_2. We then go on to discuss how we can use this mechanism to localize the Standard Model gauge group starting from an $SU(7)$ gauge theory in 5+1D.

Chapter 6 is our conclusion. We summarize the main findings of the thesis and we briefly discuss the areas of both 4+1D and 5+1D domain-wall brane models which require further work. We conclude that domain-wall brane models in five and six dimensions provide a viable framework for extending the Standard Model and that these models can reproduce many aspects of our universe.

Chapter 2

Fermion masses and mixing in a 4+1-dimensional $SU(5)$ domain-wall brane model

As described in Sec. 1.7 and Sec. 1.9 of the introduction, in the standard model (SM), three of the most open problems are how the fermion mass hierarchy is generated, the origin of small mixing angles in the Cabibbo-Kobayashi-Maskawa (CKM) matrix and near tribimaximal mixing in the lepton sector. With neutrino masses now known to be nonzero but under 1 eV, the mass hierarchy has a spread of at least 12 orders of magnitude, given that the top quark has a mass of roughly 170 GeV. Amongst approaches used for solving these problems are grand unified theories (GUTs), higher dimensional operators, and flavor symmetries.

As we have also seen in the introduction, extra-dimensional models, such as the Arkani-Hamed-Dimopoulos-Dvali (ADD) model [13], and the two Randall-Sundrum (RS) models [15, 14], have become popular due to their ability to resolve various hierarchy problems. The ADD and RS1 frameworks solve the hierarchy problem between the Planck scale and the electroweak scale, which is of a similar order of magnitude to that of the fermion mass spectra.

In RS2 models the hierarchy problem is not solved by extra-dimensional physics, but the split fermion idea of Arkani-Hamed and Schmaltz [19] can be used to generate fermion mass hierarchies from exponentially sensitive overlap integrals of extra-dimensional profile functions. Similarly, the RS1 setup can address this problem by allowing fermions to propagate in the bulk and thus acquire non-trivial profiles [17, 16]. The idea is that the 3+1D fermion zero modes are in general localized around different locations along the extra dimension, with dimensional reduction then producing an effective

3+1D Yukawa coupling constant that is the product of the 4+1D Yukawa coupling constant and an overlap integral involving profile functions. When the profiles are split, the overlap integrals are suppressed, leading to small 3+1D effective Yukawa coupling constants. This fits in well with the fact that quark and lepton masses, except for the top quark, are *suppressed* with respect to the electroweak scale. Scalar bosons will also in general be split, a phenomenon we shall use to suppress colored-Higgs-induced proton decay (see Refs. [106, 42, 43, 107, 108, 109, 110, 111, 112, 113] for more on the use of the splitting of fermions and bosons in extra dimensions to generate fermion mass textures and to suppress proton decay and other baryon number violating processes).

As we observed in Sec. 1.6, the $SU(5)$ 4+1D domain-wall brane model proposed by Davies, George and Volkas (DGV) has many of the essential components required for generating a realistic Standard Model localized to a brane. Scalars and fermions are easily localized and gauge bosons are localized via the Dvali-Shifman mechanism. Gravity can also be localized. Under the activation of the Dvali-Shifman mechanism in this model, $SU(5)$ is broken spontaneously to the SM on the wall. In this RS2-like model, the split fermion idea arises naturally, and thus the usual $SU(5)$ quark-lepton mass relations are avoided. This suggests the possibility to generate hierarchical fermion mass spectra as well as suppress colored Higgs-induced proton decay from this split mechanism. To show this explicitly is important, since if domain-wall brane models are to be of any use to describing our 3+1D universe at low energies, they must be able to naturally generate its phenomenology.

Hence, in this chapter, we will utilize the split fermion mechanism arising in the DGV model described in Sec. 1.6 to account for the fermion mass hierarchy as well as the mixing angle problems. It will be shown that the mass hierarchy problem can be solved using this method, and that the mass hierarchy and the Cabibbo angle can be accounted for in the two-generation case with Majorana neutrinos. We also explain why tribimaximal mixing cannot be accounted for without fine-tuning, and that the addition of a flavor symmetry therefore seems necessary. We are thus led to the view that extra dimensions provide an excellent way to qualitatively understand mass hierarchies, but they are insufficient to explain all the observed mixing angle patterns. The reason the flavor problem has proven to be so difficult may be because more than one ingredient is necessary: extra dimensions on their own, and flavor symmetry on its own, are only partially successful.

Given that we gave a rather thorough account of the DGV model in Sec. 1.6, including the classical domain-wall solution described by Eq. 1.95, we will not repeat most of the details of that model in this chapter. The

background domain-wall solution as well as the scalar particle content is unchanged from Sec. 1.6. We will, in the next section, give some results regarding the minor changes we have made to the model as it was originally proposed in Ref. [23], such as fermion localization when we extend the model to include all three generations, the addition of singlet right-chiral neutrinos and their localization properties, as well as the effects of adding a term which generates a Majorana mass for a right-chiral neutrino. We also outline the parameter choices we use in the Higgs sector in order to perform the analysis of the fermion mass spectra. Section 2.1 then analyses the parameter space of the model to produce the required mass and mixing angle hierarchies, with the aforementioned caveat for tribimaximal lepton mixing. Section 2.2 is the conclusion of the chapter.

2.0.1 Localizing the charged fermions and the left-chiral neutrinos: the case with more than one generation

We have already covered the localization of one generation of the charged SM fermions via coupling to the background fields η and χ in Sec. 1.6. In this section, we review the differences when we generalize to more than one generation of fermions.

In the case that we have $m > 1$ generations of fermions, Y_{DW} is generalized to

$$Y_{DW} = h^{ij}_{5\eta}\overline{\Psi^i_5}\Psi^j_5\eta + h^{ij}_{5\chi}\overline{\Psi^i_5}\chi\Psi^j_5 + h^{ij}_{10\eta}Tr(\overline{\Psi^i_{10}}\Psi^j_{10})\eta - 2h^{ij}_{10\chi}Tr(\overline{\Psi^i_{10}}\chi\Psi^j_{10}), \quad (2.1)$$

where i and j are summed from 1 to m. Hence, in the general case, there can be intergenerational mixing between the quarks and leptons through the interaction with the background. The background couplings $h_{n\eta}$ and $h_{n\chi}$ have now become 3×3 Hermitian matrices over flavor space and need not commute. To solve the equations, we look for zero mode solutions of the form,

$$\Psi^i_{nY}(x, y) = f^{ij}_{nY}(y)\psi^j_{nY}(x), \quad (2.2)$$

where the $\psi^j_{nY}(x)$ are massless left chiral 3+1d fields for $n = 5, 10$. Putting this into the 4+1D Dirac equation results in the matrix differential equation for the profiles f_{nY}, which are now 3×3 matrix valued functions of y,

$$\frac{df_{nY}(y)}{dy} + \eta(y)h_{n\eta}f_{nY}(y) + \sqrt{\frac{3}{5}}\frac{Y}{2}\chi_1(y)h_{n\chi}f_{nY}(y) = 0. \quad (2.3)$$

The case where $h_{n\eta}$ and $h_{n\chi}$ do not commute, which leads to a natural realization of the *twisted* split fermion scenario discussed in Refs. [42, 43], cannot

be solved analytically, and so for the sake of simplicity we will only search the parameter space that obeys,

$$[h_{n\eta}, h_{n\chi}] = 0, \text{ for n} = 5, 10. \tag{2.4}$$

Since both the matrices are required to be Hermitian as well, they are thus simultaneously diagonalizable, so that for some unitary matrices S_n,

$$\begin{aligned} S_n h_{n\eta} S_n^\dagger &= diag(h^1_{n\eta}, h^2_{n\eta}, \cdots, h^m_{n\eta}), \\ S_n h_{n\chi} S_n^\dagger &= diag(h^1_{n\chi}, h^2_{n\chi}, \cdots, h^m_{n\chi}), \end{aligned} \tag{2.5}$$

where the $h^i_{n\eta}$ and $h^i_{n\chi}$ are understood to be the eigenvalues of $h_{n\eta}$ and $h_{n\chi}$ respectively. Choosing to localize left-chiral zero modes for $\Psi^i_{5,10}$ is then equivalent to demanding that all the eigenvalues of $h_{n\eta}$ are positive definite. Solving the 5D Dirac equation then yields the general solution for the profiles,

$$\begin{aligned} f_{nY}(y) &= S_n^\dagger diag(C^1_{nY} e^{-b^1_{nY}(y)}, C^2_{nY} e^{-b^2_{nY}(y)}, \cdots, C^m_{nY} e^{-b^m_{nY}(y)}) V_{nY}, \\ b^i_{nY}(y) &= \tilde{h}^i_{n\eta} \log\left(\cosh\left(ky\right)\right) + Y\sqrt{\frac{3}{5}} \tilde{h}^i_{n\chi} \arctan\left(\tanh\left(\frac{ky}{2}\right)\right) \end{aligned} \tag{2.6}$$

Here we have written the multi-generation solutions in terms of the solutions for the one generation case. The C^i_{nY} are normalization constants, chosen such that the profile matrix $f_{nY}(y)$ satisfies the normalization condition,

$$\int f^\dagger_{nY}(y) f_{nY}(y)\, dy = \mathbb{1}. \tag{2.7}$$

The parameters $\tilde{h}^i_{n\eta}$ and $\tilde{h}^i_{n\chi}$ are the non-dimensionalized versions of $h^i_{n\eta}$ and $h^i_{n\chi}$, and are defined in the same way as the non-dimensionalized constants from the one generation case were in Eq. 1.100. The V_{nY} are unitary matrices which are present since the solution is unique up to matrix multiplication. The V_{nY}, in fact, correspond to a choice of which 3+1D states are the domain wall eigenstates and thus localized to the wall. Unless otherwise stated, we will assume these to be the same as the weak interaction eigenstates, and we will assume that $S_n = V_{nY} = 1$.

2.0.2 Adding singlet right-handed neutrinos

In order to generate neutrino masses, we need singlet, right-chiral neutrinos. We label these as N^i and under the $SU(5)$ and discrete reflection symmetries, they transform as

$$\begin{aligned} N^i &\sim 1, \\ N^i &\to -i\Gamma^5 N^i. \end{aligned} \tag{2.8}$$

To localize the right-chiral neutrinos, we need to couple them to the background. As they are gauge singlets, they cannot couple to the adjoint Higgs χ. Thus we can only add,

$$- h_{1\eta}^{ij} \overline{N^i} N^j \eta, \tag{2.9}$$

to Y_{DW}. The relative minus sign in front of the Yukawa interactions for the N^i is introduced because for these fields we want localized right-chiral zero modes which represent the right-handed neutrinos in the effective 3+1D theory, as opposed to left-chiral zero modes. This allows us to treat $h_{1\eta}$ in the same way as $h_{5\eta}$ and $h_{10\eta}$.

Writing down the 5D Dirac equation for the N^i, and demanding that $N^i(x,y) = f_N^{ij}(y) N^j(x)$, where the $N^j(x)$ are 3+1D right chiral zero modes, in similar fashion to the charged fermions, leads to the profile,

$$\begin{aligned} f_N(y) = S_1^\dagger diag(&C_1^1 e^{-\frac{h_{1\eta}^1 v}{k} \log(\cosh(ky))}, C_1^2 e^{-\frac{h_{1\eta}^2 v}{k} \log(\cosh(ky))}, \\ &\cdots, C_1^m e^{-\frac{h_{1\eta}^m v}{k} \log(\cosh(ky))}) V_N, \end{aligned} \tag{2.10}$$

where S_1 is again a choice of basis matrix for the 5D fields, V_N is a change of basis matrix for the 4D fields, the C_1^i are normalization constants, and the $h_{1\eta}^i$ are the positive definite eigenvalues of the Yukawa matrix $h_{1\eta}$. In the later analysis, we will also assume that $S_1 = V_N = 1$.

2.0.3 Localizing the electroweak symmetry breaking Higgs boson

We have already discussed in detail the localization properties of the electroweak Higgs as well as that of the colored Higgs scalar in Sec. 1.6. We will not repeat the details of that analysis here. In this section, we choose example choices for the non-dimensionalized parameters given in Eq. 1.111.

Note that it is possible for more than one KK excitation of the Higgs doublet to have nonzero vacuum expectation values, thus naturally generating a multi-Higgs doublet model on the brane. However, for simplicity, we will choose parameters such that only the electroweak Higgs has a tachyonic mass, and not its KK modes, and we will also have a bound state for the colored Higgs. For the purposes of this chapter, we will use three such choices.

For the first choice,

$$\begin{aligned} \mu_\Phi^2 &= k^2, \\ \lambda_4 &= \frac{0.5k^2}{v^2}, \\ \lambda_5 &= \frac{k^2}{A^2}, \\ \lambda_6 &= \frac{k^2}{A^2}, \\ \lambda_7 &= \frac{20k^2}{vA}, \end{aligned} \tag{2.11}$$

the mass eigenvalues are $m_w^2 = -0.510k^2$, and $m_c^2 = 0.380k^2$. The graphs of the profiles are shown in Fig. 2.1.

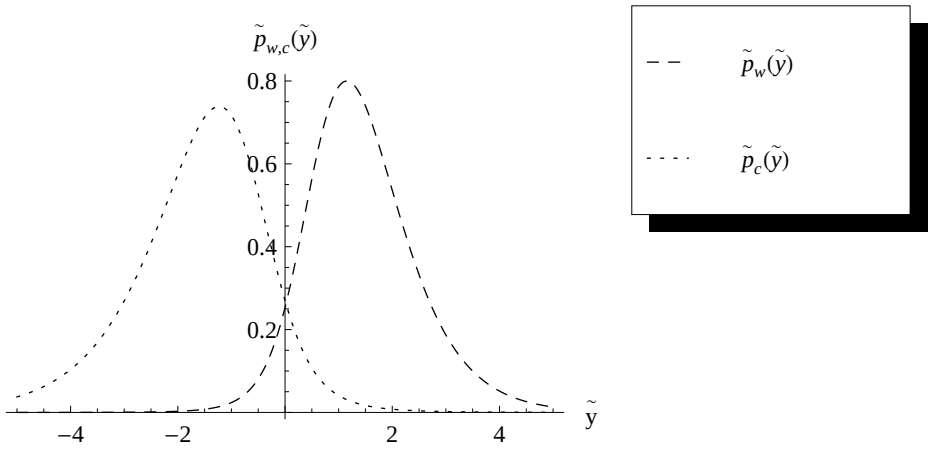

Figure 2.1: Profiles for the colored Higgs, p_c, and electroweak Higgs, p_w, for the parameter choices given in Eq. 2.11.

For the second choice,

$$\begin{aligned} \mu_\Phi^2 &= 65k^2, \\ \lambda_4 &= \frac{0.5k^2}{v^2}, \\ \lambda_5 &= \frac{10k^2}{A^2}, \\ \lambda_6 &= \frac{10k^2}{A^2} \\ \lambda_7 &= \frac{500k^2}{vA}, \end{aligned} \tag{2.12}$$

the mass eigenvalues are $m_w^2 = -16.8k^2$, and $m_c^2 = 13.2k^2$. As can be seen in Fig. 2.2, this leads to profiles which are much more localized than those for the first choice of parameters. As we will see, this has important consequences for the spread of domain wall Yukawa couplings and for the suppression of some of the decay modes for colored Higgs induced proton decay.

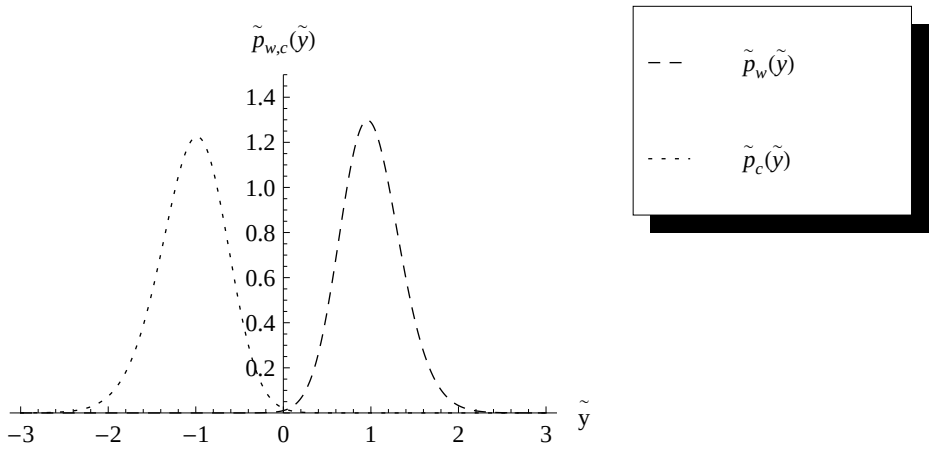

Figure 2.2: Higgs profiles for parameter choices given in Eq. 2.12.

For the third choice,

$$\begin{aligned} \mu_\Phi^2 &= 97700k^2, \\ \lambda_4 &= \frac{-75000k^2}{v^2}, \\ \lambda_5 &= \frac{15000k^2}{A^2}, \\ \lambda_6 &= \frac{-750000k^2}{A^2} \\ \lambda_7 &= \frac{20000k^2}{vA}. \end{aligned} \tag{2.13}$$

The resultant squared-masses for the lowest energy modes are $m_w^2 = -296k^2$ and $m_c^2 = 2.25 \times 10^4 k^2$. As we can see in the graphs of the profiles in Fig. 2.3, for this parameter region, the electroweak Higgs is highly peaked near the brane at $y = 0$, while the colored Higgs is more delocalized and substantially displaced from the wall. This parameter choice exploits the property of the Higgs sector that effective kink and lump couplings A_Y and B_Y are not the same for the colored and electroweak Higgs. As we will see, this kind of parameter choice can lead to suppression of all decay modes for colored

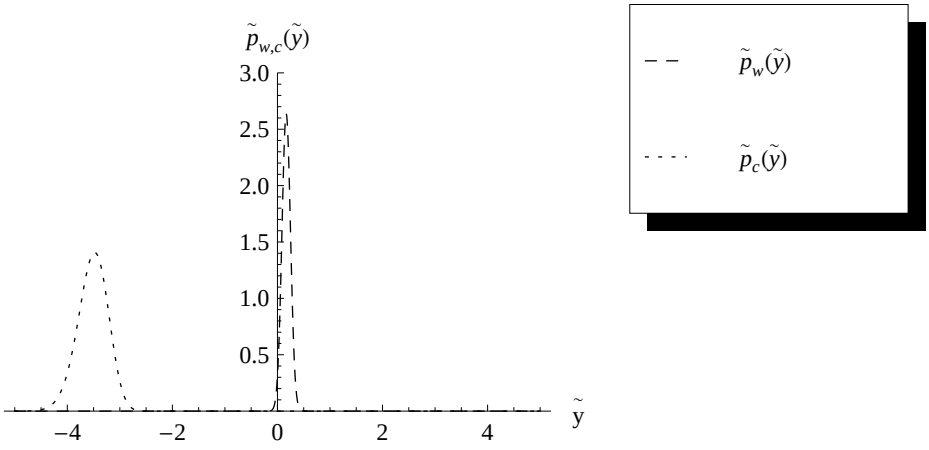

Figure 2.3: Higgs profiles for parameter choices given in Eq. 2.13.

Higgs induced proton decay, and ensure that the partial lifetimes for these modes are all many orders of magnitude above the current lower bounds.

Note that the Higgs vacuum expectation value, $\langle\phi_w\rangle$, is not uniquely determined by the constants which determine the Higgs profile. By dimensional reduction of the action,

$$S = \int d^5x \; (\partial^M \Phi)^\dagger (\partial_M \Phi) - V_\Phi, \tag{2.14}$$

one can show that the effective electroweak symmetry breaking potential is

$$V_{EW}(\phi_w) = \lambda'(\phi_w^\dagger \phi_w)^2 + m_w^2 \phi_w^\dagger \phi_w, \tag{2.15}$$

where

$$\lambda' = \lambda_3 \int p_w^4(y) \; dy. \tag{2.16}$$

Thus the VEV of the Higgs doublet is

$$\begin{aligned} \langle\phi_w\rangle &= \sqrt{\frac{-m_w^2}{2\lambda'}} \\ &= \sqrt{\frac{-m_w^2}{2\lambda_3 \int p_w^4(y) \; dy}}, \end{aligned} \tag{2.17}$$

and so whatever we choose for the other constants, we can always adjust λ_3 appropriately so that we get the correct VEV of 174 GeV.

2.0.4 Generating mass matrices for the charged fermions

The electroweak Yukawa Lagrangian, Y_5, from [23] which generates masses for the charged fermions is generalized to

$$Y_5 = h_-^{ij}\overline{(\Psi_5^i)^C}\Psi_{10}^j\Phi + h_+^{ij}\epsilon^{\alpha\beta\gamma\delta\kappa}\overline{(\Psi_{10}^i)^C}_{\alpha\beta}\Psi_{10\gamma\delta}^j\Phi_\kappa^* + h.c, \tag{2.18}$$

for m generations of fermions. Here, lower case Greek letters are $SU(5)$ indices and the lower case Roman letters indicate flavor.

The h_- terms generate mass matrices for the down-type quarks and electron type leptons, while the h_+ terms generate a mass matrix for the up-type quarks. Extracting the components from each term which generate 3+1D masses and performing dimensional reduction, one finds the mass matrices to be

$$\begin{aligned} M_u &= 4\overline{v}\int f_{u_R}^\dagger(y)h_+f_Q(y)p_w(y)\,dy, \\ M_d &= \frac{1}{\sqrt{2}}\overline{v}\int f_{d_R}^\dagger(y)h_-f_Q(y)p_w(y)\,dy, \\ M_e &= \frac{1}{\sqrt{2}}\overline{v}\int f_{e_R}^\dagger(y)h_-f_l(y)p_w(y)\,dy, \end{aligned} \tag{2.19}$$

where $p_w(y)$ is the profile of the electroweak Higgs doublet which is embedded in Φ, and $\overline{v} = 174\ GeV$ is the vacuum expectation value of the electroweak Higgs field attained on the brane.

Converting to dimensionless quantities, and defining the non-dimensionalized electroweak Yukawa couplings by

$$\begin{aligned} \tilde{h}_+ &= k^{\frac{1}{2}}h_+, \\ \tilde{h}_- &= k^{\frac{1}{2}}h_-, \end{aligned} \tag{2.20}$$

we see that these mass matrices can be rewritten as

$$\begin{aligned} M_u &= 4\overline{v}\int \tilde{f}_{u_R}^\dagger(y)\tilde{h}_+\tilde{f}_Q(y)\tilde{p}_w(y)\,d\tilde{y}, \\ M_d &= \frac{1}{\sqrt{2}}\overline{v}\int \tilde{f}_{d_R}^\dagger(y)\tilde{h}_-\tilde{f}_Q(y)\tilde{p}_w(y)\,d\tilde{y}, \\ M_e &= \frac{1}{\sqrt{2}}\overline{v}\int \tilde{f}_{e_R}^\dagger(y)\tilde{h}_-\tilde{f}_l(y)\tilde{p}_w(y)\,d\tilde{y}. \end{aligned} \tag{2.21}$$

There are some important consequences of the above forms of the mass matrices, which depend on overlap integrals of the profiles for the left and right chiral fermions and the electroweak Higgs. Firstly, the overlap integral dependence means we avoid the usual incorrect mass relations like $m_e = m_d$

which are characteristic of ordinary 3+1D $SU(5)$ models with a Higgs quintet. This is also the reason why we do not need a Higgs belonging to the 45 representation of $SU(5)$ containing an electroweak Higgs triplet to get the Georgi-Jarlskog relations [114]. Thirdly, since the fermions are split according to their hypercharges, and the splittings are dependent on the background couplings, we can potentially generate the fermion mass hierarchy and mixings by splitting the fermions appropriately so that the overlap integrals are in the desired ratios. It will be shown in a later section that this can be done.

2.0.5 Generating Dirac neutrino masses

To generate Dirac masses for the neutrinos, we need to add Yukawa interactions involving the Ψ_5^i, which contain the left handed neutrinos, the N^i, which contain the right handed neutrinos, and Φ which contains the electroweak Higgs. The correct terms to add to Y_5 which are both $SU(5)$ invariant and respect the reflection symmetry which preserves the topological stability of the domain wall are

$$(h_3^\dagger)^{ij}\overline{\Psi_5^i}\Phi N^j + h.c. \tag{2.22}$$

Reducing these terms to their SM components, and integrating out the extra-dimensional dependence, one finds the resulting Dirac mass matrix for the neutrinos to be

$$m_\nu = \overline{v}\int f_{\nu_R}^\dagger(y) h_3 f_l(y) p_w(y)\, dy. \tag{2.23}$$

Defining the dimensionless neutrino Yukawa couplings as

$$\tilde{h}_3 = k^{\frac{1}{2}} h_3, \tag{2.24}$$

and changing to non-dimensionalized quantities, we can rewrite the Dirac mass matrix for the neutrino as

$$m_\nu = \overline{v}\int \tilde{f}_{\nu_R}^\dagger(y) \tilde{h}_3 \tilde{f}_l(y) \tilde{p}_w(y)\, d\tilde{y}. \tag{2.25}$$

2.0.6 Generating Majorana neutrino masses

Let us consider one generation first. To generate a Majorana mass for the neutrino, we need to add terms to the Lagrangian that will dimensionally reduce to terms proportional to $\overline{\nu_R^c}\nu_R$ in the effective 4D theory. Thus, we might want to consider adding a term like

$$\overline{N}N^C + h.c. \tag{2.26}$$

This is obviously gauge invariant, and it turns out that it is also invariant under the discrete reflection symmetry as well. We first need to consider what implications the addition of this term has for the existence of solutions of the 5D Dirac equation. The relevant Lagrangian is

$$L_{N,DW} = i\overline{N}\Gamma^M\partial_M N + h_{1\eta}\overline{N}N\eta - \frac{1}{2}m(\overline{N}N^C + \overline{N^C}N), \tag{2.27}$$

and thus the 5d Dirac equation becomes

$$i\Gamma^M\partial_M N + h_{1\eta}N\eta - mN^C = 0. \tag{2.28}$$

Demanding the conditions that

$$\begin{aligned} N(x,y) &= f_N(y)\nu_R(x), \\ \gamma^5\nu_R &= \nu_R, \\ i\gamma^\mu\partial_\mu\nu_R &= m'(\nu_R)^c, \end{aligned} \tag{2.29}$$

and noting that the parts proportional to ν_R and $(\nu_R)^c$ must be independent of each other as the corresponding spinors transform as right-chiral and left-chiral spinors respectively, we get two independent equations for f_N,

$$\begin{aligned} &\frac{df_N}{dy} + h_{1\eta}\eta(y)f_N(y) = 0, \\ &m'f_N(y) - imf_N^*(y) = 0. \end{aligned} \tag{2.30}$$

The first of the equations above is exactly the same differential equation as before without the new term, and thus the f_N must also have the same form as before,

$$f_N(y) = C_N e^{-\frac{h_{1\eta}v}{k}\log(\cosh(ky))}. \tag{2.31}$$

The second condition then implies that $m' = |m|$, and since any phase can just be absorbed into the definition of N, we can take $m' = m$. Hence, instead of a right-chiral zero mode, we now have a right-chiral Majorana mode of mass m localized to the domain wall.

Similarly with three generations, the profiles are unaltered by the Majorana mass terms, and the 3+1d Majorana mass matrix after dimensional reduction is then

$$M_{Maj,3+1d} = \int f^T(y)m_{4+1d}f(y)\,dy. \tag{2.32}$$

We have thus successfully shown that both Dirac and Majorana masses can be generated with the addition of a right chiral singlet neutrino, and thus the see-saw mechanism can be employed. We will now demonstrate that the fermion mass hierarchy and small CKM mixing angles can be generated from split fermion idea.

2.1 Generating the flavor hierarchy and mixing angles

The fermion mass matrices depend on overlap integrals of the fermion profiles and the electroweak Higgs. Since the left-chiral and right-chiral components are naturally split according to their hypercharges, and since these overlap integrals are exponentially sensitive to these splittings, it seems we can employ the split fermion idea [19] to account for the fermion mass hierarchy from a set of domain wall couplings which are all about the same order of magnitude in this model.

Throughout the rest of this chapter, we will quote the dimensionless background Yukawa couplings to five significant figures. The reasons for this are the exponential sensitivity of the profiles to these couplings and the difficulty that was found in generating the neutrino mass squared differences (which are quadratic in overlap integrals of these profiles) to an acceptable and reasonable precision. Since this is also a classical calculation where quantum corrections are ignored, and since the quark and neutrino masses are not as precisely measured or well known as those for the charged leptons, we will quote the resultant masses of the quarks and neutrinos to two significant figures, neutrino mass squared differences to one significant figure, and the charged lepton masses to three significant figures.

2.1.1 The one-generation case with a Dirac neutrino and the suppression of colored-Higgs-induced proton decay

In this section we shall show that the mass hierarchy amongst the first generation of fermions can be generated from the split fermion idea [19] which arises naturally in our model. We will start with looking for solutions with the Higgs parameter choices of Eq. 2.11.

Firstly, we must make the neutrino light. The right chiral neutrino is always localized at $y = 0$ while the choice of Higgs parameters in Eq. 2.11 (and in fact for those in Eqs. 2.12 and 2.13 as well), the Higgs is localized to the right. Hence, the easiest way to induce a small Dirac neutrino mass is to shift the lepton doublet to the left. As the lepton doublet, L, has hypercharge -1 and the charge conjugate of d_R has hypercharge $+\frac{2}{3}$, choosing $\frac{\tilde{h_{5\chi}}}{\tilde{h_{5\eta}}}$ to be negative will displace the lepton doublet as desired while placing the right-chiral down quark to the right, near the electroweak Higgs. We now need to make the charged fermion masses significantly larger. Since the charge

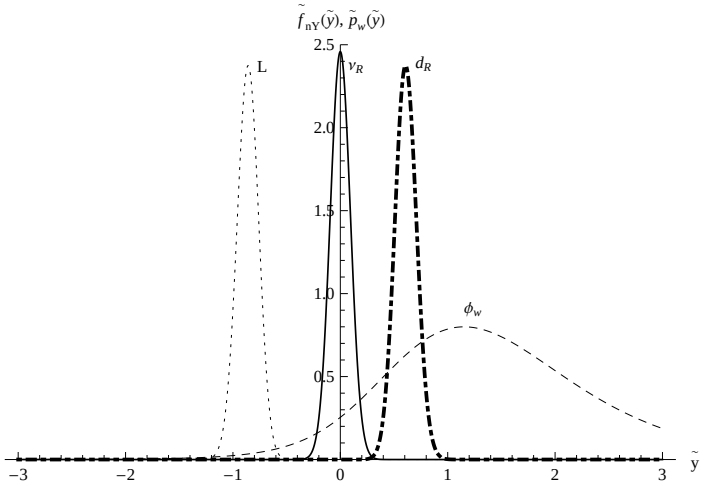

Figure 2.4: The profiles for ν_R, L, d_R and the electroweak Higgs with the Higgs parameter choice of Eq. 2.11, $\tilde{h}_{1\eta} = 115$, $\tilde{h}_{5\eta} = 100$ and $\tilde{h}_{5\chi} = -250$.

conjugates of u_R and e_R, and the quark doublet have hypercharges $-\frac{4}{3}$, $+2$ and $+\frac{1}{3}$ respectively, making the ratio $\frac{\tilde{h}_{10\chi}}{\tilde{h}_{10\eta}}$ positive will shift e_R far to the left, towards the lepton doublet, Q to slightly to the left, and u_R to the right. We found the following solution by using this configuration, making the parameter choice $\tilde{h}_{5\eta} = 100$ and $\tilde{h}_{5\chi} = -250$, plotting the contours along which the overlap integrals give the desired mass ratios, and then finding where the two contours intersected. Doing this yielded the solution for the couplings for the 10 multiplet, $\tilde{h}_{10\eta} = 8.2674$ and $\tilde{h}_{10\chi} = 27.911$. With the ratios now fixed, setting the 5D electroweak Yukawas $h_- = h_+ = h_3 = 5.2268 \times 10^{-3} k^{-\frac{1}{2}}$, and setting the kink coupling for the right handed neutrino to $\tilde{h}_{1\eta} = 115$ gives the masses,

$$\begin{aligned} m_\nu &= 0.13 \text{ eV} \\ m_e &= 0.511 \text{ MeV} \\ m_u &= 2.5 \text{ MeV} \\ m_d &= 5.0 \text{ MeV}. \end{aligned} \tag{2.33}$$

Thus, we have generated a neutrino mass below the current most stringent upper bounds of roughly 2 eV [63] , the correct electron mass, and up and down quark masses within current constraints of 1.8 MeV$< m_u <$ 3.0 MeV, and 4.5 MeV$< m_d <$ 5.3 MeV [63].

Furthermore, it turns out we get significant suppression of some modes of colored Higgs-induced proton decay with this setup. The colored Higgs

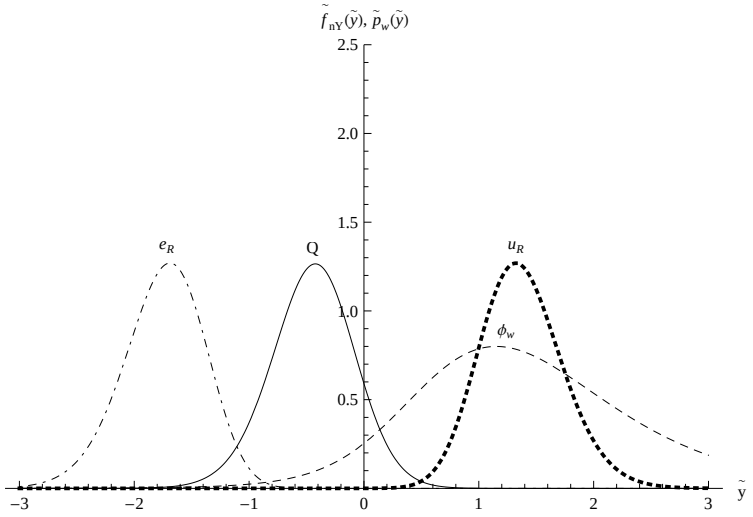

Figure 2.5: The profiles for the 10 representation, and the electroweak Higgs with the Higgs parameter choice of Eq. 2.11, $\tilde{h}_{10\eta} = 8.2674$ and $\tilde{h}_{10\chi} = 27.911$.

scalar can induce the decays $p \to e^+\pi^0$ and $p \to \nu_e\pi^+$, for which the Feynman diagrams are shown in Figures 2.7(a) and 2.7(b) respectively.

For the process $p \to e^+\pi^0$, the partial lifetime of each contribution is

$$\frac{m_c^4}{C_{v_{ue}}^2 C_{v_{ud}}^2 m_p^5}, \tag{2.34}$$

where $C_{v_{ue}}$ and $C_{v_{ud}}$ are replaced by the effective 4D couplings strengths of the operators inducing the vertices v_{ue} and v_{ud} respectively. The operators responsible for the vertex v_{ue} are $\overline{(e_R)^c} u_R \phi_c$ and $\overline{L} Q \phi_c$, and their respective coupling strengths are

$$\begin{aligned} C_{\overline{(e_R)^c} u_R \phi_c} &= 4h_+ \int f_{u_R}(y) f_{e_R}(y) p_c(y)\, dy, \\ C_{\overline{L} Q \phi_c} &= \frac{1}{\sqrt{2}} h_- \int f_L(y) f_Q(y) p_c(y)\, dy. \end{aligned} \tag{2.35}$$

The operators responsible for the vertex v_{ud} are $\overline{(u_R)^c} d_R \phi_c^*$ and $\epsilon^{ijk} Q_i Q_j (\phi_c^*)_k$, and the associated coupling strengths are

$$\begin{aligned} C_{\overline{(u_R)^c} d_R \phi_c^*} &= \frac{1}{\sqrt{2}} h_- \int f_{u_R}(y) f_{d_R}(y) p_c(y)\, dy, \\ C_{QQ\phi_c^*} &= 4h_+ \int (f_Q(y))^2 p_c(y)\, dy. \end{aligned} \tag{2.36}$$

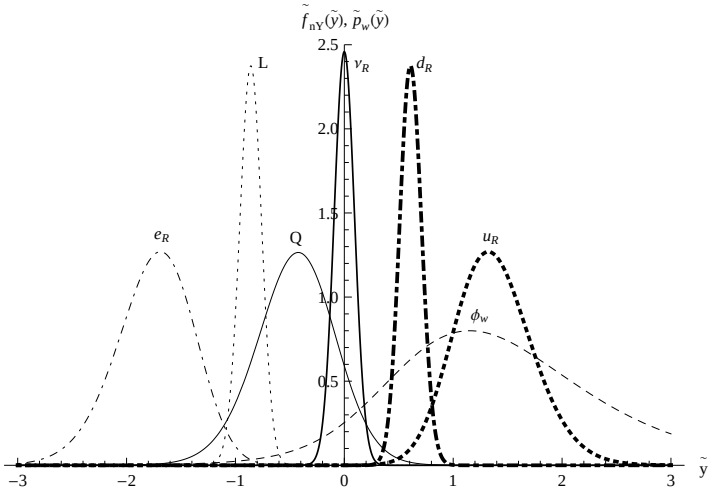

Figure 2.6: The profiles for all fermions and ϕ_w for the first solution with $\tilde{h}_{1\eta} = 115$, $\tilde{h}_{5\eta} = 100$, $\tilde{h}_{5\chi} = -250$, $\tilde{h}_{10\eta} = 8.2674$, $\tilde{h}_{10\chi} = 27.911$ and the Higgs parameter choice of Eq. 2.11.

Similarly, the partial lifetime of each contribution to $p \to \nu_e \pi^+$ is

$$\frac{m_c^4}{C_{v_{d\nu}}^2 C_{v_{ud}}^2 m_p^5}. \tag{2.37}$$

The operators responsible for the vertex v_{ud} in the $p \to \nu_e \pi^+$ are the same as that for $p \to e^+ \pi^0$, while the operators responsible for the $v_{d\nu}$ vertex are $\overline{L} Q \phi_c$ and $\overline{(\nu_R)^c} d_R \phi_c$. The coupling strength for the operator $\overline{(\nu_R)^c} d_R \phi_c$ is

$$C_{\overline{(\nu_R)^c} d_R \phi_c} = h_3 \int f_{\nu_R}(y) f_{d_R}(y) p_c(y)\, dy. \tag{2.38}$$

For the solution given above, it turns out that the partial width for $p \to e^+ \pi^0$ involving just right chiral fermions is substantially suppressed, with $C_{\overline{(e_R)^c} u_R \phi_c} = 9.6 \times 10^{-14}$ and $C_{\overline{(u_R)^c} d_R \phi_c^*} = 2.1 \times 10^{-5}$. Since the partial lifetime for $p \to e^+ \pi^0$ is at least 8.2×10^{33} years [115], and given $m_p = 0.938$ GeV [116], this sets a lower bound on the colored Higgs mass of about 3.3×10^4 TeV, much reduced compared to the standard result of $m_c \sim \Lambda_{GUT} \sim 10^{16}$ GeV. Since $C_{\overline{(\nu_R)^c} d_R \phi_c} = 3.7 \times 10^{-8}$, and the lower bound of the partial lifetime for $p \to \nu \pi^+$ is 2.5×10^{31} years [116], the contribution to $p \to \nu_e \pi^+$ involving the vertices $\overline{(\nu_R)^c} d_R \phi_c$ and $\overline{(u_R)^c} d_R \phi_c^*$ sets a lower bound on the colored Higgs mass of 4.8×10^6 TeV.

However the contribution involving just left-chiral fermions is not substantially suppressed from the splittings, with $C_{\overline{L} Q \phi_c} = 9.1 \times 10^{-4}$ and

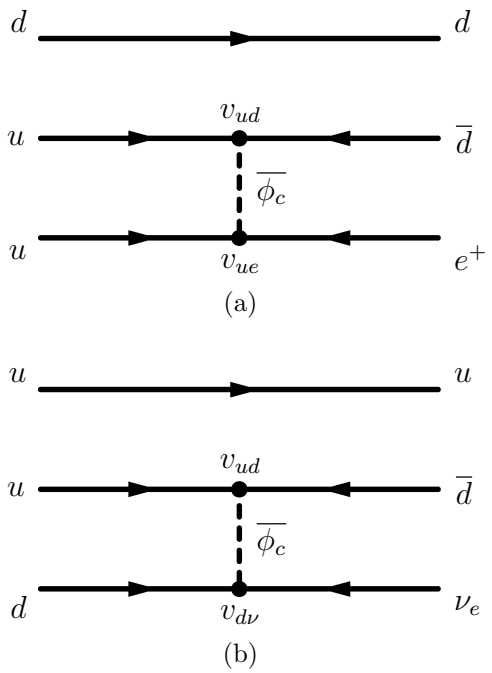

Figure 2.7: Feynman diagrams for the processes (a) $p \to e^+\pi^0$ and (b) $p \to \nu_e\pi^+$

$C_{QQ\phi_c^*} = 1.0 \times 10^{-2}$. These operators contribute to both $p \to e^+\pi^0$ and $p \to \nu_e\pi^+$, and thus the partial widths coming from the combination of these operators set lower limits on the colored Higgs mass of 7.0×10^{13} GeV for $p \to e^+\pi^0$, and 1.6×10^{13} GeV to suppress $p \to \nu_e\pi^+$. Therefore, we must still fine-tune so that the colored Higgs mass is of the order $\sim 10^{14}$ GeV to suppress all proton decay modes induced by the colored Higgs scalar.

One might then ask how to suppress proton decay even further. We could try looking for a solution where the profiles are more spread out in the extra dimension. It turns out the choice of parameters, $\tilde{h}_{1\eta} = 100$, $\tilde{h}_{5\eta} = 100$, $\tilde{h}_{5\chi} = -700$, $\tilde{h}_{10\eta} = 0.81688$, $\tilde{h}_{10\chi} = 23.868$, and $h_+ = h_- = h_3 = 0.11177k^{-\frac{1}{2}}$, yields the same masses for the electron and the quarks as the first solution, and gives a neutrino mass of the order

$$m_\nu \sim 10^{-24} \text{ eV}. \tag{2.39}$$

For proton decay, we now have for the operators involving just right chiral fermions $C_{\overline{(e_R)^c}u_R\phi_c} = 4.2 \times 10^{-17}$, $C_{\overline{(u_R)^c}d_R\phi_c^*} = 1.7 \times 10^{-5}$, and $C_{\overline{(\nu_R)^c}d_R\phi_c} = 2.8 \times 10^{-23}$, which yield $m_c > 6.1 \times 10^2$ TeV from the partial width for

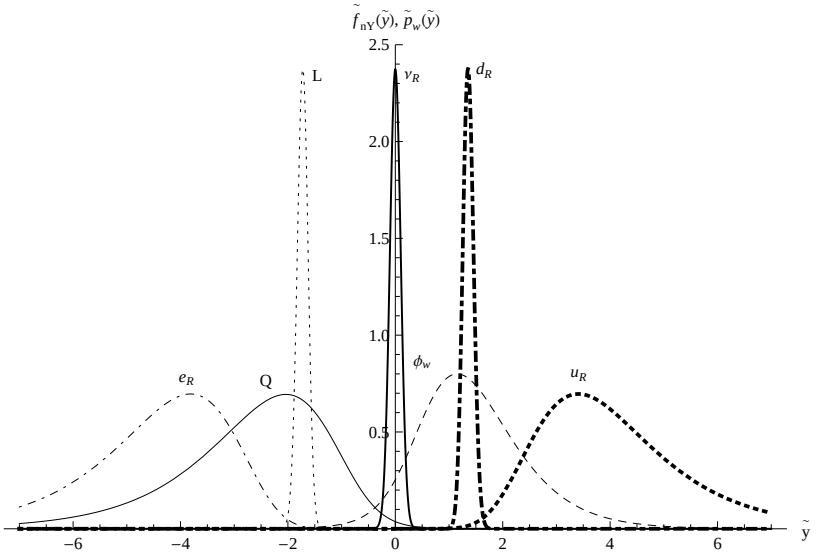

Figure 2.8: The spread of profiles for the second solution with $\tilde{h}_{1\eta} = 100$, $\tilde{h}_{5\eta} = 100$, $\tilde{h}_{5\chi} = -700$, $\tilde{h}_{10\eta} = 0.81688$, $\tilde{h}_{10\chi} = 23.868$, and the Higgs parameter choice of Eq. 2.11.

$p \to e^+\pi^0$, and $m_c > 1.2 \times 10^2$ GeV from the partial width contributed to $p \to \nu_e\pi^+$. However, the couplings for the operators involving the left chiral fermions are still not suppressed enough to solve the doublet-triplet splitting problem naturally, with $C_{\overline{L}Q\phi_c} = 2.0 \times 10^{-2}$ and $C_{QQ\phi_c^*} = 0.21$, setting the bound $m_c > 1.5 \times 10^{15}$ GeV from the more constraining decay $p \to e^+\pi^0$.

By spreading out the profiles, we have increased the spread of the domain wall parameters while only suppressing the proton decay modes induced from right chiral fermions by a further two orders of magnitude. It turns out that a choice of Higgs potential parameters giving more localized Higgs profiles can solve the first problem while yielding a similar result for proton decay. A solution for the second Higgs profile for which the Higgs parameters are those in Eq. 2.12 is $h_+ = h_- = h_3 = 82.975k^{-\frac{1}{2}}$, $\tilde{h}_{1\eta} = 200$, $\tilde{h}_{5\eta} = 100$, $\tilde{h}_{5\chi} = -250$, $\tilde{h}_{10\eta} = 60.126$, $\tilde{h}_{10\chi} = 99.829$, which again yields the same masses for the electron and the quarks as the previous solutions, and the neutrino mass

$$m_\nu = 0.024 \text{ eV}. \tag{2.40}$$

Interestingly, for these parameters, $C_{\overline{(e_R)^c}u_R\phi_c} = 2.0 \times 10^{-24}$ and $C_{\overline{(u_R)^c}d_R\phi_c^*} = 1.1 \times 10^{-3}$ suppressing the mode of $p \to e^+\pi^0$ involving just the right chiral fermions to the extent that the lower bound for the colored Higgs mass set by this mode is just 1.1 TeV. However, the decays involving the left

chiral fermions are in fact enhanced rather than suppressed by the fermion splittings with $C_{\overline{L}Q\phi_c} = 2.0 \times 10^{-2}$ and $C_{QQ\phi_c^*} = 39$, which means that the suppression factor coming from the effective coupling constants is of order 1, and so we need to make $m_c \sim M_{GUT}$. Also, the partial width involving the right chiral fermions for $p \to \nu_e \pi^+$ is not as suppressed this time, with $C_{\overline{(\nu_R)^c} d_R \phi_c} = 8.5 \times 10^{-7}$, so that an m_c of order 10^{11} GeV is required to suppress this particular mode.

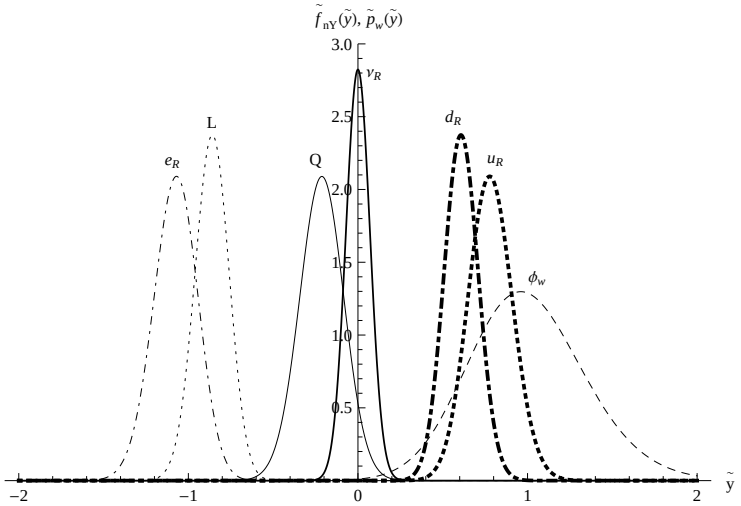

Figure 2.9: The profiles for the solution with $\tilde{h}_{1\eta} = 200$, $\tilde{h}_{5\eta} = 100$, $\tilde{h}_{5\chi} = -250$, $\tilde{h}_{10\eta} = 60.126$, $\tilde{h}_{10\chi} = 99.829$, and the choice of Higgs parameters in Eq. 2.12.

The ultimate reason we have successfully suppressed the modes of proton decay involving just the right chiral fermions but not those involving the left chiral fermions so far was that the vertices involving the right chiral fermions depended on the profiles for u_R and d_R which were localized near the electroweak Higgs away from the colored Higgs, whereas due to the setup to generate the mass hierarchy, the quark and lepton doublets were placed significantly closer to the colored Higgs. To keep the natural solution to the mass hierarchy problem, we do not wish to displace the quark and lepton doublets; a more fruitful option is to choose Higgs parameters such that the colored Higgs is well displaced from the domain wall, while at the same time the electroweak Higgs is close to $y = 0$. We have seen in Sec. 2.0.3 that this is in fact possible with the Higgs parameter choice given in Eq. 2.13. A solution for this third Higgs profile to the mass hierarchy problem is the parameter choice $h_+ = h_- = h_3 = 40987k^{-\frac{1}{2}}$, $\tilde{h}_{1\eta} = 1000$, $\tilde{h}_{5\eta} = 1000$, $\tilde{h}_{5\chi} =$

-1000, $\tilde{h}_{10\eta} = 624.62$, $\tilde{h}_{10\chi} = 382.43$, which yields the same electron, up and down quark masses as before and a neutrino mass of the order

$$m_\nu \sim 10^{-4} \text{ eV}. \tag{2.41}$$

This time, for the proton decay inducing interactions, $C_{\overline{(e_R)^c} u_R \phi_c} \sim 10^{-139}$, $C_{\overline{(u_R)^c} d_R \phi_c^*} \sim 10^{-131}$ and $C_{\overline{(\nu_R)^c} d_R \phi_c} \sim 10^{-126}$ for the operators involving just right chiral fermions and for those involving the left chiral fermions, $C_{\overline{L} Q \phi_c} \sim 10^{-92}$ and $C_{QQ\phi_c^*} \sim 10^{-98}$. Hence, all the decay modes are suppressed by roughly 90-100 orders of magnitude, with the most constraining decay mode $p \to e^+\pi^0$ with the left chiral fermions now setting a lower bound on the colored Higgs mass of $\sim 10^{-69}$ eV. Realistically, for such a solution, the colored Higgs mass should still at the very least be 45 GeV since we have not seen the Z boson decay into them, and more probably ~ 1 TeV since it is proportional to k in this model, so the partial lifetime arising from colored Higgs induced proton decay would be over 10^{100} years.

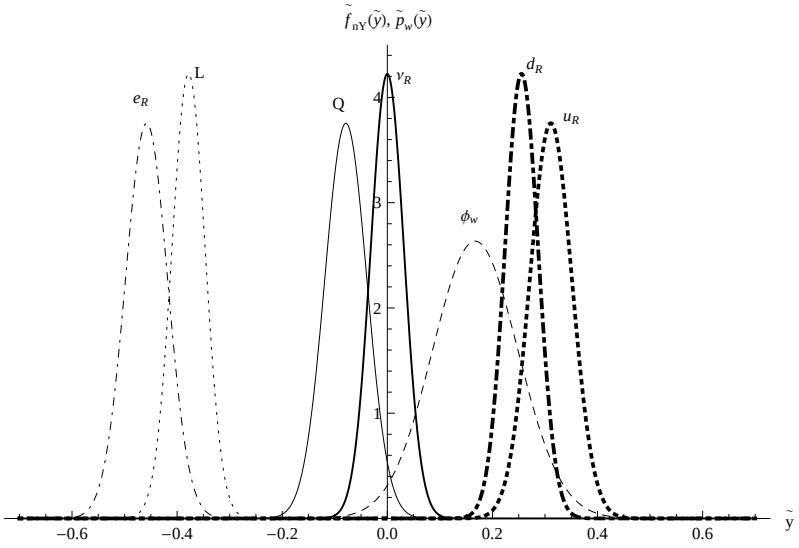

Figure 2.10: The profiles for the solution with $\tilde{h}_{1\eta} = 1000$, $\tilde{h}_{5\eta} = 1000$,$\tilde{h}_{5\chi} = -1000$, $\tilde{h}_{10\eta} = 624.62$, $\tilde{h}_{10\chi} = 382.43$, and the choice of Higgs parameters in Eq. 2.13.

The profiles for the latter two solutions are much less dispersed than those first two for the most delocalized electroweak Higgs profile, as one might expect. This is reflected in the breadth of the domain wall parameters; for the third and fourth solutions, the ratios of the magnitude of the largest background coupling ($\tilde{h}_{5\chi} = -250$ and $\tilde{h}_{1\eta} = \tilde{h}_{5\eta} = -\tilde{h}_{5\chi} = 1000$ respectively)

to the smallest ($\tilde{h}_{10\eta} = 60.126$ and $\tilde{h}_{10\chi} = 382.43$) are roughly 4.2 and 2.6 respectively, under an order of magnitude. In comparison, for the first two solutions, the corresponding ratios are about 30.2 and 860 respectively. This difference, as we will see, is exacerbated for three generations.

In summary, we have shown that the one generation mass hierarchy can be generated by splitting the fermions without fine tuning the electroweak Yukawa constants, and that for an appropriate choice of Higgs parameters, one can reduce the spread of the domain wall Yukawa constants and suppress proton decay by roughly 100 orders of magnitude without fine tuning the colored Higgs mass. In the next section, we will see that we can also do this for the three generation case without quark and lepton mixing.

2.1.2 Generating the higher generation mass hierarchies without electroweak mixing

For the sake of simplicity, we can solve the mass hierarchy problem while first omitting quark and lepton mixing by setting the off diagonal elements of the electroweak Yukawa matrices to zero. Solutions are found in analogous fashion to the one generation case by finding where the overlap integrals are in the desired ratios in parameter space.

For the first Higgs profile, setting $h^i_+ = h^i_- = h^i_3 = 1.4093k^{-\frac{1}{2}}$, the set of parameters choices for the domain wall Yukawa parameters and the resultant masses m^i_E for the electron-type leptons, m^i_U for the up-type quarks and m^i_D for the down-type quarks are shown in Table 2.1. As one can see, these masses all lie within current experimental limits [63]. We then get similar results for the second Higgs profile with $h^i_+ = h^i_- = h^i_3 = 7859.3k^{-\frac{1}{2}}$ and the third Higgs profile with $h^i_+ = h^i_- = h^i_3 = 2701.2k^{-\frac{1}{2}}$, with the solutions for these two parameter choices given in Tables 2.2 and 2.3 respectively.

i	$\tilde{h}^i_{5\eta}$	$\tilde{h}^i_{5\chi}$	$\tilde{h}^i_{10\eta}$	$\tilde{h}^i_{10\chi}$	m^i_E(MeV)	m^i_U(MeV)	m^i_D(MeV)
1	1064.0	-8563.9	0.2	25.496	0.511	2.5	5.0
2	48.986	-708.28	1.5	17.330	106	1.3×10^3	1.0×10^2
3	100	-300	10.537	8.6032	1.78×10^3	1.7×10^5	4.2×10^3

Table 2.1: A set of domain wall parameters and the resultant masses with Higgs parameters chosen in Eq. 2.11 and electroweak Yukawas set to $h^i_+ = h^i_- = h^i_3 = 1.410k^{-\frac{1}{2}}$ for $i = 1, 2, 3$

i	$\tilde{h}^i_{5\eta}$	$\tilde{h}^i_{5\chi}$	$\tilde{h}^i_{10\eta}$	$\tilde{h}^i_{10\chi}$	m^i_E(MeV)	m^i_U(MeV)	m^i_D(MeV)
1	200	-648.41	38.552	99.220	0.511	2.5	5.0
2	200	-493.42	62.128	94.251	106	1.3×10^3	1.0×10^2
3	200	-400	73.744	76.383	1.78×10^3	1.7×10^5	4.2×10^3

Table 2.2: A set of domain wall parameters and the resultant masses with Higgs parameters chosen in Eq. 2.12 and electroweak Yukawas set to $h^i_+ = h^i_- = h^i_3 = 7859.3k^{-\frac{1}{2}}$ for $i = 1, 2, 3$

i	$\tilde{h}^i_{5\eta}$	$\tilde{h}^i_{5\chi}$	$\tilde{h}^i_{10\eta}$	$\tilde{h}^i_{10\chi}$	m^i_E(MeV)	m^i_U(MeV)	m^i_D(MeV)
1	2000	-1585.2	660.91	369.07	0.511	2.5	5.0
2	2000	-1434.5	744.05	325.26	106	1.3×10^2	1.1×10^2
3	2000	-1300	708.14	256.02	1.78×10^3	1.7×10^5	4.2×10^3

Table 2.3: A set of domain wall parameters and the resultant masses with Higgs parameters chosen in Eq. 2.13 and electroweak Yukawas set to $h^i_+ = h^i_- = h^i_3 = 2701.2k^{-\frac{1}{2}}$ for $i = 1, 2, 3$

There exists a finite range of parameter space spanned by the remaining couplings $h^i_{1\eta}$ of the right handed neutrinos to the domain wall which fit the currently accepted squared neutrino mass differences of $\Delta m_{12} = 7.9^{+0.6}_{-0.5} \times 10^{-5}$ eV^2 [117] and $\Delta m_{23} = 2.74^{+0.44}_{-0.26} \times 10^{-3}$ eV^2 [118], and cosmological constraints (in some models) on the sum of the masses $\sum m_\nu < 0.3 - 0.6$ eV [119, 120], for normal, inverted, and quasi-degenerate neutrino mass hierarchies. Provided that the fermion doublets are sufficiently localized and displaced away from the domain wall at $y = 0$, where the right handed neutrinos are always situated, and the electroweak Higgs, one can just adjust the couplings of the right handed neutrinos to the kink to get the desired masses and hierarchy. For each of the three solutions given in Tables 2.1, 2.2 and 2.3, three example parameter choices for the $\tilde{h}^i_{1\eta}$ yielding normal(N), quasi-degenerate(Q), and inverted(I) neutrino mass hierarchies are given in Tables 2.4, 2.5 and 2.6 respectively.

The distribution of the fermions for each family for both the solutions with a normal neutrino mass hierarchy are shown in the Figs. 2.11, 2.12 and 2.13. As can be seen, the lighter generations are, on average, more spread apart, more distant from $y = 0$ and more delocalized. Comparing the plots

Hierarchy	$\tilde{h}^1_{1\eta}$	$\tilde{h}^2_{1\eta}$	$\tilde{h}^3_{1\eta}$	m_{ν_e}(eV)	m_{ν_μ}(eV)	m_{ν_τ}(eV)
N	100	15.44	110.4	1.5×10^{-41}	0.0089	0.053
Q	18.919	13.764	106.61	0.10	0.10	0.086
I	19.503	14.219	300	0.051	0.052	7.4×10^{-8}

$\sum m_i$(eV)	Δm^2_{21}(eV^2)	Δm^2_{32}(eV^2)
0.062	8×10^{-5}	3×10^{-3}
0.29	8×10^{-5}	-3×10^{-3}
0.10	8×10^{-5}	-3×10^{-3}

Table 2.4: Solutions for normal, quasi-degenerate and inverted neutrino mass hierarchies given the parameter choices given in Table 2.1

Hierarchy	$\tilde{h}^1_{1\eta}$	$\tilde{h}^2_{1\eta}$	$\tilde{h}^3_{1\eta}$	m_{ν_e}(eV)	m_{ν_μ}(eV)	m_{ν_τ}(eV)
N	200	132.73	262.60	3.5×10^{-15}	0.0089	0.053
Q	54.564	114.28	253.20	0.096	0.096	0.081
I	56.690	118.95	650	0.051	0.052	2.9×10^{-6}

$\sum m_i$(eV)	Δm^2_{21}(eV^2)	Δm^2_{32}(eV^2)
0.062	8×10^{-5}	3×10^{-3}
0.27	8×10^{-5}	-3×10^{-3}
0.10	8×10^{-5}	-3×10^{-3}

Table 2.5: Solutions for normal, quasi-degenerate and inverted neutrino mass hierarchies given the parameter choices given in Table 2.2

Hierarchy	$\tilde{h}^1_{1\eta}$	$\tilde{h}^2_{1\eta}$	$\tilde{h}^3_{1\eta}$	m_{ν_e}(eV)	m_{ν_μ}(eV)	m_{ν_τ}(eV)
N	2000	1449.2	2044.3	8.1×10^{-9}	0.0089	0.053
Q	826.28	1250	1948.5	0.084	0.084	0.099
I	852.44	1291	4500	0.051	0.052	2.3×10^{-6}

$\sum m_i$(eV)	Δm^2_{21}(eV^2)	Δm^2_{32}(eV^2)
0.062	8×10^{-5}	3×10^{-3}
0.27	8×10^{-5}	3×10^{-3}
0.10	8×10^{-5}	-3×10^{-3}

Table 2.6: Solutions for normal, quasi-degenerate and inverted neutrino mass hierarchies given the parameter choices given in Table 2.3

for the first Higgs profile in Fig. 2.11 to those for the second and third Higgs

profiles in Figs. 2.12 and 2.13, it is conspicuous that this increase in spread of the fermions between generations is dramatically reduced for the more localized Higgs. This is reflected in the spread of domain wall parameters, with the ratios between the smallest and largest non-dimensionalized domain wall parameters. For the parameter choices of Tables 2.1, 2.2, and 2.3 and normal neutrino mass hierarchies, these ratios are respectively 4.3×10^4, 17, and 7.8. The solution of Table 2.3 is particularly interesting since the non-dimensionalized electroweak Yukawa constant $\tilde{h}^i_{-,+,3} = h^i_{-,+,3} k^{\frac{1}{2}} = 2701.2$ is of the same order as the non-dimensionalized domain wall parameters.

With regards to proton decay, the results for the parameter choices of Tables 2.1, 2.2 and 2.3 are similar to those of Sec. 2.1.1. For the first two solutions with Higgs parameters chosen from Eqs. 2.11 and 2.12, the decay modes involving just right-chiral fermions are substantially suppressed while there is negligible suppression for the modes involving the left-chiral fermions. For the parameters chosen in Table 2.1, $C_{\overline{(e_R)^c} u_R \phi_c} \sim 10^{-18}$, $C_{\overline{(u_R)^c} d_R \phi_c^*} = 1.7 \times 10^{-5}$, $C_{\overline{L} Q \phi_c} = 5.7 \times 10^{-2}$ and $C_{QQ\phi_c^*} = 0.80$, and hence the lower bound on the colored Higgs mass from the decay mode for $p \to e^+ \pi^0$ involving just right-chiral fermions is roughly 120 TeV, while that from the decay mode involving just left-chiral fermions is of order 10^{15} GeV.

For the solution in Table 2.2, $C_{\overline{(e_R)^c} u_R \phi_c} \sim 10^{-30}$, $C_{\overline{(u_R)^c} d_R \phi_c^*} = 4.1 \times 10^{-3}$, $C_{\overline{L} Q \phi_c} = 2.5$ and $C_{QQ\phi_c^*} = 7.4 \times 10^3$, so that the decay mode involving the right-chiral fermions sets a lower bound on m_c of just 1.7 GeV, while the decay mode involving just left-chiral fermions are in fact enhanced, with the lower bound on m_c increased to order 10^{17} GeV.

For the solution of Table 2.3, just as with the one generation solution with the Higgs parameter choices of Eq. 2.13, all decay modes are suppressed since the colored Higgs is well away from the domain wall and the electroweak Higgs. For this solution, we have $C_{\overline{(e_R)^c} u_R \phi_c} \sim 10^{-135}$, $C_{\overline{(u_R)^c} d_R \phi_c^*} \sim 10^{-129}$, $C_{\overline{L} Q \phi_c} \sim 10^{-94}$ and $C_{QQ\phi_c^*} \sim 10^{-99}$, so that the bound on m_c set by the less suppressed decay mode involving the left-chiral fermions is of the order of 10^{-71} eV. For all neutrino mass hierarchies, the coupling constant $C_{\overline{(\nu_R)^c} d_R \phi_c}$ is also well below 10^{-100}, so that $p \to \nu_e \pi^+$ is also negligible.

Now that it has been demonstrated that the three generation mass hierarchies can be generated from the exponential dependences of the overlaps on the domain wall couplings while suppressing proton decay, the next step is to incorporate quark and lepton mixing.

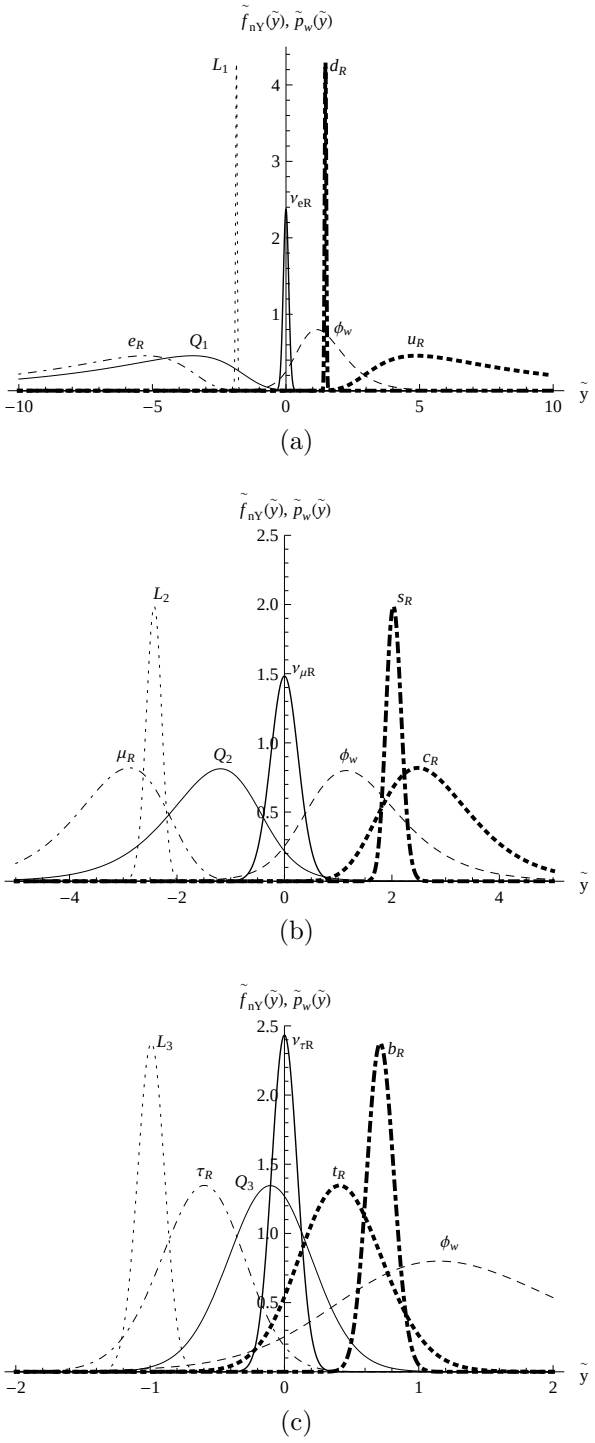

Figure 2.11: Plots of the profiles of the first (a), second (b), and third generation (c) of fermions with the parameter choice of Table 2.1 and the of the normal hierarchy parameter choice in Table 2.4.

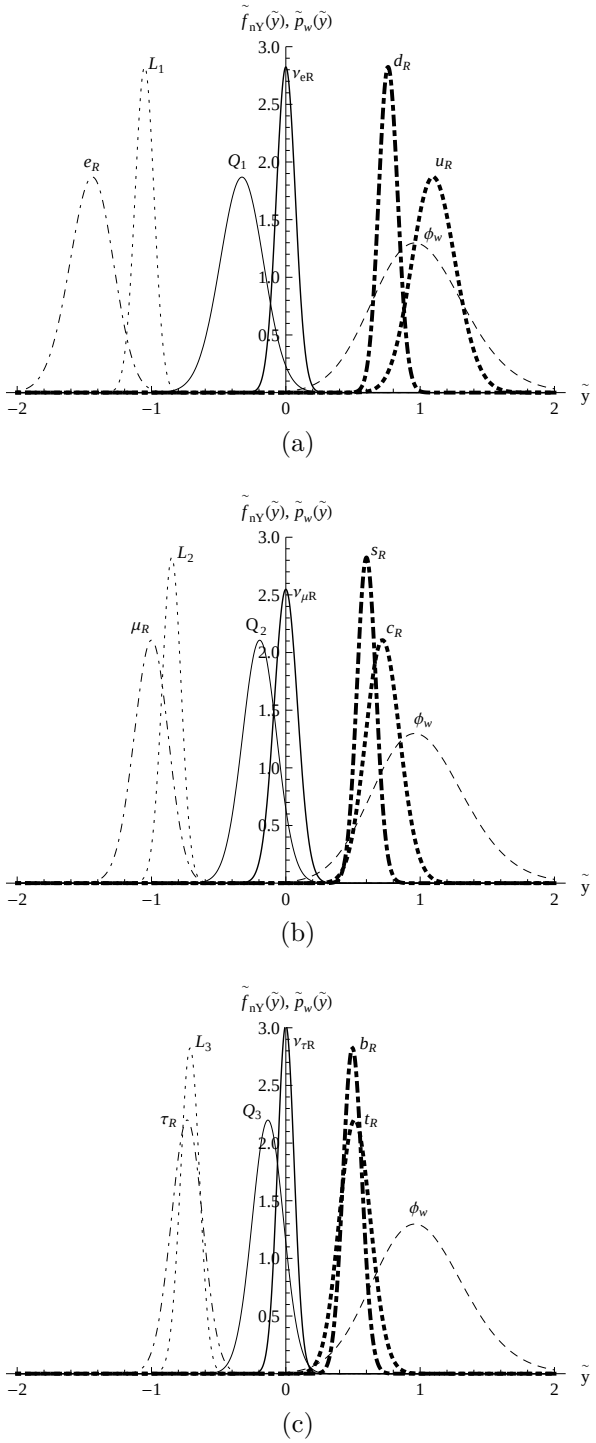

Figure 2.12: Plots of the profiles of the first (a), second (b), and third generation (c) of fermions with the parameter choice of Table 2.2 and the of the normal neutrino mass hierarchy parameter choice in Table 2.5.

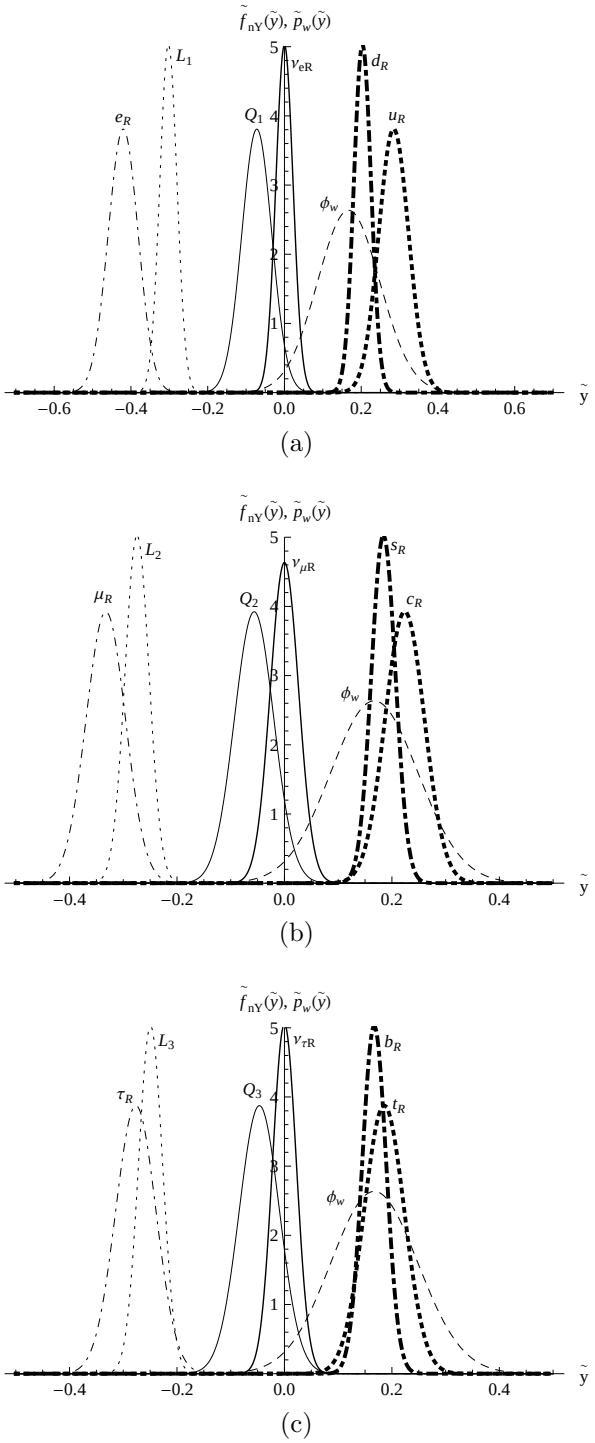

Figure 2.13: Plots of the profiles of the first (a), second (b), and third generation (c) of fermions with the parameter choice of Table 2.3 and the normal hierarchy parameter choice in Table 2.6.

2.1.3 Accounting for the Cabibbo angle in the two-generation case

To produce realistic mass matrices, we must account for the fermion mixing angles as well as the masses. For the sake of simplicity, we will work with two generations and show that the Cabibbo mixing angle can be produced along with the mass hierarchy.

Performing the required analysis is quite complicated since, if we are to assume that all the 5D Yukawa couplings are equal, including the off diagonal couplings, then the order of the analogous equations giving desired mass matrix element ratios from the overlaps is the equal to the number of families in the theory. Thus, to generate the Cabibbo angle, one must solve equations which are quadratic in the overlaps, and which are also no longer separated with respect to the domain wall parameters. For the CKM matrix it is even worse since the equations are cubic. This raises difficulties, in particular, with the down and electron sectors, since these sectors depend on all of the background couplings of the charged fermions, which amount to eight for two generations. Hence, we are forced to start with the up quark sector first, for convenience, since it only depends on four couplings. This makes it difficult to guarantee that the Dirac neutrino masses will be light.

Instead of directly solving the equations quadratic in the overlaps, we will try to generate mass matrices approximately equal to the Cholesky decompositions of the desired mass matrices squared, $M^\dagger M$. This is similar to an approach of generating mass matrices in NNI (Nearest-Neighbour-Interaction) basis for the three generation case, as was done in the analysis with Gaussian profiles done in [90], and by Mirabelli and Schmaltz [89]. The advantage of this approach is that we can now do the analysis in terms of equations linear in the overlaps instead. The main disadvantage is that we must rely on one of the off diagonal terms being significantly suppressed compared to the other couplings.

It turns out that this approach can get the charged fermion mass hierarchies and the Cabbibo angle. Taking all the electroweak Yukawa couplings to be $h_+^{ij} = h_-^{ij} = h_3^{ij} = 0.089104k^{-\frac{1}{2}}$, the Higgs parameters to be those of Eq. 2.11, and making the choices for the domain wall Yukawas in Table 2.7, we obtain the following mass matrices correct to three significant figures,

$$M_u = \begin{pmatrix} 1.04 \times 10^3 & 7.28 \times 10^2 \\ 2.77 \times 10^{-3} & 3.05 \end{pmatrix}, \tag{2.42}$$

$$M_d = \begin{pmatrix} 70.3 & 77.8 \\ \sim 0 & 7.47 \end{pmatrix}, \tag{2.43}$$

i	$\tilde{h}^i_{5\eta}$	$\tilde{h}^i_{5\chi}$	$\tilde{h}^i_{10\eta}$	$\tilde{h}^i_{10\chi}$
1	12.585	-36.719	100	53.346
2	365.78	-1708.2	2.5273	27.095

Table 2.7: The choices for the domain wall parameters with Higgs parameters from Eq. 2.11 and $h^{ij}_+ = h^{ij}_- = h^{ij}_3 = 0.089104k^{-\frac{1}{2}}$ for $i, j = 1, 2, 3$

and

$$M_e = \begin{pmatrix} 106 & \sim 0 \\ 0.465 & 0.511 \end{pmatrix}. \tag{2.44}$$

The resultant left diagonalization angle for M_u is $\Theta_u = 55°$, and the left diagonalization angle for M_d is $\Theta_d = 42°$, yielding the Cabibbo angle $\Theta_c = \Theta_u - \Theta_d = 13°$. Taking the square roots of the eigenvalues of $M_u^\dagger M_u$, $M_d^\dagger M_d$, and $M_e^\dagger M_e$ yields the masses of the charged fermions, and they turn out to be those in Table 2.8.

i	m^i_E(eV)	m^i_U(eV)	m^i_D(eV)
1	0.511	2.5	5.0
2	106	1.3×10^3	1.1×10^2

Table 2.8: The masses of the mass eigenstates in the electron, up and down type sectors respectively with the parameter choice of Table 2.7

This solution does not permit two light neutrino masses for the case of a Dirac neutrino. For example, for the parameter choice $\tilde{h}^1_{1\eta} = \tilde{h}^2_{1\eta} = 100$, the mass matrix for the neutrino is

$$M_\nu = \begin{pmatrix} 6.23 & \sim 0 \\ 6.23 & \sim 0 \end{pmatrix}, \tag{2.45}$$

which yields $m_{\nu 1} = 0$ and $m_{\nu 2} = 8.8$ MeV. Because for this solution one of the left weak eigenstates of the neutrino has a $\tilde{h}^1_{5\chi}/\tilde{h}^1_{5\eta}$ ratio larger in magnitude, and thus is more distant from the wall and the Higgs, the mass matrix for the neutrino for this solution will always have the entries of one column being larger than the other for significantly large $\tilde{h}^i_{1\eta}$ and since one of the eigenvalues is typically of the same order as the larger of the two elements

in the larger column in such a matrix. In the limit $\tilde{h}^i_{1\eta} \to \infty$ for $i = 1, 2$,

$$\begin{aligned} M_u^{ij} &= h_3 \bar{v} \int f_{\nu_R^i}(y) f_{L^j}(y) p_w(y)\, dy \\ &\to h_3 \bar{v} f_{L^j}(0) p_w(0) \end{aligned} \tag{2.46}$$

as the profiles for the right handed neutrinos converge to delta functions at $y = 0$, one obtains the mass matrix,

$$M_\nu = \begin{pmatrix} 5.81 & \sim 0 \\ 5.81 & \sim 0 \end{pmatrix}, \tag{2.47}$$

which yields neutrino masses of $m_{\nu_1} = 0$ and $m_{\nu_2} = 8.2$ MeV. Thus, the best we can do for this solution which yields Cabibbo mixing and the charged mass hierarchy, for the case of a Dirac neutrino, is to generate a massless neutrino, and a neutrino about 2-3 MeV heavier than a down quark.

This does not prove that there is no solution for a Dirac neutrino which incorporates quark mixing and the fermion mass hierarchy. The scheme we used and the section of parameter space searched led to one of the lepton doublets being placed too close to the right handed neutrino and too delocalized to support two light neutrinos. A more thorough search of the parameter space, perhaps utilizing a Monte Carlo method, will have to be done to determine whether a solution supporting two sufficiently light neutrinos exists for the case of a Dirac neutrino.

For a Majorana neutrino, however, this solution presents no such problems. As was shown earlier in this paper, the seesaw mechanism can be employed in the model, and can thus be used to suppress the mass of the heavier neutrino.

The set of domain wall parameters in Table 2.7 generate the desired mass spectrum and the Cabibbo angle. The ratio between the parameters smallest ($\tilde{h}^2_{10\eta} = 2.5273$) and largest ($\tilde{h}^2_{5\chi} = -1708.2$) in magnitude is roughly 670. To reduce this, we would need to find solutions with a more localized electroweak Higgs, such as those resulting from the parameter choices Eqs. 2.12 and 2.13. Finding such solutions has been difficult, however, and we will leave this to be done in later work.

Proton decay for this solution cannot be suppressed without fine-tuning the colored Higgs mass. Since we are using the Higgs parameter choice of Eq. 2.11 and not that of Eq. 2.13, the colored Higgs is sufficiently close to the domain wall so that the decay modes involving just the left-chiral fermions are not sufficiently suppressed. Furthermore, since the off-diagonal electroweak Yukawa constants are now non-zero, operators such $\overline{u_R}(\mu_R)\phi_c^*$ and $\overline{s_R}(u_R)^c\phi_c$ are present in the action. This means we also have to account for the decay

modes $p \to \mu^+\pi^0$, $p \to e^+K^0$ and $p \to \mu^+K^0$, which have partial lifetime lower bounds of 6.6×10^{33} years [115], 1.5×10^{32} years [116] and 1.2×10^{32} years [116]. After computing the overlaps to find the interaction strengths in the weak eigenbasis, transforming to the mass eigenbasis and then performing similar analyses for each of the decay modes, we find that even the most constraining decay mode involving just right-chiral fermions, that of $p \to \mu^+\pi^0$ sets a lower bound on the colored Higgs mass of 3.2×10^9 GeV. In fact both the modes involving the antimuon set higher bounds then those producing positrons since the coupling for the $\overline{u_R}(\mu_R)\phi_c^*$ vertex is a few orders of magnitude higher than that for the $\overline{u_R}(e_R)\phi_c^*$ vertex, due to right handed muon being closer on average to the wall. The decay modes involving left-chiral fermions are still barely suppressed, with the decay modes involving just left-chiral fermions for both $p \to e^+\pi^0$ and $p \to \mu^+\pi^0$ setting lower bounds on m_c of order 10^{15} GeV. Obviously, this situation would change if we used the Higgs parameter choice of Eq. 2.13 for which the colored Higgs is well displaced from all fermions and the domain wall.

2.1.4 Lepton mixing

It appears that generating near tribimaximal mixing in the lepton sector is incompatible with the results for the fermion mass hierarchy problem, for both Dirac and Majorana neutrinos.

As we have seen, solutions to the mass hierarchy problem typically involve shifting the lepton doublets to different locations away from the domain wall and the electroweak Higgs. This means that for such solutions, assuming the domain wall couplings for the right handed neutrinos are roughly equal, the neutrino mass matrix will take the form,

$$M_\nu \sim \begin{pmatrix} a_1 & b_1\epsilon & c_1\epsilon^2 \\ a_2 & b_2\epsilon & c_2\epsilon^2 \\ a_3 & b_3\epsilon & c_3\epsilon^2 \end{pmatrix}, \tag{2.48}$$

where $\epsilon \ll 1$ and the constants a_i, b_i and c_i are all taken to be roughly the same order of magnitude. Then the mass matrix squared will take the form

$$M_\nu^\dagger M_\nu \sim \begin{pmatrix} |\mathbf{a}|^2 & \mathbf{a}.\mathbf{b}\epsilon & \mathbf{a}.\mathbf{c}\epsilon^2 \\ \mathbf{a}.\mathbf{b}\epsilon & |\mathbf{b}|^2\epsilon^2 & \mathbf{b}.\mathbf{c}\epsilon^3 \\ \mathbf{a}.\mathbf{c}\epsilon^2 & \mathbf{b}.\mathbf{c}\epsilon^3 & |\mathbf{c}|^2\epsilon^4 \end{pmatrix}. \tag{2.49}$$

$M_\nu^\dagger M_\nu$ is clearly hierarchical, and thus the neutrino sector cannot generate two large mixing angles. From the electron sector, we know that both the lepton doublets and the right handed electrons are placed away from the

electroweak Higgs doublet, and thus their overlaps decrease rapidly with the splittings, inducing hierarchical electron mass matrices. Hence, we cannot generate large mixing angles in the electron sector either, with the generic type of solution for the mass hierarchy, and thus tribimaximal mixing cannot be produced in the lepton sector for the case of a Dirac neutrino.

The utilization of the seesaw mechanism also fails to produce tribimaximal mixing. Since all the right handed neutrinos are all localized at the same place, all the overlap integrals which contribute to the Majorana mass matrix are of the same order of magnitude unless there is a substantial hierarchy amongst their domain wall parameters. Hence, for most solutions of interest, the right handed Majorana mass matrix assumes a non-hierarchal form. However, the neutrino Dirac mass matrices will maintain their hierarchical form since the lepton doublets will still be separated, and therefore the effective left handed neutrino Majorana mass matrix, $M_L \sim -m_D^T M_R m_D$ is rendered hierarchical, and thus small lepton mixing angles for a Majorana neutrino will result.

There are several approaches one could take to the problem of lepton mixing in this model. The most obvious is the inclusion of a discrete flavor symmetry like A_4 or its double cover T'. This has in fact been employed successfully in $RS1$ [94] and orbifold models [87]. We will add a discrete A_4 symmetry in the next chapter.

It was also not surprising that a solution was not found in the Dirac case, since the initial assumption that the couplings to η and χ commuted cut the number of background Yukawa couplings to 15, and the assumption of universal electroweak Yukawa couplings cut the number of free parameters in the electroweak Yukawa sector to 1, giving 16 free parameters in total which determine the masses. If we want to generate everything except CP violation from non-hierarchical electroweak Yukawa couplings then, we need to generate the correct mass ratios for the charged fermions, quark and lepton mixing angles, the correct Δm_{12}^2 and Δm_{23}^2 and an acceptable neutrino mass scale, which amounts to 18 constraints. Thus, we were never guaranteed such a solution. Letting go of the initial assumption that the background couplings commute allows us to introduce mixing angles and CP phases from that sector. In practice, solving the relevant equations for the fermion profiles with non-commuting $h_{n\eta}$ and $h_{n\chi}$, is difficult and must be solved numerically; we do not perform an analysis of this situation in this thesis.

2.2 Conclusion

As we have seen, the utilization of extra dimensions is particularly useful in explaining the fermion mass hierarchy problem. This is particularly evident in the analysis without quark and lepton mixing, where we were able to show that the mass hierarchy which spans at least 12 orders of magnitude could be generated from a set of domain wall Yukawa parameters which have a spread of roughly an order of magnitude. Furthermore, this spread could be reduced even further by making the Higgs profile more localized. As an added bonus in this analysis, by choosing parameters such that the colored Higgs was well displaced from the domain wall and the electroweak Higgs, the doublet-triplet splitting problem was solved and proton decay suppressed to such an extent that the colored Higgs mass no longer had to be fine tuned.

Generation of quark mixing from the overlaps after initially assuming non-hierarchal $SU(5)$ electroweak Yukawa coupling constants also looks promising, and we successfully generated the Cabibbo angle and the fermion mass hierarchy for the case with two generations and Majorana neutrinos. Generically, small quark mixing angles and fermion mass hierarchies naturally arise from hierarchical mass matrices, although a more thorough numerical analysis will have to be done to find solutions for the full CKM matrix.

We have given some arguments as to why the problem of tribimaximal lepton mixing problem cannot be solved simultaneously with the quark mixing and fermion mass hierarchy problems in this braneworld model. Typically with solutions to the latter two problems, the lepton doublets are spread out away from the Higgs profile, rendering the electron and Dirac neutrino mass matrices hierarchical, leading to small mixing angles. We believe this may be amended with the addition of a discrete flavor symmetry like A_4, or by dropping the assumption that the η and χ couplings commute. The addition of a flavor symmetry to the model as well as a more thorough analysis of the parameter space will be treated in the next chapter.

Chapter 3

Large lepton mixing angles from a 4+1-dimensional $SU(5) \times A_4$ domain-wall braneworld model

In the previous chapter, we performed an analysis on the Yukawa coupling parameter space of the DGV model which showed that the fermion mass hierarchy could be accounted for naturally while satisfying the current data on the squared mass differences for the neutrinos, as well as performing a calculation with two generations which yielded the correct Cabibbo angle, showing quark mixing could likely be generated as well. We were also able to suppress proton decay by splitting the components of the Higgs quintet appropriately, using the same scheme for choosing the background and electroweak Yukawa coupling constants. We also gave reasons why large lepton mixing angles could not be generated using the same scheme used to generate the fermion mass hierarchy and quark mixing. This suggests that we need to include a further mechanism for generating the PMNS matrix.

As we have seen in Sec. 1.10, models with discrete flavor symmetries such as A_4 represent an interesting approach to explaining the quark and lepton mixing patterns. Models of this type were first proposed in [69]. For other interesting papers on discrete flavor symmetries, see [70, 71, 73]. In the simplest model using A_4 in 3+1D with just the Standard Model gauge group [73], typically the different mixing patterns are explained due to A_4 being spontaneously broken to different subgroups in each sector: $A_4 \to \mathbb{Z}_3$ in the charged fermion sector, and $A_4 \to \mathbb{Z}_2$ in the neutrino sector. This is typically achieved by the addition of two A_4 triplet Higgs fields which couple to different sectors and which attain different vacuum expectation

value (VEV) patterns. When this is done, the CKM matrix is found to be close to the identity and the PMNS matrix assumes a tribimaximal form. When interactions between the two A_4 triplet flavons are switched off, this arrangement is valid since the two non-aligned VEVs are both global minima of the potentials for each flavon. However, when interactions are switched on the two VEV patterns tend to align and thus the responsible cubic and quartic coupling constants have to be fine-tuned significantly to be small. This problem is known as the vacuum realignment problem, and is typical of theories with discrete flavor symmetries which have extended Higgs sectors of this type. There are in general three ways to ensure that the troublesome interactions are suppressed.

One is to make the theory supersymmetric so that the undesired terms are forbidden by holomorphy and renormalization constraints on the superpotential [73]. Another is to use additional discrete symmetries forbidding the interactions [85]. Yet another is to exploit the physics of extra dimensions, by localising the flavons on different branes or by splitting their extra-dimensional profiles with very little overlap so that the interactions are naturally eliminated or very suppressed [86, 87, 88].

Given that extra-dimensional models have been very successful at explaining the hierarchy problem and can ameliorate one of the major problems of discrete flavor symmetry models, and that discrete flavor symmetries can reproduce realistic leptonic mixing patterns which can be difficult to produce in extra-dimensional models, the combination of the two approaches is quite attractive. There have already been many models in the literature uniting the two approaches, particularly with regards to the warped RS1 scenario. Altarelli and Feruglio first proposed a model based on A_4 with an SM gauge group and the flavons restricted to different branes [86]. There have also been models with GUTs [87, 92, 121] as well as models with more complicated discrete flavor groups such as the double cover of A_4, T' [93]. It was also shown by Kadosh and Pallante that the flavons could be put into the bulk to allow enough cross-talk between the flavons to generate small quark mixing angles while at the same time maintaining the desired vacuum alignment [88]. It is also interesting to note that some 3+1D models with flavons in the $1'$ and $1''$ representations of A_4, which our model also contains and were not previously considered in discrete flavor symmetry models, were proposed in [122, 121]. One of these [121] was also based on $SU(5) \times A_4$.

In this chapter, we extend the $SU(5)$ 4+1D domain-wall braneworld model of Davies, George and Volkas [23] with the inclusion of a discrete A_4 flavor symmetry group. We utilize the same domain-wall background solution that we used in the previous chapter. We then dynamically localize the required fermions and flavon Higgs fields embedded in appropriate $SU(5) \times A_4$

representations to the background solution via Yukawa and quartic coupling to the kink-lump solution respectively, and we give the forms of the profiles for the resultant localized SM components which are split according to their hypercharges, yielding a natural realization of the split fermion mechanism. We show that the results in [1] with regard to the fermion mass hierarchy problem can be reproduced as well as quark mixing, neutrino mass squared differences and a tribimaximal lepton mixing matrix from a set of 5D Yukawa parameters which are all of the same order of magnitude. In our model, it turns out the required scale of the breaking of A_4 by the triplet flavons can be altered due to the fact that the Dirac masses for the neutrinos can be suppressed by the split-fermion mechanism, and these scales can vary from the electroweak scale all the way up to the GUT scale. We finally show that splitting the charged A_4-triplet flavon from the gauge singlet A_4-triplet flavon can exponentially suppress the interactions responsible for the vacuum realignment problem.

Given we are still utilizing the same background solution from Sec. 1.6, we simply begin the next section by outlining both the fermionic and scalar matter content of our model as well as the $SU(5) \times A_4$ representations to which they are assigned. Section 3.2 and Sec. 3.3 then address the dynamical localization of the fermionic matter and the Higgs flavon scalars respectively. Section 3.4 gives details of the electroweak Yukawa Lagrangian of the model and the forms of the fermion mass matrices that arise after the A_4-triplet flavons condense with the desired vacuum alignment. Our parameter fitting analysis yielding the desired fermion mass spectra, quark mixing, tribimaximal lepton mixing and the correct neutrino mass squared differences is given in Sec. 3.5. In Sec. 3.6 we discuss our solution to the vacuum realignment problem in our model, with the full flavon interaction potentials given in Appendix B. Section 3.7 is our conclusion.

3.1 The Matter Content and A_4 Representations

We now need to introduce three generations of quarks and leptons as well as Higgs fields embedded in representations of $SU(5) \times A_4$. As is usual for $SU(5)$ grand unified theories (GUTs), the lepton doublets and right-chiral down-type quarks are embedded into $SU(5)$ quintets, while the quark doublets, right-chiral up-type quarks and right-chiral charged leptons are embedded into $SU(5)$ decuplets. Right-chiral neutrinos are introduced as gauge singlets. We review the group theory of A_4 in Appendix A.

Before we discuss the fermions and the Higgs content to be localized to the wall, we should mention that the fields η and χ which form the background solution are given the same $SU(5)$ representations that they were assigned to in Sec. 1.6

In addition to the representations under the gauge group and the discrete flavor symmetry, we must also consider the transformation properties of the fields under the discrete $\mathbb{Z}_2$ reflection symmetry which ensures topological stability of the domain wall. Since interactions which localize fermions to the domain wall are Yukawa interactions of the form $\eta\overline{\Psi}\Psi$ and η has negative parity, we must have $\overline{\Psi}\Psi \to -\overline{\Psi}\Psi$, which we can satisfy by choosing $\Psi \to i\Gamma^5\Psi$ or $\Psi \to -i\Gamma^5\Psi$. Scalars can have either positive or negative parity.

The representations of the fermions, denoted as $(R_1,\ R_2)$, where R_1 denotes $SU(5)$ representation and R_2 denotes the representation under A_4, are chosen to be

$$\begin{gathered}\Psi_5 \sim (5^*,\ 1),\ \Psi_5' \sim (5^*,\ 1'),\ \Psi_5'' \sim (5^*,\ 1'') \\ \Psi_{10}^i \sim (10, 1) \text{ for } i = 1, 2, 3 \\ N \sim (1, 3)\end{gathered} \tag{3.1}$$

where N is an A_4-triplet containing all three right-chiral neutrinos. Under the reflection symmetry, $N \to -i\Gamma^5 N$ and all other fermions transform as $\Psi \to i\Gamma^5\Psi$.

For the Higgs sector, we require at least one Higgs quintet which contains an electroweak Higgs and a colored Higgs scalar, and some additional flavons as per usual in models with discrete flavor symmetries. Since the three fermion quintets Ψ_5, Ψ_5', and Ψ_5'' are in the 1, 1′, and 1″ respectively, and since all the fermion decuplets are singlets under A_4, to form A_4-invariant Yukawa interactions which generate charged lepton and down-type quark masses we similarly require a Higgs quintet under each of the A_4 representations 1, 1′, and 1″. As all three generations of right-chiral neutrino are embedded into an A_4 triplet, and since we must form Yukawa interactions involving this triplet and each of the fermion quintets to generate a Dirac neutrino mass matrix, we must have another Higgs quintet in the triplet representation of A_4. For the desired off-diagonal elements for the Majorana mass matrix for the neutrinos, we also need a gauge singlet Higgs scalar transforming as a triplet under A_4. Thus, our field content for the Higgs sector can be summarized as

$$\begin{gathered}\Phi \sim (5^*,\ 1),\ \Phi' \sim (5^*,\ 1'),\ \Phi'' \sim (5^*,\ 1'') \\ \rho \sim (5^*,\ 3),\ \varphi \sim (1,\ 3).\end{gathered} \tag{3.2}$$

Under the $\mathbb{Z}_2$ reflection symmetry, all scalars except φ are chosen to have

negative parity, while φ is chosen to have positive parity for reasons which will be discussed later in this chapter.

3.2 Localization of Chiral Fermions

To reproduce a Standard Model with an A_4 flavor symmetry on the domain wall, we still need to localize the fermions by coupling them to the background fields η and χ. The results are almost entirely the same as those in the case without the A_4 symmetry covered in the previous chapter, but given that the presence of the A_4 symmetry imposes some constraints, we go through the same analysis for the $SU(5) \times A_4$ model for the sake of completeness.

Let's consider the right-chiral neutrinos first. Since the right-chiral neutrinos are embedded into A_4 triplets and since they are gauge singlets, they couple to η only and the trapping interaction is simply

$$Y_{\eta\chi N} = -h_{1\eta}(\overline{N}N)_1\eta. \tag{3.3}$$

The 5D Dirac equation that results from this is thus

$$i\Gamma^M\partial_M N + h_{1\eta}\eta(y)N = 0. \tag{3.4}$$

To examine the effective SM Yukawa interactions for the neutrinos in the effective 4D theory on the wall, we can ignore the Kaluza-Klein (KK) modes and consider only the localized zero mode of the field N. We thus can simply look for a solution of the form $N(x,y) = f_N(y)\nu_R(x)$, where $f_N(y)$ is the zero mode profile and $\nu_R(x)$ is an A_4-triplet of 4D massless right-chiral neutrinos satisfying the ansatz

$$\begin{aligned} i\gamma^\mu\partial_\mu\nu_R(x) &= 0, \\ \gamma^5\nu_R(x) &= +\nu_R(x). \end{aligned} \tag{3.5}$$

Substituting this ansatz into Eq. 3.4, we find that the profile $f_N(y)$ satifies the first order differential equation

$$\frac{df_N(y)}{dy} + h_{1\eta}v\tanh(ky)f_N(y) = 0, \tag{3.6}$$

which can be easily solved to yield

$$\begin{aligned} f_N(y) &= C_N\,\mathrm{sech}^{\frac{h_{1\eta}v}{k}}(ky), \\ &= \tilde{C}_N k^{\frac{1}{2}}\,\mathrm{sech}^{\tilde{h}_{1\eta}}(\tilde{y}), \end{aligned} \tag{3.7}$$

where $\tilde{y} = ky$, $\tilde{h}_{1\eta} = \frac{h_{1\eta}v}{k}$ and $\tilde{C}_N = C_N k^{-\frac{1}{2}}$ are the non-dimensionalized extra-dimensional coordinate, background Yukawa coupling constant and normalization factor respectively.

For the analysis in this paper it is convenient to always work with dimensionless variables and functions, thus we define the non-dimensionalized profile $\tilde{f}_N(\tilde{y}) = k^{-\frac{1}{2}} f_N(\tilde{y})$ and normalize it to one to obtain the correct normalization for the effective 4D kinetic term for the zero mode ν_R. Since any field increases in mass dimension by half when the dimensionality of spacetime is increased by one, we non-dimensionalize the profiles for any effective 4D mode is the same way.

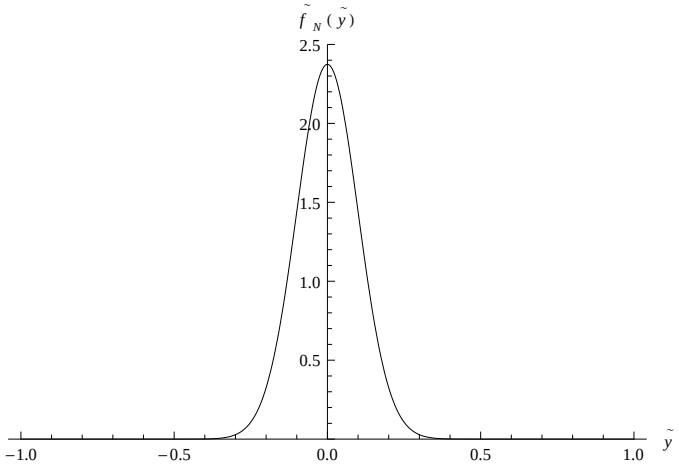

Figure 3.1: The localized right-chiral neutrino triplet profile for the parameter choice $\tilde{h}_{1\eta} = 100$.

As can be seen in Fig. 3.1, the dimensionless profile $\tilde{f}_N$ is peaked about $\tilde{y} = 0$ and decays exponentially away from the wall. Hence ν_R is indeed localized on the domain wall.

Next, we consider the fermion quintets. We have one of each of the quintets in the 1, 1′, and 1″ representations of A_4, which means that due to A_4-invariance, Yukawa interactions between different generations of the quintets and the background fields η and χ are forbidden. In this case, the coupling of each of these fermions to the background is given by

$$\begin{aligned} Y_{\eta\chi 5} = {} & h_{5\eta}\overline{\Psi_5}\Psi_5\eta + h_{5\chi}\overline{\Psi_5}\chi^T\Psi_5 \\ & + h'_{5\eta}\overline{\Psi'_5}\Psi'_5\eta + h'_{5\chi}\overline{\Psi'_5}\chi^T\Psi'_5 \\ & + h''_{5\eta}\overline{\Psi''_5}\Psi''_5\eta + h''_{5\chi}\overline{\Psi''_5}\chi^T\Psi''_5. \end{aligned} \tag{3.8}$$

Note the relative minus sign change between the interactions of η with N and η with the fermion quintets. This choice was made so that a positive $h_{5\eta}$, $h'_{5\eta}$ and $h''_{5\eta}$ correspond to the existence of left-chiral zero modes for the SM components of the respective quintets.

To find the profiles of these left-chiral zero modes embedded in the quintets, we repeat the analysis done for the field N, writing $\Psi^R_{5Y}(x,y) = f^R_{5Y}(y)\psi^R_{5Y}(x)$ for $R = 1,\ 1',\ 1''$ and $Y = +\frac{2}{3},\ -1$, and having the zero modes $\psi^R_{5Y}(x)$ satisfy the same ansatz as ν_R given in Eq. 3.5 but with the second condition of right chirality replaced with that of left chirality $\gamma^5\psi^R_{5Y}(x) = -\psi^R_{5Y}(x)$. On substituting the ansatz into the 5D Dirac equation for Ψ^R_{5Y},

$$\Big[i\Gamma^M\partial_M - h^R_{5\eta}\eta(y) - \sqrt{\frac{3}{5}}\frac{Y}{2}h^R_{5\chi}\chi_1(y)\Big]\Psi^R_{5Y}(x,y) = 0, \tag{3.9}$$

we obtain the ordinary differential equation for the profiles $f^R_{5Y}(y)$

$$\Big[\frac{d}{dy} + h^R_{5\eta}v\tanh(ky) + h^R_{5\chi}A\sqrt{\frac{3}{5}}\frac{Y}{2}\,\mathrm{sech}\,(ky)\Big]f^R_{5Y}(y) = 0. \tag{3.10}$$

From the above equation, we find that the non-dimensionalized profiles $\tilde{f}^R_{5Y}(\tilde{y})$ of the left-chiral zero modes embedded in the quintets are given by

$$\begin{aligned}
&\tilde{f}^R_{5Y}(\tilde{y}) = \tilde{C}^R_{5Y}e^{-b^R_{5Y}(\tilde{y})},\\
&b^R_{5Y}(\tilde{y}) = \tilde{h}^R_{5\eta}\log\big[\cosh(\tilde{y})\big] + \sqrt{\frac{3}{5}}\tilde{h}^R_{5\chi}Y\arctan\big[\tanh(\frac{\tilde{y}}{2})\big]
\end{aligned} \tag{3.11}$$

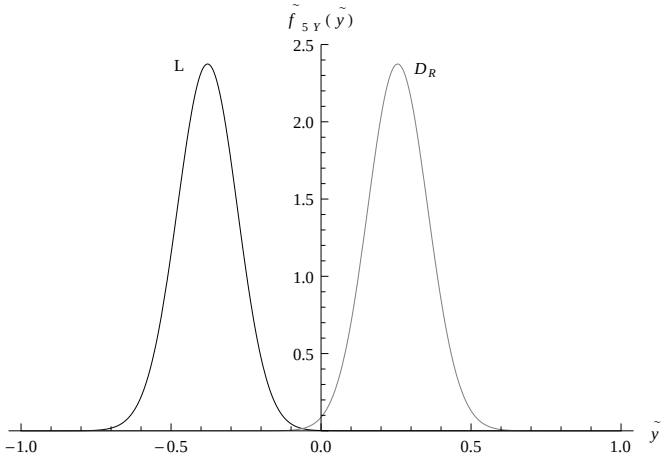

Figure 3.2: The profiles for the localized lepton doublet L and right-chiral down-type quark D_R arising from an arbitrary fermion quintet Ψ^R_5 for the parameter choice $\tilde{h}^R_{5\eta} = 100$ and $\tilde{h}^R_{5\chi} = -100$.

The profiles for the quintets are essentially the same as those of the previous chapter in the case that both matrices $h_{5\eta}$ and $h_{5\chi}$ (as defined in Sec. 2.0.1) are diagonal. Given that two of the generations are in the $1'$ and $1''$ representations, the A_4 symmetry imposes constraints so that there is no mixing between the different generations of quintets in the domain-wall Yukawa sector. A plot of the profiles for a lepton doublet L and a right-chiral down-type quark D_R, in any representation $R = 1, 1', 1''$ of A_4, for the example parameter choice $\tilde{h}^R_{5\eta} = 100$, $\tilde{h}^R_{5\chi} = -100$ is shown in Fig. 3.2.

Finally, we consider the localization of matter embedded in the decuplets Ψ^i_{10}. Since all of the decuplets are in the trivial representation of A_4, off-diagonal Yukawa couplings between η (or χ) and different generations of Ψ^i_{10} are permitted, unlike the case for the fermion quintets. This means that the localization properties of the SM components in the decuplets are essentially unchanged from the model in the previous chapter, although we will just restate the result for the sake of completeness and continuity. Therefore the most general coupling of the fermion decuplets to the background fields is

$$Y_{\eta\chi 10} = h^{ij}_{10\eta}\overline{\Psi^i_{10}}\Psi^j_{10}\eta - 2h^{ij}_{10\chi}Tr\Big(\overline{\Psi^i_{10}}\chi\Psi^j_{10}\Big). \tag{3.12}$$

Just as was the case for the decuplets in the previous chapter, the background Yukawa couplings $h_{10\eta} = \left(h^{ij}_{10\eta}\right)$ and $h_{10\chi} = \left(h^{ij}_{10\chi}\right)$ can be thought of as 3×3 matrices in the flavor space spanned by the initial 5D fields Ψ^i_{10}. Just like before, we will assume that $[h_{10\eta}, h_{10\chi}] = 0$ and that the 5D and 4D flavor rotation matrices (which were defined respectively by S_n and V_{nY} in the previous chapter) are equal to the identity matrix. In that case, since $h_{10\eta} = diag(h^1_{10\eta}, h^2_{10\eta}, h^3_{10\eta})$ and $h_{10\chi} = diag(h^1_{10\chi}, h^2_{10\chi}, h^3_{10\eta})$, each generation of decuplet Ψ^i_{10} for $i = 1, 2, 3$ obeys the Dirac equation

$$\begin{gathered}\Big[i\Gamma^M\partial_M - h^i_{10\eta}\eta(y) - \sqrt{\frac{3}{5}}\frac{Y}{2}h^i_{10\chi}\chi_1(y)\Big]\Psi^i_{10Y}(x,y) = 0, \\ \text{for } Y = -\frac{4}{3}, +\frac{1}{3}, +2.\end{gathered} \tag{3.13}$$

Writing $\Psi^i_{10Y}(x,y) = f^i_{10Y}(y)\psi^i_{10Y}(x)$ and again requiring that ψ^i_{10Y} is a left-chiral fermion which obeys the massless 4D Dirac equation, we easily find that the non-dimensionalized profiles $\tilde{f}^i_{10Y}(y)$ for the decuplet zero modes take the same form as those for the quintets,

$$\begin{aligned}\tilde{f}^i_{10Y}(\tilde{y}) &= \tilde{C}^i_{10Y}e^{-b^i_{10Y}(\tilde{y})}, \\ b^i_{10Y}(\tilde{y}) &= \tilde{h}^i_{10\eta}\log\big[\cosh(\tilde{y})\big] \\ &\quad + \sqrt{\frac{3}{5}}\tilde{h}^i_{10\chi}Y\arctan\big[\tanh(\frac{\tilde{y}}{2})\big].\end{aligned} \tag{3.14}$$

A plot of the profiles for the right-chiral electron-type lepton E_R, quark doublet Q_L and right-chiral up-type quark U_R for the example parameter choice $\tilde{h}^i_{10\eta} = 100$, $\tilde{h}^i_{10\chi} = 100$ for some generation i is shown in Fig. 3.3.

We have successfully shown that fermionic sector of the SM can be localized on the domain-wall brane. Now we must consider the localization of the Higgs scalars and show that electroweak symmetry breaking is possible.

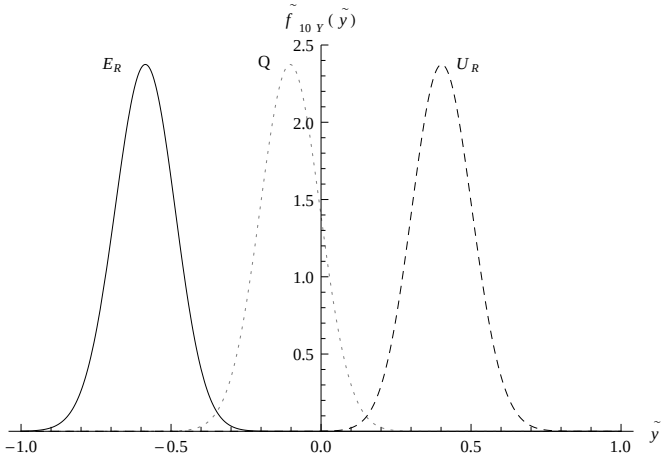

Figure 3.3: Profiles for a right-chiral electron-type lepton E_R, quark doublet Q and a right-chiral up-type quark U_R arising from an arbitrary fermion decuplet Ψ^i_{10} for the parameter choice $\tilde{h}^i_{10\eta} = 100$ and $\tilde{h}^i_{10\chi} = 100$.

3.3 Localization of Higgs fields

We now wish to localize the required Higgs scalars on the domain wall. This involves examining the Higgs scalar potential. As is typical of models with discrete flavor symmetries, we have an extended Higgs sector and the full Higgs potential is very complicated. However, most of these interactions are self-interactions amongst the flavons themselves, which do not contribute to the localization of the profiles at leading order. Hence it is sufficient to solely analyze the terms coupling the flavons to η and χ and the bulk masses of the flavons.

For the quintet scalars $\Phi = \Phi^{R=1}$, $\Phi' = \Phi^{R=1'}$, $\Phi'' = \Phi^{R=1''}$ and the A_4-triplet $\rho = \Phi^{R=3}$, the localization potentials are easy to write down. The localization potentials are essentially the same as the one for the Higgs quintet of the original $SU(5)$ model used in the previous chapter, although we will restate the result here for the sake of completeness and to define

the dimensionless constants governing the localization of these scalars in this $SU(5) \times A_4$ model. They are

$$\begin{aligned} W_{\Phi^R} &= \mu^2_{\Phi^R}(\Phi^R)^\dagger\Phi^R + \lambda_{\Phi^R\eta}(\Phi^R)^\dagger\Phi^R\eta^2 \\ &+ 2\lambda_{\Phi^R\chi 1}(\Phi^R)^\dagger\Phi^R Tr\big(\chi^2\big) + \lambda_{\Phi^R\chi 2}(\Phi^R)^\dagger\big(\chi^T\big)^2\Phi^R \\ &+ \lambda_{\Phi^R\eta\chi}(\Phi^R)^\dagger\chi^T\Phi^R\eta, \quad \text{for } R = 1,\, 1',\, 1'', \text{ and } 3. \end{aligned} \tag{3.15}$$

The mode analysis for the quintets follows that for the Higgs quintet in the original $SU(5)$ braneworld model described in [1]. Taking the ansatz

$$\begin{aligned} \Phi^R(x,y) &= \sum p^m_{RY}(y)\phi^m_{RY}(x), \\ \Box_{3+1}\phi^m_{RY}(x) &= -m^2_{RY}\phi^m_{RY}(x), \end{aligned} \tag{3.16}$$

and substituting it into the resultant 5D Klein-Gordon (KG) equation, one can show that the (non-dimensionalized) profiles for the modes of the Higgs quintets, $\tilde{p}^m_{RY}(\tilde{y})$ satisfy a Schrödinger equation with a hyperbolic Scarf potential, $V_{HS}(\tilde{y})$, which can be written as

$$\begin{aligned} -\frac{d^2\tilde{p}^m_{RY}}{d\tilde{y}^2} + V_{HS}(\tilde{y})\tilde{p}^m_{RY}(y) &= E_{RY}\tilde{p}^m_{RY}(\tilde{y}), \\ V_{HS}(\tilde{y}) = A^2_{RY} + \big(B^2_{RY} - A^2_{RY} - A_{RY}\big)\,\mathrm{sech}^2\,(\tilde{y}) \\ +B_{RY}(2A_{RY}+1)\,\mathrm{sech}\,(\tilde{y})\tanh\,(\tilde{y}), \end{aligned} \tag{3.17}$$

where A_{RY} and B_{RY} are defined as

$$\begin{aligned} A_{RY} = \frac{1}{2}\Bigg(&-1 + \Big(2\big[(\tilde{\lambda}_{\Phi^R\chi 1} + \frac{3Y^2}{20}\tilde{\lambda}_{\Phi^R\chi 2} - \tilde{\lambda}_{\Phi^R\eta} - \frac{1}{4})^2 \\ &+ \frac{3Y^2}{20}\tilde{\lambda}^2_{\Phi^R\eta\chi}\big]^{\frac{1}{2}} - 2\tilde{\lambda}_{\Phi^R\chi 1} - \frac{3Y^2}{10}\tilde{\lambda}_{\Phi^R\chi 2} \\ &+ 2\tilde{\lambda}_{\Phi^R\eta} + \frac{1}{2}\Big)^{\frac{1}{2}}\Bigg), \\ B_{RY} = \frac{\sqrt{\frac{3}{5}}\frac{Y}{2}\tilde{\lambda}_{\Phi^R\eta\chi}}{2A_{RY}+1}, & \end{aligned} \tag{3.18}$$

the bulk masses, KK mode masses and quartic coupling constants to η and χ are non-dimensionalized as

$$\begin{aligned} \tilde{\mu}^2_{\Phi^R} = \frac{\mu^2_{\Phi^R}}{k^2}, \qquad \tilde{m}^2_{RY} = \frac{m^2_{RY}}{k^2}, \\ \tilde{\lambda}_{\Phi^R\eta} = \frac{\lambda_{\Phi^R\eta}v^2}{k^2}, \qquad \tilde{\lambda}_{\Phi^R\chi 1} = \frac{\lambda_{\Phi^R\chi 1}A^2}{k^2}, \\ \tilde{\lambda}_{\Phi^R\chi 2} = \frac{\lambda_{\Phi^R\chi 2}A^2}{k^2}, \qquad \tilde{\lambda}_{\Phi^R\eta\chi} = \frac{\lambda_{\Phi^R\eta\chi}vA}{k^2}, \end{aligned} \tag{3.19}$$

and E_{RY} are the eigenvalues of the above potential, which in terms of the mode masses and fundamental constants in Eq. 3.19 are

$$E_{RY} = \tilde{m}^2_{RY} - \tilde{\mu}^2_{\Phi^R} - \tilde{\lambda}_{\Phi^R \eta} + A^2_{RY}. \tag{3.20}$$

The eigenvalues of the hyperbolic Scarf potential are well known [39, 40, 58]. In the case that $A_{RY} > 0$, it is known that there exists a set of discrete bound modes for $n = 0, 1, ..., \lfloor A_{RY} \rfloor$ with eigenvalues

$$E^n_{RY} = 2nA_{RY} - n^2. \tag{3.21}$$

This gives the mass of the nth localized mode as

$$\tilde{m}^2_{nRY} = \tilde{\mu}^2_{\Phi^R} + \tilde{\lambda}_{\Phi^R \eta} - (A_{RY} - n)^2. \tag{3.22}$$

The lowest energy modes which have the same SM charges as the electroweak Higgs doublet, the $n = 0$, $Y = -1$ modes, are the ones we identify as our candidates for the flavons of the effective 4D field theory on the wall. It should be noted that there are regions of parameter space where for a given 5D flavon field, more than one mode has a tachyonic mass. It is also possible to choose parameters such that the modes for the $Y = +2/3$ components, which transform under $SU(3)_c$, would attain tachyonic masses, which would be disastrous since then $SU(3)_c$ would be broken on the wall. Thus, to maintain an unbroken $SU(3)_c$ while employing electroweak symmetry breaking and for the sake of simplicity in the analysis of the electroweak sector, we choose parameters such that only the $n = 0$ modes of the electroweak components of Φ^R attain tachyonic masses on the wall while all modes of the colored $Y = +2/3$ components attain positive squared masses.

It turns out the profiles of the $n = 0$ modes of the quintet scalars fields have exactly the same form as for the chiral zero modes for the fermionic quintets described in the previous section, with the A_{RY} playing a role analogous to the $h^R_{5\eta}$ and the B_{RY} being analogous to the $h^R_{5\chi}$,

$$\begin{aligned} \tilde{p}_{RY}(\tilde{y}) &= \tilde{C}_{\Phi^R Y} e^{-b_{\Phi^R Y}(\tilde{y})}, \\ b_{\Phi^R Y}(\tilde{y}) &= A_{RY} \log\left[\cosh(\tilde{y})\right] \\ &\quad + 2B_{RY} Y \arctan\left[\tanh(\frac{\tilde{y}}{2})\right]. \end{aligned} \tag{3.23}$$

From now on, we denote the profiles of the $n = 0$ modes as $p_{R=1,Y=-1}(y) = p_w(y)$, $p_{R=1',Y=-1}(y) = p_{w'}(y)$, $p_{R=1'',Y=-1}(y) = p_{w''}(y)$ and $p_{R=3,Y=-1}(y) = p_{\rho w}(y)$ for the electroweak components and the same except with w replaced by c for the $Y = +2/3$ components. Similarly we will denote

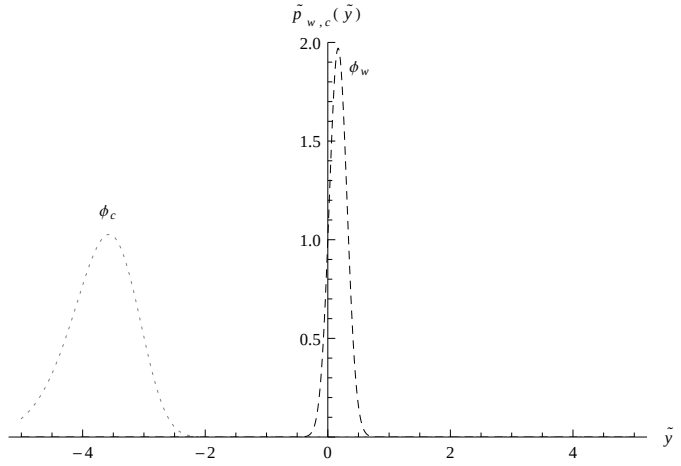

Figure 3.4: The profiles of the localized electroweak Higgs ϕ_w^R and colored Higgs scalar ϕ_c^R for an arbitrary quintet scalar Φ^R for parameters such that $\tilde{\lambda}_{\Phi^R\eta} = -7500$, $\tilde{\lambda}_{\Phi^R\chi 1} = 1500$, $\tilde{\lambda}_{\Phi^R\chi 2} = -75000$, and $\tilde{\lambda}_{\Phi^R\eta\chi} = 2000$.

the corresponding 4D fields for these modes as $\phi_{w,c}(x)$, $\phi_{w',c'}(x)$, $\phi_{w'',c''}(x)$ and $\rho_{w,c}(x)$ for $Y = -1, +2/3$ respectively. A plot of the profiles for the electroweak and colored scalar components of a Higgs quintet in any A_4 representation is shown in Fig. 3.4.

Now we turn to the gauge singlet, A_4-triplet scalar φ. The localization potential for φ is given by

$$W_\varphi = \mu_\varphi^2(\varphi\varphi)_1 + \lambda_{\varphi\eta}(\varphi\varphi)_1\eta^2 + 2\lambda_{\varphi\chi}(\varphi\varphi)_1 Tr\big(\chi^2\big). \tag{3.24}$$

In a similar fashion to the analysis of the quintet scalars, writing down the corresponding Euler-Lagrange equation, then writing $\varphi(x,y) = \sum p_\varphi^m(y)\phi_\varphi^m(x)$ and $\Box_{3+1}\phi_\varphi^m(x) = -m^2\phi_\varphi^m(x)$, we find that the modes of φ satisfy a Schrödinger equation with a well-known potential, in this case the Pöschl-Teller potential,

$$\Big[-\frac{d^2}{d\tilde{y}^2} + d(d+1)\tanh^2(\tilde{y}) - d\Big]\tilde{p}_\varphi^m(\tilde{y}) = E_\varphi^m\tilde{p}_\varphi^m(\tilde{y}), \tag{3.25}$$

where the parameter d and the eigenvalues E_φ^m are given in terms of the fundamental constants and mode masses as

$$\begin{aligned} d &= \frac{\sqrt{1 + 4(\tilde{\lambda}_{\varphi\eta} - \tilde{\lambda}_{\varphi\chi})} - 1}{2}, \\ E_\varphi^m &= \tilde{m}^2 - \tilde{\mu}^2 - \tilde{\lambda}_{\varphi\chi} - d. \end{aligned} \tag{3.26}$$

Given $d > 0$, there exists a tower of discrete localized modes with eigenvalues $E_\varphi^n = 2nd - n^2$, just as before with the hyperbolic Scarf Potentials for the quintet scalars. Similarly, we identify the effective 4D gauge singlet, A_4-triplet flavon φ_0 as the $n = 0$ mode, and we choose parameters such that this mode is the only one which attains a tachyonic mass on the domain-wall brane. The mass squared for this flavon localized to the wall is just

$$\tilde{m}_{\varphi_0}^2 = \tilde{\mu}_\varphi^2 + \tilde{\lambda}_{\varphi\chi} + d, \tag{3.27}$$

and the profile for φ_0, $\tilde{p}_{\varphi_0}(\tilde{y})$ is

$$\tilde{p}_{\varphi_0}(\tilde{y}) = \tilde{C}_{\varphi_0} \operatorname{sech}^d(\tilde{y}). \tag{3.28}$$

The lowest energy and tachyonic 4D mode of φ, φ_0, is always localized at $y = 0$. A plot of the profile for the example parameter choice $d = 500.00$ is shown in Fig. 3.5. In contrast, the profile of the electroweak component of the other A_4 triplet, ρ, is in general not localized about $y = 0$. The natural splitting between the two A_4 triplets will lead to solutions of the vacuum realignment problem, since the splitting will naturally suppress the responsible scalar interactions. This will be covered more extensively in Sec. 3.6.

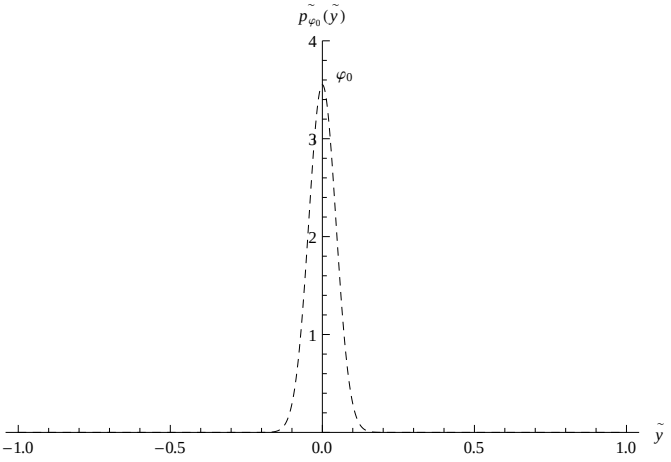

Figure 3.5: The profile of the lowest energy mode, φ_0, of the A_4 singlet flavon field φ for the parameter choice $d = 500.00$.

3.4 The Electroweak Yukawa Lagrangian and Fermion Mass Textures

Given we now have a set of localized modes for the fermions and flavons on the wall, we need to determine the electroweak Yukawa interactions in the model and the effective 4D mass textures after electroweak symmetry breaking. The full 5D electroweak Yukawa potential, Y_{EW}, is given by

$$\begin{aligned} Y_{EW} = & h_-^i \overline{(\Psi_5)^C} \Psi_{10}^i \Phi + h_-'^i \overline{(\Psi_5')^C} \Psi_{10}^i \Phi'' \\ & + h_-''^i \overline{(\Psi_5'')^C} \Psi_{10}^i \Phi' + h_+^{ij} \epsilon^{\alpha\beta\gamma\kappa\delta} \overline{(\Psi_{10}^i)^C_{\alpha\beta}} \Psi_{10}^j (\Phi_\delta)^* \\ & + h_\rho \overline{\Psi_5} (\rho N)_1 + h_\rho' \overline{\Psi_5'} (\rho N)_{1'} + h_\rho'' \overline{\Psi_5''} (\rho N)_{1''} \\ & + M (\overline{N} N^C)_1 + h_\varphi \left[(\overline{N} N^C)_{3s} . \varphi \right]_1 + h.c. \end{aligned} \tag{3.29}$$

From this, we can deduce that the elements of the effective 4D up-type quark mass matrix are given by

$$\begin{aligned} M_U^{ij} &= 4 h_+^{ij} \langle \phi_w \rangle \int f_{U_R^i}(y) f_{Q^j}(y) p_w(y) \, dy, \\ &= 4 \tilde{h}_+^{ij} \langle \phi_w \rangle \int \tilde{f}_{U_R^i}(\tilde{y}) \tilde{f}_{Q^j}(\tilde{y}) \tilde{p}_w(\tilde{y}) \, d\tilde{y}, \end{aligned} \tag{3.30}$$

where the electroweak Yukawa couplings are non-dimensionalized as $\tilde{h}_+^{ij} = h_+^{ij} k^{\frac{1}{2}}$. All electroweak Yukawas will be non-dimensionalized this way.

For the down-type quark sector, the rows of the mass matrix are given by

$$\begin{aligned} M_D^{1j} &= \frac{1}{\sqrt{2}} \tilde{h}_-^j \langle \phi_w \rangle \int \tilde{f}_{D_R}(\tilde{y}) \tilde{f}_{Q^j}(\tilde{y}) \tilde{p}_w(\tilde{y}) \, d\tilde{y}, \\ M_D^{2j} &= \frac{1}{\sqrt{2}} \tilde{h}_-'^j \langle \phi_w'' \rangle \int \tilde{f}_{D_R'}(\tilde{y}) \tilde{f}_{Q^j}(\tilde{y}) \tilde{p}_{w''}(\tilde{y}) \, d\tilde{y}, \\ M_D^{3j} &= \frac{1}{\sqrt{2}} \tilde{h}_-''^j \langle \phi_w' \rangle \int \tilde{f}_{D_R''}(\tilde{y}) \tilde{f}_{Q^j}(\tilde{y}) \tilde{p}_{w'}(\tilde{y}) \, d\tilde{y}, \end{aligned} \tag{3.31}$$

and similarly the columns of the electron-type lepton mass matrix is

$$\begin{aligned} M_E^{i1} &= \frac{1}{\sqrt{2}} \tilde{h}_-^i \langle \phi_w \rangle \int \tilde{f}_{E_R^i}(\tilde{y}) \tilde{f}_L(\tilde{y}) \tilde{p}_w(\tilde{y}) \, d\tilde{y}, \\ M_E^{i2} &= \frac{1}{\sqrt{2}} \tilde{h}_-'^i \langle \phi_w'' \rangle \int \tilde{f}_{E_R^i}(\tilde{y}) \tilde{f}_{L'}(\tilde{y}) \tilde{p}_{w''}(\tilde{y}) \, d\tilde{y}, \\ M_E^{i3} &= \frac{1}{\sqrt{2}} \tilde{h}_-''^i \langle \phi_w' \rangle \int \tilde{f}_{E_R^i}(\tilde{y}) \tilde{f}_{L''}(\tilde{y}) \tilde{p}_{w'}(\tilde{y}) \, d\tilde{y}. \end{aligned} \tag{3.32}$$

The Dirac neutrino mass matrix comes from the interaction terms coupling the fermion quintet fields, the neutrino triplet and the Higgs $(5^*, 3)$-field ρ. The form of this mass matrix is then dependent on the vacuum expectation value pattern of the lowest energy mode of ρ, $\rho_w(x)$. For this paper, we require that ρ_w takes the VEV pattern,

$$\langle \rho_w \rangle = (v_\rho, v_\rho, v_\rho). \tag{3.33}$$

Under this alignment, the form of the Dirac neutrino mass matrix takes the form

$$\begin{aligned} M_{\nu,D} &= \begin{pmatrix} m_\rho & m_\rho & m_\rho \\ m'_\rho & \omega m'_\rho & \omega^2 m'_\rho \\ m''_\rho & \omega^2 m''_\rho & \omega m''_\rho \end{pmatrix}, \\ &= \begin{pmatrix} \sqrt{3} m_\rho & 0 & 0 \\ 0 & \sqrt{3} m'_\rho & 0 \\ 0 & 0 & \sqrt{3} m''_\rho \end{pmatrix} .U(\omega), \end{aligned} \tag{3.34}$$

where the matrix $U(\omega)$ is given by

$$U(\omega) = \frac{1}{\sqrt{3}} \begin{pmatrix} 1 & 1 & 1 \\ 1 & \omega & \omega^2 \\ 1 & \omega^2 & \omega \end{pmatrix} \tag{3.35}$$

and

$$\begin{aligned} m_\rho &= \tilde{h}_\rho v_\rho \int \tilde{f}_N(\tilde{y}) \tilde{f}_L(\tilde{y}) \tilde{p}_{\rho w}(\tilde{y})\, d\tilde{y}, \\ m'_\rho &= \tilde{h}'_\rho v_\rho \int \tilde{f}_N(\tilde{y}) \tilde{f}_{L'}(\tilde{y}) \tilde{p}_{\rho w}(\tilde{y})\, d\tilde{y}, \\ m''_\rho &= \tilde{h}''_\rho v_\rho \int \tilde{f}_N(\tilde{y}) \tilde{f}_{L''}(\tilde{y}) \tilde{p}_{\rho w}(\tilde{y})\, d\tilde{y}. \end{aligned} \tag{3.36}$$

The matrix $U(\omega)$ is unitary, and such a factorization of a mass matrix where the mass eigenvalues can be arbitrary while the diagonalization angles are fixed is an example of *form diagonalizability* [72].

Lastly, the Majorana neutrino mass matrix is generated from the bare Majorana mass term $M(\overline{N}N^C)_1$ and the Yukawa interaction term $h_\varphi \left[(\overline{N}N^C)_{3s}.\varphi\right]_1$. The form of the Majorana mass matrix is obviously dependent on the VEV pattern of the lowest energy mode of φ, φ_0. Unlike for ρ_w, we instead give the field φ_0 the VEV pattern,

$$\langle \varphi_0 \rangle = (0, v_\varphi, 0). \tag{3.37}$$

This yields a Majorana neutrino mass matrix of the form,

$$M_{\nu,Maj} = \begin{pmatrix} M & 0 & M_\varphi \\ 0 & M & 0 \\ M_\varphi & 0 & M \end{pmatrix}, \tag{3.38}$$

where

$$M_\varphi = \tilde{h}_\varphi v_\varphi \int \tilde{f}_N^2(\tilde{y}) \tilde{p}_{\varphi_0}(\tilde{y})\, d\tilde{y}. \tag{3.39}$$

Clearly $M_{\nu,Maj}^{-1}$ is diagonalized by the orthogonal matrix

$$P = \frac{1}{\sqrt{2}} \begin{pmatrix} 1 & 0 & -1 \\ 0 & \sqrt{2} & 0 \\ 1 & 0 & 1 \end{pmatrix}. \tag{3.40}$$

Noting that the effective left Majorana neutrino mass matrix is given by $M_L \approx -M_{\nu,D} M_{\nu,Maj}^{-1} M_{\nu,D}^T$, in the special case that $m_\rho = m'_\rho = m''_\rho$, the left neutrino diagonalization matrix, $V_{\nu L}$ assumes the tribimaximal form

$$\begin{aligned} V_{\nu L} &= U(\omega) P, \\ &= \begin{pmatrix} \frac{2}{\sqrt{6}} & \frac{1}{\sqrt{3}} & 0 \\ -\frac{\omega}{\sqrt{6}} & \frac{\omega}{\sqrt{3}} & -\frac{e^{\pi i/6}}{\sqrt{2}} \\ -\frac{\omega^2}{\sqrt{6}} & \frac{\omega^2}{\sqrt{3}} & \frac{e^{5\pi i/6}}{\sqrt{2}} \end{pmatrix}. \end{aligned} \tag{3.41}$$

The PMNS matrix which describes lepton mixing is defined by $V_{PMNS} = V_{eL}^\dagger V_{\nu L}$, where V_{eL} is the left electron diagonalization matrix. Hence, if we obtain mass textures for the charged leptons such that $V_{eL} \approx 1$ we recover approximate tribimaximal lepton mixing which is favored by experiment.

One also finds that in the special case $m_\rho = m'_\rho = m''_\rho$, the mass eigenvalues for the left Majorana neutrino mass eigenstates are $\frac{-3m_\rho^2}{M+M_\varphi}$, $\frac{-3m_\rho^2}{M}$, and $\frac{-3m_\rho^2}{M-M_\varphi}$. For the purposes of this paper and for simplicity of analysis, we will choose parameters such that this condition is true. In the next section, we shall show that there exists a non-hierarchical parameter choice such that the Euler angles of the CKM matrix and the charged fermion masses are generated, while at the same time $V_{eL} \approx 1$, yielding the correct lepton mixing patterns, and that the neutrino mass data can be satisfied in the case that $m_\rho = m'_\rho = m''_\rho$.

3.5 Generating the Fermion Mass Hierachy, the CKM Matrix and Lepton Mixing: An Example

We now give an example parameter choice in which the fermion mass hierarchy, the Euler angles of the CKM matrix, lepton mixing and neutrino

mass squared differences are generated. With regard to the CKM matrix, at tree level the CP violating phase has to be put in by hand by giving the electroweak Yukawa coupling constants appropriate phases. We will for the sake of simplicity and clarity of the solution ignore this issue. Note that it is in principle possible for a CP phase in the CKM matrix to be generated from cross-talk between the quark and lepton sectors, since the PMNS matrix given in Eq. 3.41 contains non-zero Majorana CP phases.

Before we begin the analysis of the fermion mass spectra, let us consider the constraints on the vacuum expectation values of the gauge non-singlet Higgs fields coming from the masses of the W and Z bosons. As is typical with models with discrete flavor symmetries, our model contains an extended Higgs sector. The electroweak Higgs doublets which arise in the effective field theory on the wall are contained in the quintet Higgs flavons, Φ, Φ', Φ'' and ρ. To obtain the required W and Z boson masses, as is usual in a multiple Higgs doublet model, we must have that the sum of the squares of the vacua of these fields is equal to the square of the usual SM Higgs vacuum expectation value of 174 GeV. In our specific model, this requirement is

$$\sqrt{\langle\phi_w\rangle^2 + \langle\phi'_w\rangle^2 + \langle\phi''_w\rangle^2 + 3v_\rho^2} = 174\,\mathrm{GeV}, \tag{3.42}$$

where $\langle\phi_w\rangle$, $\langle\phi'_w\rangle$ and $\langle\phi''_w\rangle$ are the vacuum expectation values of the electroweak doublets arising from Φ, Φ' and Φ'' respectively, with v_ρ defined as before. For the sake of simplicity in our analysis, we will assume that the vacua obey $\langle\phi_w\rangle = \langle\phi'_w\rangle = \langle\phi''_w\rangle = v_\rho = (174\text{ GeV})/\sqrt{6} = 71.0\text{ GeV}$.

We first analyze the charged fermion sector. Since the charged fermion mass matrices are derived from Yukawa interactions with the Higgs fields Φ, Φ', and Φ'', we first need to localize the electroweak components of these Higgs fields. For the purpose of this analysis, we choose parameters such that $A_{R,Y=-1} = 100$ and $B_{R,Y=-1} = -10$, for $R = 1, 1', 1''$. There exists a large region of parameter space spanned by the quartic coupling constants $\tilde{\lambda}_{\Phi^R\eta}$, $\tilde{\lambda}_{\Phi^R\chi 1}$, $\tilde{\lambda}_{\Phi^R\chi 2}$, $\tilde{\lambda}_{\Phi^R\eta\chi}$ and the 5D Higgs squared masses $\mu^2_{\Phi^R}$ which yields $A_{R,Y=-1} = 100$ and $B_{R,Y=-1} = -10$. Furthermore, a subset of this parameter space is phenomenologically acceptable, namely that at least the lowest energy mode for the electroweak components attains a tachyonic mass on the wall, inducing electroweak symmetry breaking and for which all modes for the colored Higgs components have positive squared masses leaving $SU(3)_c$ intact. There also exist choices in this parameter region which satisfy all these constraints and which displace the colored Higgs well away from the wall, suppressing colored-Higgs-induced proton decay. An example from this parameter space is $\tilde{\lambda}_{\Phi^R\eta} = -39725$, $\tilde{\lambda}_{\Phi^R\chi 1} = -24396$, $\tilde{\lambda}_{\Phi^R\chi 2} = -1.6886 \times 10^5$, $\tilde{\lambda}_{\Phi^R\eta\chi} = 5189.8$, and $\mu^2_{\Phi^R} = 49700$, which gives

$\tilde{m}^2_{n=0,R,Y=-1} = -25.0$, $\tilde{m}^2_{nR,Y=-1} > 0$ for all $n > 0$, positive squared masses for all colored Higgs modes, and yields $A_{R,Y=2/3} = 9.86$ and $B_{R,Y=2/3} = 64.6$, which in turn produce a profile localized two characteristic lengths $1/k$ to the left of the center of the domain wall for the lowest energy mode of the colored Higgs.

Now that we have localized the electroweak Higgs flavons responsible for charged fermion masses after electroweak symmetry breaking, we can proceed to choose values for the background domain wall Yukawa coupling constants and electroweak Yukawa constants to generate the correct charged fermion mass spectra. We find that substituting the parameter choices,

$$\begin{aligned} \tilde{h}^1_{10\eta} &= 701.41, & \tilde{h}^1_{10\chi} &= 304.55, \\ \tilde{h}^2_{10\eta} &= 609.43, & \tilde{h}^2_{10\chi} &= 263.73, \\ \tilde{h}^3_{10\eta} &= 500.00, & \tilde{h}^3_{10\chi} &= 188.63, \end{aligned} \tag{3.43}$$

for the fermion decuplet background Yukawa coupling constants

$$\begin{aligned} \tilde{h}_{5\eta} &= 117.48, & \tilde{h}_{5\chi} &= -239.30, \\ \tilde{h}'_{5\eta} &= 185.40, & \tilde{h}'_{5\chi} &= -274.64, \\ \tilde{h}''_{5\eta} &= 203.50, & \tilde{h}''_{5\chi} &= -254.82, \end{aligned} \tag{3.44}$$

for the quintet background couplings, and

$$\begin{pmatrix} \tilde{h}^{11}_+ & \tilde{h}^{12}_+ & \tilde{h}^{13}_+ \\ \tilde{h}^{21}_+ & \tilde{h}^{22}_+ & \tilde{h}^{23}_+ \\ \tilde{h}^{31}_+ & \tilde{h}^{32}_+ & \tilde{h}^{33}_+ \end{pmatrix} = \begin{pmatrix} 640.51 & 504.28 & 580.59 \\ 501.22 & 481.66 & 524.49 \\ 129.87 & 128.95 & 431.03 \end{pmatrix}, \tag{3.45}$$

$$\begin{pmatrix} \tilde{h}^1_- & \tilde{h}^2_- & \tilde{h}^3_- \\ \tilde{h}'^1_- & \tilde{h}'^2_- & \tilde{h}'^3_- \\ \tilde{h}''^1_- & \tilde{h}''^2_- & \tilde{h}''^3_- \end{pmatrix} = \begin{pmatrix} 800.00 & 119.50 & 119.00 \\ 119.50 & 800.00 & 119.50 \\ 119.00 & 119.50 & 800.00 \end{pmatrix}, \tag{3.46}$$

for the charged fermion electroweak Yukawa couplings, we obtain the following mass matrices for the up-type quarks, down-type quarks, and electron-type leptons, all in units of MeV, respectively,

$$M_U = \begin{pmatrix} 494.21 & 1044.4 & 8037.6 \\ 1044.4 & 2389.3 & 14475 \\ 8037.2 & 14474 & 1.7139 \times 10^5 \end{pmatrix}, \tag{3.47}$$

$$M_D = \begin{pmatrix} 4.6631 & 1.0987 & 3.2390 \\ 10.408 & 116.60 & 56.779 \\ 138.17 & 218.91 & 4245.2 \end{pmatrix}, \tag{3.48}$$

$$M_E = \begin{pmatrix} 0.53478 & 15.847 & 210.19 \\ 8.1121 \times 10^{-2} & 107.52 & 217.48 \\ 5.6198 \times 10^{-2} & 13.762 & 1750.9 \end{pmatrix}. \tag{3.49}$$

The mass eigenvalues resulting from these mass matrices are

$$m_u = 2.49 \text{ MeV}, \quad m_c = 1.27 \text{ GeV}, \quad m_t = 173 \text{ GeV}, \tag{3.50}$$

for the up, charm and top quarks,

$$m_d = 4.47 \text{ MeV}, \quad m_s = 114 \text{ MeV}, \quad m_b = 4.25 \text{ GeV}, \tag{3.51}$$

for the down, strange and bottom quarks, and

$$m_e = 0.511 \text{ MeV}, \quad m_\mu = 106 \text{ MeV}, \quad m_\tau = 1.78 \text{ GeV}, \tag{3.52}$$

for the electron, muon and tauon respectively. These results obviously are in agreement within error of current data on charged lepton masses [63].

With regards to quark mixing, the Euler angles, Θ_{12}^{UL}, Θ_{13}^{UL}, and Θ_{23}^{UL} of the left up quark diagonalization matrix, V_{UL}, derived from the up quark mass matrix in Eqn. 3.47 are approximately

$$\Theta_{12}^{UL} = 17.264^\circ, \quad \Theta_{13}^{UL} = 2.6874^\circ, \quad \Theta_{23}^{UL} = 4.8658^\circ, \tag{3.53}$$

and the corresponding angles Θ_{12}^{DL}, Θ_{13}^{DL}, and Θ_{23}^{DL} of the down quark left diagonalization matrix, V_{DL}, are approximately

$$\Theta_{12}^{DL} = 4.2387^\circ, \quad \Theta_{13}^{DL} = 1.8634^\circ, \quad \Theta_{23}^{DL} = 2.9746^\circ, \tag{3.54}$$

from which one derives that the Euler angles Θ_{12}^{CKM}, Θ_{13}^{CKM}, and Θ_{23}^{CKM} of the CKM matrix, given $V_{CKM} = V_{UL}V_{DL}^\dagger$, are

$$\Theta_{12}^{CKM} = 13.0^\circ, \quad \Theta_{13}^{CKM} = 0.201^\circ, \quad \Theta_{23}^{CKM} = 2.39^\circ. \tag{3.55}$$

These results are in agreement with the current data on quark mixing angles [63].

Finally, the Euler angles Θ_{12}^{eL}, Θ_{13}^{eL}, and Θ_{23}^{eL} of the left electron diagonalization matrix, V_{eL}, are indeed small

$$\begin{gathered} \Theta_{12}^{eL} = 7.32 \times 10^{-2\,\circ}, \quad \Theta_{13}^{eL} = 4.15 \times 10^{-3\,\circ}, \\ \Theta_{23}^{eL} = 0.925^\circ. \end{gathered} \tag{3.56}$$

Thus, the left electron diagonalization matrix is indeed very close to the identity matrix, which means in choosing parameters such that $m_\rho = m'_\rho = m''_\rho$, we get a tribimaximal PMNS matrix generated entirely from the left

diagonalization matrix for the neutrinos. The only remaining things to check with regard to the mass fitting are the existence of parameter choices for the right chiral neutrinos generating the desired mass spectra and if, in the case $m_\rho = m'_\rho = m''_\rho$, the experimentally measured neutrino squared mass differences can be satisfied.

In the analysis of neutrino masses, we give two example parameter choices for the non-dimensionalized coupling of the right-handed neutrinos to the domain-wall, $\tilde{h}_{1\eta}$, the bare Majorana mass M, the non-dimensionalized Yukawa coupling $\tilde{h}_\varphi$ describing the strength of the interaction between N and the gauge singlet Higgs field φ, as well as the quartic coupling parameters determining the localization of the lowest energy modes for the A_4-triplet flavon fields ρ and φ. The Dirac masses m_ρ, m'_ρ, m''_ρ are sensitive to the splittings between the fields ρ, the lepton doublets and N, and since we still have the freedom to shift ρ, we can naturally control the scales of these masses: they can be made to be at the same order as the top quark mass or they can be made to be very light. On the other hand, since the right-handed neutrino triplet N and the flavon φ are always localized about $\tilde{y} = 0$, the overlap integral $\int f_N^2(\tilde{y}) p_{\varphi_0}(\tilde{y})\, d\tilde{y}$ on which the mass scale M_φ is dependent is always naturally of order 1, so naturally we expect that M_φ is of the same order as the bare Majorana mass for N.

In our first examples, we give parameters such that the neutrino Dirac masses are of the order of the electron mass. For the parameter choice

$$\begin{gathered} \tilde{h}_{1\eta} = 100.00, \\ \tilde{h}_\rho = 533.27, \quad \tilde{h}'_\rho = 267.97, \quad \tilde{h}''_\rho = 777.57, \\ A_{\rho Y=-1} = A_{R=3,Y=-1} = 500.00, \\ B_{\rho Y=-1} = B_{R=3,Y=-1} = 380.00, \end{gathered} \tag{3.57}$$

we get the Dirac masses to be

$$m_\rho = m'_\rho = m''_\rho = 0.100 \text{ MeV}. \tag{3.58}$$

One can then show that to satisfy the neutrino mass squared differences $\Delta m^2_{12} = 7.59 \times 10^{-5}$ eV^2 and $\Delta m^2_{23} = 2.43 \times 10^{-3}$ eV^2 from the PDG [123], we must have

$$M = 2.86 \text{ TeV}, \quad M_\varphi = 2.26 \text{ TeV}, \tag{3.59}$$

for which the neutrino masses turn out to be

$$\begin{aligned} m_1 &= \left| \frac{-3m_\rho^2}{M + M_\varphi} \right| = 5.86 \times 10^{-3} \text{ eV}, \\ m_2 &= \left| \frac{-3m_\rho^2}{M} \right| = 0.0105 \text{ eV}, \\ m_3 &= \left| \frac{-3m_\rho^2}{M - M_\varphi} \right| = 0.0504 \text{ eV}. \end{aligned} \tag{3.60}$$

Because the localized mode of φ, φ_0 is a gauge singlet and A_4-triplet and thus decoupled from the Standard Model, at least at tree level, we have the freedom to choose the scale of its vacuum expectation value, v_φ. This means we can choose the scale such that the Yukawa coupling $\tilde{h}_\varphi$ is of the same order as all the other electroweak Yukawa coupling constants; in this case, if $v_\varphi \sim 10$ GeV and $\tilde{h}_\varphi \sim 100$, we get the correct scale for M_φ.

Another example we give is one in which the Dirac neutrino masses are the same order as the top quark mass, and the Majorana mass scales are of the order $M_{GUT} = 10^{16}$ GeV, albeit with $\tilde{h}_{1\eta}$ mildly tuned. For this choice we have,

$$\begin{gathered} \tilde{h}_{1\eta} = 25.000, \\ \tilde{h}_\rho = 328.95, \quad \tilde{h}'_\rho = 208.26, \quad \tilde{h}''_\rho = 793.17, \\ A_{\rho Y=-1} = A_{R=3,Y=-1} = 900.00, \\ B_{\rho Y=-1} = B_{R=3,Y=-1} = 600.00, \end{gathered} \tag{3.61}$$

which gives

$$m_\rho = m'_\rho = m''_\rho = 174 \text{ GeV}. \tag{3.62}$$

If we then set

$$M = 8.65 \times 10^{15} \text{ GeV}, \quad M_\varphi = 6.85 \times 10^{15} \text{ GeV}, \tag{3.63}$$

we get the masses of the left neutrino mass eigenstates for this parameter choice to be the same as those for the first parameter choice in Eqn. 3.60. Given that the $M_\varphi = 6.85 \times 10^{15}$ GeV, if we have $v_\varphi \sim 10^{13}$ GeV, then we obtain $\tilde{h}_\varphi \sim 100$ as desired.

In summary, we have shown that there exist parameter choices within the model such that the fermion mass hierarchy, light neutrinos and the correct neutrino mass squared differences, quark mixing and a tribimaximal lepton mixing matrix are reproduced from a set of Yukawa coupling constants which are of the same order of magnitude. In light of the recent results of

the Daya Bay and RENO neutrino experiments [65, 66], which found that $7.9^\circ < \theta_{13} < 9.6^\circ$ for the PMNS matrix, exact tribimaximal mixing is now excluded. However, a number of assumptions in this analysis were made which ensured an exact tribimaximal form, namely that $m_\rho = m'_\rho = m''_\rho$ and requiring that the left electron diagonalization matrix was close to trivial. It is obvious that deviations from tribimaximal mixing will occur if these assumptions are relaxed, and it is clear that the correct θ_{13} mixing angle can also be generated in this model.

The $m_\rho = m'_\rho = m''_\rho$ assumption generically results in a normal neutrino mass hierarchy, since the only possible hierarchies for this parameter choice are either $m_1 < m_2 < m_3$, which is the normal hierarchy, or $m_1 > m_2 > m_3$ which is phenomenologically unacceptable. Breaking this assumption can then lead to inverted or quasidegenerate neutrino mass hierarchies as well as deviations from tribimaximal mixing.

Like many models based on A_4, our analysis relied on the alignments of the vacuum expectation values of two A_4-triplet Higgs fields being different. However, when interactions between the two flavons are switched on, this arrangement is generally destroyed and the VEVs of the two fields align, leading to the vacuum alignment problem. We will discuss the resolution of this problem within our model in the next section.

3.6 Resolving the Vacuum Alignment Problem via Splitting

Throughout this paper our analysis has depended on a particular choice of alignments for the vacuum expectation values of the two A_4-triplet Higgs fields localized to the wall. As per usual, finding valid VEVs for these fields involves finding global minima for the full scalar potential of the theory, which we have put in Appendix B. For the gauge charged triplet, ρ, we assigned a VEV of the form (v_ρ, v_ρ, v_ρ), which induces a breaking of $A_4 \to \mathbb{Z}_3$, and for the neutrally charged triplet flavon φ a VEV of the form $(0, v_\varphi, 0)$ which breaks A_4 down to $\mathbb{Z}_2$. After these fields are localized and gain tachyonic masses on the wall, one can show that these VEV patterns are indeed valid global minima of the respective self-interaction potentials V_ρ and V_φ given in Eqs. B.2 and B.3. However, when one turns on interactions between the Higgs triplets and the 1, $1'$ and $1''$ quintet scalars, this is no longer guaranteed [73, 71].

The problem is that once the cross-talking interactions are switched on, minimization of the potential yields a larger number of independent equa-

tions than known vacuum expectation values ($v_\rho, v_\varphi, \langle\phi_w\rangle, \langle\phi'_w\rangle, \langle\phi''_w\rangle$). This means that enforcing the desired vacuum alignment requires an unnatural fine-tuning of the parameters of the scalar potential. The troublesome terms are those which generate soft $A_4 \to \mathbb{Z}_2$ breaking mass terms in the potential for ρ_w after φ_0 attains its VEV, and likewise generate soft $A_4 \to \mathbb{Z}_3$ breaking terms for the potential for φ_0 when ρ_w condenses. These unwanted interactions involve coupling $1'$, $1''$, 3_s and 3_a products of ρ and φ, for example $(\rho^\dagger\rho)_{1'}(\varphi\varphi)_{1''}$ [85]. In addition to interactions with φ, there are other interactions generating $A_4 \to \mathbb{Z}_2$ breaking mass terms due to the presence of the $1'$ and $1''$ Higgs quintets Φ' and Φ'', for example $(\rho^\dagger\rho)_{1''}\Phi^\dagger\Phi'$. Analogous interactions involving just φ, Φ' and Φ'' (and technically Φ as well) are not problematic since φ, Φ' and Φ'' all break A_4 to the same $\mathbb{Z}_2$ subgroups, although there are interactions such as $\Phi''^\dagger(\rho\varphi)_{1''}$ which provide corrections to the potential for φ as well as that for ρ.

In our model, we follow the approach in [86, 88] and split the triplet flavons in the extra dimension to ensure the alignment. Typically, if we suppress the troublesome interactions such that their effective interaction strengths are extremely small, we simply expect a small classical correction to the desired vacua for ρ_w of order $\frac{\lambda_{\rho\varphi}v_\varphi^2}{\lambda_\rho v_\rho}$ for quartic interactions of ρ and φ for instance, and similarly for other troublesome mass terms impacting the alignment of φ. Since ρ is a quintet under $SU(5)$, the electroweak Higgs doublet ρ_w arising from it is in general displaced from $\tilde{y} = 0$. Since the singlet flavon φ is always localized at $\tilde{y} = 0$, it is in principle possible to separate the flavons sufficiently so that the operators in $V_{\rho\varphi}$ are naturally suppressed. As previously mentioned, we also have troublesome interactions involving ρ and the $1'$ and $1''$ Higgs quintets. Thus we place the localized mode of ρ, ρ_w, on the opposite side of the wall to those of Φ, Φ' and Φ''. The interactions coupling all three types of non-trivially A_4-charged flavons such as $\Phi''^\dagger(\rho\varphi)_{1''}$ are naturally suppressed by the splitting of the $A_4 \to \mathbb{Z}_3$ breaking sector generated by ρ from the $A_4 \to \mathbb{Z}_2$ breaking sector generated from φ, Φ' and Φ''.

In our example analysis, for the first choice with $A_{\rho Y=-1}$ and $B_{\rho Y=-1}$ given in Eq. 3.57, the same localization parameters for Φ, Φ' and Φ'' chosen in Sec. 3.5, we choose d, as defined in Eq. 3.26 and which determines how localized φ_0 is to the wall, to be set to $d = 500.00$. A graph of the profiles for ρ_w, φ_0 and those of ϕ_w, ϕ'_w, and ϕ''_w for this parameter choice is shown in Fig. 3.6.

The potentially most troublesome interactions are the cubic interactions of the form $(\rho^\dagger\rho)_{3s,a}.\varphi$ and $(\rho^\dagger\varphi)_{1,1',1''}\Phi^{R=1,1'',1'}$, for which the effective 4D couplings are proportional to the integrals $\int \tilde{p}^2_{\rho w}(\tilde{y})\tilde{p}_{\varphi_0}(\tilde{y})\, d\tilde{y}$ and

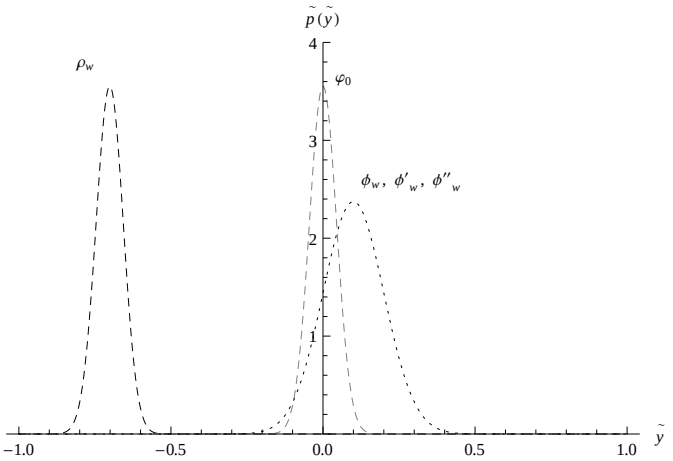

Figure 3.6: Profiles for the localized triplet flavons ρ_w and φ_0 as well as those for the 1, $1'$ and $1''$ Higgs fields ϕ_w, ϕ'_w and ϕ''_w for the parameter choices with $A_{\rho Y=-1}$ and $B_{\rho Y=-1}$ as given in Equation 3.57, the same localization parameters given for Φ, Φ' and Φ'' chosen in Sec. 3.5 and $d = 500$ for φ.

$\int \tilde{p}_{\rho w}(\tilde{y})\tilde{p}_{\varphi_0}(\tilde{y})\tilde{p}_{w,w',w''}(\tilde{y})\, d\tilde{y}$ respectively. One has to be careful in calculating the magnitude of the corrections from these interactions since quartic and cubic scalar couplings have different mass dimension; in 4+1D a quartic coupling has mass dimension -1 while a cubic coupling has mass dimension $\frac{1}{2}$. For a generic cubic interaction of the types in consideration, if the cubic coupling is a, and the quartic self-couplings for a generic A_4 triplet are of order λ, provided that the cubic interaction provides just a small perturbation, then we anticipate that this perturbation is proportional to $\frac{a}{\lambda}$. If we choose these numbers to be natural, that is $a = \overline{a}\Lambda_{DW}^{\frac{1}{2}}$ and $\lambda = \overline{\lambda}\Lambda_{DW}^{-1}$ where Λ_{DW} is the UV cut-off for our theory and $\overline{a}$ and $\overline{\lambda}$ are dimensionless numbers of order 1, this means that $\frac{a}{\lambda} \sim \Lambda_{DW}^{\frac{3}{2}}$. An overlap integral O_3 of the profiles of the scalars involved in a cubic interaction is $k^{\frac{1}{2}}$ times the non-dimensionalized integral $\tilde{O}_3$, while that for a quartic interaction self-interaction O_4 is $k\tilde{O}_4 \sim k$. Given that self-interactions only involve the one species and thus the relevant overlap integral is only dependent on the one profile, $\tilde{O}_4$ should be of order 1. If we now consider $(\rho^\dagger\rho)_{3s,a}.\varphi$, after ρ_w attains a VEV, this interaction provides a correction linear in φ_0 and so the correction to v_φ is then of order $\Lambda_{DW}^{\frac{3}{2}}k^{-\frac{1}{2}}\tilde{O}_3\frac{v_\rho^2}{v_\varphi^2}$, and likewise when φ_0 condenses this interaction provides a $A_4 \to \mathbb{Z}_2$ mass term for ρ_w which provides a correction $\Lambda_{DW}^{\frac{3}{2}}k^{-\frac{1}{2}}\tilde{O}_3\frac{v_\varphi}{v_\rho}$, where $\tilde{O}_3 = \int \tilde{p}_{\rho w}^2(\tilde{y})\tilde{p}_{\varphi_0}(\tilde{y})\, d\tilde{y}$. We do not know

what exactly the scales k and Λ_{DW} are, but for the purpose of this analysis we will assume the worst case scenario as far as these corrections are concerned: $k \sim 1\,\text{TeV}$ and $\Lambda_{DW} \sim M_{Planck} = 10^{19}\,\text{GeV}$. For this first parameter choice, $\int \tilde{p}^2_{\rho w}(\tilde{y})\tilde{p}_{\varphi_0}(\tilde{y})\,d\tilde{y}$ is of the order of 10^{-35}, which yields the correction to $\langle\varphi_0\rangle$ from this interaction to be of order $10^{-7}v_\varphi$, and the correction to $\langle\rho_w\rangle$ to be of order $10^{-10}v_\rho$. Likewise, for the interactions of the form $(\rho^\dagger\varphi)_{1,1',1''}\Phi^{R=1,1'',1'}$, the relevant overlap integral $\tilde{O}_3 = \int \tilde{p}_{\rho w}(\tilde{y})\tilde{p}_{\varphi_0}(\tilde{y})\tilde{p}_{w,w',w''}(\tilde{y})\,d\tilde{y}$ is of order 10^{-31} and after the non-triplet gauge charged Higgs fields attain VEVs these interactions give corrections linear in φ_0 and ρ_w, which turn out to be of the order of $10^{-3}v_\varphi$ and $10^{-8}v_\rho$ to $\langle\varphi_0\rangle$ and $\langle\rho_w\rangle$ respectively.

With regard to quartic cross-talk interactions, we do not have to worry about scaling of the coupling constants for obvious reasons. For the quartic interactions coupling ρ and φ, the effective 4D quartic couplings are all proportional to the integral $\int \tilde{p}^2_{\rho w}(\tilde{y})\tilde{p}^2_{\varphi_0}(\tilde{y})\,d\tilde{y}$ which for this first parameter choice turns out to be of order 10^{-53}, yielding corrections of order $(10^{-53}\frac{v_\varphi^2}{v_\rho^2})v_\rho \sim 10^{-55}v_\rho$ to $\langle\rho_w\rangle$ and $(10^{-53}\frac{v_\rho^2}{v_\varphi^2})v_\varphi \sim 10^{-52}v_\varphi$ to $\langle\varphi_0\rangle$.

Next, we deal with the quartic interactions coupling ρ, Φ and one of Φ' or Φ'', which are of the form $(\rho^\dagger\rho)_{R=1',1''}\Phi^\dagger\Phi^{R=1'',1'}$. After dimensional reduction the effective 4D coupling constants for these interactions are proportional to the overlap integral $\int \tilde{p}_{\rho w}(\tilde{y})\tilde{p}_w(\tilde{y})\tilde{p}_{w',w''}(\tilde{y})\,d\tilde{y}$. For this parameter choice these overlap integrals are of order 10^{-22}, yielding corrections of order $(10^{-22}\frac{\langle\phi_w\rangle\langle\phi_{w',w''}\rangle v_\varphi}{v_\rho^3})v_\rho \sim 10^{-22}v_\rho$ to $\langle\rho_w\rangle$.

Finally, there are quartic interactions coupling both ρ and φ to one of Φ, Φ' or Φ'', which are of the form $\left[(\varphi\varphi)_{3s}.\rho^\dagger\right]_R\Phi^{R^*}$. To leading order, since $(\langle\varphi_0\rangle\langle\varphi_0\rangle)_{3s} = ((0,v_\varphi,0).(0,v_\varphi,0))_{3s} = 0$, this interaction does not give a leading order correction to $\langle\rho_w\rangle$, although there are corrections for $\langle\varphi_0\rangle$. After dimensional reduction, the effective 4D coupling strength is proportional to the overlap integral $\int \tilde{p}^2_{\varphi_0}(\tilde{y})\tilde{p}_{\rho w}(\tilde{y})\tilde{p}_{w,w',w''}(\tilde{y})\,d\tilde{y}$, and for the first parameter choice this overlap integral is of the order 10^{-39}, leading to corrections of order $(10^{-39}\frac{v_\rho\langle\phi_w^{R=1,1',1''}\rangle}{v_\varphi^2})v_\varphi \sim 10^{-37}v_\varphi$ to $\langle\varphi_0\rangle$. Obviously any second order corrections to $\langle\rho_w\rangle$ will be much smaller than this.

For the second choice with parameters given in Eq. 3.61 with $d = 900.00$, we get the value of the relevant overlap integrals to be of order 10^{-50} for $\int \tilde{p}^2_{\rho w}(\tilde{y})\tilde{p}_{\varphi_0}(\tilde{y})\,d\tilde{y}$, 10^{-42} for $\int \tilde{p}_{\rho w}(\tilde{y})\tilde{p}_{\varphi_0}(\tilde{y})\tilde{p}_{w,w',w''}(\tilde{y})\,d\tilde{y}$, 10^{-77} for $\int \tilde{p}^2_{\rho w}(\tilde{y})\tilde{p}^2_{\varphi_0}(\tilde{y})\,d\tilde{y}$, 10^{-19} for $\int \tilde{p}^2_{\rho w}(\tilde{y})\tilde{p}^2_w(\tilde{y})\tilde{p}_{w',w''}(\tilde{y})\,d\tilde{y}$, and 10^{-54} for $\int \tilde{p}_{\rho w}(\tilde{y})\tilde{p}^2_{\varphi_0}(\tilde{y})\tilde{p}_{w,w',w''}(\tilde{y})\,d\tilde{y}$. All the corrections to $\langle\varphi_0\rangle$ are not only suppressed by the overlap integrals but by either $\frac{v_\rho}{v_\varphi} \sim 10^{-12}$ or its square $(\frac{v_\rho}{v_\varphi})^2 \sim 10^{-24}$, hence doing a similar analysis to that above shows that the corrections to $\langle\varphi_0\rangle$ are extremely negligible. Doing a similar analysis as above

shows that the the overlap integrals are small enough to overcome the ratio $\frac{v_\varphi}{v_\rho} \sim 10^{12}$ or its square $(\frac{v_\varphi}{v_\rho})^2 \sim 10^{24}$ (whichever is relevant) as well as the ratio $\Lambda_{DW}^{\frac{3}{2}} k^{-\frac{1}{2}}$ in the case of the cubic interactions and still ensure that the corrections to $\langle \rho_w \rangle$ are more than several orders of magnitude less than v_ρ.

3.7 Conclusion

We found that the A_4 extension of the $SU(5)$ 4+1D domain-wall braneworld model of [23] can generate large mixing angles in the lepton sector. We explicitly demonstrated parameter values that yield tribimaximal lepton mixing with a normal neutrino mass hierarchy, together with successful predictions for the hierarchical charged fermion masses and quark mixing angles. Through small departures from this parameter point, the small but nonzero θ_{13} leptonic mixing angle can be generated, and the neutrino mass spectrum altered to give an inverted hierarchy or a quasi-degenerate pattern. This is a significant extension of the results found in [1].

We also discovered that the troublesome interactions which are responsible for the vacuum realignment problem in analogous 4D models could be suppressed by splitting the profile of ρ, which initiates $A_4 \to \mathbb{Z}_3$ breaking, from the profiles of the $A_4 \to \mathbb{Z}_2$ breaking flavons φ, Φ' and Φ''. This led to exponential suppression of the overlap integrals of these profiles determining the effective 4D coupling constants for interactions between the A_4-triplets as well as the troublesome interactions which involve Φ' and Φ'', ensuring that the contributions of these interactions to the vacua of the localized components of ρ and φ were sufficiently small compared to the classical vacua of their respective self-interaction potentials. This maintained the desired vacuum alignments for these flavons required to generate large lepton mixing angles.

We have shown in this chapter and in [1] that domain-wall braneworld models with an $SU(5)$ gauge group are generically good for generating the fermion mass hierarchy and quark mixing, and that with the inclusion of the discrete flavor group A_4 we can attain large lepton mixing angles. Further work along these lines could involve extending either the gauge group (to $SO(10)$ for example [124], or to even larger groups such as E_6 [25]), the discrete flavor group (for example, to T' which is the double cover of A_4), or both. Further work could also look at the case where gravity is included or quantum corrections to the fermion mass spectra.

Chapter 4

Solutions for Intersecting Domain Walls with Internal Structure in Six Dimensions from a $\mathbb{Z}_2 \times \mathbb{Z}_2$-invariant Action

This chapter represents the beginning of our studies into increasing the scope of the domain-wall brane framework to two additional dimensions rather than just one.

Topological defects of co-dimension 2 have been considered as candidates for the localization of fields onto a 3+1D subspace. The simplest example of a co-dimension 2 defect is a string and it has already been shown that 3+1D gravity can be reproduced on such an object in a 5+1D spacetime [95, 96]. Extensions of the RS2 model for the intersection of n fundamental branes in 4+n-dimensional spacetime were proposed in [33, 99]. Other than strings, we could instead consider the possibility of using a pair of domain walls in 6D spacetime to localize fields on to a 4D world volume.

There are two ways of introducing a second domain wall in order to freeze out a second extra dimension. One way is to localize a scalar field onto a domain wall and have that scalar field develop a tachyonic mass which induces a breaking of a second discrete symmetry, yielding a second domain wall localized to the first. This is called a nested domain wall or domain ribbon and there is some literature that has dealt with this scenario [4, 100, 101] and with the possible localization of gravity on such a defect [102]. A second way to produce a dimensional reduction from 5+1D to 3+1D is to have two stable domain walls which intersect. There have been some supersymmetric models which yield rare exact solutions for a pair of non-trivially intersecting walls [104]. For more on models with intersecting domain walls or domain-wall

junctions, see [103, 125, 126, 105].

In this chapter, we present a $\mathbb{Z}_2 \times \mathbb{Z}_2$-invariant 5+1D interacting scalar field theory with four real scalar fields, where the 6D masses are tachyonic for two of the scalar fields and positive definite for the other two, in which a rare analytic solution for two intersecting domain walls can be obtained for a particular parameter choice. We find that there exists a class of energy degenerate solutions with two domain walls: one in which the walls are perpendicular, a range of solutions where the walls intersect at an angle between 0 and 90 degrees and another in which the walls are parallel. We give topological arguments for why the perpendicular solution cannot evolve to the parallel solution given for the particular parameter choice, as well as an argument for why the perpendicular solution might be energetically favorable to the solutions with intersection angle less than 90 degrees in a nearby region of parameter space (assuming they are not topologically distinct). We also show that chiral fermions and scalars can be localized to the intersection of the domain wall. This is important because these chiral fermions and scalars form the building blocks of the quarks, leptons and Higgs bosons of an effective Standard Model-like theory dynamically localized to the intersection.

We have already given a number of solutions to $\mathbb{Z}_2$-symmetric scalar field theories in which one scalar field generates a domain wall and another condenses in the domain-wall interior. These single-wall solutions all have the same qualitative features. Hence, we begin with Sec. 4.1, in which we outline the model generating the intersecting domain wall solution, give the form of the solution for which the walls are perpendicular and give a topological argument for why this solution cannot evolve to the solution where the walls are parallel despite these solutions being energy degenerate. We also give an argument for why the perpendicular solution and the solutions which intersect at an angle between 0 and 90 degrees are not energy degenerate in general. In Sec. 4.2, we discuss fermion localization and we show that localization of a single chiral zero mode on the intersection of the domain walls is possible. In Sec. 4.3, we show that scalars can also be localized to the domain-wall intersection. Section 4.4 is our conclusion.

4.1 The Background Scalar Field Theory

Our model describing the background fields is a 5+1-dimensional (5+1D) quartic scalar field theory with four scalar fields invariant under a $\mathbb{Z}_2 \times \mathbb{Z}_2$ symmetry. The role of the $\mathbb{Z}_2 \times \mathbb{Z}_2$ symmetry is to ensure topological stability of the resultant intersecting walls in a manner analogous to that of the $\mathbb{Z}_2$ symmetry in the single wall case. Under this symmetry, we assign the

following parities to these fields:

$$\begin{aligned} \eta_1 &\sim (-,+) \qquad & \chi_1 &\sim (-,+), \\ \eta_2 &\sim (+,-) \qquad & \chi_2 &\sim (+,-). \end{aligned} \tag{4.1}$$

The fields η_1 and η_2 will form the two perpendicular background domain-wall kinks while χ_1 and χ_2 will attain lump-like profiles parallel to each respective wall.

Given the parity assignments, we may write the most general quartic scalar potential of this theory as

$$\begin{aligned} V_{DW} = &\frac{1}{4}\lambda_{\eta_1}(\eta_1^2 - v_1^2)^2 + \frac{1}{2}\lambda_{\eta_1\chi_1}(\eta_1^2 - v_1^2)\chi_1^2 + \frac{1}{2}\mu_{\chi_1}^2\chi_1^2 + \frac{1}{4}\lambda_{\chi_1}\chi_1^4 + g_{\eta_1\chi_1}\eta_1^3\chi_1 \\ &+ h_{\eta_1\chi_1}\eta_1\chi_1^3 + \frac{1}{4}\lambda_{\eta_2}(\eta_2^2 - v_2^2)^2 + \frac{1}{2}\lambda_{\eta_2\chi_2}(\eta_2^2 - v_2^2)\chi_2^2 + \frac{1}{2}\mu_{\chi_2}^2\chi_2^2 + \frac{1}{4}\lambda_{\chi_2}\chi_2^4 \\ &+ g_{\eta_2\chi_2}\eta_2^3\chi_2 + h_{\eta_2\chi_2}\eta_2\chi_2^3 + \frac{1}{2}\lambda_{\eta_1\eta_2}(\eta_1^2 - v_1^2)(\eta_2^2 - v_2^2) + \frac{1}{2}\lambda_{\eta_1\chi_2}(\eta_1^2 - v_1^2)\chi_2^2 \\ &+ \frac{1}{2}\lambda_{\chi_1\eta_2}\chi_1^2(\eta_2^2 - v_2^2) + \frac{1}{2}\lambda_{\chi_1\chi_2}\chi_1^2\chi_2^2 + \frac{1}{2}\lambda_{\eta_1\eta_2\chi_2}\eta_1^2\eta_2\chi_2 + \frac{1}{2}\lambda_{\chi_1\eta_2\chi_2}\chi_1^2\eta_2\chi_2 \\ &+ \frac{1}{2}\lambda_{\eta_1\chi_1\eta_2}\eta_1\chi_1\eta_2^2 + \frac{1}{2}\lambda_{\eta_1\chi_1\chi_2}\eta_1\chi_1\chi_2^2 + \lambda_{\eta_1\chi_1\eta_2\chi_2}\eta_1\chi_1\eta_2\chi_2. \end{aligned} \tag{4.2}$$

Choosing parameters such that this potential is bound from below, including $\lambda_{\eta_1}, \lambda_{\eta_2}, \lambda_{\chi_1}, \lambda_{\chi_2}, \lambda_{\eta_1\eta_2}, \lambda_{\eta_1\chi_2}, \lambda_{\chi_1\eta_2}, \lambda_{\chi_1\chi_2} > 0$, there are four global minima given by $\eta_1 = \pm v_1$, $\eta_2 = \pm v_2$, $\chi_1 = \chi_2 = 0$. Furthermore, we require that $\lambda_{\eta_1\chi_1}v_1^2 > \mu_{\chi_1}^2$ and $\lambda_{\eta_2\chi_2}v_2^2 > \mu_{\chi_2}^2$ to ensure that χ_1 and χ_2 attain tachyonic masses in the interiors of of the respective walls generated by η_1 and η_2. This ensure solutions where χ_1 and χ_2 form lump-like profiles are the most stable ones, analogously to the single kink-lump case. We also make the parameter choices $\mu_{\chi_1}^2 > \lambda_{\chi_1\eta_2}v_2^2$ and $\mu_{\chi_2}^2 > \lambda_{\eta_1\chi_2}v_1^2$. We choose the last two conditions so that χ_1 does not condense along the edges at infinity along which the $\eta_2 - \chi_2$ kink-lump solution interpolates and vice versa.

To set up an intersecting domain wall solution, we must find a static solution for all of the four fields η_1, η_2, χ_1 and χ_2 to the Euler-Lagrange equations which at the very least interpolate amongst the four vacua at infinity along the corners of each quadrant in the $y - z$ plane. Firstly, we attempt to find a solution in which the walls are mutually perpendicular. Along one edge where η_1 is constant at one of its vacua $\pm v_1$ and where also $\chi_1 = 0$, the field η_2 should interpolate between the values $\pm v_2$ and χ_2 should be zero at infinity along the edge and condense in the middle of the edge, much like the one-dimensional kink-lump solutions discussed in the

previously. The same should apply to η_1 and χ_1 along the edges where η_2 and χ_2 are fixed. This motivates us to look for solutions obeying boundary conditions of the type

$$\begin{aligned}
&\eta_1(y=\pm\infty,z)=\pm v_1,\ \eta_1(y,z=\pm\infty)=v_1\tanh(ky),\\
&\eta_2(y=\pm\infty,z)=v_2\tanh(lz),\ \eta_2(y,z=\pm\infty)=\pm v_2,\\
&\chi_1(y=\pm\infty,z)=0,\ \chi_1(y,z=\pm\infty)=A_1\,\mathrm{sech}(ky),\\
&\chi_2(y=\pm\infty,z)=A_2\,\mathrm{sech}(lz),\ \chi_2(y,z=\pm\infty)=0.
\end{aligned} \tag{4.3}$$

By making the parameter choice,

$$\begin{aligned}
\lambda_{\eta_1\eta_2\chi_2}=\lambda_{\chi_1\eta_2\chi_2}=\lambda_{\eta_1\chi_1\eta_2}=\lambda_{\eta_1\chi_1\chi_2}=\lambda_{\eta_1\chi_1\eta_2\chi_2}=0,\\
g_{\eta_1\chi_1}=h_{\eta_1\chi_1}=g_{\eta_2\chi_2}=h_{\eta_2\chi_2}=0,\\
\lambda_{\eta_1\eta_2}v_1^2=\lambda_{\chi_1\eta_2}A_1^2,\quad \lambda_{\eta_1\eta_2}v_2^2=\lambda_{\eta_1\chi_2}A_2^2,\\
\lambda_{\eta_1\chi_2}v_1^2=\lambda_{\chi_1\chi_2}A_1^2,\quad \lambda_{\chi_1\eta_2}v_2^2=\lambda_{\chi_1\chi_2}A_2^2,\\
2\mu_{\chi_1}^2(\lambda_{\eta_1\chi_1}-\lambda_{\chi_1})+(\lambda_{\eta_1}\lambda_{\chi_1}-\lambda_{\eta_1\chi_1}^2)v^2=0,\\
2\mu_{\chi_2}^2(\lambda_{\eta_2\chi_2}-\lambda_{\chi_2})+(\lambda_{\eta_2}\lambda_{\chi_2}-\lambda_{\eta_2\chi_2}^2)v^2=0,
\end{aligned} \tag{4.4}$$

one finds that

$$\begin{aligned}
\eta_1(y)=v_1\tanh(ky),\quad \chi_1(y)=A_1\,\mathrm{sech}(ky),\\
\eta_2(z)=v_2\tanh(lz),\quad \chi_2(z)=A_2\,\mathrm{sech}(lz),
\end{aligned} \tag{4.5}$$

where $k^2=\mu_{\chi_1}^2$, $l^2=\mu_{\chi_2}^2$, $A_1^2=\frac{\lambda_{\eta_1\chi_1}v_1^2-2\mu_{\chi_1}^2}{\lambda_{\chi_1}}$, $A_2^2=\frac{\lambda_{\eta_2\chi_2}v_2^2-2\mu_{\chi_2}^2}{\lambda_{\chi_2}}$, is a solution to the four coupled Euler-Lagrange equations resulting from the potential in Eq. 4.2 and satisfies the boundary conditions in Eq. 4.3. We give plots for η_1, χ_1, η_2 and χ_2 for the solution in Eq. 4.5 in Fig. 4.1, Fig. 4.2, Fig. 4.3 and Fig. 4.4 respectively, in terms of the non-dimensionalized coordinates $\tilde{y}=ky$ and $\tilde{z}=lz$.

It is important to note that there are other solutions with two kink-lump pairs to the coupled Euler-Lagrange equations. Without loss of generality, assume that η_1 and χ_1 are the same as in Eq. 4.5 but consider instead that η_2 and χ_2 take the form

$$\begin{aligned}
\eta_2(y,z)=v_2\tanh[l(\cos\theta y+\sin\theta z)],\\
\chi_2(y,z)=A_2\,\mathrm{sech}[l(\cos\theta y+\sin\theta z)].
\end{aligned} \tag{4.6}$$

Acting with the d'Alembertian operator on η_2 and χ_2 yields

$$\begin{aligned}
\Box\eta_2&=\frac{2l^2}{v_2^2}(\eta_2^2-v_2^2)\eta_2,\\
\Box\chi_2&=\frac{2l^2}{A_2^2}\chi_2^3-l^2\chi_2.
\end{aligned} \tag{4.7}$$

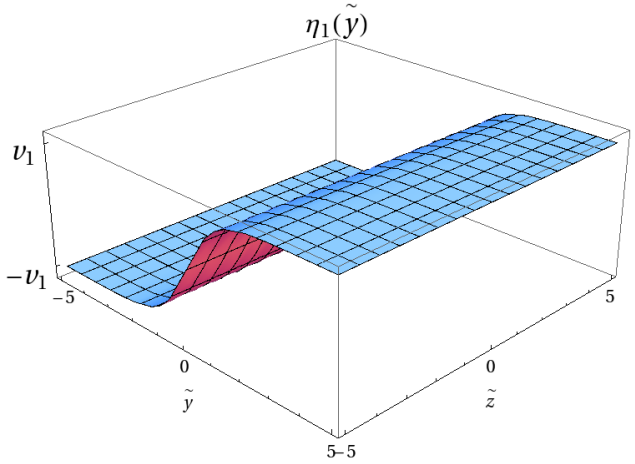

Figure 4.1: A plot of η_1 for the solution in Eq. 4.5.

The resulting relations of the kinetic terms of η_2 and χ_2 to themselves given in Eq. 4.7 are independent of the relative angle, θ, between this kink-lump pair and that for η_1 and χ_1. Hence, under the same parameter choice as in Eq. 4.4,

$$\begin{aligned} \eta_1(y) &= v_1 \tanh(ky), \\ \chi_1(y) &= A_1 \operatorname{sech}(ky), \\ \eta_2(y,z) &= v_2 \tanh[l(\cos\theta y + \sin\theta z)], \\ \chi_2(y,z) &= A_2 \operatorname{sech}[l(\cos\theta y + \sin\theta z)], \end{aligned} \tag{4.8}$$

is a solution to the Euler-Lagrange equations for general θ. This means we have a whole class of solutions ranging from a solution in which the two walls are parallel ($\theta = 0$), through intermediate angles of intersection, to the perpendicular solution of Eq. 4.5. The parallel and angled solutions obviously do not satisfy the same boundary conditions as the perpendicular solution given in Eq. 4.3. The angled solutions still divide the $y - z$ plane into four domains which tend to all four of the discrete global minima out at infinity. The parallel solution is a wall between two of these discrete vacua out at infinity along one direction. In calculating the energy density, the kinetic terms and the potentials describing the self-interactions and mass terms involving only η_1 and χ_1 and likewise only η_2 and χ_2 are associated with the energy density of the single kink-lump pairs, and integrating them over the directions normal to the walls yields the tensions associated with each kink-lump pair. In general, in theories with multiple domain-walls, the

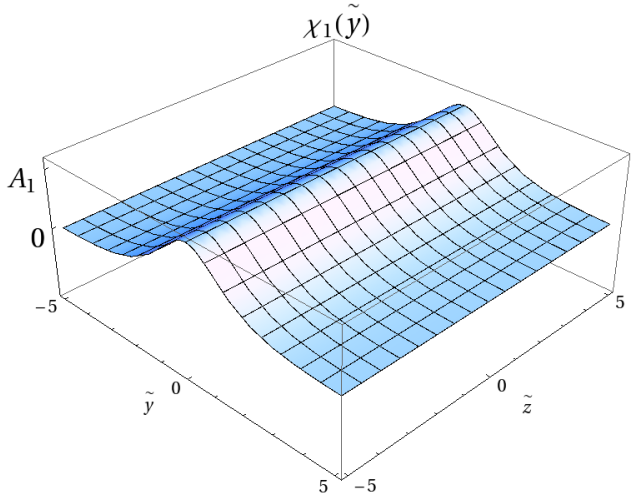

Figure 4.2: A plot of χ_1 for the solution in Eq. 4.5.

quartic interactions between the fields yielding different domain walls lead to a tension associated with the intersection or junction of those walls. In this scalar field theory and with the parameter choices we made in Eq. 4.4, we find that this tension is precisely zero,

$$\begin{aligned}\varepsilon_{int} &= \frac{1}{2}\lambda_{\eta_1\eta_2}(\eta_1^2 - v_1^2)(\eta_2^2 - v_2^2) + \frac{1}{2}\lambda_{\eta_1\chi_2}(\eta_1^2 - v_1^2)\chi_2^2 + \frac{1}{2}\lambda_{\chi_1\eta_2}\chi_1^2(\eta_2^2 - v_2^2) \\ &\quad + \frac{1}{2}\lambda_{\chi_1\chi_2}\chi_1^2\chi_2^2, \\ &= \frac{1}{2}\lambda_{\eta_1\eta_2}v_1^2v_2^2\,\mathrm{sech}^2\,(ky)\,\mathrm{sech}^2\,(lu) - \frac{1}{2}\lambda_{\eta_1\chi_2}v_1^2A_2^2\,\mathrm{sech}^2\,(ky)\,\mathrm{sech}^2\,(lu) \\ &\quad - \frac{1}{2}\lambda_{\chi_1\eta_2}A_1^2v_2^2\,\mathrm{sech}^2\,(ky)\,\mathrm{sech}^2\,(lu) + \frac{1}{2}\lambda_{\chi_1\chi_2}A_1^2A_2^2\,\mathrm{sech}^2\,(ky)\,\mathrm{sech}^2\,(lu), \\ &= 0,\end{aligned} \tag{4.9}$$

for all angles θ where here we have used $u = \cos\theta y + \sin\theta z$. These solutions are degenerate in energy.

It turns out that despite the energy degeneracy, neither the perpendicular nor angled solutions can evolve into the parallel solution. This is not surprising as the former two interpolate amongst the four vacua along the boundary, while the latter only interpolates between two of them so we expect them to be topologically distinct. To be precise, there exists a topological charge associated with the 2-dimensional boundary of the $y-z$ plane. The associated

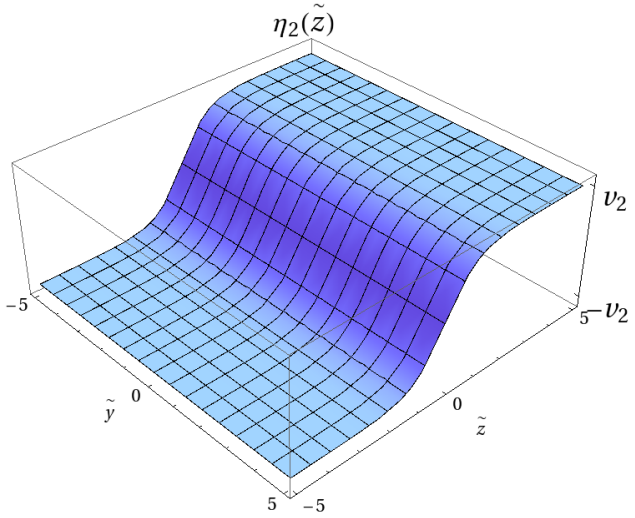

Figure 4.3: A plot of η_2 for the solution in Eq. 4.5.

topological current is defined by

$$J^{MNOP} = \epsilon^{MNOPQR}\epsilon^{ij}\partial_Q\eta_i\partial_R\eta_j. \tag{4.10}$$

Clearly, the 6-divergence of this current vanishes and is thus conserved. The conserved topological charge associated with this current is just

$$Q^{ABC} = \int d^6x J^{0ABC}. \tag{4.11}$$

Since the background fields are solely dependent on y and z, only the elements Q^{ijk} where $i, j, k = 1, 2, 3$ are non-zero. One can show that these charges are proportional to the integral

$$I = \int_\Sigma dydz\big(\partial_4\eta_1\partial_5\eta_2 - \partial_5\eta_1\partial_4\eta_2\big), \tag{4.12}$$

where Σ denotes the $y-z$ plane. Using Stokes' theorem, one can also write this as

$$\begin{aligned} I &= \int_{\partial\Sigma} \eta_1\partial_4\eta_2 dy + \eta_1\partial_5\eta_2 dz, \\ &= \int_{\partial\Sigma} \eta_1\nabla\eta_2.\mathbf{dl}. \end{aligned} \tag{4.13}$$

One can easily show from Eqs. 4.12 and 4.13 that for the perpendicular and angled solutions $I = 4v_1v_2$ whereas for the parallel solution $I = 0$. Thus

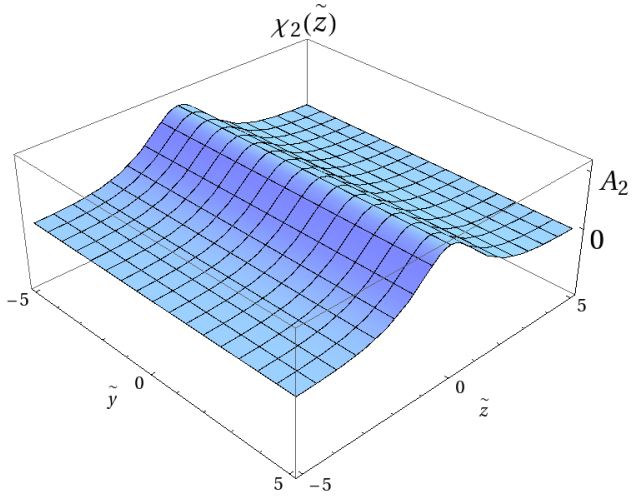

Figure 4.4: A plot of χ_2 for the solution in Eq. 4.5.

the perpendicular and angled solutions are stable against decay or evolution to the parallel solution despite the energy degeneracy.

The topological charge in Eq. 4.11 does not differentiate between the perpendicular and angled solutions. It is not clear whether this means that these solutions are in the same topological class as there could exist other topological charges which differ between the two types of solution. In case they are topologically equivalent, one can imagine that one could perform a small perturbation from the parameter region considered in generating the analytic solutions to ensure that the perpendicular solution is the most energetically favorable one since the energy degeneracy between the solutions is likely not true in general. From a rough glance at the interactions in Eq. 4.9 one can see that if one performs a perturbation $\lambda_{\eta_1\eta_2} \to \lambda_{\eta_1\eta_2} + \epsilon$, with $\epsilon > 0$, that the contribution $\epsilon\eta_1^2\eta_2^2$ is minimized for $\theta = 90°$ and tends towards infinity as $\theta \to 0$. Unfortunately, there are also resultant perturbations to the fields η_1, η_2, χ_1 and χ_2, and these perturbations satisfy four coupled partial differential equations which can only be solved numerically, so we can not give a definitive answer here.

We also need to perform a local stability analysis of the solutions given in this section. Likewise, this requires numerically solving four non-linear coupled partial differential equations and we defer this to a later study. For the rest of this paper, we will assume that the perpendicular solution is stable and that one can always choose this to be the background solution.

4.2 Fermion Localization

In this section, we show that fermions can be localized to the intersection of the two domain walls. Normally, in the case of a single domain wall, one localizes fermions to the center by Yukawa coupling them to the relevant scalar field. In the case of a single domain wall with a Yukawa coupling of the form $\overline{\Psi}\Psi\eta$, as $\eta \to -\eta$ under the discrete $\mathbb{Z}_2$ symmetry, to preserve the symmetry and maintain topological stability, we require that the Dirac bilinear $\overline{\Psi}\Psi \to -\overline{\Psi}\Psi$ under the symmetry. This can be achieved by choosing the fermionic fields to transform individually as $\Psi \to \pm i\Gamma\Psi$, where Γ is the gamma matrix associated with the direction parametrizing the profile of the domain-wall solution. In 4+1-dimensional (4+1D) theory, one often chooses $\Gamma = \Gamma^4 = -i\gamma^5$ for example.

In six dimensions, with our background set-up, if one wishes to localize chiral fermions to the intersection region of the background solution, one must Yukawa couple the desired fermionic fields to all four scalar fields. However, with two independent $\mathbb{Z}_2$ symmetries, one has a problem in attempting to couple a fermionic field to both defects since if we perform the first $\mathbb{Z}_2$ transformation $\eta_1 \to -\eta_1$, $\chi_1 \to -\chi_1$, $\eta_2 \to \eta_2$, $\chi_2 \to \chi_2$, and maintain that $\overline{\Psi}\Psi \to -\overline{\Psi}\Psi$ under such a transformation, then $\overline{\Psi}\Psi\eta_2$ and $\overline{\Psi}\Psi\chi_2$ are not invariant under the first symmetry, and likewise $\overline{\Psi}\Psi\eta_1$ and $\overline{\Psi}\Psi\chi_1$ won't be if we impose the second $\mathbb{Z}_2$ symmetry. Hence, we cannot localize fermions to the defect by using just scalar Yukawa interactions to all fields without compromising topological stability. This reflects the fact that we must choose our effective $6D$ localization bulk mass matrix carefully in order to localize chiral fermions on the intersection, an issue that was first raised in [99].

However, in 5+1D there is another possibility, since in spacetimes of even dimensionality there always exists a chirality operator and thus there always exists a pseudoscalar bilinear in these spacetime dimensionalities. In 5+1D, the chirality operator Γ^7 is defined

$$\begin{aligned}\Gamma^7 &= \Gamma^0\Gamma^1\Gamma^2\Gamma^3\Gamma^4\Gamma^5, \\ &= \frac{1}{6!}\epsilon_{MNOPQR}\Gamma^M\Gamma^N\Gamma^O\Gamma^P\Gamma^Q\Gamma^R.\end{aligned} \tag{4.14}$$

One can then define the pseudoscalar bilinear $\overline{\Psi}\Gamma^7\Psi$. Now we consider the Yukawa terms

$$\begin{aligned}\mathcal{L}_{Yuk} = &-ih_{\eta_1}\overline{\Psi}\Gamma^7\Psi\eta_1 - ih_{\chi_1}\overline{\Psi}\Gamma^7\Psi\chi_1 \\ &+ h_{\eta_2}\overline{\Psi}\Psi\eta_2 + h_{\chi_2}\overline{\Psi}\Psi\chi_2,\end{aligned} \tag{4.15}$$

and ask if it is possible to define two independent transformations for each $\mathbb{Z}_2$ symmetry for Ψ such that for the first symmetry in which $\eta_1 \to -\eta_1$ and $\chi_1 \to$

$-\chi_1$ we have $\overline{\Psi}\Gamma^7\Psi \to -\overline{\Psi}\Gamma^7\Psi$ but $\overline{\Psi}\Psi \to \overline{\Psi}\Psi$, while for the second reflection symmetry $\eta_2 \to -\eta_2$ and $\chi_2 \to -\chi_2$ we have $\overline{\Psi}\Gamma^7\Psi$ unchanged but $\overline{\Psi}\Psi \to -\overline{\Psi}\Psi$. Due to the fact that Γ^7 anticommutes with the gamma matrices, for the second $\mathbb{Z}_2$ one can easily show that the usual type of transformation $\Psi \to i\Gamma^5\Psi$ can be chosen. For the first $\mathbb{Z}_2$, one can show that the transformation $\Psi \to i\Gamma^4\Gamma^7\Psi$ induces the transformation $\overline{\Psi}\Psi \to \overline{\Psi}\Psi$ and $\overline{\Psi}\Gamma^7\Psi \to -\overline{\Psi}\Gamma^7\Psi$. Hence, we have shown that there exists a mechanism to couple a fermionic field to all four background scalar fields with the combination of scalar and pseudoscalar Yukawa couplings given in Eq. 4.15.

Henceforth, we assume boundary conditions such that we have the perpendicular intersecting domain-wall solution and we take the following sets of transformations to be our reflection symmetries which ensure topological stability of the background,

$$\begin{aligned} y &\to -y, \\ z &\to z, \\ \eta_1 &\to -\eta_1, \\ \chi_1 &\to -\chi_1, \\ \eta_2 &\to \eta_2, \\ \chi_2 &\to \chi_2, \\ \Psi &\to i\Gamma^4\Gamma^7\Psi, \end{aligned} \tag{4.16}$$

and

$$\begin{aligned} y &\to y, \\ z &\to -z, \\ \eta_1 &\to \eta_1, \\ \chi_1 &\to \chi_1, \\ \eta_2 &\to -\eta_2, \\ \chi_2 &\to -\chi_2, \\ \Psi &\to i\Gamma^5\Psi. \end{aligned} \tag{4.17}$$

We now need to show that there is indeed a chiral zero mode localized to the intersection of the domain walls. Writing down the resultant 6D Dirac equation for Ψ, we have

$$i\Gamma^M\partial_M\Psi + iW_1(y)\Gamma^7\Psi - W_2(z)\Psi = 0, \tag{4.18}$$

where

$$\begin{aligned} W_1(y) &= h_{\eta_1}\eta_1(y) + h_{\chi_1}\chi_1(y), \\ W_2(z) &= h_{\eta_2}\eta_2(z) + h_{\chi_2}\chi_2(z). \end{aligned} \tag{4.19}$$

In order to perform dimensional reduction and calculate the profiles of the modes of Ψ, we must choose a basis for the 5+1D Clifford algebra. One can show that

$$\begin{aligned}\Gamma^\mu &= \sigma_1 \otimes \gamma^\mu = \begin{pmatrix} 0 & \gamma^\mu \\ \gamma^\mu & 0 \end{pmatrix}, \\ \Gamma^4 &= \sigma_1 \otimes -i\gamma^5 = \begin{pmatrix} 0 & -i\gamma^5 \\ -i\gamma^5 & 0 \end{pmatrix}, \\ \Gamma^5 &= -i\sigma_3 \otimes \mathbb{1} = \begin{pmatrix} -i & 0 \\ 0 & i \end{pmatrix},\end{aligned} \tag{4.20}$$

satisfies the 5+1D Clifford algebra

$$\{\Gamma^M, \Gamma^N\} = 2\eta^{MN}, \tag{4.21}$$

and is thus an appropriate choice of basis for the 5+1D gamma matrices. In this basis the 6D chirality operator is

$$\Gamma^7 = \sigma_2 \otimes \mathbb{1} = \begin{pmatrix} 0 & i \\ -i & 0 \end{pmatrix}. \tag{4.22}$$

Decomposing Ψ into components $\Psi_\pm$ which have 4 complex components and are eigenvectors of Γ^5,

$$\Psi = \begin{pmatrix} \Psi_+ \\ \Psi_- \end{pmatrix}, \tag{4.23}$$

one can shown that the 6D Dirac equation reduces to

$$(i\gamma^\mu \partial_\mu + \gamma^5 \partial_4 + W_1(y))\Psi_+ - \partial_5 \Psi_- - W_2(z)\Psi_- = 0, \tag{4.24a}$$
$$(i\gamma^\mu \partial_\mu + \gamma^5 \partial_4 - W_1(y))\Psi_- + \partial_5 \Psi_+ - W_2(z)\Psi_+ = 0. \tag{4.24b}$$

To calculate the profiles of all modes, due to the fact that the excited Kaluza-Klein (KK) modes are usually Dirac fermions it is useful to find the corresponding Klein-Gordon (KG) equation that the components $\Psi_\pm$ satisfy. Operating with $(i\gamma^\mu \partial_\mu + \gamma^5 \partial_4 - W_1(y))$ from the left on Eq. 4.24a and likewise $(i\gamma^\mu \partial_\mu + \gamma^5 \partial_4 + W_1(y))$ on Eq. 4.24b, one obtains the KG equations

$$\Box \Psi_\pm + (W_1(y)^2 \mp W_1'(y)\gamma_5)\Psi_\pm + (W_2(z)^2 \pm W_2'(z))\Psi_\pm = 0. \tag{4.25}$$

Now we expand each of $\Psi_\pm$ as a series of modes. As one can see from Eq. 4.24, the y-dependent piece is chirality-dependent while the z-dependent piece is not. The z-dependent piece is only dependent on whether the component is Ψ_- or Ψ_+. Thus we make the expansion

$$\begin{aligned}&\Psi_\pm(x_\mu, y, z) = \\ &\quad \sum_m f^m_{\pm L}(y) g^m_\pm(z) \varphi^m_{\pm L}(x_\mu) + f^m_{\pm R}(y) g^m_\pm(z) \varphi^m_{\pm R}(x_\mu).\end{aligned} \tag{4.26}$$

Here, m just denotes some mass eigenvalue, $\varphi^m_{\pm L,R}$ denotes the 3+1D left/right-chiral mode of mass m embedded in the component $\Psi_\pm$ of Ψ, and $f^m_{\pm L,R}(y)$ and $g^m_\pm(z)$ are profiles for these modes along the y and z directions respectively. Since any 3+1D fermionic mode should satisfy a corresponding Klein-Gordon equation, let us substitute the expansion into Eq. 4.25 and demand that modes satisfy $\Box_{3+1}\varphi^m_{\pm L,R}(x_\mu) = -m^2\varphi^m_{\pm L,R}(x_\mu)$. We find that Eq. 4.25 reduces to

$$\begin{aligned}
&\big[-\frac{d^2 f^m_{\pm L}}{dy^2} + (W_1(y)^2 \pm W_1'(y))f^m_{\pm L}(y)\big]g^m_\pm(z) \\
&+ f^m_{\pm L}(y)\big[-\frac{d^2 g^m_\pm}{dz^2} + (W_2(z)^2 \pm W_2'(z))g^m_\pm(z)\big] \\
&= m^2 f^m_{\pm L}(y) g^m_\pm(z), \\
&\big[-\frac{d^2 f^m_{\pm R}}{dy^2} + (W_1(y)^2 \mp W_1'(y))f^m_{\pm R}(y)\big]g^m_\pm(z) \\
&+ f^m_{\pm R}(y)\big[-\frac{d^2 g^m_\pm}{dz^2} + (W_2(z)^2 \pm W_2'(z))g^m_\pm(z)\big] \\
&= m^2 f^m_{\pm R}(y) g^m_\pm(z),
\end{aligned} \tag{4.27}$$

for the left and right-chiral components respectively.

Demanding that the profiles satisfy the following Schrödinger equations (SE)

$$-\frac{d^2 f^m_{\pm L}}{dy^2} + (W_1(y)^2 \pm W_1'(y))f^m_{\pm L}(y) = \lambda^1_{\pm L} f^m_{\pm L}(y), \tag{4.28a}$$

$$-\frac{d^2 f^m_{\pm R}}{dy^2} + (W_1(y)^2 \mp W_1'(y))f^m_{\pm R}(y) = \lambda^1_{\pm R} f^m_{\pm R}(y), \tag{4.28b}$$

$$-\frac{d^2 g^m_\pm}{dz^2} + (W_2(z)^2 \pm W_2'(z))g^m_\pm(z) = \lambda^2_\pm g^m_\pm(z), \tag{4.28c}$$

we find that the values of the squared masses of the localized KK modes are

$$m^2_{\pm L,R} = \lambda^1_{\pm L,R} + \lambda^2_\pm, \tag{4.29}$$

for the modes embedded in $\Psi_\pm$.

Given the definitions for W_1 and W_2 in Eq. 4.19, one can see that the potentials of Eq. 4.28 are hyperbolic Scarf potentials. These potentials are well known and can be solved analytically [58, 39, 40]. For simplicity, let us assume that both h_{η_1} and h_{η_2} are positive definite. Non-dimensionalizing all

variables and parameters except m as

$$\begin{aligned} \tilde{y} &= ky, \qquad \tilde{z} = lz, \\ \tilde{h}_{\eta_1} &= \frac{h_{\eta_1} v_1}{k}, \qquad \tilde{h}_{\chi_1} = \frac{h_{\chi_1} A_1}{k}, \\ \tilde{h}_{\eta_2} &= \frac{h_{\eta_2} v_2}{l}, \qquad \tilde{h}_{\chi_2} = \frac{h_{\chi_2} A_2}{l}, \\ \tilde{\lambda}^1_{\pm L,R} &= \frac{\lambda^1_{\pm L,R}}{k^2}, \qquad \tilde{\lambda}^2_{\pm} = \frac{\lambda^2_{\pm}}{l^2}, \end{aligned} \tag{4.30}$$

and non-dimensionalizing the profiles as

$$\begin{aligned} \tilde{f}^m_{\pm L,R}(\tilde{y}) &= k^{-\frac{1}{2}} f^m_{\pm L,R}(y), \\ \tilde{g}^m_{\pm}(\tilde{z}) &= l^{-\frac{1}{2}} g^m_{\pm}(z), \end{aligned} \tag{4.31}$$

one can show that each of the Eqs. 4.28a, 4.28b, and 4.28c has a finite number of localized, square-normalizable solutions as well as a delocalized continuum. First, let us start with the z-dependent equations. For positive h_{η_2}, it is the potential for Ψ_-, $\tilde{W}_2^2 - \tilde{W}_2'$ which generates a series of $\lceil h_{\eta_2} \rceil$ localized modes starting from an eigenvalue of $\tilde{\lambda}^2_{-0} = 0$. The eigenvalues of these modes are given as

$$\tilde{\lambda}^2_{-n} = 2n\tilde{h}_{\eta_2} - n^2, \quad n = 0, 1, ..., \lfloor \tilde{h}_{\eta_2} \rfloor. \tag{4.32}$$

The $\tilde{\lambda}^2_{-0}$ profile is given by

$$\tilde{g}^0_-(\tilde{z}) = \tilde{D}^0_- e^{-\tilde{h}_{\eta_2} \log[\cosh(\tilde{z})] - 2\tilde{h}_{\chi_2} \arctan[\tanh(\tilde{z}/2)]}, \tag{4.33}$$

and the profiles for the excited localized modes can be generated by applying the ladder operator which is proportional to $W_2(\tilde{z}) - \frac{d}{d\tilde{z}}$. As for the potential for Ψ_+, $\tilde{W}_2^2 + \tilde{W}_2'$, given our parameter choice there is no solution with $\tilde{\lambda}^2_{+0} = 0$. Rather, there are $\lfloor \tilde{h}_{\eta_2} \rfloor$ localized modes starting from an eigenvalue $\tilde{\lambda}^2_{+1} = 2\tilde{h}_{\eta_2} - 1$ (provided $\tilde{h}_{\eta_2} > 1$). All this implies that, in considering just the interaction with the z-dependent kink-lump, for $\tilde{h}_{\eta_2} > 0$, there is a massless 4+1D Dirac zero mode generated in Ψ_- and then a tower of massive 4+1D Dirac modes embedded in both Ψ_- and Ψ_+. In then further considering the interaction with the y-dependent part of the solution and calculating the $f_{\pm L,R}$, each of these 4+1D modes will generate a tower of 3+1D left- and right-chiral modes localized to the domain-wall intersection. Obviously, any chiral zero mode produced on the intersection must be embedded in the massless 4+1D zero mode of Ψ_- in this case. If we choose $\tilde{h}_{\eta_2}$ to be negative instead, the roles of Ψ_- and Ψ_+ in this situation are reversed, and the chiral zero mode must therefore be embedded in Ψ_+.

Now let us analyze the y-dependent equations. These equations are also SE's with the hyperbolic Scarf potentials. In this case the particular form of the hyperbolic Scarf potential for the modes is dependent on chirality. Since we are assuming $\tilde{h}_{\eta_2} > 0$ without loss of generality, let us focus on the left- and right-chiral modes embedded in Ψ_- first, since as noted above this is the component containing any potential chiral zero mode. Looking at Eqs. 4.28a and 4.28b, one sees that the potentials for the left- and right-chiral components in Ψ_- are $\tilde{W}_1(\tilde{y})^2 - \tilde{W}_1'(\tilde{y})$ and $\tilde{W}_1(\tilde{y})^2 + \tilde{W}_1'(\tilde{y})$ respectively. Hence, we easily deduce that for $\tilde{h}_{\eta_1} > 0$, the equation for the left-chiral modes of Ψ_- has the same form as that for the z-dependent profile equation for Ψ_- and thus has a mode starting from an eigenvalue of $\tilde{\lambda}^1_{-L0} = 0$, and likewise that for the right-chiral modes has the same form as that for the $\tilde{g}^m_+(\tilde{z})$ and thus only has solutions with positive definite eigenvalues. Since from Eq. 4.29, we know that these eigenvalues directly contribute to the mass, this implies that for the choice $\tilde{h}_{\eta_1} > 0$, $\tilde{h}_{\eta_2} > 0$, there is a single massless left-chiral zero mode embedded in Ψ_- localized to the intersection.

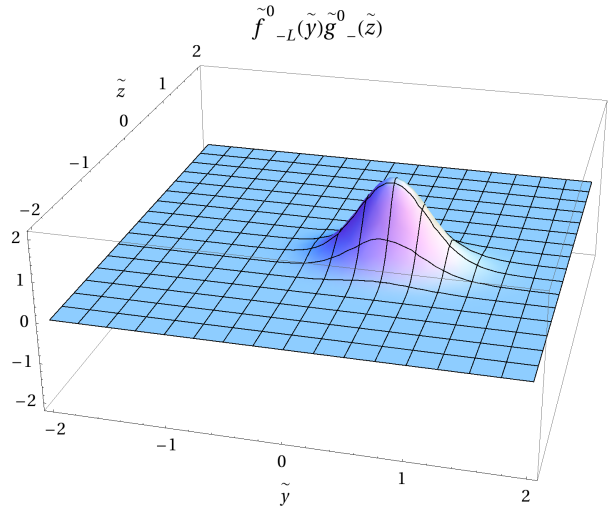

Figure 4.5: A plot of the profile for the left chiral zero mode embedded in Ψ_- for the parameter choice $\tilde{h}_{\eta_1} = 10$, $\tilde{h}_{\chi_1} = -5$, $\tilde{h}_{\eta_2} = 20$, and $\tilde{h}_{\chi_2} = 4$.

The resultant solution for the $\lambda^1_{-L0} = 0$ eigenfunction, $\tilde{f}^0_{-L}(\tilde{y})$ is given by

$$\tilde{f}^0_{-L}(\tilde{y}) = \tilde{C}^0_{-L} e^{-\tilde{h}_{\eta_1} \log[\cosh(\tilde{y})] - 2\tilde{h}_{\chi_1} \arctan[\tanh(\tilde{y}/2)]}, \tag{4.34}$$

and thus the full profile over the $y - z$ plane for the left chiral zero mode is

$$\tilde{F}^0_{-L}(\tilde{y}, \tilde{z}) = \tilde{f}^0_{-L}(\tilde{y})\tilde{g}^0_-(\tilde{z}), \tag{4.35}$$

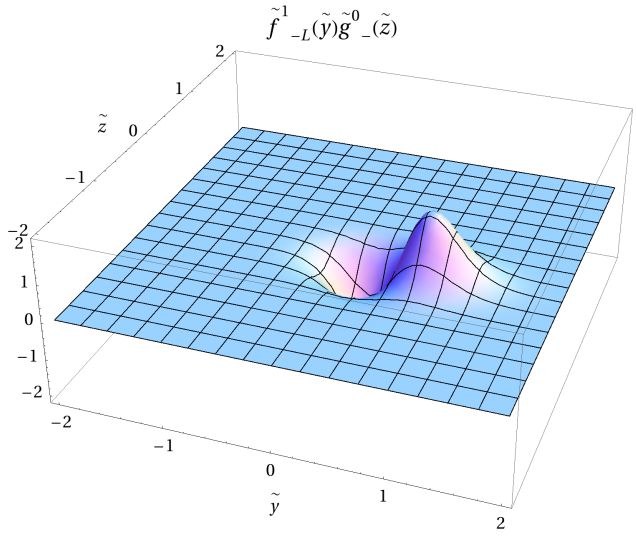

Figure 4.6: A plot of the profile for the left-chiral $i = 1$, $j = 0$ mode in Ψ_- for the parameter choice $\tilde{h}_{\eta_1} = 10$, $\tilde{h}_{\chi_1} = -5$, $\tilde{h}_{\eta_2} = 20$, and $\tilde{h}_{\chi_2} = 4$.

and a plot of this is shown in Fig. 4.5.

The y-dependent profiles for the higher localized left-chiral modes can be accessed by applying a ladder operator proportional to $W_1(\tilde{y}) - \frac{d}{d\tilde{y}}$. The eigenvalues of these $\tilde{f}^n_{-L}$ profiles are given as

$$\tilde{\lambda}^1_{-Ln} = 2\tilde{h}_{\eta_1} n - n^2. \tag{4.36}$$

Putting Eqs. 4.32 and 4.36 together and converting back to dimensionful variables, we can see that the resultant squared masses of the left-chiral modes embedded in Ψ_- are

$$\begin{aligned} m^2_{-Lij} &= \tilde{\lambda}^1_{-Li} k^2 + \tilde{\lambda}^2_{-j} l^2, \\ &= 2ih_{\eta_1} v_1 k - 2i^2 k^2 + 2jh_{\eta_2} v_2 l - 2j^2 l^2, \\ &i = 0, 1, ..., \lfloor \tilde{h}_{\eta_1} \rfloor, \quad j = 0, 1, ..., \lfloor \tilde{h}_{\eta_2} \rfloor. \end{aligned} \tag{4.37}$$

For the parameter choice $\tilde{h}_{\eta_1} = 10$, $\tilde{h}_{\chi_1} = -5$, $\tilde{h}_{\eta_2} = 20$, and $\tilde{h}_{\chi_2} = 4$, we give a plot of the full profile $\tilde{F}^0_{-L}(\tilde{y}, \tilde{z})$ for the zero mode ($i = 0$, $j = 0$) in Fig. 4.5. We also give plots for the analogous profiles of the left-chiral $i = 1$, $j = 0$, $i = 1$, $j = 2$, and $i = 2$, $j = 2$ KK modes in Fig. 4.6, Fig. 4.7 and Fig. 4.8 respectively.

For the right-chiral modes of Ψ_-, there is no zero mode, but the massive modes have the same mass as the left-chiral counterparts, and the masses

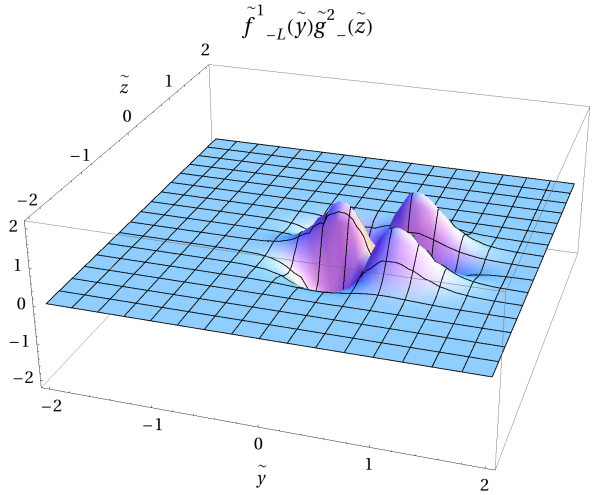

Figure 4.7: A plot of the profile for the left-chiral $i = 1$, $j = 2$ mode in Ψ_- for the parameter choice $\tilde{h}_{\eta_1} = 10$, $\tilde{h}_{\chi_1} = -5$, $\tilde{h}_{\eta_2} = 20$, and $\tilde{h}_{\chi_2} = 4$.

are

$$\begin{aligned} m^2_{-Rij} &= \tilde{\lambda}^1_{-Ri}k^2 + \tilde{\lambda}^2_{-j}l^2, \\ &= 2ih_{\eta_1}v_1k - 2i^2k^2 + 2jh_{\eta_2}v_2l - 2j^2l^2, \\ &i = 1, ..., \lfloor \tilde{h}_{\eta_1} \rfloor, \quad j = 0, 1, ..., \lfloor \tilde{h}_{\eta_2} \rfloor. \end{aligned} \tag{4.38}$$

For the left-chiral and right-chiral localized modes embedded in Ψ_+, the eigenvalue associated with the z-dependent profiles, λ^2_{+j}, is always more than zero, thus all these modes are massive. Also, $\lambda^2_{+j} = \lambda^2_{-j}$ for $j = 1, 2, ..., \lfloor \tilde{h}_{\eta_2} \rfloor$. If one looks at Eqs. (4.28a) and (4.28b), one sees that the y-dependent profiles $f^m_{\pm L}$ of the chiral modes of Ψ_- satisfy the same equation as those of equal mass and opposite chirality in Ψ_+, In other words, $f^m_{\pm L} = f^m_{\mp R}$, which in turn implies that $\lambda^1_{+L,R} = \lambda^1_{-R,L}$. Thus the masses for these modes are simply

$$\begin{aligned} m^2_{+Lij} &= \tilde{\lambda}^1_{+Li}k^2 + \tilde{\lambda}^2_{+j}l^2, \\ &= 2ih_{\eta_1}v_1k - 2i^2k^2 + 2jh_{\eta_2}v_2l - 2j^2l^2, \\ &i = 1, ..., \lfloor \tilde{h}_{\eta_1} \rfloor, \quad j = 1, ..., \lfloor \tilde{h}_{\eta_2} \rfloor, \end{aligned} \tag{4.39}$$

and

$$\begin{aligned} m^2_{+Rij} &= \tilde{\lambda}^1_{+Ri}k^2 + \tilde{\lambda}^2_{+j}l^2, \\ &= 2ih_{\eta_1}v_1k - 2i^2k^2 + 2jh_{\eta_2}v_2l - 2j^2l^2, \\ &i = 0, 1, ..., \lfloor \tilde{h}_{\eta_1} \rfloor, \quad j = 1, ..., \lfloor \tilde{h}_{\eta_2} \rfloor. \end{aligned} \tag{4.40}$$

Obviously, these modes should satisfy a 3+1D Dirac equation. The above KG equations and the resultant equations for the profiles give clues for what

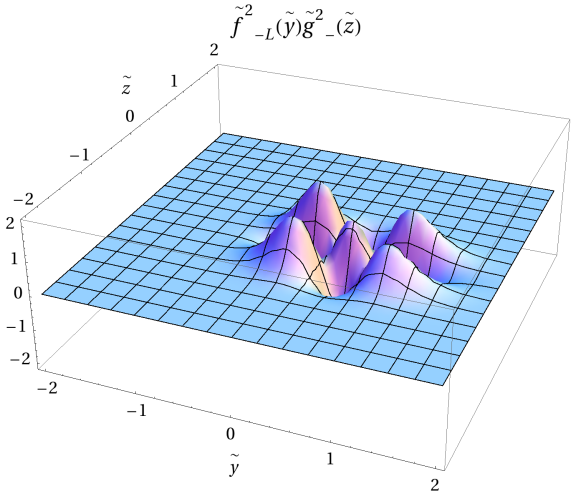

Figure 4.8: A plot of the profile for the left-chiral $i = 2$, $j = 2$ mode in Ψ_- for the parameter choice $\tilde{h}_{\eta_1} = 10$, $\tilde{h}_{\chi_1} = -5$, $\tilde{h}_{\eta_2} = 20$, and $\tilde{h}_{\chi_2} = 4$.

the form of these should be. Each mode belonging to Ψ_- or Ψ_+ has a z-dependent profile g^m_- or g^m_+ respectively. In turn, each chiral mode inside Ψ_- and Ψ_+ has a y-dependent profile $f^m_{\pm L,R}$, and as we noted above, $f^m_{\pm L} = f^m_{\mp R}$. In using this expansion and performing dimensional reduction, one expects a left-chiral mode of Ψ_- with a particular mass to not only attain a mass term with the corresponding right-chiral modes of Ψ_- but also those of Ψ_+. This is particularly important when considering that for a left-chiral mode in Ψ_- which has $\lambda^1_{-L} = 0$ but $\lambda^2_- \neq 0$ (ie. the mode is a zero mode with respect to the y-dependent wall) given that there is no corresponding right-chiral mode of the same eigenvalues and thus mass in Ψ_-. However, there is in Ψ_+ and thus with such modes there is a single Dirac fermion of the given mass formed from the left-chiral mode in Ψ_- and the right-chiral mode of Ψ_+. Hence, the correct ansatz is that the effective 3+1D mass Lagrangian should be of the form

$$\mathcal{L} = \begin{pmatrix} \overline{\varphi^m_{-L}} & \overline{\varphi^m_{+L}} \end{pmatrix} \begin{pmatrix} -\sqrt{\lambda^1_{-L}} & \sqrt{\lambda^2_-} \\ \sqrt{\lambda^2_-} & \sqrt{\lambda^1_{-L}} \end{pmatrix} \begin{pmatrix} \varphi^m_{-R} \\ \varphi^m_{+R} \end{pmatrix} + h.c. \tag{4.41}$$

For the massive modes with both λ^1_{-L} and λ^2_- non-zero, one can deduce from the mass matrix in Eq. 4.41 that there exist two Dirac fermion modes of mass $\sqrt{\lambda^1_{-L} + \lambda^2_-}$. After putting this ansatz into the 5D Dirac equation and doing some algebra, one can show that the equations yielded for the y and z-dependent profiles are exactly the same as those derived above from

the Klein-Gordon equation.

In this section we have shown that there exists a single chiral zero mode localized to the domain-wall intersection when the 5+1D fermionic field Ψ is subject to the Yukawa interactions in Eq. 4.15. In addition to this single chiral zero mode, there is a single tower of Dirac modes which are zero modes with respect to one wall but not the other, and then for each given squared mass value for which the eigenvalues associated with each wall are both non-zero there exist two Dirac modes. There will also be modes with one of $\lambda^1_{\pm L,R}$ or $\lambda^2_{\pm}$ being more than the maximum value for the localized KK modes and the other corresponding to a value associated with a localized mode; these modes can propagate along one wall and behave as 5D delocalized modes. Modes for which both the eigenvalues $\lambda^1_{\pm L,R}$ and $\lambda^2_{\pm}$ are more than the maximum values for the localized modes are completely delocalized from both walls and can propagate through the entire 6D bulk.

4.3 Scalar Localization

Scalar localization can be similarly achieved via quartic coupling to the background scalar fields. Generally, in a model that is to be physically viable we are interested in localizing Higgs fields which have gauge charges. Thus for this section we will assume that our candidate scalar field is a complex scalar field Φ. The scalar potential for Φ is then

$$\begin{aligned} V_\phi = &\frac{1}{2}\mu_\Phi^2\Phi^\dagger\Phi + \frac{1}{4}\lambda_\Phi(\Phi^\dagger\Phi)^2 + \frac{1}{2}\lambda_{\Phi\eta_1}\eta_1^2\Phi^\dagger\Phi \\ &+ \frac{1}{2}\lambda_{\Phi\chi_1}\chi_1^2\Phi^\dagger\Phi + \frac{1}{2}\lambda_{\Phi\eta_1\chi_1}\eta_1\chi_1\Phi^\dagger\Phi + \frac{1}{2}\lambda_{\Phi\eta_2}\eta_2^2\Phi^\dagger\Phi \\ &+ \frac{1}{2}\lambda_{\Phi\chi_2}\chi_2^2\Phi^\dagger\Phi + \frac{1}{2}\lambda_{\Phi\eta_2\chi_2}\eta_2\chi_2\Phi^\dagger\Phi. \end{aligned} \tag{4.42}$$

Assuming that either Φ has a vanishing vacuum expectation value (VEV) or one of much smaller magnitude than those that the background fields attain (as it would be in the case of an electroweak Higgs boson), we can ignore the quartic self-coupling for Φ in the determination of the profiles when we do a mode expansion. Hence, we can focus solely on the couplings of Φ to the background fields and the mass term, and to calculate the profiles we must solve the 5+1D KG equation

$$\begin{aligned} \big[\Box + \mu_\Phi^2 + \lambda_{\Phi\eta_1}\eta_1^2 + \lambda_{\Phi\chi_1}\chi_1^2 + \lambda_{\Phi\eta_1\chi_1}\eta_1\chi_1 \\ + \lambda_{\Phi\eta_2}\eta_2^2 + \lambda_{\Phi\chi_2}\chi_2^2 + \lambda_{\Phi\eta_2\chi_2}\eta_2\chi_2\big]\Phi = 0. \end{aligned} \tag{4.43}$$

Again assuming the same perpendicular solution for the background that we assumed in the previous section, we expand Φ as a series of modes

$$\Phi(x_\mu, y, z) = \sum_m p_m(y) q_m(z) \phi_m(x_\mu), \tag{4.44}$$

where the $\phi_m(x_\mu)$ are 3+1D scalar modes satisfying the KG equation $\Box\phi_m(x_\mu) = -m^2\phi_m(x_\mu)$ and the $p_m(y)$ and $q_m(z)$ are the associated profiles along the y and z directions respectively. Subsitituting this expansion into Eq. 4.43, and then demanding that profiles satisfy the Schrödinger equations

$$\begin{aligned}
&\big[-\frac{d^2}{dy^2} + \lambda_{\Phi\eta_1}\eta_1^2(y) + \lambda_{\Phi\chi_1}\chi_1^2(y) \\
&+ \lambda_{\Phi\eta_1\chi_1}\eta_1(y)\chi_1(y)\big] p_m(y) = \lambda_m^1 p_m(y) \qquad (4.45a) \\
&\big[-\frac{d^2}{dz^2} + \lambda_{\Phi\eta_2}\eta_2^2(z) + \lambda_{\Phi\chi_2}\chi_2^2(z) \\
&+ \lambda_{\Phi\eta_2\chi_2}\eta_2(z)\chi_2(z)\big] q_m(z) = \lambda_m^2 q_m(z), \qquad (4.45b)
\end{aligned}$$

reduces Eq. 4.43 to a relation between the masses of the KK modes m to the eigenvalues λ_m^1, λ_m^2 and the 5D bare mass μ_Φ

$$m^2 = \mu_\Phi^2 + \lambda_m^1 + \lambda_m^2. \tag{4.46}$$

Working in the non-dimensionalised coordinates $\tilde{y}_1 = \tilde{y} = ky$, $\tilde{y}_2 = \tilde{z} = lz$, using the notation $p_m^1 = p_m$ and $p_m^2 = q_m$, and given the perpendicular solution given in Eq. 4.5, the Schrödinger equations 4.45 can both be rewritten in the form

$$\begin{aligned}
&-\frac{d^2 p_m^i}{d\tilde{y}_i^2} + V_{HS}^i(\tilde{y}_i) p_m^i(\tilde{y}_i) = E_m^i p_m^i(\tilde{y}_i), \\
&V_{HS}^i(\tilde{y}_i) = a_i^2 + \left(b_i^2 - a_i^2 - a_i\right) \mathrm{sech}^2(\tilde{y}_i) + b_i(2a_i+1)\,\mathrm{sech}(\tilde{y}_i)\tanh(\tilde{y}_i),
\end{aligned} \tag{4.47}$$

where the a_i and b_i are defined as

$$\begin{aligned}
a_i &= \frac{1}{2}\bigg(-1 + \big(2[(\tilde{\lambda}_{\Phi\chi_i} - \tilde{\lambda}_{\Phi\eta_i} - \frac{1}{4})^2 + \tilde{\lambda}_{\Phi\eta_i\chi_i}^2]^{\frac{1}{2}} - 2\tilde{\lambda}_{\Phi\chi_i} + 2\tilde{\lambda}_{\Phi\eta_i} + \frac{1}{2}\big)^{\frac{1}{2}}\bigg), \\
b_i &= \frac{\tilde{\lambda}_{\Phi\eta_i\chi_i}}{2a_i+1},
\end{aligned} \tag{4.48}$$

the non-dimensionalized versions of the original eigenvalues and quartic scalar couplings are defined as

$$\begin{aligned}
&\tilde{\lambda}_m^1 = \frac{\lambda_m^1}{k^2},\ \tilde{\lambda}_{\Phi\eta_1} = \frac{\lambda_{\Phi\eta_1} v_1^2}{k^2},\ \tilde{\lambda}_{\Phi\chi_1} = \frac{\lambda_{\Phi\chi_1} A_1^2}{k^2},\ \tilde{\lambda}_{\Phi\eta_1\chi_1} = \frac{\lambda_{\Phi\eta_1\chi_1} v_1 A_1}{k^2} \\
&\tilde{\lambda}_m^2 = \frac{\lambda_m^2}{l^2},\ \tilde{\lambda}_{\Phi\eta_2} = \frac{\lambda_{\Phi\eta_2} v_2^2}{l^2},\ \tilde{\lambda}_{\Phi\chi_2} = \frac{\lambda_{\Phi\chi_2} A_2^2}{l^2},\ \tilde{\lambda}_{\Phi\eta_2\chi_2} = \frac{\lambda_{\Phi\eta_2\chi_2} v_2 A_2}{l^2},
\end{aligned} \tag{4.49}$$

and the eigenvalues of these potentials E_m^i given in terms of $\tilde{\lambda}_m^i$, $\tilde{\lambda}_{\Phi\eta_i}$ and a_i are

$$E_m^i = \tilde{\lambda}_m^i - \tilde{\lambda}_{\Phi\eta_i} + a_i^2. \tag{4.50}$$

Assuming a_1 and a_2 are positive[1], these hyperbolic scarf potentials yield a discrete set of modes localized to the intersection of the domain walls. A localized ϕ_m mode must clearly have both of p_m and q_m decay to zero as $y \to \pm\infty$ and $z \to \pm\infty$ respectively. Since the respective hyperbolic scarf potentials for the p_m and q_m yield $\lceil a_1 \rceil$ and $\lceil a_2 \rceil$ localized functions respectively, there are $\lceil a_1 \rceil \lceil a_2 \rceil$ modes localized to the domain-wall intersection. For each potential, the eigenvalues for the localized modes are known to be

$$E_n^i = 2na_i - n^2, \tag{4.51}$$

for $n = 0, 1, ..., \lfloor a_i \rfloor$, and using Eqs. 4.46, 4.50, and 4.51 we thus find that the squared masses of the localized 3+1D modes are

$$m_{ij}^2 = \mu_\Phi^2 + \tilde{\lambda}_{\Phi\eta_1} k^2 + \tilde{\lambda}_{\Phi\eta_2} l^2 - (a_1 - i)^2 k^2 - (a_2 - j)^2 l^2, \tag{4.52}$$

for $i = 0, 1, ..., \lfloor a_1 \rfloor$ and $j = 0, 1, ..., \lfloor a_2 \rfloor$.

There will also exist modes with sufficient average momenta transverse to one domain wall but not the other such that these modes are localized to one wall but not the other. These modes have a profile with one of the quantum numbers described above with respect to one wall but will have energies above that of the most energetic localized mode of the other. These modes are essentially 5D particles.

For modes with energies above all localized modes, their profiles along both directions are delocalized and they are thus 6D particles with can propogate along the full extent of the bulk.

In any potentially phenomenological model based on this type, we are usually interested in the lowest energy localized mode, as this 4D scalar mode would correspond to Higgs particles in the effective field theory on the domain-wall intersection. In our model, this mode is the $i = 0$, $j = 0$ mode of Eq. 4.52. The resultant (non-dimensionalized) profiles for this mode $\tilde{p}_0(\tilde{y})$ and $\tilde{q}_0(\tilde{z})$ are simply given by

$$\begin{aligned} \tilde{p}_0(\tilde{y}) &= \tilde{C}_0 e^{-a_1 \log[\cosh(\tilde{y})] - 2b_1 \arctan[\tanh(\tilde{y}/2)]}, \\ \tilde{q}_0(\tilde{z}) &= \tilde{D}_0 e^{-a_2 \log[\cosh(\tilde{z})] - 2b_2 \arctan[\tanh(\tilde{z}/2)]}. \end{aligned} \tag{4.53}$$

Here, $\tilde{p}_0(\tilde{y}) = k^{-\frac{1}{2}} p_0(\tilde{y})$ and $\tilde{q}_0(\tilde{z}) = l^{-\frac{1}{2}} q_0(\tilde{z})$.

[1]If one of a_1 or a_2 is negative, then there are no modes localized to the intersection and there will exist modes localized to one wall but delocalized from the other. If both are negative, then all modes are delocalized from both walls.

4.4 Conclusion

In this chapter, we have generated a rare analytic solution to a $\mathbb{Z}_2 \times \mathbb{Z}_2$-invariant scalar field theory with four real scalar fields in 5+1D spacetime describing a pair of intersecting domain walls with internal structure. We found that with respect to the desirable perpendicular solution, there also existed a class of solutions describing kink-lump solutions which intersect at an angle between 0 and 90 degrees, as well as a solution where the walls are parallel and that these solutions were energy degenerate. We then argued that there exists a conserved topological charge related to the one-dimensional boundary of the $y-z$ plane which differed between the intersecting solutions and the parallel solution, meaning that the intersecting solutions cannot evolve to the parallel one despite this energy degeneracy. We also gave an argument as to why the perpendicular solution might be energetically favorable to the solutions with intersection angle less than 90 degrees in a nearby region of parameter space.

In addition to finding this solution, we showed in the case that the two domain walls were perpendicular that fermions and scalars could be dynamically localized to the intersection of the two walls. We found that coupling a 6D fermionic field to one kink-lump pair with ordinary scalar Yukawa couplings and to the other with pseudoscalar Yukawa couplings allowed the fermionic sector to be invariant under the full $\mathbb{Z}_2 \times \mathbb{Z}_2$ symmetry, and resulted in the localization of a 4D chiral zero mode on the intersection of the kinks, followed by a tower of localized KK modes and 5D and 6D delocalized modes.

Standard quartic couplings of a complex scalar field to the background scalar fields resulted in a tower of localized 4D localized scalar modes with the squared masses starting from some potentially non-zero value. This result is similar to the result for scalar localization to a single domain wall in 5D. Furthermore, the squared mass of the lowest energy scalar mode can be negative, allowing the possibility of the localized scalar field inducing spontaneous symmetry breaking should that scalar field transform under a non-trivial gauge group representation.

Localization of gravity and gauge bosons is left to later work. Localization of gravity would involve searching for a similar solution to the 6D Einstein field equations as well as the Einstein-Klein-Gordon equations. These equations are highly non-linear and difficult to solve so it remains to be seen if an analytic solution could be found. It could also be the case that such a solution could have qualitative differences as in principle the two domain-wall branes should interact gravitationally, whereas in this flat space case the net interaction between the two kink-lump solutions was zero.

For the localization of gauge bosons, we conjecture that the Dvali-Shifman

mechanism works in 5+1D spacetime. This ultimately depends on whether or not non-Abelian gauge theories are confining in 5+1D. In previous work in 4+1D, particularly in the $SU(5)$ model [23], the Dvali-Shifman mechanism was facilitated by the addition of a scalar field transforming under the gauge group which attained a lump-like profile and induced symmetry breaking in the interior of the domain wall. Hence, the background solution of this model was of the kink-lump type discussed in this thesis, and the additional fields χ_1 and χ_2 which attained lump-like profiles in the 6D model are potentially well motivated. With the assignment of gauge representations, these fields can break a gauge group to different subgroups which then *clash* at the intersection, leading to further symmetry breaking and a different realization of the Clash-of-Symmetries mechanism [24, 25]. We will discuss in detail this realization of the Clash-of-Symmetries mechanism and its applications to model building in the next chapter.

Chapter 5

A Clash-of-Symmetries Mechanism from Intersecting Domain-Wall Branes

In the previous chapter, we proposed a model in 5+1D based on the discrete group $\mathbb{Z}_2 \times \mathbb{Z}_2$ with four real scalar fields in which two of the scalar fields generate intersecting domain walls and the other two attain lump-like profiles parallel to each of the walls. It was found that there existed a small, special region of parameter space generating analytic solutions. It was also shown that fermions and scalars could be localized to the domain wall intersection, with the couplings to the lumps shifting the profiles away from the center. To construct a realistic model with a Standard Model localized to the domain-wall intersection then requires that we introduce mechanisms for the localization of gravity and the localization of gauge bosons. This chapter focuses on the latter.

As was discussed in Sec. 1.5, the only plausible mechanism for localizing gauge bosons to domain walls is the Dvali-Shifman mechanism. In its most basic form, it involves a non-Abelian gauge group G, which is confining in the bulk, being broken to a subgroup H. The H-bosons are then confined to the domain wall by the confinement dynamics of G. Previously, we have dealt with the DGV model in which $G = SU(5)$ and $H = SU(3) \times SU(2) \times U(1)$. Other domain-wall brane models utilizing Dvali-Shifman dynamics have been constructed based on the gauge groups $SO(10)$ [124] and E_6 [25].

The E_6 model in Ref. [25] is particularly interesting as it is based on a generalization of the Dvali-Shifman mechanism called the Clash-of-Symmetries (CoS) mechanism [127, 128, 24, 25, 129, 130, 131]. The condition of the original Dvali-Shifman mechanism where G was unbroken is not a necessary one: one just has to ensure that the subgroup preserved on the wall is con-

tained by a larger non-Abelian subgroup of G which is in confinement phase in the bulk. It was realized that a smaller subgroup on the wall could still be localized if G was broken respectively to isomorphic but *differently embedded* subgroups H and H' on each side of the domain wall. In the interior of the wall, the symmetry respected is the intersection of these subgroups $H \cap H'$ and some of the factors of this final subgroup will be localized to the domain wall provided they are proper subgroups of non-Abelian factors of both H and H' which are confining in the respective halves of the bulk. In proposing the CoS mechanism, we have many tools in our framework in which to extend domain-wall brane models to larger gauge groups.

Just as we saw in the previous chapter that there is more freedom in constructing braneworlds based on solitons such as domain walls in 5+1D and higher, there is clearly also more freedom in how we localize gauge fields from the Dvali-Shifman mechanism assuming that 5+1D non-Abelian theories have a confinement phase. Although we are unaware of any work which attempts to prove that a confinement phase exists in 5+1D non-Abelian gauge theories, we are encouraged by lattice gauge simulations which have shown that there exist confining phases in 4+1D SU(2) [57] and SU(5) [41] Yang-Mills gauge theories. The simplest scenario one could think of in both intersecting and nested wall scenarios is a simple codimension-2 generalization of the standard Dvali-Shifman picture on a single wall where a scalar field attains a tachyonic mass in the center of the defect or intersection region and breaks a non-Abelian gauge group G to a subgroup H with the entire 5+1D bulk around the core of the defect in confinement phase. With domain ribbons, one could imagine a nested Dvali-Shifman scenario where we use scalar fields to break G to a subgroup H on the first wall with another scalar field localized to the first domain wall breaking a non-Abelian factor of H to yet a smaller gauge group on the core of the domain ribbon.

This chapter focuses on an application of the Dvali-Shifman mechanism suited for intersecting domain walls and which is the natural one to consider in the context of the model proposed in the previous chapter, namely that of what we call an intersecting Clash-of-Symmetries mechanism. Here, we utilize the two scalar fields which attain one-dimensional lump-like profiles parallel to each domain wall by giving them gauge charges so that they break G to two subgroups H_1 and H_2 on the respective domain walls. Here, the 5+1D bulk away from both domain walls is assumed to be in confinement phase so that H_1 and H_2 are localized to the respective walls by the standard Dvali-Shifman mechanism. On the intersection of these walls, there in general is a further symmetry breaking to the overlap of these subgroups $H_1 \cap H_2$. We in turn assume that the non-Abelian factors of H_1 and H_2 are in confinement phase in the 4+1D bulk of the respective domain walls outside

the intersection. This means that non-Abelian factors of $H_1 \cap H_2$ are localized by Dvali-Shifman dynamics if they are proper subgroups of both H_1 and H_2. Further, Abelian factors of $H_1 \cap H_2$ are localized if their generators can be written completely in terms of generators belonging to the non-Abelian factors of both H_1 and H_2. Given that the scalar fields generating lumps need not be in the same representation or have the same symmetry breaking pattern, in this version of the CoS mechanism we need not have H_1 and H_2 isomorphic. In general, the clashing groups H_1 and H_2 are determined by the 4+1D energy densities (or brane tensions) of the two perpendicular kink-lump pairs which can be calculated in terms of the kink-lump solutions that we set as the boundary conditions at infinity around the plane spanned by the two extra dimensions. Given that the 4+1D energy density is degenerate for single kink-lump solutions which break G to different embeddings of the same subgroup, it is then the minimization of the 3+1D junction tension or energy density which arises due to interactions between the perpendicular kink-lump solutions which determines the exact form of the resultant $H_1 \cap H_2$ on the intersection.

After laying out the details of the intersecting CoS mechanism, we give several toy models based on the gauge group $SU(7)$. It turns out that it is possible to localize a Standard Model gauge group[1] under this mechanism with $G = SU(7)$. The first three examples we give are all with the fields attaining lump-like profiles in the adjoint representation. The first example is one where the lump fields attain vacua such that $H_1 = SU(5) \times SU(2) \times U(1)$ and $H_2 = SU(4) \times SU(3) \times U(1)$. We show that a particular intersecting CoS solution yields a localized Standard Model gauge group with the hypercharge generator proportional to $\mathrm{diag}(-2/3, -2/3, -2/3, +1, +1, -2, +2)$. This arrangement does have some problems since a single kink-lump solution breaking $SU(7)$ to $H_1 = SU(5) \times SU(2) \times U(1)$ is not the most stable one for the interaction potential between the two scalar fields involved in this kink-lump pair, but we give some suggestions about how to overcome this, including adding a cubic invariant for the lump field and accepting metastability or alternatively extending the model to a sextic potential. We also find that we can embed the SM fermions in the anomaly-free combination $\overline{7} + \overline{7} + \overline{7} + 21$ and we outline how to embed the electroweak Higgs doublet and the additional Higgs fields required to break the semi-delocalized $U(1)$ groups that we get in addition to the SM.

The second example we give is one in which H_1 and H_2 are differently embedded subgroups isomorphic to $SU(4) \times SU(3) \times U(1)$. This can also

[1]Let us note that by saying that a gauge group is localized, we mean that all the gauge bosons associated with that gauge group are localized.

yield a localized Standard Model gauge group but this time with a hypercharge generator which acts on the fundamental as
$\mathrm{diag}(-2/3, -2/3, -2/3, -1, -1, +2, +2)$. This seems like it might not work due to the highly unusual form of this hypercharge generator but it actually turns out that the SM fermions can still be embedded into $SU(7)$ multiplets with the correct quantum numbers, this time in the anomaly-free combination $7 + \overline{21} + 35$. This model has the advantage over the previous one in that the energetics of the single kink-lump solutions used as the boundary conditions can be assured in a model of the form given in Ref. [3] without resorting to a sextic potential or other additional physics.

The third example we give for adjoint scalars is one in which we show that this form of the Clash-of-Symmetries mechanism can also be used to implement the approach taken in Ref. [25] by localizing a grand unification group to the domain wall. Here, we have H_1 and H_2 as differently embedded subgroups isomorphic to $SU(6) \times U(1)$, yielding an $SU(5)$ gauge group which is fully localized to the intersection along with some semi-delocalized $U(1)$ gauge groups which must be broken.

The last example we give is one in which we have one of the lump-forming fields in the 21 representation and the other in the 35 representation. The 21 can naturally break $SU(7)$ to $H_1 = SU(5) \times SU(2)$ and the 35 can naturally induce a breaking to $H_2 = SU(4) \times SU(3)$. This is the most elegant example we give in the paper since we attain the same Standard Model gauge group as we get in the first example with adjoint scalars with the generators corresponding to the semi-delocalized $U(1)$ generators that we got previously already broken naturally. Furthermore, we can choose parameters such that the desired solution is the most energetically favorable one.

In Sec. 5.1, we give a review of the Clash-of-Symmetries mechanism, which includes giving the conditions necessary for localization of both Abelian and non-Abelian gauge fields under this mechanism. In Sec. 5.2, we outline the proposal for the intersecting Clash-of-Symmetries mechanism, again outlining the necessary conditions for localization which are similar to those for the original CoS mechanism. In Sec. 5.3, we give all four of the examples we have discussed applying this mechanism in the case that $G = SU(7)$. Section 5.4 is our conclusion.

5.1 The Clash-of-Symmetries mechanism in the single domain-wall scenario

In single domain-wall models, we can generalize the Dvali-Shifman mechanism to the clash-of-symmetries (CoS) mechanism. Several applications of the CoS mechanism were given in Refs. [127, 128, 24, 25] and for a more detailed treatment of the underlying group theory behind the CoS mechanism, see Ref. [132]. Some other papers in which the CoS mechanism is utilized but with different motivations to ours are given in Refs. [129, 130, 131]. Under the CoS mechanism, only the field generating the kink, η, is retained and it assigned to the adjoint representation of the gauge group G rather than being a singlet. To employ this mechanism we require a disconnected vacuum manifold and the way we achieve this is to ensure that the discrete $\mathbb{Z}_2$ symmetry is *outside* the gauge group. Hence, the full symmetry group is $G \times \mathbb{Z}_2$. In the CoS mechanism, η attains a vacuum expectation value towards spatial infinity on each side of the wall except this time these vacua spontaneously break G. In general, η can break G to two *differently embedded* but isomorphic subgroups H and H' on each side of the wall. On such a CoS domain wall, there is a further breaking in the interior to the subgroup $H \cap H'$. Assuming the H and H' respecting bulks are confining, there should be a similar Dvali-Shifman mechanism localizing the gauge fields of $H \cap H'$.

Whether the full clashing group $H \cap H'$ or only some of its factor groups are localized on the wall depends on how they are embedded within the subgroups of G respected on each wall. Generically, the subgroups on each side of the wall, H and H', will be semi-simple and may be written in the form

$$\begin{aligned} H &= N_1 \times N_2 \times N_3 \times ... \times N_{k-1} \times N_k \times U(1)_{Q_1} \times U(1)_{Q_2} \\ &\quad \times U(1)_{Q_3} ... \times U(1)_{Q_{l-1}} \times U(1)_{Q_l}, \\ H' &= N'_1 \times N'_2 \times N'_3 \times ... \times N'_{k'-1} \times N'_{k'} \times U(1)_{Q'_1} \times U(1)_{Q'_2} \\ &\quad \times U(1)_{Q'_3} ... \times U(1)_{Q'_{l'-1}} \times U(1)_{Q'_{l'}}, \end{aligned} \tag{5.1}$$

where the N_i and N'_i denote the non-Abelian factor groups and the Q_i and Q'_i denote the generators of the Abelian factor groups belonging to H and H' respectively. Since, H and H' are semi-simple, $H \cap H'$ is also semi-simple. We will denote its non-Abelian factor groups as n_i and the generators of its Abelian factor groups as q_i and write

$$\begin{aligned} H \cap H' &= n_1 \times n_2 \times n_3 \times ... \times n_{r-1} \times n_r \times U(1)_{q_1} \times U(1)_{q_2} \\ &\quad \times U(1)_{q_3} \times ... \times U(1)_{q_{s-1}} \times U(1)_{q_s}. \end{aligned} \tag{5.2}$$

The above is the general form of the entire $H \cap H'$ group respected on the domain wall at the level of symmetries. In general, not all of the factor groups, both Abelian and non-Abelian, of $H \cap H'$ will be fully localized to the wall. For a factor group of $H \cap H'$ to be localized, it must be fully embedded in the non-Abelian factor groups of both H and H' respected in each semi-infinite region of the bulk, since for a gauge group to be localized via a Dvali-Shifman mechanism, it must lie inside a larger non-Abelian group which is confining in the bulk.

In the non-Abelian case, this means that a non-Abelian factor of $H \cap H'$, n_i $(1 \leq i \leq r)$, is localized only if it is a *proper* subgroup of simple, non-Abelian factors N_a and N'_b of both H and H' respectively. In other words, we require

$$n_i \subset N_a \text{ and } n_i \subset N'_b, \tag{5.3}$$

for some $1 \leq a \leq k$ and $1 \leq b \leq k'$. If for any a, n_i is precisely equal to N_a but is still a proper subgroup of N'_b for some b, there will be no Dvali-Shifman mechanism taking place in the H-respecting part of the bulk and thus the gauge bosons of n_i will be semi-delocalized. Likewise, if $n_i \subset N_a$ but $n_i = N'_b$, n_i will be semi-delocalized and its gauge bosons will be able to propagate into the H'-respecting bulk. If $n_i = N_a = N'_b$ for some a and b, then there is no Dvali-Shifman mechanism acting on n_i on either side of the bulk and it is thus fully delocalized: its gauge bosons are able to propagate through the whole bulk.

The Abelian case is a little more complicated but follows similar principles. All the generators q_i from Eq. 5.2 which are preserved on the wall at the level of symmetries must be linear combinations of generators residing in both H and H'. Obviously, the respective $U(1)$ generators Q_i and Q'_i can contribute to both these linear combinations, but there are also generators that belong to the non-Abelian factor groups N_a and N'_b which lie *outside* the resultant non-Abelian factors n_i of the clash. For example, suppose we had for some a and b the factors $N_a = SU(4)$ and $N'_b = SU(3)$ and the resultant clash was a group $n_i = SU(2)$. Then there exists a generator $T = \text{diag}(+1, +1, -1, -1)$ in N_a for which the first two eigenvalues act on components transforming under n_i and the latter two act on the two components which do not. Because this generator acts non-trivially on components not acted upon by the resultant $SU(2)$ subgroup, it is outside n_i. Similarly N'_b will have some generator $T' = \text{diag}(-2, +1, +1)$ in which the latter two components act on n_i which is also outside n_i. We will label these generators T_i and T'_i for H and H' respectively. Hence, for a generator q_i to be a preserved generator on the domain wall at the level of symmetries, it must

be that

$$\begin{aligned} q_i &= \sum_{i=1}^{l} \alpha_i Q_i + \sum_{i=1}^{m} \beta_i T_i, \\ &= \sum_{i=1}^{l'} \alpha'_i Q'_i + \sum_{i=1}^{m'} \beta'_i T'_i, \end{aligned} \tag{5.4}$$

where all the α_i, β_i, α'_i and β'_i are real numbers and m and m' are some non-negative integers.

Equation 5.4 is just the condition for the generator to be respected at the level of symmetries: the condition for the Abelian generator to be localized is more stringent. For an Abelian generator q_i to be fully localized to the domain wall, it must be always embedded inside non-Abelian subgroups of both H and H' for the photon to experience the Dvali-Shifman mechanism from both sides of the bulk. This means that it cannot contain any partition proportional to one of the Q_i or Q'_i in either of the linear combinations describing q_i in terms of generators from H and H', otherwise it will be delocalized in at least one part of the bulk. This means that the condition for full *localization* of an Abelian generator q_i to the domain wall is

$$q_i = \sum_{i=1}^{m} \beta_i T_i = \sum_{i=1}^{m'} \beta'_i T'_i, \qquad \alpha_i = \alpha'_{i'} = 0 \; \forall \; i, i'. \tag{5.5}$$

If some α_i are non-zero but all the α'_i are zero, then q_i is free to propagate and leak into the H-respecting side of the bulk. Likewise, if all the α_i are zero but some α'_i are non-zero, q_i is semi-delocalized with respect to the H'-respecting side of the bulk. If there exist some α_a and some α'_b which are non-zero, the photon corresponding to q_i is free to propagate in both sides of the bulk and is thus fully delocalized.

Several attempts have been made at constructing a realistic model via the CoS mechanism [25]. In this paper, the authors first mentioned an attempt to construct a model based on $SO(10)$, as noted in the paragraphs above. Notwithstanding some issues with the energetics, this model fails because the resultant photon is semi-delocalized. Here, on one side of the wall $H = SU(5) \times U(1)$ and on the other $H' = SU(5)' \times U(1)'$. Depending on the vacua at the two ends at spatial infinity, there are three possible outcomes for $H \cap H'$: $SU(5) \times U(1)$, $SU(3) \times SU(2) \times U(1) \times U(1)$ and $SU(4) \times U(1) \times U(1)$. Obviously, it is the second of these two outcomes which is potentially the desirable one. It turned out that in the region of parameter space that was assumed in that paper to generate analytic solutions, the third option was the most energetically favorable one, that is it minimized the domain-wall

tension. However, the authors continued the analysis assuming the second outcome on the basis that there existed a different region of parameter space where the second outcome was the most energetically favorable. If we do this we immediately notice that the $SU(3)$ color and $SU(2)$ weak isospin subgroups are localized to the domain wall since these groups are contained in both $SU(5)$ of H and $SU(5)'$ of H'. Where even the second outcome fails is in considering the localization of the hypercharge generator Y. Since the hypercharge generator can be embedded entirely in an $SU(5)$ subgroup, we can choose it to be embedded in either $SU(5)$ or $SU(5)'$. Without loss of generality, we will assume that Y is contained in $SU(5)$ subgroup of H. However, since $SU(5)'$ is a differently embedded subgroup of $SO(10)$, it cannot be that the analogous generator Y' is equal to Y. Hence, the hypercharge generator Y must be a non-trivial linear combination of the Y' and the generator of the $U(1)'$ subgroup of H'. From the analysis above, it follows that the hypercharge generator is semi-delocalized (the other $U(1)$ of $H \cap H'$ will also be semi-delocalized).

There are several approaches that one could take to get around the problem of semi-delocalized photons in generating a theory in which the Standard Model is reproduced on the domain-wall, or as it turns out in the different Clash-of-Symmetries mechanism on a domain-wall intersection in the 6D model that we will discuss in the rest of the paper. One approach is to localize the gauge fields corresponding to a grand unification group containing the Standard Model on the domain wall instead of just the Standard Model gauge group (plus some additional $U(1)$'s perhaps). This is indeed the approach taken in Ref. [25] in which the authors utilize the gauge group E_6 instead of $SO(10)$ and break it down to $H = SO(10) \times U(1)$ and $H' = SO(10)' \times U(1)'$ on each side of the wall. One particular outcome for the clash is $H \cap H' = SU(5) \times U(1) \times U(1)$ for which the $SU(5)$ subgroup is always localized since it is contained in both $SO(10)$ and $SO(10)'$. Assuming there is a region of parameter space where this is the most stable configuration, to reproduce an acceptable model it is just a case of breaking the localized $SU(5)$ subgroup to the Standard Model as well as breaking the additional $U(1)$ subgroups and localizing the required matter content to the wall.

A second approach, the one we will take when we utilize the Clash-of-Symmetries mechanism for intersecting domain walls in a theory based on $SU(7)$, is to employ a gauge group which is large enough to generate and localize the $SU(3)$ color and $SU(2)$ weak isospin subgroups and at the same type generate more contributing $U(1)$ generators of the second type described in this section, those that initially belong to non-Abelian subgroups respected in the bulk. If at the very least one of the clashing subgroups contained at

least two $U(1)$ generators coming from non-Abelian groups and the other at least one, then as noted above if there exists a $U(1)$ generator which is a linear combination of $U(1)$ generators derived solely from non-Abelian subgroups of both the subgroups of G which clash, then this photon will be localized. This is exactly how the $SU(7)$ theory localizes a generator containing the correct hypercharge quantum numbers for the Standard Model components, along with quantum numbers of ± 2 for non-SM components (so we get the Standard Model along with some exotics with $Y = \pm 2$). Before discussing the Clash-of-Symmetries mechanism for intersecting domain walls, we will discuss the generation of intersecting kink-lump solutions in the next section.

5.2 The Clash-of-Symmetries Mechanism from Intersecting Kink-Lump Solutions

We now give an outline for a new Clash-of-Symmetries mechanism applicable in the context of the intersecting domain-wall model treated in the previous chapter, which is the main purpose of this chapter. We now add a gauge group G and give the fields which form lumps, χ_1 and χ_2, gauge charges. When these fields condense in the interior of each of the respective domain walls η_1 and η_2, they break G to subgroups H_1 and H_2 on each wall. Now consider what happens on the intersection of the domain walls. Naturally, we assume G is again confining in the bulk, just as it usually is in the single-wall case. Then by the Dvali-Shifman mechanism, H_1 is localized to the domain wall described by η_1 and H_2 is localized to the domain wall described by η_2. In general H_1 and H_2 are not the same group, so in the intersection these groups will *clash* and the subgroup respected on the intersection will be $H_1 \cap H_2$, analogously to the single-wall CoS mechanism. A graph of this scenario is shown in Fig. 5.1.

Unlike the single-wall CoS mechanism, H_1 and H_2 need not be differently embedded isomorphic subgroups of G. This is because χ_1 and χ_2 are independent fields and so they potentially can attain vacuum expectation values which break G to two different *non-isomorphic* subgroups. Furthermore, χ_1 and χ_2 need not be in the adjoint representation nor do they need to be in the same representation. These phenomena open up a whole new set of theoretical possibilities for the CoS mechanism. For instance, consider $G = SU(4)$. With an adjoint, we can break G to $SU(3) \times U(1)$ or to $SU(2) \times SU(2) \times U(1)$. Unlike the single wall case where we only had one adjoint field, here we have two adjoint fields so we could break G to $SU(3) \times U(1)$ on one wall and to $SU(2) \times SU(2) \times U(1)$ on the other, lead-

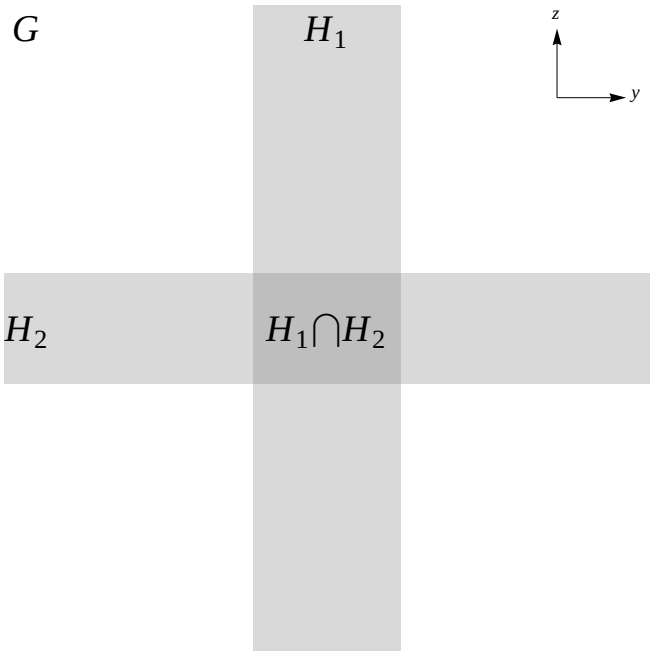

Figure 5.1: A picture of the intersecting Clash-of-Symmetries mechanism in the y-z plane. The gauge group G is spontaneously broken to subgroups H_1 and H_2 along the walls parallel to the y and z axes respectively. Further symmetry breaking occurs in the intersection region of the walls where the total symmetry respected is $H_1 \cap H_2$. If $H_1 \cap H_2$ is semi-simple, then provided each factor subgroup is entirely contained in a non-Abelian subgroup or factor group of each of H_1 and H_2, it will be completely localized to the intersection. Otherwise there is at least a subgroup of $H_1 \cap H_2$ which will be semi-delocalized along one of the domain walls.

ing to possible CoS groups which are isomorphic to $SU(2) \times U(1) \times U(1)$. On the other hand we could make, say, χ_2 transform under the fundamental representation which always breaks G to $SU(3)$ and consider the possible CoS groups when χ_1 breaks G to $SU(3) \times U(1)$ or when it breaks G to $SU(2) \times SU(2) \times U(1)$. Yet another possibility is the case where both η_1 and η_2 are fundamentals, leading to both H_1 and H_2 being isomorphic to $SU(3)$. In fact, for the case where $G = SU(7)$ it turns out that there is a phenomenologically acceptable solution which breaks to the Standard Model (plus two $U(1)$ gauge groups) which results from a clash between non-isomorphic subgroups, with $H_1 = SU(5) \times SU(2) \times U(1)$ and $H_2 = SU(4) \times SU(3) \times U(1)$. We will discuss all these possibilities in further detail in the sections that follow.

When interactions between these fields are switched on, the configuration of vacua attained by these fields will be the one that minimizes the energy of the solution. This is not necessarily the one where both vacua are the same and aligned. To see this one needs to see the different contributions to the energy density. The contributions will be the energy densities of each 4+1-dimensional domain wall as well as a 3+1-dimensional junction tension which is associated with the interactions between the walls. Due to the additional dimensionality, the 4+1-dimensional wall tensions will be positive and infinity larger in magnitude than the junction tension. As an illustrative example to describe this set of physics, let χ_1 and χ_2 transform under the adjoint representation, although this also works more generally. Each kink-lump pair can by itself break G to a number of subgroups depending on the VEV pattern of the respective lump fields χ_1 and χ_2. Since the value of these VEVs depends on the coordinates, we can write these patterns in the form $\chi_1(y) = A_1^a T_a \chi_{A_1}(y)$ and $\chi_2(z) = A_2^a T_a \chi_{A_2}(z)$, where $\chi_{A_1}(y)$ and $\chi_{A_2}(z)$ are just one-dimensional real fields corresponding to the generators encompassed by the breaking patterns A_1 and A_2 respectively. Due to the presence (in general) of $\mathrm{Tr}[\chi_{1,2}^4]$ terms, each of the different configurations with the lumps breaking G to different subgroups will generate different effective quartic self-couplings for $\chi_{A_1}(y)$ and $\chi_{A_2}(z)$ and thus affects the energy densities of these kink-lump solutions. The resultant clashing groups H_1 and H_2 will be determined by which breakings minimize the 4D brane tensions. After determining the subgroups respected on each wall up to isomorphism, since single kink-lump configurations which respect isomorphic but differently embedded subgroups will not differ in energy, it will be the minimization of the 3D junction tension energy density that will determine which particular *clash* gives the minimal energy configuration and thus the intersection group $H_1 \cap H_2$. Taking a given embedding of H_2 as a reference, then the resultant intersection of H_2 with different embeddings of H_1 will

not be the same in general. It turns out that the various interaction terms between the two sets of fields generating the kink-lump pairs, like $\mathrm{Tr}[\chi_1^2\chi_2^2]$, $\mathrm{Tr}[\chi_1\chi_2\chi_1\chi_2]$ and $[\mathrm{Tr}(\chi_1\chi_2)]^2$, are sensitive to the exact clash and thus the surviving subgroup resulting from the clash of H_1 and H_2. Thus the final subgroup respected on the domain-wall intersection firstly depends on the subgroups respected on each wall, which are more or less determined by the coupling constants in the $\eta_1 - \chi_1$ and $\eta_2 - \chi_2$ sectors, and then secondly on which particular embeddings of those subgroups minimize the junction energy density which is determined from the couplings between the $\eta_1 - \chi_1$ and $\eta_2 - \chi_2$ sectors.

The localization of the subgroups of $H_1 \cap H_2$ in the Clash-of-Symmetries mechanism in the intersecting wall scenario follows analogously to the single domain wall case discussed in Sec. 5.1. As discussed above, since G is non-Abelian and confining in the bulk, H_1 and H_2 are automatically localized to the respective domain walls. Again, as in the single wall scenario, H_1 and H_2 are in general semi-simple and may be written in the form described by Eq. 5.1 and their overlap $H_1 \cap H_2$ is also described by Eq. 5.2. The conditions for the full localization of non-Abelian and Abelian groups to the junction are the same as those for the single-kink Clash-of-Symmetries; a non-Abelian subgroup n of $H_1 \cap H_2$ must satisfy Eq. 5.3 and an Abelian generator q must satisfy Eq. 5.5. In the case that these conditions are not satisfied, the gauge bosons are semi-delocalized and there are obvious physical differences to the single-wall case; in this case semi-delocalized gauge bosons are able to propagate along one or both walls (but not into the G-respecting parts of the bulk) rather than being able to propagate through one half of the bulk or through the entire bulk in the single-wall case.

For this application of the Dvali-Shifman mechanism to work, there is a certain hierarchy of scales which needs to be respected. This hierarchy is very similar to that stated for the single-wall $SU(5)$ model of Ref. [23], and it is based on similar principles. Firstly, as our theory is a 5+1D field theory, it is non-renormalizable and a UV cutoff Λ_{UV} must be imposed. Secondly, there are the symmetry breaking scales for H_1 and H_2 on each wall which are roughly of the order of $A_1^{1/2}$ and $A_2^{1/2}$ respectively, where here A_1 and A_2 simply denote the maximum value of the lump profiles in the components of χ_1 and χ_2 which condense. Due to the bulk being in confinement phase, there exists the bulk confinement scale for G which we call $\Lambda_{G,\mathrm{conf}}$. There are also the confinement scales for the non-Abelian factor groups of H_1 and H_2, which we label collectively as $\Lambda_{H_1,\mathrm{conf}}$ and $\Lambda_{H_2,\mathrm{conf}}$ as well as the confinement scales of the localized non-Abelian factor groups of $H_1 \cap H_2$, which we label $\Lambda_{H_1\cap H_2,\mathrm{conf}}$. Finally, there are the inverse widths of each domain wall, k and

l. The required hierarchy is

$$\Lambda_{UV} > A_1^{1/2}, A_2^{1/2} > \Lambda_{G,\text{conf}} > \Lambda_{H_1,\text{conf}}, \Lambda_{H_2,\text{conf}} > k, l > \Lambda_{H_1\cap H_2,\text{conf}}. \quad (5.6)$$

Obviously, Λ_{UV} must be the highest scale of the theory. Next, the symmetry breaking scales $A_1^{1/2}$ and $A_2^{1/2}$ must be larger than the confinement scale in the bulk $\Lambda_{G,\text{conf}}$ so that our background solutions for χ_1 and χ_2 are not destroyed by the confinement dynamics of G. In turn, $\Lambda_{G,\text{conf}}$ must be higher than any of the confinement scales $\Lambda_{H_1,\text{conf}}$ and $\Lambda_{H_2,\text{conf}}$ in order to localize H_1 and H_2 by the Dvali-Shifman mechanism and ensure that there is a mass gap between the masses of the glueballs of G and those of the non-Abelian factor groups of H_1 and H_2. The confinement scales $\Lambda_{H_1,\text{conf}}$ and $\Lambda_{H_2,\text{conf}}$ on each wall must be larger the the inverse widths of the domain walls k and l for the same reasons that the bulk confinement scale must be larger than the domain wall scale in the single wall case utilizing Dvali-Shifman, as discussed in [56]. Finally, $\Lambda_{H_1\cap H_2,\text{conf}}$ must be lower than $\Lambda_{H_1,\text{conf}}$ and $\Lambda_{H_2,\text{conf}}$ to ensure that its gauge bosons are localized by the Dvali-Shifman mechanism. In fact, $\Lambda_{H_1\cap H_2,\text{conf}}$ should be the lowest scale of the theory since if we reproduce the Standard Model on the domain-wall intersection we naturally expect $\Lambda_{H_1\cap H_2,\text{conf}} \sim \Lambda_{QCD}$. All the scales except $\Lambda_{H_1\cap H_2,\text{conf}}$ should be above the electroweak scale.

In the next section, we will discuss applying this realization of the Clash-of-Symmetries mechanism in practice. In Section 5.3, we will discuss how to build a realistic model from an $SU(7)$ gauge group.

5.3 Some Slices of Heaven From $SU(7)$: A Construction of a Realistic Model from the Clash-of-Symmetries Mechanism

In this section we discuss how to build a realistic model on an $SU(7)$ gauge group. In the forthcoming analysis, we will assume that both χ_1 and χ_2 are charged under the adjoint representation, that is the 48 of $SU(7)$. We give details on the representation theory of $SU(7)$ as well as the embeddings of the subgroups $SU(6)\times U(1)$, $SU(5)\times SU(2)\times U(1)$ and $SU(4)\times SU(3)\times U(1)$ in Appendix C. Firstly, we need to consider the possible breaking patterns of a single adjoint scalar field, which can be analyzed by simply looking at the Cartan subalgebra.

We can always gauge rotate the vacuum expectation value of an adjoint scalar field χ (which could be either χ_1 and χ_2 here) such that it is represented

by a traceless diagonal matrix, which in the case of $SU(7)$ may be written

$$\chi = \mathrm{diag}(\mathrm{a}_1, \mathrm{a}_2, \mathrm{a}_3, \mathrm{a}_4, \mathrm{a}_5, \mathrm{a}_6, \mathrm{a}_7), \tag{5.7}$$

where the a_i are numbers parametrizing the Cartan subalgebra and satisfy the traceless condition $\sum_{i=1}^{7} a_i = 0$. From considering various values of the six independent a_i it is possible to generate all the possible symmetry breaking patterns for a single adjoint. The most stable configuration will depend on the potential for χ in the theory. In Ref. [133], Ruegg showed that the quartic Higgs potential resulting for the a_i after substitution for χ only has extrema (and thus minima) if at most two of the a_i are different. Hence the possible resulting subgroups after breaking with the 48 of $SU(7)$ are $SU(6) \times U(1)$, for which six of the a_i are equal and the other differs, $SU(5) \times SU(2) \times U(1)$ when five a_i are equal and the remaining two a_i are equal to a different value, and $SU(4) \times SU(3) \times U(1)$ which results when one eigenvalue of χ has a multiplicity of four and the other three.

In the context of our model with intersecting kink-lump solutions, this means that each of χ_1 and χ_2 break $SU(7)$ to one of these three subgroups. As a result, the possible clashes are between two different embeddings of one of the three subgroups $SU(6) \times U(1)$, $SU(5) \times SU(2) \times U(1)$ or $SU(4) \times SU(3) \times U(1)$ or between particular embeddings of two different choices of these groups. Most of the possibilities are physically uninteresting; a full description of all the possibilities is given in Appendix D.

The most physically interesting possibility with χ_1 and χ_2 in the adjoint representation is a clash between a particular embedding of $H_1 = SU(5) \times SU(2) \times U(1)$ and $H_2 = SU(4) \times SU(3) \times U(1)$. It turns out that a possible subgroup resulting from the clash contains a Standard Model gauge group, including the Abelian group generated by hypercharge, which is fully *localized* to the domain-wall intersection, along with some semi-delocalized $U(1)$ gauge groups that we must break by adding additional Higgs fields in the appropriate representations. Given that the top 5×5 block of the localized Abelian generator is just the usual $SU(5)$ hypercharge generator, the Standard Model fermions can be embedded in $SU(7)$ multiplets in the most obvious way: in a combination of the anti-fundamental $\overline{7}$ representation and the anti-symmetric 21 representation, along with a couple of additional fermions in the $\overline{7}$ to ensure that the effective 3+1D field theory is anomaly-free. The main difficulty with this arrangement is ensuring that the kink-lump solution breaking $SU(7)$ to $H_1 = SU(5) \times SU(2) \times U(1)$ is the most energetically favorable one in the η_1-χ_1 sector. This cannot be generated in the parameter region with analytic solutions with a quartic potential and it seems necessary to utilize a sextic potential.

Another particular choice that we mention that works in an unusual way is that between two different embeddings of $SU(4) \times SU(3) \times U(1)$. Having looked at the possibility mentioned in the previous paragraph, it might seem perfectly reasonable to consider two different embeddings of $SU(4) \times SU(3) \times U(1)$ and particularly so since it avoids some of the problems of the previous solution in ensuring that it is energetically favorable. This choice indeed can localize a SM-like gauge group but with a localized $U(1)$ subgroup whose generator has the *wrong* relative sign between the charges of the right-handed down quark and the lepton doublet! In spite of this, the Standard Model fermions can be successfully embedded in to representations of $SU(7)$, albeit in a rather unusual way: they are embedded in the combination of a 7, a $\overline{21}$ and a 35 rather than the more obvious combination of a $\overline{7}$ and a 21. This means that this solution yields a Standard Model with more exotics.

The third possibility we mention is one between two different embeddings of $SU(6) \times U(1)$. Like the case with two embeddings of $SU(4) \times SU(3) \times U(1)$, one can easily choose energetically favored solutions for the two different walls. In the case of differently embedded $SU(6) \times U(1)$ subgroups, there will be a localized $SU(5)$ gauge group on the intersection along with two semi-delocalized $U(1)$ gauge groups. Hence, this example provides a six-dimensional realization of the approach taken in the single wall case in [25] to localizing the photon along with the non-Abelian gauge bosons of the Standard Model, namely that of localizing a grand unified gauge group to the intersection containing our 3+1D universe. It then follows that one just needs to break the semi-delocalized Abelian groups and then break the $SU(5)$ group to the SM in the usual way.

The last possibility we illustrate is a case where neither χ_1 or χ_2 are adjoint scalars but transform instead under the totally antisymmetric 21 and 35 representations respectively. The 21 can break $SU(7)$ to $H_1 = SU(5) \times SU(2)$ and the 35 can induce a breaking to $H_2 = SU(4) \times SU(3)$. A particular clash between these two groups leads directly to the localization of the same Standard Model gauge group as that generated in the first example given with adjoint scalars. There are two main advantages with this situation over the one with two adjoint scalars in generating the same Standard Model gauge group. Obviously, the first is that we have a localized Standard Model without the need to break any additional semi-delocalized Abelian groups. The second is that, unlike the case with an adjoint scalar, for a particular parameter choice the arrangement on the first wall where the 21 induces the breaking to the $SU(5) \times SU(2)$ subgroup can be guaranteed to be the most stable one with a quartic potential. The breaking to $SU(4) \times SU(3)$ on the second wall with the 35 can also be guaranteed to be the most stable arrangement with a quartic potential.

We discuss these four possibilities in the following four subsections.

5.3.1 A fully localized Standard Model with $H_1 = SU(5) \times SU(2) \times U(1)$ and $H_2 = SU(4) \times SU(3) \times U(1)$ on a Domain-Wall Intersection

Here we will describe firstly the group theoretic background behind the solution with $H_1 = SU(5) \times SU(2) \times U(1)$ and $H_2 = SU(4) \times SU(3) \times U(1)$ which localizes the Standard Model along with some $Y = \pm 2$ exotics. Later we will discuss the energetics and parameter choices needed to ensure that such a solution is the most stable one.

Let's list all the possible subgroups resulting from a clash between an $SU(5) \times SU(2) \times U(1)$ subgroup and an $SU(4) \times SU(3) \times U(1)$ subgroup of $SU(7)$, at the level of symmetries. There are three possibilities: $H_1 \cap H_2 = SU(4) \times SU(2) \times U(1) \times U(1)$, $H_1 \cap H_2 = SU(3) \times SU(2) \times SU(2) \times U(1) \times U(1)$ and $H_1 \cap H_2 = SU(3) \times SU(2) \times U(1) \times U(1) \times U(1)$. The first two are physically uninteresting since, in both these cases, one of the non-Abelian subgroups is semi-delocalized due to being respected along one wall (the $SU(4)$ subgroup in the first case, the $SU(3)$ subgroup in the second). It is the last case which is interesting since here the whole Standard Model gauge group is localized. Along with the Standard Model come two $U(1)$ subgroups which are semi-delocalized and thus must be broken at a sufficiently high energy scale to avoid a leakage of energy into the bulk in the low energy field theory.

As an example which yields this desired situation, consider the case where the component of χ_1 which condenses is proportional to the matrix

$$Q_1 = \begin{pmatrix} 2 & 0 & 0 & 0 & 0 & 0 & 0 \\ 0 & 2 & 0 & 0 & 0 & 0 & 0 \\ 0 & 0 & 2 & 0 & 0 & 0 & 0 \\ 0 & 0 & 0 & 2 & 0 & 0 & 0 \\ 0 & 0 & 0 & 0 & 2 & 0 & 0 \\ 0 & 0 & 0 & 0 & 0 & -5 & 0 \\ 0 & 0 & 0 & 0 & 0 & 0 & -5 \end{pmatrix}, \tag{5.8}$$

and the component of χ_2 which condenses is proportional to

$$Q_1' = \begin{pmatrix} 3 & 0 & 0 & 0 & 0 & 0 & 0 \\ 0 & 3 & 0 & 0 & 0 & 0 & 0 \\ 0 & 0 & 3 & 0 & 0 & 0 & 0 \\ 0 & 0 & 0 & -4 & 0 & 0 & 0 \\ 0 & 0 & 0 & 0 & -4 & 0 & 0 \\ 0 & 0 & 0 & 0 & 0 & -4 & 0 \\ 0 & 0 & 0 & 0 & 0 & 0 & 3 \end{pmatrix}. \tag{5.9}$$

The former clearly induces the breaking $SU(7) \to SU(5) \times SU(2) \times U(1)$ and the latter induces the breaking $SU(7) \to SU(4) \times SU(3) \times U(1)$. Inspecting these two matrices, one notices that there is an $SU(3)$ subgroup which preserves the top-left 3×3 blocks of these two matrices. This $SU(3)$ subgroup is the one common to the $SU(5)$ and $SU(4)$ subgroups induced by the respective vacua. Similarly, an $SU(2)$ subgroup represented by generators with non-trivial components in the 2×2 block on the intersection of the fourth and fifth rows and fourth and fifth columns preserves the fourth and fifth elements along the diagonal along both matrices, which is common to the $SU(5)$ and $SU(3)$ subgroups. Looking at the lower-right 2×2 block, one sees that the $SU(2)$ subgroup induced by the condensation of χ_1 does not survive and is thus broken since this same group does not preserve the corresponding elements of the diagonal in the VEV pattern of χ_2, represented by Q_1'. Hence, the non-Abelian sector surviving the clash is $SU(3) \times SU(2)$, which is precisely that required for a localized SM. Since both these non-Abelian subgroups are entirely contained in larger non-Abelian subgroups respected along each wall ($SU(5)$ and $SU(4)$ in the case of $SU(3)$ color, and $SU(5)$ and $SU(3)$ in the case of $SU(2)$ weak isospin), they are fully localized as required to the domain-wall intersection.

Next, we need to determine the remaining $U(1)$ subgroups respected on the wall at the level of symmetries, and then determine if any of them are localized. As is well known, any spontaneous breaking by an adjoint scalar field always preserves a $U(1)$ subgroup and the generator of this $U(1)$ subgroup is precisely equal to the generator which condenses. Hence, Q_1 and Q_1' are the generators of these associated $U(1)$ subgroups in the case of the walls generated by η_1 and η_2 respectively. We now look at any potential leftover generators inside the non-Abelian groups respected on each wall but which are outside the smaller non-Abelian subgroups respected on the intersection (ie. $U(1)$ generators of the T, T' type discussed previously). For H_1, one sees

that the usual $SU(5)$ hypercharge generator is one of the leftover generators,

$$T_1 = \begin{pmatrix} +\frac{2}{3} & 0 & 0 & 0 & 0 & 0 & 0 \\ 0 & +\frac{2}{3} & 0 & 0 & 0 & 0 & 0 \\ 0 & 0 & +\frac{2}{3} & 0 & 0 & 0 & 0 \\ 0 & 0 & 0 & -1 & 0 & 0 & 0 \\ 0 & 0 & 0 & 0 & -1 & 0 & 0 \\ 0 & 0 & 0 & 0 & 0 & 0 & 0 \\ 0 & 0 & 0 & 0 & 0 & 0 & 0 \end{pmatrix}, \tag{5.10}$$

which lies inside the $SU(5)$ subgroup respected on the first wall but is outside both its $SU(3)$ and $SU(2)$ subgroups that survive the clash. Similarly,

$$T_2 = \begin{pmatrix} 0 & 0 & 0 & 0 & 0 & 0 & 0 \\ 0 & 0 & 0 & 0 & 0 & 0 & 0 \\ 0 & 0 & 0 & 0 & 0 & 0 & 0 \\ 0 & 0 & 0 & 0 & 0 & 0 & 0 \\ 0 & 0 & 0 & 0 & 0 & 0 & 0 \\ 0 & 0 & 0 & 0 & 0 & 1 & 0 \\ 0 & 0 & 0 & 0 & 0 & 0 & -1 \end{pmatrix}, \tag{5.11}$$

is inside the $SU(2)$ subgroup respected on the first wall and could potentially contribute to a surviving $U(1)$. For H_2, the respective generators inside $SU(4)$ and $SU(3)$ but outside the preserved non-Abelian groups are respectively

$$T_1' = \begin{pmatrix} +\frac{2}{3} & 0 & 0 & 0 & 0 & 0 & 0 \\ 0 & +\frac{2}{3} & 0 & 0 & 0 & 0 & 0 \\ 0 & 0 & +\frac{2}{3} & 0 & 0 & 0 & 0 \\ 0 & 0 & 0 & 0 & 0 & 0 & 0 \\ 0 & 0 & 0 & 0 & 0 & 0 & 0 \\ 0 & 0 & 0 & 0 & 0 & 0 & 0 \\ 0 & 0 & 0 & 0 & 0 & 0 & -2 \end{pmatrix}, \tag{5.12}$$

and

$$T_2' = \begin{pmatrix} 0 & 0 & 0 & 0 & 0 & 0 & 0 \\ 0 & 0 & 0 & 0 & 0 & 0 & 0 \\ 0 & 0 & 0 & 0 & 0 & 0 & 0 \\ 0 & 0 & 0 & -1 & 0 & 0 & 0 \\ 0 & 0 & 0 & 0 & -1 & 0 & 0 \\ 0 & 0 & 0 & 0 & 0 & 2 & 0 \\ 0 & 0 & 0 & 0 & 0 & 0 & 0 \end{pmatrix}. \tag{5.13}$$

We have listed all the possible contributing generators above. For a $U(1)$ subgroup to be respected on the wall at the level of symmetries, as discussed

previously it must be a linear combination of generators satisfying Eq. 5.4. By inspection, one can easily see from the above generators that there exists a generator Y which can be written solely in terms of the T_i and T'_i generators:

$$Y = -T_1 - 2T_2 = -T'_1 - T'_2 = \begin{pmatrix} -\frac{2}{3} & 0 & 0 & 0 & 0 & 0 & 0 \\ 0 & -\frac{2}{3} & 0 & 0 & 0 & 0 & 0 \\ 0 & 0 & -\frac{2}{3} & 0 & 0 & 0 & 0 \\ 0 & 0 & 0 & +1 & 0 & 0 & 0 \\ 0 & 0 & 0 & 0 & +1 & 0 & 0 \\ 0 & 0 & 0 & 0 & 0 & -2 & 0 \\ 0 & 0 & 0 & 0 & 0 & 0 & +2 \end{pmatrix}. \quad (5.14)$$

Thus, Y satisfies Eq. 5.5 and is thus localized to the domain-wall intersection. Furthermore, the upper left 5×5 block of Y is precisely the usual hypercharge generator so it has the desired properties of a localized Abelian generator on the components which transform under the $SU(3)$ color and $SU(2)$ isospin subgroups. Hence, this configuration successfully localizes the Standard Model gauge group.

Along with the localized Standard Model, we also get a couple of semi-delocalized $U(1)$ gauge groups. The generators of these Abelian groups may be taken to be

$$A = 4Q_1 + 7T_1 - 6T_2 = 2Q'_1 + 10T'_1 + 9T'_2 = \begin{pmatrix} \frac{38}{3} & 0 & 0 & 0 & 0 & 0 & 0 \\ 0 & \frac{38}{3} & 0 & 0 & 0 & 0 & 0 \\ 0 & 0 & \frac{38}{3} & 0 & 0 & 0 & 0 \\ 0 & 0 & 0 & +1 & 0 & 0 & 0 \\ 0 & 0 & 0 & 0 & +1 & 0 & 0 \\ 0 & 0 & 0 & 0 & 0 & -26 & 0 \\ 0 & 0 & 0 & 0 & 0 & 0 & -14 \end{pmatrix}, \quad (5.15)$$

and

$$B = -3Q_1 + 12T_1 + 12T_2 = \frac{3}{2}Q'_1 - \frac{3}{8}T'_1 - 15'T_2 = \begin{pmatrix} 2 & 0 & 0 & 0 & 0 & 0 & 0 \\ 0 & 2 & 0 & 0 & 0 & 0 & 0 \\ 0 & 0 & 2 & 0 & 0 & 0 & 0 \\ 0 & 0 & 0 & -18 & 0 & 0 & 0 \\ 0 & 0 & 0 & 0 & -18 & 0 & 0 \\ 0 & 0 & 0 & 0 & 0 & 27 & 0 \\ 0 & 0 & 0 & 0 & 0 & 0 & 3 \end{pmatrix}. \quad (5.16)$$

Evidently, both A and B satisfy Eq. 5.4 but not Eq. 5.5, as one expects for semi-delocalized generators. The resultant photons are able to propagate along both walls and thus these Abelian groups must be broken on the

domain-wall intersection as the existence of massless 5D states coupling to the Standard Model fermions would obviously be disastrous.

Since the lower right 2×2 block is proportional to twice the third Pauli matrix, once we include the fermionic particle content and Higgs fields required for electroweak symmetry breaking, we expect exotic scalars and fermions. If we embed the right-handed down quark and the lepton doublet in a $\overline{7}$ for instance, there will be exotics with hypercharge $Y = \pm 2$. Thus, to construct realistic models, we need to ensure that the masses of the localized modes for these exotics are sufficiently more massive than those corresponding to the SM particle content. The exact breakdowns of the $\overline{7}$, 21 and 35 representations in terms of the full $SU(3)_c \times SU(2)_I \times U(1)_Y \times U(1)_A \times U(1)_B$ subgroup preserved at the level of symmetries on the domain-wall intersection are

$$\begin{aligned}\overline{7} = &(\overline{3}, 1, +\frac{2}{3}, -\frac{38}{3}, -2) + (1, 2, -1, -1, +18) + (1, 1, +2, +26, -27) \\ &+ (1, 1, -2, +14, -3),\end{aligned} \tag{5.17}$$

$$\begin{aligned}21 = &(\overline{3}, 1, -\frac{4}{3}, +\frac{76}{3}, +4) + (3, 2, +\frac{1}{3}, +\frac{41}{3}, -16) + (1, 1, +2, +2, -36) \\ &+ (3, 1, -\frac{8}{3}, -\frac{40}{3}, +29) + (3, 1, +\frac{4}{3}, -\frac{4}{3}, +5) + (1, 2, -1, -25, +9) \\ &+ (1, 2, +3, -13, -15) + (1, 1, 0, -40, +30),\end{aligned} \tag{5.18}$$

and

$$\begin{aligned}35 = &(3, 1, +\frac{4}{3}, +\frac{44}{3}, -34) + (\overline{3}, 2, -\frac{1}{3}, +\frac{79}{3}, -14) + (1, 1, -2, +38, +6) \\ &+ (\overline{3}, 1, -\frac{10}{3}, -\frac{2}{3}, +31) + (3, 2, -\frac{5}{3}, -\frac{37}{3}, +11) + (1, 1, 0, -24, -9) \\ &+ (\overline{3}, 1, +\frac{2}{3}, +\frac{34}{3}, +7) + (3, 2, +\frac{7}{3}, -\frac{1}{3}, -13) + (1, 1, +4, -12, -33) \\ &+ (3, 1, -\frac{2}{3}, -\frac{82}{3}, +32) + (1, 2, +1, -39, +12).\end{aligned} \tag{5.19}$$

Thus we can easily see that we can embed the Standard Model fermions in the most obvious way with the charge conjugate of the right-chiral down quark $(d_R)^c$ and the lepton doublet L embedded in the $\overline{7}$, and the charge conjugates of the right-chiral up quark $(u_R)^c$ and of the right-chiral electron $(e_R)^c$ along with the quark doublet Q embedded in the 21. There is also a component which is a singlet under the SM, the $(1, 1, 0, -40, +30)$ component, inside the 21 which could be potentially used as a right-chiral neutrino or its charge conjugate.

One thing that is not completely clear is what is the *minimal* content necessary for anomaly cancellation. Fermion localization in the model described in Sec. 4.1 was treated in Ref. [3], and it was shown that a single chiral zero mode was reproduced on the intersection when a 5+1D *Dirac* fermion was coupled to the background scalar fields through scalar and pseudoscalar Yukawa couplings. The fact that we use full eight-component Dirac spinors to embed 3+1D chiral zero modes is important since this means that the underlying 5+1D theory is vector-like and is thus free from both 5+1D gravitational and gauge anomalies. However, the effective 3+1D theory reproduced on the intersection is in general chiral since each 5+1D Dirac fermion produces a single chiral zero mode. Hence, one may plausibly reproduce an *anomalous* 3+1D theory from an *anomaly-free* 5+1D theory, as would be the case if we chose the only fermionic content to be a single 5+1D Dirac fermion in the $\overline{7}$ representation and another in the 21 representation to embed each generation of the SM fermions. In an $SU(7)$ theory in 3+1D with chiral fermions, $\overline{7}+21$ is anomalous and the minimal anomaly-free combination is in fact a left-chiral fermion in the 21 representation along with *three* transforming as a $\overline{7}$. This phenomenon of an anomalous lower dimensional theory reproduced from an anomaly-free one in higher dimensions has been noted previously [134, 135] and in some cases the anomalies of the lower dimensional theory have been shown to be canceled by effects coming from the bulk [134]. It is not clear to us if this is the case in our model and that bulk effects will protect our 3+1D theory from anomalies if we simply choose a single $\overline{7}$ Dirac fermion and a 21 Dirac fermion in 5+1D for each SM generation. Nevertheless, we can always make the safe choice and include the full $\overline{7}+\overline{7}+\overline{7}+21$ combination for our initial 5+1D Dirac fermion content. Alternatively, there is the next-to-minimal choice $\overline{7}+21+\overline{35}$.

With regards to the Higgs sector, we not only need a Higgs field in which to embed the electroweak Higgs doublet but we also need to include the requisite Higgs fields to break the semi-delocalized Abelian groups generated by A and B. Both the Abelian groups $U(1)_A$ and $U(1)_B$ must be broken without breaking $U(1)_Y$ so the required Higgs fields must contain components which transform as singlets under the Standard Model but are charged under the semi-delocalized Abelian groups. The obvious candidates are the 21 and the 35 since the 21 contains a component transforming as $(1,1,0,-40,+30)$ and the 35 contains a component transforming as $(1,1,0,-24,-9)$. Furthermore, it is obvious that these two different components will completely break $U(1)_A \times U(1)_B$ since each component will preserve different linear combinations of A and B after attaining a VEV. Hence the $21+35$ combination will do the job. For embedding the electroweak Higgs, one might first consider the anti-fundamental $\overline{7}$. While a scalar transforming as a $\overline{7}$ can form a gauge

invariant Yukawa coupling with fermion in the $\overline{7}$ and another in the 21, it cannot form a Yukawa coupling with the 21 fermion and its charge conjugate, which we need to get a mass matrix for the up-like quarks. Neither can a scalar in the 21 representation, even though it contains a component transforming as an electroweak doublet. On the other hand, the $\overline{35}$ representation can both form a Yukawa coupling between a $\overline{7}$ and a 21 as well as a gauge invariant Yukawa coupling between the 21 and its charge conjugate. Further, the $\overline{35}$ contains a component transforming as an electroweak doublet, the $(1, 2, -1, +39, -12)$ component, and thus it is necessary to embed the electroweak Higgs in this representation. Although a phenomenological analysis of the fermion and scalar modes is beyond the scope of this paper, it would be interesting to see if we can embed the electroweak Higgs field along with the SM singlet required to break one of the semi-delocalized Abelian groups in the same $\overline{35}$ scalar and choose parameters such that these components attain tachyonic masses on the intersection while all other components attain positive definite squared masses.

To ensure that we get this configuration, we need to ensure that it is the most energetically favorable and stable one. The most general $\mathbb{Z}_2 \times \mathbb{Z}_2$-invariant quartic potential for η_1, χ_1, η_2, and χ_2 with χ_1 and χ_2 as adjoint scalar fields is

$$V = V_{\eta_1\chi_1} + V_{\eta_2\chi_2} + V_{\eta_1\chi_1\eta_2\chi_2}, \tag{5.20}$$

where $V_{\eta_i\chi_i}$ for $i = 1, 2$ are the self interaction potentials

$$\begin{aligned} V_{\eta_i\chi_i} = {} & \frac{1}{4}\lambda_{\eta_i}(\eta_i^2 - v_i^2)^2 + \lambda_{\eta_i\chi_i}(\eta_i^2 - v_i^2)\mathrm{Tr}[\chi_{\mathrm{i}}^2] + \mu_{\chi_{\mathrm{i}}}^2\,\mathrm{Tr}[\chi_{\mathrm{i}}^2] + \mathrm{h}_{\eta_{\mathrm{i}}\chi_{\mathrm{i}}}\eta_{\mathrm{i}}\mathrm{Tr}[\chi_{\mathrm{i}}^3] \\ & + \lambda_{\chi_i}^1\,\mathrm{Tr}[\chi_{\mathrm{i}}^2]^2 + \lambda_{\chi_{\mathrm{i}}}^2\,\mathrm{Tr}[\chi_{\mathrm{i}}^4], \end{aligned} \tag{5.21}$$

for the η_1-χ_1 and η_2-χ_2 sectors respectively and $V_{\eta_1\chi_1\eta_2\chi_2}$ is the interaction potential between these two sectors, which may be written

$$\begin{aligned} V_{\eta_1\chi_1\eta_2\chi_2} = {} & \frac{1}{2}\lambda_{\eta_1\eta_2}(\eta_1^2 - v_1^2)(\eta_2^2 - v_2^2) + \lambda_{\eta_1\chi_2}(\eta_1^2 - v_1^2)\mathrm{Tr}[\chi_2^2] \\ & + \lambda_{\chi_1\eta_2}(\eta_2^2 - v_2^2)\mathrm{Tr}[\chi_1^2] + 2\lambda_{\chi_1\chi_2}^1\mathrm{Tr}[\chi_1^2]\mathrm{Tr}[\chi_2^2] + 2\lambda_{\chi_1\chi_2}^2\big[\mathrm{Tr}[\chi_1\chi_2]\big]^2 \\ & + 2\lambda_{\chi_1\chi_2}^3\mathrm{Tr}[\chi_1^2\chi_2^2] + 2\lambda_{\chi_1\chi_2}^4\mathrm{Tr}[\chi_1\chi_2\chi_1\chi_2] + \lambda_{\eta_1\chi_1\chi_2}\eta_1\mathrm{Tr}[\chi_1\chi_2^2] \\ & + \lambda_{\chi_1\eta_2\chi_2}\eta_2\mathrm{Tr}[\chi_1^2\chi_2] + \lambda_{\eta_1\chi_1\eta_2\chi_2}\eta_1\eta_2\mathrm{Tr}[\chi_1\chi_2]. \end{aligned} \tag{5.22}$$

Firstly, we need to ensure that the configurations on the boundary leading to the desired subgroups being respected on each wall are the most stable. This involves analyzing the respective one-dimensional kink-lump solutions which we utilize as the boundary conditions generated by the self-interaction

potentials $V_{\eta_i\chi_i}$ given in Eq. 5.21. At the boundaries, we obviously set $\eta_i(y_i \to \pm\infty) = \pm v_i$ (here, $y_1 = y$, $y_2 = z$), and here the corresponding χ_i must be zero since here it experiences a potential bounded from below with a positive definite squared mass. At some point, on the wall where η_i traverses from one vacuum to the other, $\eta_i = 0$ and here the squared mass of χ_i becomes tachyonic and is thus expected to condense. In this region, χ_i experiences a standard quartic symmetry-breaking potential for an adjoint scalar. In generating analytic solutions, we normally set the coupling constant for the $\eta_i \mathrm{Tr}[\chi_{\mathrm{i}}^3]$ term to zero (and other terms involving odd powers of η_i and χ_i in the full potential for similar reasons). This means that the resultant effective quartic potential experienced by χ_i in the region where it is tachyonic has a $\mathbb{Z}_2$ symmetry, with its breaking patterns determined by Li [136]. Since all generators are normalized to 1/2, the $[\mathrm{Tr}(\chi_{\mathrm{i}}^2)]^2$ always yields a quartic self-interaction term which has the same strength no matter which breaking pattern is chosen. On the other hand the value of $\mathrm{Tr}[\chi_{\mathrm{i}}^4]$ differs depending on the VEV pattern chosen. Hence, the real components of χ_i corresponding to different symmetry breaking patterns experience different effective quartic self-couplings, which will be linear combinations of $\lambda^1_{\chi_i}$ and $\lambda^2_{\chi_i}$. If we write the effective $\lambda_{\chi_i eff}$ coupling constants for these different components with the normalization given in Eq. 4.2 in terms of $\lambda^1_{\chi_i}$ and $\lambda^2_{\chi_i}$, then for an $SU(6) \times U(1)$ breaking pattern the effective coupling is $\lambda^1_{\chi_i} + 31\lambda^2_{\chi_i}/42$, for an $SU(5) \times SU(2) \times U(1)$ breaking pattern it is $\lambda^1_{\chi_i} + 19\lambda^2_{\chi_i}/70$ and for $SU(4) \times SU(3) \times U(1)$ it is $\lambda^1_{\chi_i} + 13\lambda^2_{\chi_i}/84$. Since the energy of the effective potential for χ_i at the respective vacuum is $-\mu^4_{\chi_i}/4\lambda_{\chi_i eff}$, the configuration with the lowest effective quartic coupling will have the lowest energy and consequently the most stable vacuum. Thus, of the three breaking patterns, for $\lambda^2_{\chi_i} > 0$ the $SU(4) \times SU(3) \times U(1)$ is the most stable and for $\lambda^2_{\chi_i} < 0$ the $SU(6) \times U(1)$ vacuum is the most stable (provided $\lambda^1_{\chi_i} + \lambda^2_{\chi_i} > 0$ to ensure the potential is bound from below); these results agree with Ref. [136].

The energy of the effective potential for an $SU(5) \times SU(2) \times U(1)$ symmetry breaking pattern thus always lies in between that for the $SU(6) \times U(1)$ and $SU(4) \times SU(3) \times U(1)$ symmetry breaking patterns in the case that the effective potential for χ_i has the $\mathbb{Z}_2$ symmetry (not the ones initially imposed). This means that for a quartic potential with the $\eta_1\chi_1^3$ term set to zero, that the configuration where the component of χ_1 which is proportional to Q_1 condenses to form the lump is never the most stable one. We can ensure that the $SU(4) \times SU(3) \times U(1)$ breaking pattern is the most stable one in the $\eta_2 - \chi_2$ sector, but we need some way to ensure that $SU(5) \times SU(2) \times U(1)$ breaking kink-lump configuration is the most stable one for the $\eta_1 - \chi_1$ sector if we are to generate the desired outcome with a localized Standard Model outlined in this section.

There are several ways around the problem in the previously mentioned paragraph. One might first think that one of these would be to switch on the $\eta_1 \mathrm{Tr}[\chi_1^3]$ term. However, there will still be a point where $\eta_1 = 0$ and thus around this point one of the other breaking patterns would still be expected to be more stable. Furthermore, this term will affect the localization of the lump and once again the effective coupling for this interaction is largest in magnitude for the $SU(6) \times U(1)$ breaking pattern followed by that for $SU(5) \times SU(2) \times U(1)$ followed again by $SU(4) \times SU(3) \times U(1)$. By examining this term, we have noticed that it generally lowers the energy density of the solutions and the more the lump is delocalized from the center of the kink, the more the energy density lowers. Thus, one initially thinks that there may be a way to make the $SU(5) \times SU(2) \times U(1)$ preserving configuration the lowest in energy. The magnitude of its effective coupling constant for this term is greater than the $SU(4) \times SU(3) \times U(1)$ one, so if we choose $\lambda_{\chi_1}^2 > 0$ initially and then slowly increase $h_{\eta_1 \chi_1}$ from zero, one may expect the energy density of the $SU(5) \times SU(2) \times U(1)$ to become lower. Unfortunately, in the exploration of the parameter space that we have done, it seems that the energy density of the $SU(6) \times U(1)$ decreases too rapidly for there to be some point at which $SU(5) \times SU(2) \times U(1)$ becomes the most stable one. Thus, the $\eta_1 \mathrm{Tr}[\chi_1^3]$ term seems unlikely to solve this problem.

In terms of the cubic invariant, what one would really like is just a bare cubic term of the form $d_{\chi_1} \mathrm{Tr}[\chi_1^3]$. Let us first mention that in Ref. [133], Ruegg also showed that when $\lambda_{\chi_i}^2 > 0$, as the ratio between d_{χ_1} and $\lambda_{\chi_i}^2$ increases from zero to infinity the most stable breaking pattern cascades from $SU(N-n) \times SU(n) \times U(1)$, where $n = \lfloor N/2 \rfloor$, to $SU(N-n+1) \times SU(n-1) \times U(1)$, then to $SU(N-n+2) \times SU(n-2) \times U(1)$ and so on up to $SU(N-1) \times U(1)$. Hence, in the case of $SU(7)$, there would exist a parameter region where the configuration breaking to $SU(5) \times SU(2) \times U(1)$ would become the most stable one if we had a bare cubic term for χ_1. The main difficulty would then be ensuring that this cubic term would be allowed, as it is not under the current symmetries and parities imposed in our theory. One could imagine changing the parity of χ_1 to $(+,+)$ under the $\mathbb{Z}_2 \times \mathbb{Z}_2$ symmetry or perhaps utilizing a different discrete symmetry with which to form a domain wall between discrete vacua, so that such a cubic term is allowed. Provided χ_1 could then be coupled to scalars and fermions in an acceptable way, this would be an ideal approach.

Another obvious solution is to go to a sextic potential. Resorting to a sextic potential in our extra-dimensional theory is not a problem since any interacting field theory in a spacetime with dimension more than four is non-renormalizable anyway. One of the problems we had was ensuring that there were enough different invariant operators, and hence parameters, for

χ_1 to permit greater freedom in symmetry breaking outcomes. For the sake of simplicity and as an example, make the quartic self-couplings for χ_1 and any sextic term involving η_1 zero, with just the sextic self-couplings for χ_1 non-zero. In this case, the effective potential for χ_1 where $\eta_1 = 0$ is just a tachyonic mass term with a positive definite sextic term. Just as before with the quartic case, the symmetry breaking pattern will be determined by the effective sextic coupling and the configuration with the lowest effective sextic coupling will be the most stable. Unlike the quartic case, there are more invariants to play with since we can have $\mathrm{Tr}[\chi_1^6]$, $(\mathrm{Tr}[\chi_1^2])^3$, $\mathrm{Tr}[\chi_1^2]\mathrm{Tr}[\chi_1^4]$ and $(\mathrm{Tr}[\chi_1^3])^2$. With this number of invariants, one can easily manipulate the parameters such that the $SU(5) \times SU(2) \times U(1)$ respecting configuration has the lowest effective sextic coupling, and thus yields the kink-lump solution where the corresponding component for Q_1 condenses is the most stable. A potential difficulty with this approach is that the theorem proven by Ruegg [133] where any extrema and thus minima of the potential for an adjoint scalar exist only if at most two of the eigenvalues of the VEV of the adjoint scalar differ may not apply here since we are dealing with a sextic potential and the aforementioned theorem was only proven for a quartic potential. Thus, with a sextic there may be configurations where the VEV pattern has more than two distinct eigenvalues and one would need to check through these to ensure that the desired configuration is the most stable one.

Once one has ensured that one wall generating $SU(5) \times SU(2) \times U(1)$ is stable and has chosen parameters such that the other wall breaks $SU(7)$ to $SU(4) \times SU(3) \times U(1)$, we need to determine the possible symmetries and localized groups on the intersection under the clash-of-symmetries mechanism. As we stated in the previous section, the most stable clash-of-symmetries arrangement will be the one that minimizes the 3+1D junction energy density. Just as there existed effective quartic self-couplings for the components of χ_1 and χ_2 chosen to condense after computing the traces of the powers of the respective generators involved, so there will exist other effective coupling constants describing interactions between these different components. In fact, each different configuration will lead to a different effective scalar potential of the form given in Eq. 4.2. For the analytic solution given in Eq. 4.5 yielded by the parameter conditions in Eq. 4.4, only the terms in $V_{\eta_1\chi_1\eta_2\chi_2}$ contribute to the junction energy density. For parameters not satisfying Eq. 4.4, the self-interaction potentials $V_{\eta_i\chi_i}$ will in general make a small contribution. Fortunately, there is a way to extract the energy density by defining the fields $\overline{\eta_1}$, $\overline{\chi_1}$, $\overline{\eta_2}$ and $\overline{\chi_2}$ as differences between the real two-dimensional interacting kink-lump solutions and the one-dimensional kink-lump solutions which are

used as the boundary conditions. In other words, these fields are defined as

$$\begin{aligned}
\overline{\eta_1}(y,z) &= \eta_1(y,z) - \eta_1^{1d}(y) = \eta_1(y,z) - v_1 \tanh(ky), \\
\overline{\chi_1}(y,z) &= \chi_1(y,z) - \chi_1^{1d}(y) = \chi_1(y,z) - A_1 \operatorname{sech}(ky), \\
\overline{\eta_2}(y,z) &= \eta_2(y,z) - \eta_2^{1d}(z) = \eta_2(y,z) - v_2 \tanh(lz), \\
\overline{\chi_2}(y,z) &= \chi_2(y,z) - \chi_2^{1d}(z) = \chi_2(y,z) - A_2 \operatorname{sech}(lz).
\end{aligned} \tag{5.23}$$

Given the boundary conditions in Eq. 4.3 for the full fields η_1, η_2, χ_1 and χ_2, one can show that $\overline{\eta_1}$, $\overline{\chi_1}$, $\overline{\eta_2}$ and $\overline{\chi_2}$ all vanish along the entire two-dimensional boundary at infinity. Since for a sensible solution the deviations from the 1D solutions should be largest on the intersection with the solutions for η_1, η_2, χ_1 and χ_2 asymptoting to the 1D solutions out at infinity, it should also be the case that $\overline{\eta_1}$, $\overline{\chi_1}$, $\overline{\eta_2}$ and $\overline{\chi_2}$ should decay to zero faster than $1/y$ and $1/z$ in both directions towards infinity. Given this, since η_1, η_2, χ_1 and χ_2 are all bounded functions, when we expand the potential V in terms of $\overline{\eta_1}$, $\overline{\chi_1}$, $\overline{\eta_2}$ and $\overline{\chi_2}$ and η_1^{1d}, χ_1^{1d}, η_2^{1d} and χ_2^{1d}, any term proportional to any power of $\overline{\eta_1}$, $\overline{\chi_1}$, $\overline{\eta_2}$ or $\overline{\chi_2}$ should be integrable over the $y-z$ plane and should thus give a finite contribution to the junction energy density.

If we make choices consistent with those of Eq. 4.4 and set $\lambda_{\eta_1\chi_1\chi_2} = \lambda_{\chi_1\eta_2\chi_2} = \lambda_{\eta_1\chi_1\eta_2\chi_2} = 0$, then the most important terms in $V_{\eta_1\chi_1\eta_2\chi_2}$ which decide which clash-of-symmetries solutions are most energetically favorable are the quartic couplings between χ_1 and χ_2 which are $\mathrm{Tr}[\chi_1^2]\mathrm{Tr}[\chi_2^2]$, $\mathrm{Tr}[\chi_1\chi_2]^2$, $\mathrm{Tr}[\chi_1^2\chi_2^2]$ and $\mathrm{Tr}[\chi_1\chi_2\chi_1\chi_2]$. For a given solution, after we take the relevant traces of these operators, we obtain an effective quartic coupling between the components of χ_1 and χ_2. After integrating this effective term over the $y-z$ plane, we should obtain its contribution to the junction energy density. Since this effective term is proportional to the squares of the condensing components of χ_1 and χ_2, if the effective coupling constant for a particular solution is positive, the contribution to the junction energy density will be positive. Furthermore, if we compare it with the contributions coming from the perturbations to the fields as a result of turning on interactions, the former will be proportional to $A_1^2 A_2^2 \operatorname{sech}^2(ky)\operatorname{sech}^2(lz)$ but the latter will be proportional to say (at first order) $v_1^3 \tanh(ky)\operatorname{sech}^2(ky)\overline{\eta_1}(y,z)$. The v_i and A_i $(i=1,2)$ should be roughly the same order and they will be associated with a high energy scale (typically Λ_{GUT}) and given we expect the perturbations $\overline{\eta_1}$, $\overline{\chi_1}$, $\overline{\eta_2}$ and $\overline{\chi_2}$ to be small, the contribution coming from the background dependent terms arising from the quartic couplings of $V_{\eta_1\chi_1\eta_2\chi_2}$ are naturally expected to be one power of this energy scale larger and will dominate the overall contribution to the junction energy density. It then follows that the clash-of-symmetries solution with the lowest effective coupling between the

components of χ_1 and χ_2 which condense will minimize the energy density and thus be the most stable intersecting kink-lump solution.

We now have to determine the effective quartic couplings between χ_1 and χ_2 for each of the different clash-of-symmetries solutions. If χ_{1a} and χ_{2b} are the components which condense, we define the effective quartic coupling between them to have the same normalization as the $\chi_1^2\chi_2^2$ term in the original intersecting kink-lump model given in Eq. 4.2. That is, after computing the relevant traces of the generators in which χ_1 and χ_2 condense, the effective coupling $\lambda^{eff}_{\chi_1\chi_2}$ is defined such that the quartic term appears in the effective potential as $\frac{1}{2}\lambda^{eff}_{\chi_1\chi_2}\chi^2_{1a}\chi^2_{2b}$.

There are three possible clash-of-symmetries solutions coming from $H_1 = SU(5)\times SU(2)\times U(1)$ and $H_2 = SU(4)\times SU(3)\times U(1)$. The other patterns along with the one we have discussed in this section can be found in the appendix. We will label these resultant CoS groups $X_1 = SU(4)\times SU(2)\times U(1)\times U(1)$, $X_2 = SU(3)_c\times SU(2)_I\times U(1)_Y\times U(1)\times U(1)$ and $X_3 = SU(3)\times SU(2)\times SU(2)\times U(1)\times U(1)$. Obviously, the solution with X_2 is the one we have discussed and the one we desire to be the most stable. It turns out that the effective $\chi_1-\chi_2$ couplings for the three breaking patterns are

$$\begin{aligned}
\lambda^{X_1}_{\chi_1\chi_2} &= \lambda^1_{\chi_1\chi_2} + \frac{1}{15}\lambda^2_{\chi_1\chi_2} + \frac{6}{35}(\lambda^3_{\chi_1\chi_2}+\lambda^4_{\chi_1\chi_2}),\\
\lambda^{X_2}_{\chi_1\chi_2} &= \lambda^1_{\chi_1\chi_2} + \frac{1}{120}\lambda^2_{\chi_1\chi_2} + \frac{41}{280}(\lambda^3_{\chi_1\chi_2}+\lambda^4_{\chi_1\chi_2}),\\
\lambda^{X_3}_{\chi_1\chi_2} &= \lambda^1_{\chi_1\chi_2} + \frac{3}{10}\lambda^2_{\chi_1\chi_2} + \frac{407}{5880}(\lambda^3_{\chi_1\chi_2}+\lambda^4_{\chi_1\chi_2}).
\end{aligned} \tag{5.24}$$

From this it follows that the solution generating the Standard Model that we have discussed above has the lowest $\lambda^{eff}_{\chi_1\chi_2}$ and is thus the most stable CoS solution if the parameter conditions $\lambda^2_{\chi_1\chi_2} > 0$ and $-\frac{7}{3}\lambda^2_{\chi_1\chi_2} < \lambda^3_{\chi_1\chi_2}+\lambda^4_{\chi_1\chi_2} < \frac{1715}{454}\lambda^2_{\chi_1\chi_2}$ are imposed. We also impose $\lambda^1_{\chi_1\chi_2}+\lambda^2_{\chi_1\chi_2}+\lambda^3_{\chi_1\chi_2}+\lambda^4_{\chi_1\chi_2} > 0$ to ensure that the potential is bounded from below.

After doing the above analysis, one notices that there is actually another solution to the problem of making the kink-lump generating the $SU(5)\times SU(2)\times U(1)$ subgroup stable, although it involves a fine-tuning that is not ideal. If we fine-tune the self-coupling $\lambda^2_{\chi_1}$ to zero, then all three solutions generating the respective subgroups $SU(6)\times U(1)$, $SU(5)\times SU(2)\times U(1)$ and $SU(4)\times SU(3)\times U(1)$ become degenerate. The other reason this is problematic is that it introduces an accidental $O(48)$ symmetry amongst the components of χ_1 in the potential $V_{\eta_1\chi_1}$ and thus we would naturally expect these solutions to fluctuate. However, the interactions in $V_{\eta_1\chi_1\eta_2\chi_2}$ do not respect this $O(48)$ symmetry, breaking it explicitly back to $SU(7)$. The resultant possible solutions then are not only the three with $H_1 = SU(5)\times$

$SU(2) \times U(1)$ and $H_2 = SU(4) \times SU(3) \times U(1)$, but also those where $H_1 = SU(6) \times U(1)$ and $H_2 = SU(4) \times SU(3) \times U(1)$ as well as those coming from $H_1 = SU(4) \times SU(3) \times U(1)$ and $H_2 = SU(4)' \times SU(3)' \times U(1)'$ (which includes the alternate SM we discuss in the next subsection). In other words, making the fine-tuning $\lambda^2_{\chi_1} = 0$, our desired solution simply has more competitors. Amazingly, when one computes all the effective $\chi_1 - \chi_2$ couplings of the additional CoS solutions, it is still possible to make the solution with the SM discussed in this subsection the most stable one. This is largely due to the very small coefficient in front of the $\lambda^2_{\chi_1\chi_2}$ coupling constant. One finds that the solution discussed in this subsection is still the most stable in this scenario if we tighten the parameter conditions to $\lambda^2_{\chi_1\chi_2} > 0$ and $-\frac{7}{3}\lambda^2_{\chi_1\chi_2} < \lambda^3_{\chi_1\chi_2} + \lambda^4_{\chi_1\chi_2} < \frac{98}{383}\lambda^2_{\chi_1\chi_2}$.

5.3.2 A Rather Non-Standard Standard Model from $H_1 = SU(4) \times SU(3) \times U(1)$ and $H_2 = SU(4)' \times SU(3)' \times U(1)'$

In the last subsection, we described a scenario which produced a Standard Model-like gauge group with the correct hypercharge quantum numbers for the known SM field content along with some $Y = \pm 2$ exotics from a clash between $SU(5) \times SU(2) \times U(1)$ and $SU(4) \times SU(3) \times U(1)$. As noted above, there are some problems in ensuring that the arrangement where we have an $SU(5) \times SU(2) \times U(1)$ subgroup as one of the clashing groups is the most stable one for one kink-lump pair. One naturally might then be motivated to consider obtaining a Standard Model-like gauge group from a clash between two differently embedded copies of $SU(4) \times SU(3) \times U(1)$. Firstly, this has the advantage that we can ensure the most stable arrangement for each kink-lump pair from a one-dimensional point of view is the one generating a $SU(4) \times SU(3) \times U(1)$ subgroup, since to do this we simply choose $\lambda^2_{\chi_1} > 0$ and $\lambda^2_{\chi_2} > 0$ in each sector. Furthermore, it is obvious that we can obtain the non-Abelian part of the Standard Model gauge group since if we call the second group $H_2 = SU(4)' \times SU(3)' \times U(1)'$, we can easily choose the embeddings such that $SU(4) \cap SU(4)' \supset SU(3)_c$ and $SU(3) \cap SU(3)' \supset SU(2)_I$. One also suspects that we can get a localized $U(1)$ in this case since like the case in the previous section, there will be four leftover diagonal generators from all four non-Abelian groups involved in the clash. Indeed, it turns out that this is the case. In this case, we obtain a rather different localized hypercharge generator, one that makes it seem like a successful embedding of the Standard Model fermion content is not possible

To realize the above described situation, we make χ_1 condense in a com-

ponent proportional to the Abelian generator

$$Q_1 = \begin{pmatrix} 3 & 0 & 0 & 0 & 0 & 0 & 0 \\ 0 & 3 & 0 & 0 & 0 & 0 & 0 \\ 0 & 0 & 3 & 0 & 0 & 0 & 0 \\ 0 & 0 & 0 & -4 & 0 & 0 & 0 \\ 0 & 0 & 0 & 0 & -4 & 0 & 0 \\ 0 & 0 & 0 & 0 & 0 & -4 & 0 \\ 0 & 0 & 0 & 0 & 0 & 0 & 3 \end{pmatrix}, \tag{5.25}$$

and let the component of χ_2 which condenses be proportional to

$$Q_1' = \begin{pmatrix} 3 & 0 & 0 & 0 & 0 & 0 & 0 \\ 0 & 3 & 0 & 0 & 0 & 0 & 0 \\ 0 & 0 & 3 & 0 & 0 & 0 & 0 \\ 0 & 0 & 0 & -4 & 0 & 0 & 0 \\ 0 & 0 & 0 & 0 & -4 & 0 & 0 \\ 0 & 0 & 0 & 0 & 0 & 3 & 0 \\ 0 & 0 & 0 & 0 & 0 & 0 & -4 \end{pmatrix}. \tag{5.26}$$

From this we easily see that the groups preserved by the clash are, as noted in the first paragraph of this section, $SU(3)_c \subset SU(4) \cap SU(4)'$ and $SU(2)_I \subset SU(3) \cap SU(3)'$. The leftover generators from $SU(4)$, $SU(3)$ from H_1 and $SU(4)'$, $SU(3)'$ from H_2 are respectively

$$T_1 = \begin{pmatrix} +\frac{2}{3} & 0 & 0 & 0 & 0 & 0 & 0 \\ 0 & +\frac{2}{3} & 0 & 0 & 0 & 0 & 0 \\ 0 & 0 & +\frac{2}{3} & 0 & 0 & 0 & 0 \\ 0 & 0 & 0 & 0 & 0 & 0 & 0 \\ 0 & 0 & 0 & 0 & 0 & 0 & 0 \\ 0 & 0 & 0 & 0 & 0 & 0 & 0 \\ 0 & 0 & 0 & 0 & 0 & 0 & -2 \end{pmatrix}, \tag{5.27}$$

$$T_2 = \begin{pmatrix} 0 & 0 & 0 & 0 & 0 & 0 & 0 \\ 0 & 0 & 0 & 0 & 0 & 0 & 0 \\ 0 & 0 & 0 & 0 & 0 & 0 & 0 \\ 0 & 0 & 0 & +1 & 0 & 0 & 0 \\ 0 & 0 & 0 & 0 & +1 & 0 & 0 \\ 0 & 0 & 0 & 0 & 0 & -2 & 0 \\ 0 & 0 & 0 & 0 & 0 & 0 & 0 \end{pmatrix}, \tag{5.28}$$

$$T_1' = \begin{pmatrix} +\frac{2}{3} & 0 & 0 & 0 & 0 & 0 & 0 \\ 0 & +\frac{2}{3} & 0 & 0 & 0 & 0 & 0 \\ 0 & 0 & +\frac{2}{3} & 0 & 0 & 0 & 0 \\ 0 & 0 & 0 & 0 & 0 & 0 & 0 \\ 0 & 0 & 0 & 0 & 0 & 0 & 0 \\ 0 & 0 & 0 & 0 & 0 & -2 & 0 \\ 0 & 0 & 0 & 0 & 0 & 0 & 0 \end{pmatrix}, \tag{5.29}$$

and

$$T_2' = \begin{pmatrix} 0 & 0 & 0 & 0 & 0 & 0 & 0 \\ 0 & 0 & 0 & 0 & 0 & 0 & 0 \\ 0 & 0 & 0 & 0 & 0 & 0 & 0 \\ 0 & 0 & 0 & +1 & 0 & 0 & 0 \\ 0 & 0 & 0 & 0 & +1 & 0 & 0 \\ 0 & 0 & 0 & 0 & 0 & 0 & 0 \\ 0 & 0 & 0 & 0 & 0 & 0 & -2 \end{pmatrix}. \tag{5.30}$$

Again there is an Abelian generator surviving the clash which is solely a linear combination of the above four generators and thus satisfies the localization condition described in Eq. 5.5, namely

$$Y' = -T_1 - T_2 = -T_1' - T_2' = \begin{pmatrix} -\frac{2}{3} & 0 & 0 & 0 & 0 & 0 & 0 \\ 0 & -\frac{2}{3} & 0 & 0 & 0 & 0 & 0 \\ 0 & 0 & -\frac{2}{3} & 0 & 0 & 0 & 0 \\ 0 & 0 & 0 & -1 & 0 & 0 & 0 \\ 0 & 0 & 0 & 0 & -1 & 0 & 0 \\ 0 & 0 & 0 & 0 & 0 & +2 & 0 \\ 0 & 0 & 0 & 0 & 0 & 0 & +2 \end{pmatrix}. \tag{5.31}$$

Again, we also get a couple of semi-delocalized $U(1)$ gauge groups. In this case, the semi-delocalized generators A and B may be taken to be

$$A = 4Q_1 + T_1 - T_2 = 2Q_1' + 10T_1' - 9T_2' = \begin{pmatrix} \frac{38}{3} & 0 & 0 & 0 & 0 & 0 & 0 \\ 0 & \frac{38}{3} & 0 & 0 & 0 & 0 & 0 \\ 0 & 0 & \frac{38}{3} & 0 & 0 & 0 & 0 \\ 0 & 0 & 0 & -17 & 0 & 0 & 0 \\ 0 & 0 & 0 & 0 & -17 & 0 & 0 \\ 0 & 0 & 0 & 0 & 0 & -14 & 0 \\ 0 & 0 & 0 & 0 & 0 & 0 & 10 \end{pmatrix}, \tag{5.32}$$

and

$$B = Q_1 - 2T_1 + 2T_2 = -\frac{1}{2}Q_1' + \frac{29}{4}T_1' - 6T_2' = \begin{pmatrix} \frac{5}{3} & 0 & 0 & 0 & 0 & 0 & 0 \\ 0 & \frac{5}{3} & 0 & 0 & 0 & 0 & 0 \\ 0 & 0 & \frac{5}{3} & 0 & 0 & 0 & 0 \\ 0 & 0 & 0 & -2 & 0 & 0 & 0 \\ 0 & 0 & 0 & 0 & -2 & 0 & 0 \\ 0 & 0 & 0 & 0 & 0 & -8 & 0 \\ 0 & 0 & 0 & 0 & 0 & 0 & 7 \end{pmatrix}. \tag{5.33}$$

Thus, we have a localized hypercharge generator with a relative sign between the charge for the lepton doublet and the charge for the conjugate of the right-chiral down quark which is opposite that of the usual $SU(5)$ hypercharge generator. It seems that it would be extremely difficult to pick representations containing the SM field content in a simple way, since the charges for the components in the antisymmetric 21 representation would also be affected, which is problematic since the 21 is the natural candidate for embedding the right-chiral up quark, right-chiral electron and the quark doublet. For instance, instead of having a hypercharge $Y = +1/3$, the component inside the 21 that transforms as $(3, 2)$ under $SU(3)_c \times SU(2)_I$ now has $Y = -5/3$. This rules out using the minimal anomaly-free fermion combination of $\overline{7} + \overline{7} + \overline{7} + 21$ to embed each generation of the Standard Model fermions. However, it in fact turns out that the SM fermion content can be embedded in the next-to-minimal anomaly-free fermion combination of $7 + \overline{21} + 35$. Under $SU(3)_c \times SU(2)_I \times U(1)_{Y'} \times U(1)_A \times U(1)_B$, the $SU(7)$ representations break down as

$$\begin{aligned} 7 = {} & (3, 1, -\frac{2}{3}, +\frac{38}{3}, +\frac{5}{3}) + (1, 2, -1, -17, -2) + (1, 1, +2, -14, -8) \\ & + (1, 1, +2, +10, +7), \end{aligned} \tag{5.34}$$

$$\begin{aligned} \overline{21} = {} & (3, 1, +\frac{4}{3}, -\frac{76}{3}, -\frac{10}{3}) + (\overline{3}, 2, +\frac{5}{3}, +\frac{13}{3}, +\frac{1}{3}) + (1, 1, +2, +34, +4) \\ & + (\overline{3}, 1, -\frac{4}{3}, +\frac{4}{3}, +\frac{19}{3}) + (\overline{3}, 1, -\frac{4}{3}, -\frac{68}{3}, -\frac{26}{3}) + (1, 2, -1, +31, +10) \\ & + (1, 2, -1, +7, -5) + (1, 1, -4, +4, +1), \end{aligned} \tag{5.35}$$

$$\begin{aligned}35 = &(3,1,-\frac{8}{3},-\frac{64}{3},-\frac{7}{3}) + (\overline{3},2,-\frac{7}{3},+\frac{25}{3},+\frac{4}{3}) + (1,1,-2,+38,+5)\\ &+ (\overline{3},1,+\frac{2}{3},+\frac{34}{3},-\frac{14}{3}) + (\overline{3},1,+\frac{2}{3},+\frac{106}{3},+\frac{31}{3}) + (3,2,+\frac{1}{3},-\frac{55}{3},-\frac{25}{3})\\ &+ (3,2,+\frac{1}{3},+\frac{17}{3},+\frac{20}{3}) + (3,1,+\frac{10}{3},+\frac{26}{3},+\frac{2}{3}) + (1,2,+3,-21,-3)\\ &+ (1,1,0,-48,-12) + (1,1,0,-24,+3).\end{aligned} \tag{5.36}$$

Hence, if we choose the couplings to the background scalar fields such that each of the fermion fields charged under these representations has a localized left-chiral zero mode, both the lepton doublet L and the charge conjugate of the right-chiral electron $(e_R)^c$ can be embedded in either the 7 or the $\overline{21}$, the charge conjugate of the right-chiral up quark $(u_R)^c$ can be embedded in the $\overline{21}$ and the quark doublet Q can be embedded in the 35. In choosing the representations in this way, the charge conjugate of the right-chiral down quark, $(d_R)^c$, must be embedded in the 35. We can even fit in the charge conjugate of the right-chiral neutrino as the 35 contains two singlet representations. In fact, we can fit in two generations of quarks and 3 generations of charged leptons along with two right-chiral neutrinos.

The electroweak Higgs could fit into either a 7 or a 21. However, given both Q and $(d_R)^c$ are embedded in a 35, to form a down-quark mass matrix we need an invariant between a Higgs field and the Dirac bilinear formed from a fermion field in the 35 representation and its charge conjugate. The only choice that can do the job is a 7 since the tensor product 35×35 contains a $\overline{7}$ but not a $\overline{21}$. Since the tensor products $7 \times 7 \times \overline{21}$ and $\overline{7} \times \overline{21} \times 35$ contain singlets, we can form mass matrices for the charged leptons and the up-type quarks with the electroweak Higgs in a 7. With regards to breaking the semi-delocalized photons, we can utilize the $(1,1,0,-48,-12)$ and $(1,1,0,-24,+3)$ of the 35. It would be interesting to see whether we could use both these components from the one 35 and choose parameters such that both these components attain tachyonic masses. Otherwise, we can use two 35's. From there, like with the previous realization of the SM, the main task is to ensure that the profiles for the scalars and fermions are split appropriately so that the exotic states, other extra states and the semi-delocalized photons become sufficiently massive. Like before, we also need to make sure that there are no unwanted breakings coming from additional localized Higgs components.

Lastly, we need to check that we can make the aforementioned CoS solution the most stable one. As in the previous section, the relevant operators are $\mathrm{Tr}[\chi_1^2]\mathrm{Tr}[\chi_2^2]$, $\mathrm{Tr}[\chi_1\chi_2]^2$, $\mathrm{Tr}[\chi_1^2\chi_2^2]$ and $\mathrm{Tr}[\chi_1\chi_2\chi_1\chi_2]$ and we need to take the relevant traces to compute $\lambda_{\chi_1\chi_2 eff}$ for each different solution. There

are three other clash-of-symmetries breaking patterns, the VEV patterns for which are listed in Appendix D, along with the one we have described. These other solutions break $SU(7)$ down to $W_1 = SU(4) \times SU(3) \times U(1)$, $W_2 = SU(2) \times SU(2) \times SU(2) \times U(1) \times U(1) \times U(1)$ and $W_3 = SU(3) \times SU(3) \times U(1) \times U(1)$. After taking the relevant traces, it turns out that the effective coupling constants are in this case

$$\begin{aligned}
\lambda^{SM\times U(1)^2}_{\chi_1\chi_2 eff} &= \lambda^1_{\chi_1\chi_2} + \frac{25}{576}\lambda^2_{\chi_1\chi_2} + \frac{149}{1008}(\lambda^3_{\chi_1\chi_2} + \lambda^4_{\chi_1\chi_2}),\\
\lambda^{W_1}_{\chi_1\chi_2 eff} &= \lambda^1_{\chi_1\chi_2} + \lambda^2_{\chi_1\chi_2} + \frac{13}{84}(\lambda^3_{\chi_1\chi_2} + \lambda^4_{\chi_1\chi_2}),\\
\lambda^{W_2}_{\chi_1\chi_2 eff} &= \lambda^1_{\chi_1\chi_2} + \frac{1}{36}\lambda^2_{\chi_1\chi_2} + \frac{71}{1008}(\lambda^3_{\chi_1\chi_2} + \lambda^4_{\chi_1\chi_2}),\\
\lambda^{W_3}_{\chi_1\chi_2 eff} &= \lambda^1_{\chi_1\chi_2} + \frac{9}{16}\lambda^2_{\chi_1\chi_2} + \frac{15}{112}(\lambda^3_{\chi_1\chi_2} + \lambda^4_{\chi_1\chi_2}).
\end{aligned} \tag{5.37}$$

Again we can easily choose parameters such that $\lambda^{SM\times U(1)^2}_{\chi_1\chi_2 eff}$ is the smallest of the effective couplings, rendering the arrangement we have described above the most stable. In fact, one can show that $\lambda^{SM\times U(1)^2}_{\chi_1\chi_2 eff}$ is smaller than all of $\lambda^{W_1}_{\chi_1\chi_2 eff}$, $\lambda^{W_2}_{\chi_1\chi_2 eff}$ and $\lambda^{W_3}_{\chi_1\chi_2 eff}$ if we choose parameters such that $\lambda^2_{\chi_1\chi_2} > 0$ and $-551\lambda^2_{\chi_1\chi_2}/4 < \lambda^3_{\chi_1\chi_2} + \lambda^4_{\chi_1\chi_2} < -21\lambda^2_{\chi_1\chi_2}/104$.

5.3.3 The GUT Approach: A Localized $SU(5)$ theory from $H_1 = SU(6) \times U(1)$ and $H_2 = SU(6) \times U(1)$

We can also take the approach of Ref. [25] and localize a grand unification group. If we choose our clashing subgroups to be differently embedded copies of $SU(6) \times U(1)$, then it is clear that we can obtain a localized $SU(5)$ subgroup. Again, from what we know from Ref. [136], if we choose $\lambda^2_{\chi_1} < 0$ and $\lambda^2_{\chi_2} < 0$ then an $SU(6) \times U(1)$ breaking pattern will be the most stable 1D kink-lump configuration for each sector, provided we also choose parameters such that $\lambda^1_{\chi_1} + \lambda^2_{\chi_1} > 0$ and $\lambda^1_{\chi_2} + \lambda^2_{\chi_2} > 0$ still hold so that it is absolutely guaranteed that the potentials are bounded from below. This means that the only thing we really need to check is that the arrangement where the clash yields a localized $SU(5)$ subgroup is the most stable arrangement, which in this case just means that it is more stable than the only other arrangement where $H_1 = H_2$ to give a semi-delocalized $SU(6) \times U(1)$.

The VEV pattern we desire is one in which χ_1 condenses in the component

corresponding to the matrix

$$Q_1 = \begin{pmatrix} 1 & 0 & 0 & 0 & 0 & 0 & 0 \\ 0 & 1 & 0 & 0 & 0 & 0 & 0 \\ 0 & 0 & 1 & 0 & 0 & 0 & 0 \\ 0 & 0 & 0 & 1 & 0 & 0 & 0 \\ 0 & 0 & 0 & 0 & 1 & 0 & 0 \\ 0 & 0 & 0 & 0 & 0 & 1 & 0 \\ 0 & 0 & 0 & 0 & 0 & 0 & -6 \end{pmatrix}, \tag{5.38}$$

and χ_2 condenses in the component corresponding to

$$Q_1' = \begin{pmatrix} 1 & 0 & 0 & 0 & 0 & 0 & 0 \\ 0 & 1 & 0 & 0 & 0 & 0 & 0 \\ 0 & 0 & 1 & 0 & 0 & 0 & 0 \\ 0 & 0 & 0 & 1 & 0 & 0 & 0 \\ 0 & 0 & 0 & 0 & 1 & 0 & 0 \\ 0 & 0 & 0 & 0 & 0 & -6 & 0 \\ 0 & 0 & 0 & 0 & 0 & 0 & 1 \end{pmatrix}. \tag{5.39}$$

Clearly, $SU(6) \cap SU(6)' = SU(5)$. The leftover generators coming from inside the $SU(6)$ and $SU(6)'$ generators are

$$T_1 = \begin{pmatrix} 1 & 0 & 0 & 0 & 0 & 0 & 0 \\ 0 & 1 & 0 & 0 & 0 & 0 & 0 \\ 0 & 0 & 1 & 0 & 0 & 0 & 0 \\ 0 & 0 & 0 & 1 & 0 & 0 & 0 \\ 0 & 0 & 0 & 0 & 1 & 0 & 0 \\ 0 & 0 & 0 & 0 & 0 & -5 & 0 \\ 0 & 0 & 0 & 0 & 0 & 0 & 0 \end{pmatrix}, \tag{5.40}$$

and χ_2 condenses in the component corresponding to

$$T_1' = \begin{pmatrix} 1 & 0 & 0 & 0 & 0 & 0 & 0 \\ 0 & 1 & 0 & 0 & 0 & 0 & 0 \\ 0 & 0 & 1 & 0 & 0 & 0 & 0 \\ 0 & 0 & 0 & 1 & 0 & 0 & 0 \\ 0 & 0 & 0 & 0 & 1 & 0 & 0 \\ 0 & 0 & 0 & 0 & 0 & 0 & 0 \\ 0 & 0 & 0 & 0 & 0 & 0 & -5 \end{pmatrix}. \tag{5.41}$$

There are therefore a couple of semi-delocalized $U(1)$ generators which may

be taken to be

$$q_1 = 5/6Q_1 + 7/6T_1 = 5/6Q_1' + 7/6T_1' = \begin{pmatrix} 2 & 0 & 0 & 0 & 0 & 0 & 0 \\ 0 & 2 & 0 & 0 & 0 & 0 & 0 \\ 0 & 0 & 2 & 0 & 0 & 0 & 0 \\ 0 & 0 & 0 & 2 & 0 & 0 & 0 \\ 0 & 0 & 0 & 0 & 2 & 0 & 0 \\ 0 & 0 & 0 & 0 & 0 & -5 & 0 \\ 0 & 0 & 0 & 0 & 0 & 0 & -5 \end{pmatrix}, \quad (5.42)$$

and

$$q_2 = 1/6(Q_1 - T_1) = 1/6(T_1' - Q_1') = \begin{pmatrix} 0 & 0 & 0 & 0 & 0 & 0 & 0 \\ 0 & 0 & 0 & 0 & 0 & 0 & 0 \\ 0 & 0 & 0 & 0 & 0 & 0 & 0 \\ 0 & 0 & 0 & 0 & 0 & 0 & 0 \\ 0 & 0 & 0 & 0 & 0 & 0 & 0 \\ 0 & 0 & 0 & 0 & 0 & 1 & 0 \\ 0 & 0 & 0 & 0 & 0 & 0 & -1 \end{pmatrix}. \quad (5.43)$$

Thus the full symmetry respected on the wall is $SU(5) \times U(1)_{q_1} \times U(1)_{q_2}$ but only the $SU(5)$ subgroup is fully localized to the junction, and just as before in the other cases with adjoint scalars, we will have to introduce additional Higgs fields to break the residual Abelian groups.

To work out if this arrangement is the most stable one, again we just analyze the effective quartic coupling constants coming from the interactions $\mathrm{Tr}[\chi_1^2]\mathrm{Tr}[\chi_2^2]$, $(\mathrm{Tr}[\chi_1\chi_2])^2$, $\mathrm{Tr}[\chi_1^2\chi_2^2]$ and $\mathrm{Tr}[\chi_1\chi_2\chi_1\chi_2]$. Firstly, note that a pattern generating a clash between identical $SU(6) \times U(1)$ subgroups is simply one where both χ_1 and χ_2 condense in the component proportional to Q_1 in Eq. 5.38. In calculating the relevant traces of the generators involved, we find that the effective quartic coupling $\lambda_{\chi_1\chi_2 eff} = 1/2\lambda^1_{\chi_1\chi_2} + 1/72\lambda^2_{\chi_1\chi_2} + 11/504(\lambda^3_{\chi_1}\chi_2 + \lambda^4_{\chi_1\chi_2})$ for the $SU(5) \times U(1) \times U(1)$ breaking pattern and it is $\lambda_{\chi_1\chi_2 eff} = 1/2(\lambda^1_{\chi_1\chi_2} + \lambda^2_{\chi_1\chi_2}) + 31/84(\lambda^3_{\chi_1}\chi_2 + \lambda^4_{\chi_1\chi_2})$ for the $SU(6) \times U(1)$ pattern. Thus there is a very large parameter space where the $SU(5) \times U(1) \times U(1)$ has the lowest effective quartic coupling given that the coefficients coming from the traces of the $(\mathrm{Tr}[\chi_1\chi_2])^2$, $\mathrm{Tr}[\chi_1^2\chi_2^2]$ and $\mathrm{Tr}[\chi_1\chi_2\chi_1\chi_2]$ terms are much lower than those for the $SU(6) \times U(1)$ pattern. Indeed, one can ensure that $SU(5) \times U(1) \times U(1)$ has the lowest effective $\chi_1 - \chi_2$ coupling by choosing all of $\lambda^2_{\chi_1\chi_2}$, $\lambda^3_{\chi_1\chi_2}$ and $\lambda^4_{\chi_1\chi_2}$ to be positive.

Having now ensured that the desired Clash-of-Symmetries breaking pattern where we have a localized $SU(5)$ subgroup on the domain-wall intersection can be the most stable one, let us comment briefly on how to construct

a realistic scenario. We obviously have to break $SU(5)$ on the domain-wall intersection. We do this by introducing another adjoint scalar since under $SU(5) \times U(1)_A \times U(1)_B$ the 48 breaks down as

$$\begin{aligned} 48 = &(24,0,0) + (5,+7,-1) + (\overline{5},-7,+1) + (5,+7,+1) + (\overline{5},-7,-1) \\ &+ (1,0,-2) + (1,0,+2) + (1,0,0) + (1,0,0), \end{aligned} \tag{5.44}$$

and subsequently we perform dynamical localization on this additional adjoint scalar field. As usual, each of the different $SU(5) \times U(1)_A \times U(1)_B$ components of the 48 will have their own set of discrete localized modes and continuum modes. To break to the SM, we need the $(24,0,0)$ component to have at least one localized mode and we need its lowest energy localized mode to attain a tachyonic mass on the domain-wall intersection. Although doing the exact full analysis is beyond the scope of this paper, it would be interesting to see if we can make the lowest energy localized mode of one of the $(1,0,-2)$ and $(1,0,+2)$ components tachyonic simultaneously with that of the $(24,0,0)$ component in order to efficiently break one of the semi-delocalized subgroups.

We need to break both the semi-delocalized $U(1)$ subgroups to produce a phenomenologically acceptable model. As noted above we can break one of them by utilizing some of the components inside the additional adjoint scalar. Under $SU(5) \times U(1)_A \times U(1)_B$ symmetry, the 7, 21 and 35 reduce respectively to

$$7 = (5,+2,0) + (1,-5,+1) + (1,-5,-1), \tag{5.45}$$

$$21 = (10,+4,0) + (5,-3,+1) + (5,-3,-1) + (1,-10,0), \tag{5.46}$$

$$35 = (\overline{10},+6,0) + (10,-1,+1) + (10,-1,-1) + (5,-8,0). \tag{5.47}$$

Thus, we can utilize the $(1,-5,\pm 1)$ components inside the 7 or the $(1,-10,0)$ components in conjunction with one of the $(1,0,\pm 2)$ components inside the 48 to break both the semi-delocalized Abelian groups. Alternatively, we could use any two $SU(5)$ singlet components which have different non-trivial charges under the Abelian symmetries in any combination of 7's and 21's.

From the above equations for the representations, we can easily see how to make the exotic and unwanted fermionic states much more massive than the $SU(5)$ states yielding the SM quark and lepton field content. If we choose the standard anomaly-free combination $\overline{7} + \overline{7} + \overline{7} + 21$ for each generation, we can see that if we use the combination of a 7 and a 21 to break the semi-delocalized $U(1)$ gauge symmetries by giving the respective $(1,-5,+1)$ and $(1,-5,-1)$ components tachyonic masses, the quintets $(\overline{5},-2,0)$ from

the extra two anti-fundamentals can form singlets with the $(5, -3, +1)$ and $(5, -3, -1)$ components inside the 21 and thus decouple as heavy fermions.

Finally, one needs to break electroweak symmetry. In principle one could do this with any of the quintets embedded in the 7, 21, or 35 representations. If we embed the usual fermionic quintet in a 7, we can form the electron and down quark mass matrices with two conjugates of the $(5, +2, 0)$ component and the $(10, +4, 0)$ component in the 21. On the other hand, we can't use the same quintet to yield the up quark mass matrix: we instead require the $(5, -8, 0)$ component to give the SM fermions inside the $(10, +4, 0)$ component of the 21 masses. Thus, it seems we require a two-Higgs doublet model in this scenario, along with more singlet Higgs fields than is necessary to break the semi-delocalized $U(1)$'s in order to give the exotic states masses.

5.3.4 An Alternative Path to the Standard Model with $\chi_1 \sim 21$ and $\chi_2 \sim 35$

Finally, we give an example yielding a Standard Model gauge group where the scalar fields responsible for the breakings on each wall are not in the adjoint representation. Instead, the field χ_1 will be chosen to transform under the 21 representation and χ_2 will be chosen to transform under the 35 representation. With these representations, we can end up with exactly the Standard Model gauge group *without* any semi-delocalized $U(1)$ gauge groups.

The full scalar potential is

$$V = V_{\eta_1\chi_1} + V_{\eta_2\chi_2} + V_{\eta_1\chi_1\eta_2\chi_2}, \tag{5.48}$$

where in this case the self-interaction potentials for each kink-lump generating pair are

$$\begin{aligned} V_{\eta_1\chi_1} = {} & \frac{1}{4}\lambda_{\eta_1}(\eta_1^2 - v_1^2)^2 + \lambda_{\eta_1\chi_1}(\eta_1^2 - v_1^2)\chi_1^{ab}\chi_{1ba} + \mu_{\chi_1}^2\chi_1^{ab}\chi_{1ba} \\ & + \lambda_{\chi_1}^1[\chi_1^{ab}\chi_{1ab}]^2 + \lambda_{\chi_1}^2\chi_1^{ab}\chi_{1bc}\chi_1^{cd}\chi_{1da}, \end{aligned} \tag{5.49}$$

and

$$\begin{aligned} V_{\eta_2\chi_2} = {} & \frac{1}{4}\lambda_{\eta_2}(\eta_2^2 - v_2^2)^2 + \lambda_{\eta_2\chi_2}(\eta_2^2 - v_2^2)\chi_2^{abc}\chi_{2abc} + \mu_{\chi_2}^2\chi_2^{abc}\chi_{2abc} \\ & + \lambda_{\chi_2}^1[\chi_2^{abc}\chi_{2abc}]^2 + \lambda_{\chi_2}^2\chi_1^{abc}\chi_{1bcd}\chi_1^{def}\chi_{1efa}, \end{aligned} \tag{5.50}$$

and the interaction potential between the two sectors is

$$\begin{aligned} V_{\eta_1\chi_1\eta_2\chi_2} = & \frac{1}{2}\lambda_{\eta_1\eta_2}(\eta_1^2 - v_1^2)(\eta_2^2 - v_2^2) + \lambda_{\eta_1\chi_2}(\eta_1^2 - v_1^2)\chi_2^{abc}\chi_{2abc} \\ & + \lambda_{\chi_1\eta_2}(\eta_2^2 - v_2^2)\chi_1^{ab}\chi_{1ab} + 2\lambda^1_{\chi_1\chi_2}\chi_1^{ab}\chi_{1ab}\chi_2^{cde}\chi_{2cde} \\ & + 2\lambda^2_{\chi_1\chi_2}\chi_1^{ab}\chi_{1bc}\chi_2^{cde}\chi_{2dea} + 2\lambda^3_{\chi_1\chi_2}\chi_1^{ab}\chi_{2abc}\chi_2^{cde}\chi_{1de} \\ & + \lambda_{\chi_1\eta_2\chi_2}\epsilon^{abcdefg}\chi_{1ab}\chi_{1cd}\chi_{2efg}\eta_2 + \lambda^*_{\chi_1\eta_2\chi_2}\epsilon_{abcdefg}\chi_1^{ab}\chi_1^{cd}\chi_2^{efg}\eta_2. \end{aligned} \tag{5.51}$$

There are some clear advantages with regards to the energetics by choosing $\chi_1 \sim 21$ and $\chi_2 \sim 35$. Firstly, the 21 representation corresponds to a rank 2 antisymmetric tensor. It was shown in Ref. [136] that for a potential just involving a rank 2 antisymmetric $SU(N)$ tensor that for $\lambda^2_{\chi_1} > 0$ the lowest energy breaking pattern was one where a single 2×2 block of the tensor is non-zero and proportional to the rank 2 alternating tensor while all other components vanish, yielding $SU(N-2) \times SU(2)$ as the unbroken subgroup. Thus, if we choose $\lambda^2_{\chi_1} > 0$ then in the region where χ_1 is tachyonic it should condense with this pattern and therefore the lowest energy 1D kink-lump solution should have $SU(7)$ broken to $SU(5) \times SU(2)$! Thus we have done what we had trouble doing in a simple way with an adjoint scalar in Sec. 5.3.1 and ensured that one wall generates the same $SU(5) \times SU(2)$ subgroup. Furthermore, as the 21 is an antisymmetric tensor rather than an adjoint, the $U(1)$ subgroup of $SU(5) \times SU(2) \times U(1)$ that we got with an adjoint scalar is already broken.

In a similar way to how the 21 attains a VEV pattern with one block proportional to the rank 2 alternating tensor ϵ_{ij}, one might think that for a certain region of parameter space that a rank 3 totally antisymmetric tensor such as the 35 of $SU(7)$ might attain a VEV pattern in which just three indices trace over the elements of the rank 3 alternating tensor ϵ_{ijk} with all other components zero. If this were the case, since ϵ_{ijk} is an invariant tensor under $SU(3)$ and the VEV patttern of the 35 would vanish for the remaining four indices, one would expect the unbroken subgroup would to be $SU(4) \times SU(3)$. Although obtaining the canonical form for a rank 3 alternating tensor is a much more non-trivial problem than that for a rank 2 antisymmetric tensor, this was indeed shown to be the case [137, 138]. Choosing $7\lambda^1_{\chi_2} + \lambda^2_{\chi_2} > 0$ to ensure boundedness from below, if we choose $\lambda^2_{\chi_1} > 0$ then the 35 will indeed condense with the aforementioned pattern. In choosing the 35 we also automatically break the $U(1)$ that usually comes with the $SU(4) \times SU(3)$ subgroup if we perform the breaking with an adjoint, which is analogous to how the 21 breaks the $U(1)$ associated with $SU(5) \times SU(2)$. Hence, in choosing $\chi_1 \sim 21$ and $\chi_2 \sim 35$ we have already broken the semi-delocalized $U(1)$ subgroups that we get when we utilize adjoint scalars.

The last thing to check is whether we can guarantee that the pattern generating a Standard Model gauge group localized to the intersection is the most stable one. It is obvious that we can generate the same Standard Model gauge group given Sec. 5.3.1. It is this precise SM group since if we choose our VEV's such that $SU(5) \cap SU(4) \supset SU(3)$ and $SU(5) \cap SU(3) \supset SU(2)$, we still obtain the same leftover generators from each group given in Eqs. 5.10, 5.11, 5.12 and 5.13, yielding the same hypercharge generator as in Eq. 5.14. To show this outcome can be achieved obviously requires looking at the possible VEV patterns.

As χ_1 is a rank 2 antisymmetric tensor, it will attain a VEV of the form

$$V^{21}_{ab} = A_1(\epsilon_{12}\delta^m_a\delta^n_b + \epsilon_{21}\delta^n_a\delta^m_b), \tag{5.52}$$

where here $1 \leq m < n \leq 7$ denote some fixed, distinct integers. In a similar manner, $\chi_2 \sim 35$ will attain a VEV of the form

$$V^{35}_{abc} = A_2\big(\epsilon_{123}(\delta^q_a\delta^r_b\delta^s_c+\delta^s_a\delta^q_b\delta^r_c+\delta^r_a\delta^s_b\delta^q_c)+\epsilon_{132}(\delta^q_a\delta^s_b\delta^r_c+\delta^s_a\delta^r_b\delta^q_c+\delta^r_a\delta^q_b\delta^s_c)\big), \tag{5.53}$$

where again $1 \leq q < r < s \leq 7$ are fixed, distinct integers.

Up to rearrangement of the indices and gauge transformations, there are three distinct clashing patterns. The first is where neither of the integers m or n of Eq. 5.52 are equal to any of the integers q, r or s of Eq. 5.53. For this first pattern, the $SU(2)$ subgroup preserving the rank 2 alternating tensor of V^{21}_{ab} is outside the $SU(3)$ alternating tensor preserving the rank 3 alternating tensor of the pattern V^{35}_{abc}, and thus the unbroken symmetry in the intersection region is $SU(3) \times SU(2) \times SU(2)$, with only one of the $SU(2)$ subgroups localized and the other $SU(2)$ and the $SU(3)$ semi-delocalized.

The second pattern is where, without loss of generality, $n = q$ with m not equal to neither of r or s. Here, since the two indices r and s overlap with the remaining five indices for which any element of V^{21}_{ab} is zero, the $SU(2)$ subgroup of the $SU(3)$ preserving V^{35}_{abc} is also contained in the $SU(5)$ subgroup preserved by V^{21}_{ab}. Also, three of the indices transformed by the $SU(4)$ subgroup left unbroken by V^{35}_{abc} also transform under the $SU(5)$ subgroup left unbroken by V^{21}_{ab}. Hence this is the pattern we want, with $SU(3)_c \times SU(2)_I \times U(1)_Y$ localized to the domain-wall intersection.

The last possible pattern is where, without loss of generality, $m = q$ and $n = r$. Here, the $SU(2)$ subgroup preserving V^{21}_{ab} is also a subgroup of the $SU(3)$ subgroup preserving V^{35}_{abc}. Also, the $SU(4)$ subgroup left unbroken by V^{35}_{abc} is also a subgroup of the $SU(5)$ subgroup preserved by V^{21}_{ab}. Thus, the group respected on the wall with this pattern is $SU(4) \times SU(2)$, with both non-Abelian factor groups semi-delocalized.

Having outlined the possible groups resulting from the clash-of-symmetries mechanism, we now need to look at the effective couplings between the relevant components of χ_1 and χ_2 involved in each clash. For simplicity of analysis, we will ignore the $\epsilon^{abcdefg}\chi_{1ab}\chi_{1cd}\chi_{2efg}\eta_2$ term and set $\lambda_{\chi_1\eta_2\chi_2} = 0$. This leaves as the relevant terms $\chi_1^{ab}\chi_{1ba}\chi_2^{cde}\chi_{2cde}$, $\chi_1^{ab}\chi_{1bc}\chi_2^{cde}\chi_{2dea}$, and $\chi_1^{ab}\chi_{2abc}\chi_2^{cde}\chi_{1de}$. To determine the effective quartic coupling constants, we need to calculate the contractions of the various epsilon tensors involved in the products, which can be though of as products between V_{ab}^{21}/A_1 and V_{abc}^{35}/A_2. For $\chi_1^{ab}\chi_{1ba}\chi_2^{cde}\chi_{2cde}$, the resulting coefficient is always the same, namely we have $\chi_1^{ab}\chi_{1ba}\chi_2^{cde}\chi_{2cde} \propto \epsilon^{ij}\epsilon_{ij}\epsilon^{uvw}\epsilon_{uvw} = 2 \times 6 = 12$. Hence, the $\chi_1^{ab}\chi_{1bc}\chi_2^{cde}\chi_{2dea}$ and $\chi_1^{ab}\chi_{2abc}\chi_2^{cde}\chi_{1de}$ terms are ultimately the ones which determine which clash-of-symmetries group is favored.

For the $SU(3) \times SU(2) \times SU(2)$ pattern, $\chi_1^{ab}\chi_{1bc}\chi_2^{cde}\chi_{2dea}$ and $\chi_1^{ab}\chi_{2abc}\chi_2^{cde}\chi_{1de}$ both vanish since the rank 2 and rank 3 tensors contained in V_{ab}^{21} and V_{abc}^{35} do not have any indices in common. Therefore, the effective quartic coupling in this situation is simply $\lambda_{\chi_1\chi_2 eff} = \lambda^1_{\chi_1\chi_2}$.

For the pattern generating a localized $SU(3)_c \times SU(2)_I \times U(1)_Y$ to the intersection, there is one index in common between the rank 2 alternating tensor from V_{ab}^{21} and the rank 3 alternating tensor from V_{abc}^{35}. This means that $\chi_1^{ab}\chi_{2abc}\chi_2^{cde}\chi_{1de}$ must vanish because it involves a contraction between V_{ab}^{21} and V_{abc}^{35} over two indices rather than just one. On the other hand, since $\epsilon^{ij}\epsilon_{jk} = \delta^i_k$ and $V^{21ab}V^{21}_{bc} \propto \delta^a_m\delta^m_c + \delta^a_n\delta^n_c$, we have

$$\begin{aligned}
\chi_1^{ab}\chi_{1bc}\chi_2^{cde}\chi_{2dea} &\propto (\delta^a_m\delta^m_c + \delta^a_n\delta^n_c)V^{35cde}V^{35}_{dea} \\
&= V^{35mde}V^{35}_{dem} + V^{35nde}V^{35}_{den} \\
&= 0 + 2V^{35qrs}V^{35}_{rsq} \\
&= 2V^{35qrs}V^{35}_{qrs} \\
&\propto 2\epsilon^{ijk}\epsilon_{ijk} \\
&= 12.
\end{aligned} \tag{5.54}$$

Thus for the pattern we want, $\lambda_{\chi_1\chi_2 eff} = \lambda^1_{\chi_1\chi_2} + \lambda^2_{\chi_1\chi_2}$. For the $SU(4) \times SU(2)$ pattern, both indices of the rank 2 alternating tensor in V_{ab}^{21} coincide with indices of the rank 3 alternating tensor in V_{abc}^{35}. Thus, in this case, both the non-trivial quartic coupling terms are non-vanishing. For $\chi_1^{ab}\chi_{1bc}\chi_2^{cde}\chi_{2dea}$ we

have

$$\begin{aligned}\chi_1^{ab}\chi_{1bc}\chi_2^{cde}\chi_{2dea} &\propto (\delta^a_m\delta^m_c+\delta^a_n\delta^n_c)V^{35cde}V^{35}_{dea}\\ &= V^{35mde}V^{35}_{dem}+V^{35nde}V^{35}_{den}\\ &= 2V^{35qrs}V^{35}_{rsq}+2V^{35rsq}V^{35}_{sqr}\\ &= 4V^{35qrs}V^{35}_{qrs}\\ &\propto 4\epsilon^{ijk}\epsilon_{ijk}\\ &= 24.\end{aligned} \tag{5.55}$$

Given $V^{21}_{ab}V^{35cab} \propto \delta^m_a\delta^n_b V^{35cab} - \delta^n_a\delta^m_b V^{35cab} = 2V^{35cmn}$ and $V^{21ab}V^{35}_{abc} \propto -\delta^a_m\delta^b_n V^{35}_{abc} + \delta^a_n\delta^b_m V^{35abc} = -2V^{35}_{mnc}$, we have

$$\begin{aligned}\chi_1^{ab}\chi_{2abc}\chi_2^{cde}\chi_{1de} &\propto -4V^{35}_{mnc}V^{35cmn}\\ &= -4V^{35}_{mnc}V^{35mnc}\\ &\propto -4\epsilon_{ijk}\epsilon^{ijk}\\ &= -24.\end{aligned} \tag{5.56}$$

Thus for the $SU(4)\times SU(2)$ pattern, $\lambda_{\chi_1\chi_2 eff} = \lambda^1_{\chi_1\chi_2} + 2\lambda^2_{\chi_1\chi_2} - 2\lambda^3_{\chi_1\chi_2}$.

We can easily choose parameters such that the pattern yielding the localized Standard Model has the lowest effective $\chi_1-\chi_2$ coupling and is thus the most stable solution. One can easily see by inspection that choosing $\lambda^1_{\chi_1\chi_2}>0$, $\lambda^2_{\chi_1\chi_2}<0$, $\lambda^1_{\chi_1\chi_2}+\lambda^2_{\chi_1\chi_2}>0$ and $\lambda^2_{\chi_1\chi_2}-\lambda^3_{\chi_1\chi_2}>0$ that $\lambda_{\chi_1\chi_2 eff}$ will be positive for all three patterns and will always be lowest for the $SU(3)_c\times SU(2)_I\times U(1)_Y$ pattern and highest for the $SU(4)\times SU(2)$ pattern.

We have successfully shown that an intersecting kink-lump solution with $\chi_1\sim 21$ and $\chi_2\sim 35$ yields a subgroup localized to the domain-wall intersection which is precisely the Standard Model gauge group with no other localized or semi-delocalized gauge symmetries respected there. Furthermore, we have shown that this solution can be the most stable one possible. From here, aside from the semi-delocalized $U(1)$'s which are already broken in this case, we face many of the same challenges as with the models produced from adjoint scalars. We need to localize the requisite Higgs fields to the intersection with tachyonic masses and we need to ensure that other unwanted components have positive definite squared masses. As the Standard Model produced here is equivalent to the one produced with two adjoint scalars in Sec. 5.3.1, we will have to embed the electroweak Higgs doublet inside another scalar field charged under the 35 representation if we embed the Standard Model fermions inside a $\overline{7}$ and a 21 with a couple of $\overline{7}$'s in addition to ensure anomaly cancellation.

Since the 21 and 35 representations are complex, the fermion couplings to χ_1 and χ_2 are not exactly vector-like as they are in the case in which they

are adjoint scalars. They involve Dirac scalar products between spinor fields $\Psi_7 \sim \overline{7}$ and $\Psi_{21} \sim 21$ and their charge conjugates. Note that if a 5+1D spinor Ψ transforms under the two discrete $\mathbb{Z}_2$ symmetries as $\Psi \to i\Gamma^4\Gamma^7\Psi$ and $\Psi \to i\Gamma^5\Psi$ respectively, then its charge conjugate Ψ^C also transforms as $\Psi^C \to i\Gamma^4\Gamma^7\Psi^C$ and $\Psi \to i\Gamma^5\Psi^C$. This implies that it is also the case that $\overline{\Psi^C}\Psi \to \overline{\Psi^C}\Psi$ and $\overline{\Psi^C}\Gamma^7\Psi \to -\overline{\Psi^C}\Gamma^7\Psi$ under the first $\mathbb{Z}_2$ symmetry and $\overline{\Psi^C}\Psi \to -\overline{\Psi^C}\Psi$ and $\overline{\Psi^C}\Gamma^7\Psi \to \overline{\Psi^C}\Gamma^7\Psi$ under the second. Hence, in this scenario, the background Yukawa Lagrangian for one generation, with the SM fermions embedded in Ψ_7 and Ψ_{21} and with the fermionic fields $K^1 \sim \overline{7}$ and $K^2 \sim \overline{7}$ added for anomaly cancellation, is

$$\begin{aligned}
\mathcal{L}_{Yuk} = & -ih_{7\eta_1}\overline{\Psi_7}\Gamma^7\Psi_7\eta_1 + h_{7\eta_2}\overline{\Psi_7}\Psi_7\eta_2 - ih_{7K^i\eta_1}\overline{\Psi_7}\Gamma^7K^i\eta_1 + h_{7K^i\eta_2}\overline{\Psi_7}K^i\eta_2 \\
& - ih^*_{7K^i\eta_1}\overline{K^i}\Gamma^7\Psi_7\eta_1 + h^*_{7K^i\eta_2}\overline{K^i}\Psi_7\eta_2 - ih_{K^iK^j\eta_1}\overline{K^i}\Gamma^7K^j\eta_1 \\
& + h_{K^iK^j\eta_2}\overline{K^i}K^j\eta_2 - 2ih_{21\eta_1}\mathrm{Tr}[\overline{\Psi_{21}}\Gamma^7\Psi_{21}]\eta_1 + 2\mathrm{h}_{21\eta_2}\mathrm{Tr}[\overline{\Psi_{21}}\Psi_{21}]\eta_2 \\
& - ih_{7\chi_1}\overline{\Psi_7}\chi_1^\dagger\Gamma^7\Psi_7^C - ih^*_{7\chi_1}\overline{\Psi_7^C}\chi_1\Gamma^7\Psi_7 - ih_{7K^i\chi_1}\overline{\Psi_7}\chi_1^\dagger\Gamma^7K^{iC} \\
& - ih^*_{7K^i\chi_1}\overline{K_7^{iC}}\chi_1\Gamma^7\Psi_7 - ih_{K^iK^j\chi_1}\overline{K^i}\chi_1^\dagger\Gamma^7K^{jC} - ih^*_{K^iK^j\chi_1}\overline{K^{jC}}\chi_1^\dagger\Gamma^7K^i \\
& + h_{7\chi_2 21}\overline{\Psi_{21}}^{ab}\Psi_7^c\chi_{2abc} + h^*_{7\chi_2 21}\overline{\Psi_{7c}}\Psi_{21ab}\chi_2^{abc}.
\end{aligned} \tag{5.57}$$

It would be interesting to see what effect some of these non-standard background couplings have on the profiles. There should still be chiral zero modes localized on the intersection since their existence is mainly due to the couplings to the fields generating the kinks η_1 and η_2. If the couplings are vector-like, the interactions with χ_1 and χ_2 tend to affect the localization centers, although in this case we also have interactions mixing the fermionic fields so one would expect some mixing induced in the profiles. The analysis for fermion localization is beyond the scope of the paper.

In showing that there is an interesting solution in a case where the fields inducing the symmetry breaking on each wall are not adjoint scalar fields, we have demonstrated that the scope for application of this new realization of the clash-of-symmetries mechanism is broad. One of the advantages of using complex representations to induce the breakings on the walls is that the residual $U(1)$'s are automatically broken. Indeed, one can imagine using different representations from the ones chosen in this section to reproduce other interesting scenarios. For example, it is obvious that the SM-like gauge group produced and described in Sec. 5.3.2 could alternatively be produced by utilizing two scalars in the 35 representation since they both induce breakings to $SU(4) \times SU(3)$ subgroups. Likewise, an $SU(5)$ theory equivalent to the one produced in Sec. 5.3.3 could also be reproduced by replacing the adjoint scalars with fundamental scalars.

5.4 Conclusion

In this chapter, we have proposed a new version of the Clash-of-Symmetries mechanism, which is an extension of the Dvali-Shifman mechanism, in the context of intersecting domain walls in 5+1D spacetime. Here, a large gauge group G was assumed to be in confinement phase in the 6D bulk away from both domain-wall branes and on the branes G was broken to subgroups H_1 and H_2 on each wall by the fields which attain lump-like VEV patterns on the wall. H_1 and H_2 are taken to be localized via the Dvali-Shifman mechanism. In turn, there is a clash-of-symmetries mechanism on the domain-wall intersection between H_1 and H_2, where the symmetry respected is $H_1 \cap H_2$. Subgroups of $H_1 \cap H_2$ are then taken to be localized to the domain-wall intersection by confinement dynamics if they are proper subgroups of confining, non-Abelian factor subgroups of both H_1 and H_2. Assuming that both 5D and 6D non-Abelian Yang-Mills gauge theories exhibit confinement, this is a plausible mechanism to localize subgroups of a larger group on the intersection of two domain walls.

We then dealt with a toy $SU(7)$ model which yielded some interesting results. In a model in which both χ_1 and χ_2 were charged under the adjoint representation, we showed that two choices for the VEV patterns for these fields yielded SM-like gauge groups fully localized to the domain-wall intersection, and another yielded a localized $SU(5)$ gauge theory. We found that in these cases, there are always left-over photons that are semi-delocalized and thus must be broken. We then gave the most elegant example in the paper in which χ_1 is charged under the 21 representation and χ_2 is charged under the 35 representation, yielding exactly an SM-like gauge group localized to the intersection with no leftover semi-delocalized photons. This case also has another advantage over the case with adjoint scalars generating the same SM, namely that it is possible to ensure that the desired configuration is the most stable in a quartic scalar field theory.

In all the examples that we have given, we only briefly touched on some of the basics of how to construct realistic fermionic and scalar sectors localized to the domain-wall intersection. We did not, for example, go into the specifics of scalar and fermion localization and show that realistic masses for the Standard Model fermions could be generated and that all the extra exotic fermions and scalars could be made massive enough. In some of the examples we have used, this seems to be quite a formidable task and one that is truly beyond the scope of this thesis. Nevertheless, we have achieved something quite non-trivial in showing that in principle it is possible to localize and break straight down to a Standard Model gauge group by using the Clash-of-Symmetries mechanism. We showed this could be done both

by using adjoint scalars and scalars in complex representations, and we have thus shown that the scope for use of this particular version of the Clash-of-Symmetries mechanism is very broad. It may not turn out that the particular models we have described in this paper are of phenomenological relevance after a more thorough analysis of the fermionic and scalar sectors, but we have laid the foundations for building a successful intersecting domain-wall braneworld model with gauge bosons localized to the intersection.

There is still further work that needs to be done in the intersecting domain-wall braneworld framework. We also need to successfully localize gravity and we also need to analyze the local stability properties of these intersecting domain-wall solutions.

Chapter 6

Conclusion

In this thesis, we have essentially discussed two different aspects of domain-wall brane models; the first being how to account for the fermiom mass spectra in such models and the second on how to extend the domain-wall brane framework to six dimensions. The first was necessary to show that a domain-wall brane model could realistically and naturally account for the fermion masses and mixing angles, and it served as a test for whether these models can fit phenomenological constraints. The second was motivated by the desire to extend the domain-wall brane framework beyond one additional dimension, just as has been done previously by extending the framework to gauge groups more complicated than $SU(5)$ [124, 25].

In Chapter 2, we showed that the split fermion mechanism which arose naturally in the $SU(5)$ model could account for the fermion mass hierarchy as well as small quark mixing angles. We showed that this could be done by choosing a set of Yukawa coupling constants associated with interactions with the background fields which were all of the same order of magnitude and with all electroweak Yukawa coupling constants equal. Given that the non-dimensionalized versions of the background and electroweak Yukawa coupling constants that we gave depend differently on the diverse set of energy scales in the theory, there could very well be a hierarchy between these sets of coupling constants, although it could also be possible to choose the energy scales of the theory such that they are of the same order of magnitude. Knowing what the relevent energy scales are, such as the domain-wall scale and the bulk confinement scale, requires further work. We were also able to show that the mass squared differences between the neutrino mass eigenstates could be satisfied using the split fermion mechanism and we also were able to suppress proton decay via use of the split scalar mechanism. However, we failed to generate large leptonic mixing angles in the same regime as the one we used to generate the fermion mass hierarchy and quark mixing. This motivated

us to consider adding a discrete flavor symmetry.

In Chapter 3, we extended the $SU(5)$ model by adding a discrete A_4 flavor symmetry. This meant that the full symmetry group of the model was extended from $SU(5) \times \mathbb{Z}_2$ to $SU(5) \times A_4 \times \mathbb{Z}_2$. We introduced two A_4-triplet Higgs scalars, one of which, ρ, was charged under the quintet of $SU(5)$, and the other, φ, was a gauge singlet. We also added some Higgs quintents in the 1, $1'$ and $1''$ representations of A_4. We then assigned the Standard Model fermions to appropriate representations, such that we were able to generate the fermion mass hierarchy and quark mixing with the split fermion mechanism just as before, while generating a tribimaximal PMNS matrix from the neutrino sector by utilizing the form diagonalizability properties typical of models based on A_4. Furthermore, we showed that the split scalar mechanism could be utilized to suppress the interactions between the two A_4 triplet scalars and resolve the VEV alignment problem. Given that we put some strong assumptions on the parameter space to get a tribimaximal PMNS matrix, we also suggested that deviations from tribimaximal mixing, in particular a non-zero θ_{13} mixing angle, could be generated by breaking those assumptions.

Chapter 4 was the start of our endeavor to construct a 5+1D intersecting domain-wall brane model, in which we proposed a simple $\mathbb{Z}_2 \times \mathbb{Z}_2$ scalar field theory with four scalar fields, with two of them generating kinks and the other two forming lump-like profiles. We showed that an analytic solution in which the domain walls are perpendicular exists in a special region of parameter space. We also showed that there was a class of energy-degenerate solutions in the same parameter space in which the angle between the walls was less than ninety degrees and potentially zero, yielding the solution with the walls parallel. We then showed that any solution with a non-zero intersection angle could not deform into the solution with parallel walls, due to the existence of a conserved topological charge associated with the boundary of the plane spanned by the two extra-dimensional coordinates. We also suggested that the perpendicular solution and the solutions for which the intersection angle was non-zero but less than ninety degrees are no longer energy degenerate if we perturb to a nearby region of parameter space. Assuming the perpendicular solution, we proceeded to show that scalars and fermions could be localized to the intersection.

In Chapter 5, we sought to extend the work of the previous chapter to include gauge structure and to localize gauge fields through Dvali-Shifman dynamics. In this section, we proposed a realization of the Clash-of-Symmetries mechanism in which a gauge group G is broken to different subgroups H_1 and H_2 on the two different walls by giving the scalar fields which generate the lumps gauge charges, with further breaking to $H_1 \cap H_2$ on the intersec-

tion of the domain walls. We then outlined the conditions in which Abelian and non-Abelian gauge fields of $H_1 \cap H_2$ are fully localized to the domain-wall intersection. We then proposed several toy models and scenarios. We gave three examples in the case with the lump-generating fields χ_1 and χ_2 being charged under the adjoint representation, two of which localized SM-like gauge theories and another in which there was an $SU(5)$ GUT localized to the domain-wall intersection. We then gave an example with $\chi_1 \sim 21$ and $\chi_2 \sim 35$ which for a particular parameter region generated a localized Standard Model without the semi-delocalized photons and we found that we could ensure that the SM-generating configuration could be made the most stable one.

There is still much more work to be done in order to demonstrate that domain-wall brane models are viable. On the phenomenological front, having passed the test with regards to the fermion mass spectra and the suppression of colored-Higgs-induced proton decay, we need to show that other experimental limits and tests can be satisfied. In the context of the basic $SU(5)$ model, an obvious one is proton decay mediated by X and Y gauge bosons which become massive on the wall. Another is the unification of the gauge coupling constants, which is not only desirable but in fact required in domain-wall brane models utilizing the Dvali-Shifman mechanism, since any realistic model will have the Standard Model embedded in a grand unification group. Given that the running of the gauge coupling constants depends on the fermions in the effective field theory on the wall as well as their masses, the parameter fitting done in Chapters 2 and 3 will be invaluable.

Clearly the work we have done in this thesis on intersecting domain-wall brane models in 5+1D is not finished. The next goal is to localize gravity onto the domain-wall intersection. In doing this, one would take very much the same approach as for a single-wall model by taking an appropriate ansatz for the warped background metric and proceed to show that the resultant warped metric has all the same properties as before and that there exists a graviton zero mode localized to the domain-wall intersection. Such work will probably have to be done numerically. We also need to further analyze local stability of the solutions given in Chapters 4 and 5, which will involve studying the translational zero modes, as well as any other possible massless modes arising in the KK spectrum of the background fields. There is also phenomenological work to be done although one would naturally expect, given that the split fermion and split scalar mechanisms would still arise, that fermion mass spectra could still be reproduced in much the same way.

Domain-wall brane models are an exciting approach to extra dimensions, and such models are capable of explaining the fermion mass hierarchy problem as well as quark and lepton mixing. There is also now a framework for

extending the number of extra dimensions through the utilization of intersecting domain walls. The work done in this thesis represents another step in this corpus of work and further motivates its extension.

Bibliography

[1] B. D. Callen and R. R. Volkas, "Fermion Masses and Mixing in a 4+1D $SU(5)$ Domain-Wall Braneworld Model," *Phys. Rev. D83, 056004*, 2011.

[2] B. D. Callen and R. R. Volkas, "Large Lepton Mixing Angles from a 4+1-Dimensional $SU(5) \times A_4$ Domain-Wall Braneworld Model," *Phys. Rev. D86, 056007*, 2012.

[3] B. D. Callen and R. R. Volkas, "Solutions for Intersecting Domain Walls with Internal Structure in Six Dimensions from a $\mathbb{Z}_2 \times \mathbb{Z}_2$-invariant Action," *Phys. Rev. D87, 116002*, 2013.

[4] N. Pesor, "Elegant brane-world models: ribbons and bowties," 2007.

[5] B. D. Callen and R. R. Volkas, "Clash-of-Symmetries Mechanism from Intersecting Domain-Wall Branes," *Phys. Rev. D89, 056004*, 2014.

[6] T. Kaluza, "Zum unitätsproblem in der physik," *Sitzungsber. Preuss. Akad. Wiss. Berlin. (Math. Phys.) 96: 69-72*, 1921.

[7] O. Klein, "Quantentheorie und fünfdimensionale Relativitätstheorie," *Zeitschrift für Physik A 37 (12): 895-906*, 1926.

[8] D. Bailin and A. Love, "Kaluza-Klein Theories," *Rep. Prog. Phys., 50, 1087*, 1987.

[9] M. J. Duff, "Kaluza-Klein Theory in Perspective," 1994. arXiv:hep-th/9410046v1.

[10] M. B. Green and J. H. Schwarz, "Anomaly Cancellations in Supersymmetric D=10 Gauge Theory and Superstring Theory," *Phys. Lett. B149, 117*, 1984.

[11] J. Dai, R. G. Leigh and J. Polchinski, "New Connections Between String Theories," *Mod. Phys. Lett. A4, 2073*, 1989.

[12] J. Polchinski, "Dirichlet Branes and Ramond-Ramond Charges," *Phys. Rev. Lett. 75, 4724*, 1995.

[13] N. Arkani-Hamed, S. Dimopoulos and G. R. Dvali, "The Hierarchy Problem and New Dimensions at a Millimeter," *Phys. Lett. B429, 263*, 1998.

[14] L. Randall and R. Sundrum, "A Large Mass Hierarchy from a Small Extra Dimension," *Phys. Rev. Lett. 83, 3370*, 1999.

[15] L. Randall and R. Sundrum, "An Alternative to Compactification," *Phys. Rev. Lett. 83, 4690*, 1999.

[16] T. Gherghetta and A. Pomarol, "Bulk fields and supersymmetry in a slice of AdS," *Nucl. Phys. B586, 141*, 2000.

[17] Y. Grossman and M. Neubert, "Neutrino masses and mixings in non-factorizable geometry," *Phys. Lett. B474 (3-4), 361-371*, 2000.

[18] S. J. Huber and Q. Shafi, "Fermion Masses, Mixings and Proton Decay in a Randall-Sundrum Model," *Phys. Lett. B498, 256-262*, 2001.

[19] N. Arkani-Hamed and M. Schmaltz, "Hierarchies without Symmetries from Extra Dimensions," *Phys. Rev. D61, 033005*, 2000.

[20] V. A. Rubakov and M. E. Shaposhnikov, "Do We Live Inside A Domain Wall?," *Phys. Lett. B125, 136*, 1983.

[21] R. Jackiw and C. Rebbi, "Solitons with fermion number $\frac{1}{2}$," *Phys. Rev. D 13, 3398*, 1976.

[22] R. Davies and D. P. George, "Fermions, scalars and Randall-Sundrum gravity on domain-wall branes," *Phys. Rev. D76, 104010*, 2007.

[23] R. Davies, D. P. George and R. R. Volkas, "The Standard Model on a Domain-Wall Brane?," *Phys. Rev. D77, 124038*, 2008.

[24] A. Davidson, B. F Toner, R. R. Volkas and K. C. Wali, "Clash of Symmetries on the Brane," *Phys. Rev. D 65, 125013*, 2002.

[25] A. Davidson, D. P. George, A. Kobakhidze, R. R. Volkas and K. C. Wali, "SU(5) grand unification on a domain-wall brane from an E6-invariant action," *Phys. Rev. D77, 085031*, 2008.

[26] G. Nordström, "On The Possibility of Unifying The Electromagnetic and The Gravitational Fields," *Physik. Zeitschr. XV, 504-506*, 1914. arXiv:physics/0702221 [physics.gen-ph].

[27] G. Nordström, "On a Theory of Electricity and Gravitation," $\ddot{O}versigt\ af\ Finska\ Vetenskaps\text{-}Societetens\ F\ddot{o}rhandlingar(Helsingfors), Bd.LVII.1914 - 1915Afd.A.N : o4, p.1 - 15$, 1914. arXiv:physics/0702222 [physics.gen-ph].

[28] G. Nordström, "On a Possible Foundation of a Theory of Matter," $\ddot{O}versigt\ af\ Finska\ Vetenskaps\text{-}Societetens\ F\ddot{o}rhandlingar(Helsingfors), Bd.LVII.1914 - 1915Afd.A.N : o28, p.1 - 21$, 1915. arXiv:physics/0702223 [physics.gen-ph].

[29] K. Becker, M. Becker and J. H. Schwarz, *String Theory and M-Theory: A Modern Introduction.* Cambridge University Press., 1st ed., 2007.

[30] J. Polchinski, "Tasi Lectures on D-Branes," 1996. arXiv:hep-th/9611050.

[31] I. Antoniadis, "A Possible New Dimension at a Few TeV," *Phys. Lett. B246, 377*, 1990.

[32] I. Antoniadis, N. Arkani-Hamed, S. Dimopoulos and G. Dvali, "New Dimensions at a Millimeter to a Fermi and Superstrings at a TeV," *Phys. Lett. B436, 257*, 1998.

[33] N. Arkani-Hamed, S. Dimopoulos, G. Dvali and N. Kaloper, "Infinitely Large New Dimensions," *Phys. Rev. Lett. 84, 586*, 2000.

[34] A Patani, M Schlindwein and Q Shafi, "Topological charges in field theory," *J. Phys. A: Math. Gen. 9 1513*, 1976.

[35] D. P. George and R. R. Volkas, "Kink Modes and Effective Four Dimensional Fermion and Higgs Brane Models," *Phys. Rev. D75, 105007*, 2007.

[36] N. Rosen and P. M. Morse, "On the Vibrations of Polyatomic Molecules," *Phys. Rev. 42, 210*, 1932.

[37] M. M. Nieto, "Exact wave-function normalization constants for the $B_0 \tanh z - U_0 \cosh^{-2} z$ and Pöschl-Teller potentials," *Phys. Rev. A17, 1273*, 1978.

[38] R. Rajaraman, *Solitons and Instantons: An Introduction to Solitons and Instantons in Quantum Field Theory.* North-Holland Publishing Company, 1982.

[39] G. Lévai, "A search for shape-invariant solvable potentials," *J.Phys. A: Math. Gen. 22, 689-702*, 1989.

[40] J. W. Dabrowska, A. Khare and U. P. Sukhatme, "Explicit wavefunctions for shape-invariant potentials by operator techniques," *J. Phys. A: Math. Gen. 21 L195-L200*, 1988.

[41] D. George, *Domain-Wall Brane Models of an Infinite Extra Dimension.* Ph.D thesis, University of Melbourne, 2009.

[42] Y. Grossman, R. Harnik, G. Perez, M. D. Schwartz, and Z. Surujon, "Twisted Split Fermions," *Phys. Rev. D71, 056007*, 2005.

[43] R. Harnik, G. Perez, M. D. Schwartz, and Y. Shirman, "Strong CP, Flavor, and Twisted Split Fermions," *JHEP 0503, 068*, 2005.

[44] O. DeWolfe, D. Z. Freedman, S. S. Gubser and A. Karch, "Modeling the fifth dimension with scalars and gravity," *Phys. Rev. D62, 046008*, 2000.

[45] M. Gremm, "Four-dimensional gravity on a thick domain wall," *Phys. Lett. B478, 434*, 2000.

[46] A. Davidson and P. D. Mannheim, "Dynamical localization of gravity," 2000. hep-th/0009064.

[47] G. Dando, A. Davidson, D. P. George, R. R. Volkas, and K. C. Wali, "The clash of symmetries in a Randall-Sundrum-like spacetime," *Phys. Rev. D72, 045016*, 2005.

[48] A. Kehagias and K. Tamvakis, "Localized Gravitons, Gauge Bosons and Chiral Fermions in Smooth Spaces Generated by a Bounce," *Phys. Lett. B504, 38*, 2001.

[49] T. R. Slatyer and R. R. Volkas, "Cosmology and Fermion Confinement in a Scalar-Field-Generated Domain Wall Brane in Five Dimensions," *JHEP04, 062*, 2007.

[50] S. Kobayashi, K. Koyama, and J. Soda, "Thick Brane Worlds and Their Stability," *Phys. Rev. D65, 064014*, 2002.

[51] S. L. Dubovsky and V. A. Rubakov, "On Models of Gauge Field Localisation on a Brane," *Int. J. Mod. Phys. A16, 4331*, 2001.

[52] G. R. Dvali and M. A. Shifman, "Domain Walls in Strongly Coupled Theories," *Phys. Lett. B396, 64*, 1997.

[53] G. 't Hooft, "Gauge theories with unified weak, electromagnetic and strong interactions," 1976. in *High Energy Physics*, Proceedings of the EPS International Conference, Palermo 1975, ed. A Zichichi, Editrice Compositori, Bologna.

[54] S. Mandelstam, "II Vortices and Confinement in non-Abelian Gauge Theories," *Phys. Rep. C23, 245*, 1976.

[55] N. Arkani-Hamed and M. Schmaltz, "Field Theoretic Branes and Tachyons of the QCD String," *Phys. Lett. B450, 92*, 1999.

[56] M. Laine, H. B. Meyer, K. Rummukainen and M. Shaposhnikov, "Effective gauge theories on domain walls via bulk confinement?," *JHEP, 04, 027*, 2004.

[57] M. Creutz, "Confinement and the Critical Dimensionality of Space-Time," *Phys. Rev. Lett. 43, 553*, 1979.

[58] D. E. Alvarez-Castillo and M. Kirchbach, "Exact Spectrum and Wave Functions of the Hyperbolic Scarf Potential in Terms of Finite Romanovski Polynomials," *Rev. Mex. Fis. E53 (2) 143-154*, 2007.

[59] C. Csaki, J. Erlich, T. J. Hollowood and Y. Shirman, "Universal Aspects of Gravity Localized on Thick Branes," *Nucl. Phys. B581, 309*, 2000.

[60] S.L. Dubovsky, V.A. Rubakov and P.G. Tinyakov, "Brane world: disappearing massive matter," *Phys. Rev. D 62, 105011*, 2000.

[61] Planck Collaboration, "Planck 2013 results. XVI. Cosmological parameters," 2013. arXiv:1303.5076.

[62] S. A. Thomas, F. B. Abdalla, and O. Lahav, "Upper Bound of 0.28 eV on Neutrino Masses from the Largest Photometric Redshift Survey," *Phys. Rev. Lett. 105, 031301*, 2010.

[63] J. Beringer et al. (Particle Data Group), "Review of Particle Physics," *Phys. Rev. D86, 010001*, 2012.

[64] G. L. Fogli, E. Lisi, A. Marrone, D. Montanino, A. Palazzo and A. M. Rotunno, "Global analysis of neutrino masses, mixings, and phases: Entering the era of leptonic CP violation searches," *Phys. Rev. D 86, 013012*, 2012.

[65] F. P. An *et al.* (Daya Bay Collaboration), "Observation of electron-antineutrino disappearance at Daya Bay," *Phys. Rev. Lett. 108, 171803*, 2012.

[66] S-B Kim *et al.* (RENO Collaboration), "Observation of Reactor Electron Antineutrinos Disappearance in the RENO Experiment," *Phys. Rev. Lett. 108, 191802*, 2012.

[67] Y. Abe *et al.* (Double Chooz Collaboration), "Indication of Reactor $\overline{\nu_e}$ Disappearance in the Double Chooz Experiment," *Phys. Rev. Lett. 108, 131801*, 2012.

[68] K. Abe *et al.* (T2K Collaboration), "Evidence of electron neutrino appearance in a muon neutrino beam," *Phys. Rev. D 88, 032002*, 2013.

[69] E. Ma and G. Rajasekaran, "Softly Broken A_4 Symmetry for Nearly Degenerate Neutrino Masses," *Phys. Rev. D64, 113012*, 2001.

[70] E. Ma, "Quark Mass Matrices in the A_4 Model," *Mod. Phys. Lett. A17, 627*, 2002.

[71] G. Altarelli and F. Feruglio, "Tri-Bimaximal Neutrino Mixing, A_4 and the Modular Symmetry," *Nucl. Phys. B741, 215*, 2006.

[72] C. I. Low and R. R. Volkas, "Tri-bimaximal Mixing, Discrete Family Symmetries, and a Conjecture Connecting the Quark and Lepton Mixing Matrices," *Phys. Rev. D68, 033007*, 2003.

[73] X.G. He, Y. Y. Keum and R. R. Volkas, "A4 Flavour Symmetry Breaking Scheme for Understanding Quark and Neutrino Mixing Angles," *JHEP04(2006)039*, 2006.

[74] A. Aranda, "Neutrino mixing from the double tetrahedral group T'," *Phys. Rev. D 76, 111301*, 2007.

[75] M. C. Chen and K.T. Mahanthappa, "CKM and tri-bimaximal MNS matrices in a $SU(5) \times T(d)$ model," *Phys. Lett. B 652, 34*, 2007.

[76] F. Feruglio, C. Hagedorn, Y. Lin and L. Merlo, "Tri-bimaximal neutrino mixing and quark masses from a discrete flavour symmetry," *Nucl. Phys. B 775, 120*, 2007.

[77] I. de Medeiros Varzielas, S.F. King and G.G. Ross, "Neutrino tri-bimaximal mixing from a non-Abelian discrete family symmetry," *Phys. Lett. B 648, 201*, 2007.

[78] W. Grimus and L. Lavoura, "A model for trimaximal lepton mixing," *JHEP 09, 106*, 2008.

[79] R. N. Mohapatra, M. K. Parida and G. Rajasekaran, "High scale mixing unification and large neutrino mixing angles," *Phys. Rev. D 69, 053007 (2004)*, 2004.

[80] Y. Cai and H. B. Yu, "SO(10) grand unification model with S4 flavor symmetry," *Phys. Rev. D 74, 115005*, 2006.

[81] C. Hagedorn, M. Lindner and R. N. Mohapatra, "S4 flavor symmetry and fermion masses: towards a grand unified theory of flavor," *JHEP 06, 042*, 2006.

[82] C. Luhn, S. Nasri, and P. Ramond, "Simple finite non-Abelian flavor groups," *J. Math. Phys. 48, 123519*, 2007.

[83] S. F. King and C. Luhn, "A new family symmetry for SO(10) GUTs," *Nucl. Phys. B 820, 269*, 2009.

[84] G. Altarelli and F. Feruglio, "Discrete flavor symmetries and models of neutrino mixing," *Rev. Mod. Phys. 82, 2701*, 2010.

[85] M. Holthausen and M. A. Schmidt, "Natural Vacuum Alignment from Group Theory: The Minimal Case," *JHEP 1201, 126*, 2012.

[86] G. Altarelli and F. Feruglio, "Tri-Bimaximal Neutrino Mixing from Discrete Symmetry in Extra Dimensions," *Nucl.Phys. B720, 64*, 2005.

[87] G. Altarelli, F. Feruglio and C. Hagedorn, "A SUSY SU(5) Grand Unified Model of Tri-Bimaximal Mixing from A4," *JHEP03(2008)052*, 2008.

[88] A. Kadosh and E. Pallante, "An A4 flavor model for quarks and leptons in warped geometry," *JHEP 1008, 115*, 2010.

[89] E. A. Mirabelli and M. Schmaltz, "Yukawa Hierarchies from Split Fermions in Extra Dimensions," *Phys. Rev. D61 113011*, 2000.

[90] G. C. Branco, A. de Gouvêa and M. N. Rebelo, "Split Fermions in Extra Dimensions and CP Violation," *Phys. Lett. B506, 115*, 2001.

[91] G. Barenboim, G. C. Branco, A. de Gouvêa and M. N. Rebelo, "Neutrino Masses and Lepton Flavour Violation in Thick Brane Scenarios," *Phys. Rev. D64, 073005*, 2001.

[92] T. J. Burrows and S. F. King, "A4 Family Symmetry from SU(5) SUSY GUTs in 6d," *Nucl. Phys. B835, 174*, 2010.

[93] M. C. Chen, K. T. Mahanthappa and F. Yu, "Viable Randall-Sundrum Model for Quarks and Leptons with T' Family Symmetry," *Phys. Rev. D81, 036004*, 2010.

[94] C. Csáki, C. Delaunay, C. Grojean and Y. Grossman, "A Model of Lepton Masses from a Warped Extra Dimension," *JHEP10(2008)055*, 2008.

[95] M. Giovannini, H. Meyer and M. Shaposhnikov, "Warped compactification on Abelian vortex in six dimensions," *Nucl. Phys. B619, 615*, 2001.

[96] T. Gherghetta and M. Shaposhnikov, "Localizing Gravity on a String-like Defect in Six Dimensions," *Phys. Rev. Lett. 85, 240*, 2000.

[97] H. Davoudiasl and T. G. Rizzo, "New Dimensions for Randall-Sundrum Phenomenology," *JHEP 0811, 013*, 2008.

[98] K. L. McDonald, "Warping, extra dimensions, and a slice of AdS_d," $Phys.Rev.D81, 024006, 2010$.

[99] A. Flachi and M. Minamitsuji, "Field localization on a brane intersection in anti-de Sitter spacetime," *Phys. Rev. D79, 104021*, 2009.

[100] J. R. Morris, "Domain Defects in Strings and Walls," *Phys. Rev. D 51, 697*, 1995.

[101] J. D. Edelstein, M. L. Trobo, F. A. Brito and D. Bazeia, "Kinks Inside Supersymmetric Domain Ribbons," *Phys. Rev. D 57, 7561*, 1998.

[102] R. Gregory and A. Padilla, "Nested Braneworlds and Strong Brane Gravity," *Phys. Rev. D 65, 084013*, 2002.

[103] H. Oda, K. Ito, M. Naganuma and N. Sakai, "An Exact Solution of BPS Domain Wall Junction," *Phys. Lett. B471, 140*, 1999.

[104] J. P. Gauntlett, D. Tong and P. K. Townsend, "Supersymmetric Intersecting Domain Walls in Massive Hyper-Kähler Sigma Models," *Phys.Rev. D63, 085001*, 2001.

[105] S.V. Troitskya and M.B. Voloshin, "On intersection of domain walls in a supersymmetric model," *Phys. Lett. B449, 17*, 1999.

[106] A. Coulthurst, K. L. McDonald, and B. H. J. McKellar, "Supressing Proton Decay by Separating Quarks and Leptons," *Phys. Rev. D74, 127701*, 2006.

[107] Y. Grossman and G. Perez, "Realistic construction of split fermion models," *Phys. Rev. D67, 015011*, 2003.

[108] Z. Surujon, "Higgs Localization in Split Fermion Models," *Phys. Rev. D73, 016008*, 2006.

[109] W. F. Chang and J. N. Ng, "CP violation in 5D Split Fermions Scenario," *JHEP 0212, 077*, 2002.

[110] S. Nussinov and R. Shrock, "$n - \overline{n}$ Oscillations in Models with Large Extra Dimensions," *Phys. Rev. Lett. 88, 171601*, 2002.

[111] S. Nussinov and R. Shrock, "Coulombic Effects on Fermion Masses in Models with Standard Model Fields in Large Extra Dimensions," *Phys. Lett. B526, 137-143*, 2002.

[112] M. Kakizaki and M. Yamaguchi, "Splitting Triplet and Doublet in Extra Dimensions," *Prog. Theor. Phys. 107, 433-441,*, 2002.

[113] M. Kakizaki and M. Yamaguchi, "Proton Decay, Fermion Masses and Texture from Extra Dimensions in SUSY GUTs," *Int.J.Mod.Phys. A19, 1715-1736*, 2004.

[114] H. Georgi and C. Jarlskog, "A New Lepton-Quark Mass Relation in a Unified Theory," *Phys. Lett. B86 (3-4), 297-300*, 1979.

[115] The Super-Kamiokande Collaboration, "Search for Proton Decay via $p \to e^+\pi^0$ and $p \to \mu^+\pi^0$ in a Large Water Cherenkov Detector," *Phys. Rev. Lett. 102(14), 141801*, 2009.

[116] C. Amsler *et al. (Particle Data Group)*, 2008. (URL: http://pdg.lbl.gov).

[117] KamLAND Collaboration, "Measurement of Neutrino Oscillation with KamLAND: Evidence of Spectral Distortion," *Phys. Rev. Lett. 94(8), 081801*, 2005.

[118] MINOS Collaboration, "Observation of Muon Neutrino Disappearance with the MINOS Detectors in the NuMI Neutrino Beam," *Phys. Rev. Lett. 97(19), 191801*, 2006.

[119] A. Goobar, S. Hannestad, E. Mörtsell and H. Tu, "The neutrino mass bound from WMAP 3 year data, the baryon acoustic peak, the SNLS supernovae and the Lyman-α forest," *JCAP06(2006)019*, 2006.

[120] F. De Bernardis, P. Serra, A. Cooray and A. Melchiorri, "An improved limit on the neutrino mass with CMB and redshift-dependent halo bias-mass relations from SDSS, DEEP2, and Lyman-Break Galaxies," *Phys. Rev. D78, 083535*, 2008.

[121] I. K. Cooper, S. F. King and C. Luhn, "$A4 \times SU(5)$ SUSY GUT of Flavour with Trimaximal Neutrino Mixing," *arXiv:1203.1324v2 [hep-ph]*, 2012.

[122] S. F. King and C. Luhn, "Trimaximal neutrino mixing from vacuum alignment in A_4 and S_4 models," *JHEP 1109, 042*, 2011.

[123] K. Nakamura *et al. (Particle Data Group)*, 2010. (URL: http://pdg.lbl.gov).

[124] J. E. Thompson and R. R. Volkas, "SO(10) domain-wall brane models," *Phys. Rev. D80, 125016*, 2009.

[125] K. Ito, M. Naganuma, H. Oda and N. Sakai, "Nonnormalizable Zero Modes on BPS Junctions," *Nucl. Phys. B586, 231*, 2000.

[126] G. W. Gibbons and P. K. Townsend, "Bogomol'nyi Equation for Intersecting Domain Walls," *Phys. Rev. Lett. 83, 1727*, 1999.

[127] E. M. Shin and R. R. Volkas, "O(10) kinks: clash of symmetries on the brane and the gauge hierarchy problem," *Phys. Rev. D69, 045010*, 2004.

[128] J. S. Rozowsky, R. R. Volkas and K. C. Wali, "Domain wall solutions with Abelian gauge fields," *Phys. Lett. B580, 249-256*, 2004.

[129] L. Pogosian and T. Vachaspati, "Domain Walls in SU(5)," *Phys. Rev. D62, 123506*, 2000.

[130] T. Vachaspati, "A Class of Kinks in $SU(N) \times Z(2)$," *Phys. Rev. D63, 105010*, 2001.

[131] L. Pogosian and T. Vachaspati, "Space of kink solutions in $SU(N) \times Z_2$," *Phys. Rev. D64, 105023*, 2001.

[132] D. P. George, A. Ram, J. E. Thompson and R. R. Volkas, "Symmetry breaking, subgroup embeddings and the Weyl group," *Phys. Rev. D 87, 105009*, 2013.

[133] H. Ruegg, "Extrema of SU(n) Higgs potentials and symmetry-breaking pattern," *Phys. Rev. D 22, 2040*, 1980.

[134] S. Randjbar-Daemi and M. Shaposhnikov, "QED from six-dimensional vortex and gauge anomalies," *JHEP 0304, 016*, 2003.

[135] A. Boyarsky, O. Ruchayskiy and M. Shaposhnikov, "Anomalies as a signature of extra dimensions," *Phys. Lett. B 626, 184*, 2005.

[136] L-F. Li, "Group theory of the spontaneously broken gauge symmetries," *Phys. Rev. D 9, 1723*, 1974.

[137] C. J. Cummins and R. C. King, "Symmetry breaking patterns for third-rank totally antisymmetric tensor representations of unitary groups," *J.Phys. A: Math. Gen. 17, 627-633*, 1984.

[138] C. J. Cummins, "Canonical forms of tensor representations and spontaneous symmetry breaking," *J.Phys. A: Math. Gen. 19, 1055-1063*, 1986.

Appendix A

Group Theoretic Properties and Representations of The Discrete Flavor Group A_4

In this appendix, we follow heavily the appendix given in Ref. [73]. The discrete flavor group A_4 is a non-Abelian finite group with twelve elements. It is the set of even permutations of four objects (and thus a subgroup of S_4) and is also the symmetry group of a tetrahedron. Formally, the group is generated by two generators S and T and is defined by the presentation

$$A_4 =< S, T | S^2 = T^3 = 1 > . \tag{A.1}$$

The generator T by itself generates a $\mathbb{Z}_3 \simeq C_3$ subgroup and the generator S generates a $\mathbb{Z}_2$ reflection subgroup. There is one real triplet representation 3 as well as three one-dimensional representations 1, $1'$ and $1''$, where the 1 representation is the usual singlet and the $1'$ and $1''$ representations transform non-trivially under A_4 and a complex conjugates of each other, $1'' = (1')^*$. The generators S and T may be represented as real 3×3 matrices acting on the 3 representation and these representations may be written as

$$S = \begin{pmatrix} 1 & 0 & 0 \\ 0 & -1 & 0 \\ 0 & 0 & -1 \end{pmatrix} \qquad T = \begin{pmatrix} 0 & 0 & 1 \\ 1 & 0 & 0 \\ 0 & 1 & 0 \end{pmatrix}, \tag{A.2}$$

with the other ten elements being the 3×3 identity matrix, the inverse of T

$$T^{-1} = \begin{pmatrix} 0 & 1 & 0 \\ 0 & 0 & 1 \\ 1 & 0 & 0 \end{pmatrix}, \tag{A.3}$$

as well as two other reflection matrices $S' = TST^{-1} = diag(-1, 1, -1)$, $S'' = T^{-1}ST = diag(-1, -1, 1)$ and six other rotations STS, $ST^{-1}S$, $S'TS'$, $S'T^{-1}S'$, $S''TS''$, and $S''T^{-1}S''$.

The non-trivial one-dimensional representations $1'$ and $1''$ transform trivially under the generator S but non-trivially under T. Under the action of T,

$$\begin{aligned} 1' &\to \omega 1', \\ 1'' &\to \omega^2 1'', \end{aligned} \tag{A.4}$$

where $\omega = e^{2\pi i/3}$ is the complex cube root of one.

The tensor products of the non-trivial A_4 representations are

$$1' \otimes 1' = 1'', \qquad 1' \otimes 1'' = 1, \tag{A.5}$$

and

$$3 \otimes 3 = 3_s \oplus 3_a \oplus 1 \oplus 1' \oplus 1''. \tag{A.6}$$

In Eq. A.6, s and a stand for symmetric and antisymmetric products respectively. If we represent two 3 representations as three-dimensional vectors (x_1, x_2, x_3) and (y_1, y_2, y_3), the various irreducible representations resulting from their tensor product are

$$(3 \otimes 3)_{3_s} = (x_2y_3 + x_3y_2, x_3y_1 + x_1y_3, x_1y_2 + x_2y_1) \tag{A.7}$$

$$(3 \otimes 3)_{3_a} = (x_2y_3 - x_3y_2, x_3y_1 - x_1y_3, x_1y_2 - x_2y_1) \tag{A.8}$$

$$(3 \otimes 3)_1 = x_1y_1 + x_2y_2 + x_3y_3 \tag{A.9}$$

$$(3 \otimes 3)_{1'} = x_1y_1 + \omega x_2y_2 + \omega^2 x_3y_3 \tag{A.10}$$

$$(3 \otimes 3)_{1''} = x_1y_1 + \omega^2 x_2y_2 + \omega x_3y_3. \tag{A.11}$$

Appendix B

The Higgs Flavon Scalar Interaction Potential

In this appendix, we give the potentials describing the interactions amongst different Higgs flavon fields localized to the domain wall. The background scalar field potential $V_{\eta\chi}$ yielding the background kink-lump solution was given in Eq. 1.89 in Sec. 1.6. The potentials coupling the flavons to the background fields η and χ, W_{Φ}, $W_{\Phi'}$, $W_{\Phi''}$, W_{ρ} and W_{φ}, were given in Sec. 3.3 in Eqs. 3.15 and 3.24, which after localization of the scalars and an appropriate choice of parameters contribute tachyonic masses to the effective self-interaction potentials for the lightest localized modes of these fields. Thus let V_{ρ}, V_{φ}, V_{Φ}, $V_{\Phi'}$, and $V_{\Phi''}$ be potentials containing the quartic self-interactions for each of these fields along with their localization potentials. Let the potentials $V_{\rho\varphi}$, $V_{\rho\Phi\Phi'\Phi''}$, $V_{\varphi\Phi\Phi'\Phi''}$, $V_{\rho\varphi\Phi\Phi'\Phi''}$, and $V_{\Phi\Phi'\Phi''}$ be those containing cross-talk interactions between the fields in the subscripts. Then the full scalar potential of the theory, V, is given by

$$\begin{aligned} V = {} & V_{\eta\chi} + V_{\rho} + V_{\varphi} + V_{\Phi} + V_{\Phi'} + V_{\Phi''} + V_{\rho\varphi} \\ & + V_{\rho\Phi\Phi'\Phi''} + V_{\varphi\Phi\Phi'\Phi''} + V_{\rho\varphi\Phi\Phi'\Phi''} + V_{\Phi\Phi'\Phi''}, \end{aligned} \tag{B.1}$$

where

$$
\begin{aligned}
V_\rho &= \lambda^1_\rho(\rho^\dagger\rho)_1(\rho^\dagger\rho)_1 + \lambda^2_\rho(\rho^\dagger\rho)_{1'}(\rho^\dagger\rho)_{1''} \\
&+ \lambda^3_\rho\big[(\rho^\dagger\rho)_{3s}.(\rho^\dagger\rho)_{3s}\big]_1 + \lambda^4_\rho\big[(\rho^\dagger\rho)_{3a}.(\rho^\dagger\rho)_{3a}\big]_1 \\
&+ i\lambda^5_\rho\big[(\rho^\dagger\rho)_{3s}.(\rho^\dagger\rho)_{3a}\big]_1 + W_\rho \\
&= \lambda^1_\rho(\rho^\dagger\rho)_1(\rho^\dagger\rho)_1 + \lambda^2_\rho(\rho^\dagger\rho)_{1'}(\rho^\dagger\rho)_{1''} \\
&+ \lambda^3_\rho\big[(\rho^\dagger\rho)_{3s}.(\rho^\dagger\rho)_{3s}\big]_1 + \lambda^4_\rho\big[(\rho^\dagger\rho)_{3a}.(\rho^\dagger\rho)_{3a}\big]_1 \\
&+ i\lambda^5_\rho\big[(\rho^\dagger\rho)_{3s}.(\rho^\dagger\rho)_{3a}\big]_1 + \mu^2_\rho(\rho^\dagger\rho)_1 + \lambda_{\rho\eta}(\rho^\dagger\rho)_1\eta^2 \\
&+ 2\lambda_{\rho\chi1}(\rho^\dagger\rho)_1 Tr\big(\chi^2\big) + \lambda_{\rho\chi2}(\rho^\dagger\big(\chi^T\big)^2\rho)_1 \\
&+ \lambda_{\rho\eta\chi}(\rho^\dagger\chi^T\rho)_1\eta,
\end{aligned}
\tag{B.2}
$$

$$
\begin{aligned}
V_\varphi &= \delta_\varphi(\varphi\varphi\varphi)_1 + \lambda^1_\varphi(\varphi\varphi)_1(\varphi\varphi)_1 \\
&+ \lambda^2_\varphi(\varphi\varphi)_{1'}(\varphi\varphi)_{1''} + \lambda^3_\varphi\big[(\varphi\varphi)_{3s}(\varphi\varphi)_{3s}\big]_1 + W_\varphi \\
&= \delta_\varphi(\varphi\varphi\varphi)_1 + \lambda^1_\varphi(\varphi\varphi)_1(\varphi\varphi)_1 \\
&+ \lambda^2_\varphi(\varphi\varphi)_{1'}(\varphi\varphi)_{1''} + \lambda^3_\varphi\big[(\varphi\varphi)_{3s}(\varphi\varphi)_{3s}\big]_1 \\
&+ \mu^2_\varphi(\varphi\varphi)_1 + \lambda_{\varphi\eta}(\varphi\varphi)_1\eta^2 + 2\lambda_{\varphi\chi}(\varphi\varphi)_1 Tr\big(\chi^2\big),
\end{aligned}
\tag{B.3}
$$

$$
\begin{aligned}
V_{\Phi^R} &= \lambda_{\Phi^R}((\Phi^R)^\dagger\Phi^R)^2 + W_{\Phi^R} \\
&= \lambda_{\Phi^R}((\Phi^R)^\dagger\Phi^R)^2 + \mu^2_{\Phi^R}(\Phi^R)^\dagger\Phi^R + \lambda_{\Phi^R\eta}(\Phi^R)^\dagger\Phi^R\eta^2 \\
&+ 2\lambda_{\Phi^R\chi1}(\Phi^R)^\dagger\Phi^R Tr\big(\chi^2\big) + \lambda_{\Phi^R\chi2}(\Phi^R)^\dagger\big(\chi^T\big)^2\Phi^R \\
&+ \lambda_{\Phi^R\eta\chi}(\Phi^R)^\dagger\chi^T\Phi^R\eta, \quad \text{for } R = 1,\, 1',\, 1'',
\end{aligned}
\tag{B.4}
$$

$$
\begin{aligned}
V_{\rho\varphi} &= \delta^s_{\rho\varphi}\big[(\rho^\dagger\rho)_{3s}.\varphi\big]_1 + i\delta^a_{\rho\varphi}\big[(\rho^\dagger\rho)_{3a}.\varphi\big]_1 \\
&+ \lambda^1_{\rho\varphi}(\rho^\dagger\rho)_1(\varphi\varphi)_1 + \lambda^2_{\rho\varphi}(\rho^\dagger\rho)_{1'}(\varphi\varphi)_{1''} \\
&+ \lambda^{2*}_{\rho\varphi}(\rho^\dagger\rho)_{1''}(\varphi\varphi)_{1'} + \lambda^3_{\rho\varphi}\Big[(\rho^\dagger\rho)_{3s}.(\varphi\varphi)_{3s}\Big]_1 \\
&+ i\lambda^4_{\rho\varphi}\Big[(\rho^\dagger\rho)_{3a}.(\varphi\varphi)_{3s}\Big]_1
\end{aligned}
\tag{B.5}
$$

$$
\begin{aligned}
V_{\rho\Phi\Phi'\Phi''} &= \lambda^1_{\rho\Phi}(\rho^\dagger\rho)_1(\Phi^\dagger\Phi) + \lambda_{\rho\Phi'}(\rho^\dagger\rho)_1(\Phi'^\dagger\Phi') \\
&+ \lambda_{\rho\Phi''}(\rho^\dagger\rho)_1(\Phi'^\dagger\Phi') + \lambda_{\rho\Phi\Phi'}(\rho^\dagger\rho)_{1''}(\Phi^\dagger\Phi') \\
&+ \lambda^*_{\rho\Phi\Phi'}(\rho^\dagger\rho)_{1'}(\Phi'^\dagger\Phi) + \lambda_{\rho\Phi\Phi''}(\rho^\dagger\rho)_{1'}(\Phi^\dagger\Phi'') \\
&+ \lambda^*_{\rho\Phi\Phi''}(\rho^\dagger\rho)_{1''}(\Phi''^\dagger\Phi) + \lambda^1_{\rho\Phi'\Phi''}(\rho^\dagger\rho)_{1''}(\Phi'^\dagger\Phi'') \\
&+ \lambda^{1*}_{\rho\Phi'\Phi''}(\rho^\dagger\rho)_{1'}(\Phi''^\dagger\Phi') + \lambda^2_{\rho\Phi}\big[(\rho^\dagger\Phi).(\rho^\dagger\Phi)\big]_1 \\
&+ \lambda^{2*}_{\rho\Phi}\big[(\Phi^\dagger\rho).(\Phi^\dagger\rho)\big]_1 + \lambda^2_{\rho\Phi'\Phi''}\big[(\rho^\dagger\Phi').(\rho^\dagger\Phi'')\big]_1 \\
&+ \lambda^{2*}_{\rho\Phi'\Phi''}\big[(\Phi'^\dagger\rho).(\Phi''^\dagger\rho)\big]_1
\end{aligned}
\tag{B.6}
$$

$$
\begin{aligned}
V_{\varphi\Phi\Phi'\Phi''} = {} & \lambda_{\varphi\Phi}(\Phi^\dagger\Phi)(\varphi\varphi)_1 + \lambda_{\varphi\Phi'}(\Phi'^\dagger\Phi')(\varphi\varphi)_1 \\
& + \lambda_{\varphi\Phi''}(\Phi''^\dagger\Phi'')(\varphi\varphi)_1 + \lambda_{\varphi\Phi\Phi'}(\Phi^\dagger\Phi')(\varphi\varphi)_{1''} \\
& + \lambda^*_{\varphi\Phi\Phi'}(\Phi'^\dagger\Phi)(\varphi\varphi)_{1'} + \lambda_{\varphi\Phi\Phi''}(\Phi^\dagger\Phi'')(\varphi\varphi)_{1'} \\
& + \lambda^*_{\varphi\Phi\Phi''}(\Phi''^\dagger\Phi)(\varphi\varphi)_{1''} + \lambda_{\varphi\Phi'\Phi''}(\Phi'^\dagger\Phi'')(\varphi\varphi)_{1''} \\
& + \lambda^*_{\varphi\Phi'\Phi''}(\Phi''^\dagger\Phi')(\varphi\varphi)_{1'},
\end{aligned}
\tag{B.7}
$$

$$
\begin{aligned}
V_{\rho\varphi\Phi\Phi'\Phi''} = {} & \delta_{\rho\varphi\Phi}(\varphi\rho^\dagger)_1\Phi + \delta^*_{\rho\varphi\Phi}\Phi^\dagger(\rho\varphi)_1 \\
& + \delta_{\rho\varphi\Phi'}(\varphi\rho^\dagger)_{1''}\Phi' + \delta^*_{\rho\varphi\Phi'}\Phi'^\dagger(\rho\varphi)_{1'} \\
& + \delta_{\rho\varphi\Phi''}(\varphi\rho^\dagger)_{1'}\Phi'' + \delta^*_{\rho\varphi\Phi''}\Phi''^\dagger(\rho\varphi)_{1''} \\
& + \lambda_{\rho\varphi\Phi}\left[(\varphi\varphi)_{3s}.\rho^\dagger\right]_1\Phi + \lambda^*_{\rho\varphi\Phi}\Phi^\dagger\left[\rho.(\varphi\varphi)_{3s}\right]_1 \\
& + \lambda_{\rho\varphi\Phi'}\left[(\varphi\varphi)_{3s}.\rho^\dagger\right]_{1''}\Phi' + \lambda^*_{\rho\varphi\Phi'}\Phi'^\dagger\left[\rho.(\varphi\varphi)_{3s}\right]_{1'} \\
& + \lambda_{\rho\varphi\Phi''}\left[(\varphi\varphi)_{3s}.\rho^\dagger\right]_{1'}\Phi'' + \lambda^*_{\rho\varphi\Phi''}\Phi''^\dagger\left[\rho.(\varphi\varphi)_{3s}\right]_{1''},
\end{aligned}
\tag{B.8}
$$

$$
\begin{aligned}
V_{\Phi\Phi'\Phi''} = {} & \lambda^1_{\Phi\Phi'}(\Phi^\dagger\Phi)(\Phi'^\dagger\Phi') + \lambda^2_{\Phi\Phi'}(\Phi^\dagger\Phi')(\Phi'^\dagger\Phi) \\
& + \lambda^1_{\Phi\Phi''}(\Phi^\dagger\Phi)(\Phi''^\dagger\Phi'') + \lambda^2_{\Phi\Phi''}(\Phi^\dagger\Phi'')(\Phi''^\dagger\Phi) \\
& + \lambda^1_{\Phi'\Phi''}(\Phi'^\dagger\Phi')(\Phi''^\dagger\Phi'') + \lambda^2_{\Phi'\Phi''}(\Phi'^\dagger\Phi'')(\Phi''^\dagger\Phi') \\
& + \lambda^1_{\Phi\Phi'\Phi''}(\Phi^\dagger\Phi')(\Phi^\dagger\Phi'') + \lambda^{1*}_{\Phi\Phi'\Phi''}(\Phi'^\dagger\Phi)(\Phi''^\dagger\Phi) \\
& + \lambda^2_{\Phi\Phi'\Phi''}(\Phi'^\dagger\Phi)(\Phi'^\dagger\Phi'') + \lambda^{2*}_{\Phi\Phi'\Phi''}(\Phi^\dagger\Phi')(\Phi''^\dagger\Phi') \\
& + \lambda^3_{\Phi\Phi'\Phi''}(\Phi''^\dagger\Phi)(\Phi''^\dagger\Phi') + \lambda^{3*}_{\Phi\Phi'\Phi''}(\Phi^\dagger\Phi'')(\Phi'^\dagger\Phi'')
\end{aligned}
\tag{B.9}
$$

Appendix C

Some $SU(7)$ Representations, Products and Embeddings

C.1 Basic $SU(7)$ Representations

$$
\begin{aligned}
7 &= (1,0,0,0,0,0) \\
21 &= (0,1,0,0,0,0) \\
35 &= (0,0,1,0,0,0) \\
\overline{35} &= (0,0,0,1,0,0) \\
\overline{21} &= (0,0,0,0,1,0) \\
\overline{7} &= (0,0,0,0,0,1) \\
28 &= (2,0,0,0,0,0) \\
48 &= (1,0,0,0,0,1) \\
84 &= (3,0,0,0,0,0) \\
112 &= (1,1,0,0,0,0) \\
140 &= (1,0,0,0,1,0) \\
189 &= (2,0,0,0,0,1)
\end{aligned}
\qquad
\begin{aligned}
196 &= (0,2,0,0,0,0) \\
210' &= (1,0,1,0,0,0) \\
224 &= (1,0,0,1,0,0) \\
392 &= (0,1,0,0,1,0) \\
490' &= (0,1,1,0,0,0) \\
540 &= (2,0,0,0,1,0) \\
588 &= (0,1,0,1,0,0) \\
735 &= (2,0,0,0,0,2) \\
735' &= (1,1,0,0,0,1) \\
784 &= (0,0,1,1,0,0) \\
1323 &= (1,0,1,0,0,1)
\end{aligned}
\qquad \text{(C.1)}
$$

C.2 Some Tensor Products of $SU(7)$ Representations

$$
\begin{aligned}
7 \times \overline{7} &= 1 + 48 & 21 \times \overline{21} &= 1 + 48 + 392 \\
7 \times 7 &= 21 + 28 & 21 \times 35 &= \overline{21} + 224 + 490' \\
7 \times 21 &= 35 + 112 & 21 \times \overline{35} &= \overline{7} + 140 + 588 \\
7 \times \overline{21} &= \overline{7} + 140 & 21 \times 48 &= 21 + 28 + \overline{224} + 735' \\
7 \times 35 &= \overline{35} + 210' & 35 \times 35 &= \overline{7} + 140 + 490' + 588 \\
7 \times \overline{35} &= \overline{21} + 224 & 35 \times \overline{35} &= 1 + 48 + 392 + 784 \\
7 \times 48 &= 7 + \overline{140} + 189 & 35 \times 48 &= 35 + 112 + \overline{210'} + 1323 \\
21 \times 21 &= \overline{35} + 196 + 210' & 48 \times 48 &= 1 + 48 + 48 + 392 + 540 + \overline{540} + 735
\end{aligned}
\tag{C.2}
$$

C.3 Embeddings of Subgroups of $SU(7)$

C.3.1 $SU(7) \supset SU(6) \times U(1)$

$$
\begin{aligned}
7 &= (6, +1) + (1, -6) \\
21 &= (15, +2) + (6, -5) \\
28 &= (21, +2) + (6, -5) + (1, -12) \\
35 &= (20, +3) + (15, -4) \\
48 &= (35, 0) + (6, +7) + (\overline{6}, -7) + (1, 0) \\
112 &= (70, +3) + (21, -4) + (15, -4) + (6, -11)
\end{aligned}
\tag{C.3}
$$

C.3.2 $SU(7) \supset SU(5) \times SU(2) \times U(1)$

$$
\begin{aligned}
7 &= (5, 1, +2) + (1, 2, -5) \\
21 &= (10, 1, +4) + (5, 2, -3) + (1, 1, -10) \\
28 &= (15, 1, +4) + (5, 2, -3) + (1, 3, -10) \\
35 &= (\overline{10}, 1, +6) + (10, 2, -1) + (5, 1, -8) \\
48 &= (24, 1, 0) + (5, \overline{2}, +7) + (\overline{5}, 2, -7) + (1, 3, 0) + (1, 1, 0) \\
112 &= (40, 1, +6) + (15, 2, -1) + (10, 2, -1) + (5, 3, -8) + (5, 1, -8) + (1, 2, -15)
\end{aligned}
\tag{C.4}
$$

C.3.3 $SU(7) \supset SU(4) \times SU(3) \times U(1)$

$$
\begin{aligned}
7 &= (4,1,+3) + (1,3,-4) \\
21 &= (6,1,+6) + (4,3,-1) + (1,\overline{3},-8) \\
28 &= (10,1,+6) + (4,3,-1) + (1,6,-8) \\
35 &= (\overline{4},1,+9) + (6,3,+2) + (4,\overline{3},-5) + (1,1,-12) \\
48 &= (15,1,0) + (4,\overline{3},+7) + (\overline{4},3,-7) + (1,8,0) + (1,1,0) \\
112 &= (20,1,+9) + (10,3,+2) + (6,3,+2) + (4,6,-5) + (4,\overline{3},-5) + (1,8,-12)
\end{aligned}
\tag{C.5}
$$

Appendix D

All Possible Clash-of-Symmetries Groups from $SU(7)$ With Two Adjoint Scalars

In this appendix, we list all the possible Clash-of-Symmetries breaking patterns with both of χ_1 and χ_2 transforming under the adjoint representation. For each possibility, we give example VEV patterns for χ_1 and χ_2 which generate them. We also state which resultant gauge groups are localized to the domain-wall intersection under the Dvali-Shifman formalism and which are semi-delocalized. We start by detailing the possibilities when $H_1 \simeq H_2 \simeq SU(6) \times U(1)$.

D.1 $H_1 = SU(6) \times U(1)$ and $H_2 = SU(6)' \times U(1)'$

D.1.1 Case 1: $H_1 \cap H_2 = H_1 = H_2 = SU(6) \times U(1)$

- Example VEV pattern: both χ_1 and χ_2 condense in the component proportional to the generator $Q_1 = \text{diag}(1, 1, 1, 1, 1, 1, -6)$.
- Here, $SU(6) \cap SU(6)' = SU(6)$
- There are no leftover diagonal generators.
- Hence, the only Abelian symmetry preserved on the wall is Q_1.

- The full symmetry respected on the intersection is $H_1 \cap H_2 = SU(6) \times U(1)_{Q_1}$. Both the gauge groups are semi-delocalized and able to propagate along both walls.

D.1.2 Case 2: $H_1 \cap H_2 = SU(5) \times U(1) \times U(1)$

- Example VEV pattern: χ_1 condenses in the component proportional to the generator $Q_1 = \text{diag}(1, 1, 1, 1, 1, 1, -6)$ and χ_2 condenses in the component proportional to the generator $Q_1' = \text{diag}(1, 1, 1, 1, 1, -6, 1)$.

- Here, $SU(6) \cap SU(6) = SU(5)$

- The leftover diagonal generators are $T_1 = \text{diag}(1, 1, 1, 1, 1, -5, 0)$ and $T_1' = \text{diag}(1, 1, 1, 1, 1, 0, -5)$.

- Hence, the Abelian symmetries preserved on the wall are $q_1 = 5/6Q_1 + 7/6T_1 = 5/6Q_1' + 7/6T_1' = \text{diag}(2, 2, 2, 2, 2, -5, -5)$ and $q_2 = 1/6(Q_1 - T_1) = 1/6(T_1' - Q_1') = \text{diag}(0, 0, 0, 0, 0, 1, -1)$.

- The full symmetry respected on the intersection is $H_1 \cap H_2 = SU(5) \times U(1)_{q_1} \times U(1)_{q_2}$. The $SU(5)$ subgroup is fully localized, the Abelian subgroups are not localized to the intersection and are free to propagate along both walls.

D.2 $H_1 = SU(6) \times U(1)$ and $H_2 = SU(5) \times SU(2) \times U(1)$

D.2.1 Case 1: $H_1 \cap H_2 = SU(5) \times U(1) \times U(1)$

- Example VEV pattern: χ_1 condenses in the component proportional to the generator $Q_1 = \text{diag}(1, 1, 1, 1, 1, 1, -6)$ and χ_2 condenses in the component proportional to the generator $Q_1' = \text{diag}(2, 2, 2, 2, 2, -5, -5)$.

- Here, $SU(6) \cap SU(5) = SU(5)$

- The leftover diagonal generators are $T_1 = \text{diag}(1, 1, 1, 1, 1, -5, 0)$ and $T_1' = \text{diag}(0, 0, 0, 0, 0, 1, -1)$

- Hence, the Abelian symmetries preserved on the wall are $q_1 = Q_1 + T_1 = Q_1' + T_1' = \text{diag}(2, 2, 2, 2, 2, -4, -6)$ and $q_2 = 1/6(Q_1 - T_1) = T_1' = \text{diag}(0, 0, 0, 0, 0, 1, -1)$.

- The full symmetry respected on the intersection is $H_1 \cap H_2 = SU(5) \times U(1)_{q_1} \times U(1)_{q_2}$. None of the gauge groups are localized; the $SU(5)$ gauge bosons are free to propagate along the H_2-respecting wall, the $U(1)_{q_2}$ photon can propagate along the H_1-respecting wall and the $U(1)_{q_1}$ photon can propagate along both walls.

D.2.2 Case 2: $H_1 \cap H_2 = SU(4) \times SU(2) \times U(1) \times U(1)$

- Example VEV pattern: $\langle\chi_1\rangle \propto Q_1 = \text{diag}(1,1,1,1,1,1,-6)$ and $\langle\chi_2\rangle \propto Q_1' = \text{diag}(-5,-5,2,2,2,2,2)$.
- Hence, $SU(6) \cap SU(5) = SU(4)$ and $SU(6) \cap SU(2) = SU(2)$.
- Leftover diagonal generators: $T_1 = \text{diag}(-2,-2,1,1,1,1,0)$ from H_1 and $T_1' = \text{diag}(0,0,1,1,1,1,-4)$ from H_2.
- Preserved Abelian generators: $q_1 = Q_1 - 2T_1 = T_1' - Q_1' = \text{diag}(5,5,-1,-1,-1,-1,-6)$ and $q_2 = 2Q_1 + T_1 = 3T_1' = \text{diag}(0,0,1,1,1,1,-4)$.
- Preserved symmetry on intersection: $H_1 \cap H_2 = SU(4) \times SU(2) \times U(1)_{q_1} \times U(1)_{q_2}$. The $SU(4)$ subgroup is fully localized, the $SU(2)$ and $U(1)_{q_2}$ subgroup is semi-delocalized and able to propagate along the H_2-respecting wall, $U(1)_{q_1}$ is semi-delocalized and able to propagate along both walls.

D.3 $H_1 = SU(6) \times U(1)$ and $H_2 = SU(4) \times SU(3) \times U(1)$

D.3.1 Case 1: $H_1 \cap H_2 = SU(4) \times SU(2) \times U(1) \times U(1)$

- Example VEV pattern: $\langle\chi_1\rangle \propto Q_1 = \text{diag}(1,1,1,1,1,1,-6)$ and $\langle\chi_2\rangle \propto Q_1' = \text{diag}(3,3,3,3,-4,-4,-4)$.
- Hence, $SU(6) \cap SU(4) = SU(4)$ and $SU(6) \cap SU(3) = SU(2)$.
- Leftover diagonal generators: $T_1 = \text{diag}(1,1,1,1,-2,-2,0)$ from H_1 and $T_1' = \text{diag}(0,0,0,0,1,1,-2)$ from H_2.
- Preserved Abelian generators: $q_1 = Q_1 + 2T_1 = Q_1' + T_1' = \text{diag}(3,3,3,3,-3,-3,-6)$ and $q_2 = 2Q_1 - T_1 = 1/3(Q_1' + 16T_1') = \text{diag}(1,1,1,1,4,4,-12)$.

- Preserved symmetry on intersection: $H_1 \cap H_2 = SU(4) \times SU(2) \times U(1)_{q_1} \times U(1)_{q_2}$. The $SU(2)$ subgroup is fully localized, the $SU(4)$ subgroup is semi-delocalized and able to propagate along the H_2-respecting wall, and the $U(1)_{q_1}$ and $U(1)_{q_2}$ subgroups are semi-delocalized and able to propagate along both walls.

D.3.2 Case 2: $H_1 \cap H_2 = SU(3) \times SU(3) \times U(1) \times U(1)$

- Example VEV pattern: $\langle \chi_1 \rangle \propto Q_1 = \text{diag}(1, 1, 1, 1, 1, 1, -6)$ and $\langle \chi_2 \rangle \propto Q_1' = \text{diag}(3, 3, 3, -4, -4, -4, 3)$.
- Hence, $SU(6) \cap SU(4) = SU(3)_1$ and $SU(6) \cap SU(3) = SU(3)_2$.
- Leftover diagonal generators: $T_1 = \text{diag}(1, 1, 1, -1, -1, -1, 0)$ from H_1 and $T_1' = \text{diag}(1, 1, 1, 0, 0, 0, -3)$ from H_2.
- Preserved Abelian generators: $q_1 = 3T_1 - Q_1 = Q_1' - T_1' = \text{diag}(2, 2, 2, -4, -4, -4, 6)$ and $q_2 = 3Q_1 + T_1 = 1/2(11T_1' - Q_1') = \text{diag}(4, 4, 4, 2, 2, 2, -18)$.
- Preserved symmetry on intersection: $H_1 \cap H_2 = SU(3)_1 \times SU(3)_2 \times U(1)_{q_1} \times U(1)_{q_2}$. The $SU(3)_1$ subgroup is fully localized while the $SU(3)_2$ subgroup is semi-delocalized and able to propagate along the H_2-respecting wall, and the $U(1)_{q_1}$ and $U(1)_{q_2}$ subgroups are semi-delocalized and able to propagate along both walls.

D.4 $H_1 = SU(5) \times SU(2) \times U(1)$ and $H_2 = SU(5)' \times SU(2)' \times U(1)'$

D.4.1 Case 1: $H_1 \cap H_2 = H_1 = H_2 = SU(5) \times SU(2) \times U(1)$

- Example VEV pattern: $\langle \chi_1 \rangle \propto Q_1 = \text{diag}(2, 2, 2, 2, 2, -5, -5)$ and $\langle \chi_2 \rangle \propto Q_1' = \text{diag}(2, 2, 2, 2, 2, -5, -5)$.
- Hence, $SU(5) \cap SU(5)' = SU(5)$ and $SU(2) \cap SU(2)' = SU(2)$.
- Leftover diagonal generators: None
- Preserved Abelian generators: $q_1 = Q_1 = Q_1' = \text{diag}(2, 2, 2, 2, 2, -5, -5)$
- Preserved symmetry on intersection: $H_1 \cap H_2 = SU(5) \times SU(2) \times U(1)_{q_1}$. All the factor gauge groups are semi-delocalized and free to propagate along both walls.

D.4.2 Case 2: $H_1 \cap H_2 = SU(4) \times U(1) \times U(1) \times U(1)$

- Example VEV pattern: $\langle\chi_1\rangle \propto Q_1 = \text{diag}(2,2,2,2,2,-5,-5)$ and $\langle\chi_2\rangle \propto Q_1' = \text{diag}(2,2,2,2,-5,-5,2)$.
- Hence, $SU(5) \cap SU(5)' = SU(4)$.
- Leftover diagonal generators: $T_1 = \text{diag}(1,1,1,1,-4,0,0)$, $T_2 = \text{diag}(0,0,0,0,0,1,-1)$ from H_1 and $T_1' = \text{diag}(1,1,1,1,0,0,-4)$, $T_2' = \text{diag}(0,0,0,0,1,-1,0)$ from H_2.
- Preserved Abelian generators: $q_1 = T_1 + 4T_2 = T_1' - 4T_2' = \text{diag}(1,1,1,1,-4,4,-4)$, $q_2 = 1/2(Q_1 - 7T_2) = 1/2(Q_1' + 7T_2') = \text{diag}(1,1,1,1,1,-6,1)$, and $q_3 = 1/5(2Q_1+T_1) = 1/5(Q_1'+3T_1'+5T_2') = \text{diag}(1,1,1,1,0,-2,-2)$.
- Preserved symmetry on intersection: $H_1 \cap H_2 = SU(4) \times U(1)_{q_1} \times U(1)_{q_2} \times U(1)_{q_3}$. The $SU(4)$ and $U(1)_{q_1}$ subgroups are fully localized to the intersection while the $U(1)_{q_2}$ and $U(1)_q$ subgroups are semi-delocalized and able to propagate along both walls.

D.4.3 Case 3: $H_1 \cap H_2 = SU(3) \times SU(2) \times SU(2) \times U(1) \times U(1)$

- Example VEV pattern: $\langle\chi_1\rangle \propto Q_1 = \text{diag}(2,2,2,2,2,-5,-5)$ and $\langle\chi_2\rangle \propto Q_1' = \text{diag}(2,2,2,-5,-5,2,2)$.
- Hence, $SU(5) \cap SU(5)' = SU(3)$, $SU(2) \cap SU(5)' = SU(2)_1$ and $SU(5) \cap SU(2)' = SU(2)_2$.
- Leftover diagonal generators: $T_1 = \text{diag}(2/3,2/3,2/3,-1,-1,0,0)$ from H_1 and $T_1' = \text{diag}(2/3,2/3,2/3,0,0,-1,-1)$ from H_2.
- Preserved Abelian generators: $q_1 = 9/5Q_1 + 3/5T_1 = 3/5Q_1' - 9/5T_1' = \text{diag}(4,4,4,3,3,-9,-9)$ and $q_2 = Q_1 - 3T_1 = -Q_1' + 3T_1' = \text{diag}(0,0,0,5,5,-5,-5)$.
- Preserved symmetry on intersection: $H_1 \cap H_2 = SU(3) \times SU(2)_1 \times SU(2)_2 \times U(1)_{q_1} \times U(1)_{q_2}$. The $SU(3)$ subgroup is fully localized to the intersection, the $SU(2)_1$ gauge bosons are semi-delocalized and free to propagate along the H_1-respecting wall, similarly the $SU(2)_2$ gauge bosons are semi-delocalized and free to propagate along the H_2-respecting wall and the Abelian groups $U(1)_{q_1}$ and $U(1)_{q_2}$ are semi-delocalized and free to propagate along both walls.

D.5 $H_1 = SU(5) \times SU(2) \times U(1)$ and $H_2 = SU(4) \times SU(3) \times U(1)$

D.5.1 Case 1: $H_1 \cap H_2 = SU(4) \times SU(2) \times U(1) \times U(1)$

- Example VEV pattern: $\langle \chi_1 \rangle \propto Q_1 = \text{diag}(2, 2, 2, 2, 2, -5, -5)$ and $\langle \chi_2 \rangle \propto Q_1' = \text{diag}(3, 3, 3, 3, -4, -4, -4)$.

- Hence, $SU(5) \cap SU(4) = SU(4)$ and $SU(2) \cap SU(3) = SU(2)$.

- Leftover diagonal generators: $T_1 = \text{diag}(1, 1, 1, 1, -4, 0, 0)$ from H_1 and $T_1' = \text{diag}(0, 0, 0, 0, -2, 1, 1)$ from H_2.

- Preserved Abelian generators: $q_1 = Q_1 + T_1 = Q_1' - T_1' = \text{diag}(3, 3, 3, 3, -2, -5, -5)$ and $q_2 = -Q_1 + 5T_1 = Q_1' + 9T_1' = \text{diag}(3, 3, 3, 3, -22, 5, 5)$.

- Preserved symmetry on intersection: $H_1 \cap H_2 = SU(4) \times SU(2) \times U(1)_{q_1} \times U(1)_{q_2}$. None of the subgroups are fully localized. The $SU(4)$ gauge bosons are semi-delocalized and free to propagate along the H_2-respecting wall, similarly the $SU(2)$ gauge bosons are semi-delocalized and free to propagate along the H_1-respecting wall and the Abelian groups $U(1)_{q_1}$ and $U(1)_{q_2}$ are semi-delocalized and free to propagate along both walls.

D.5.2 Case 2: $H_1 \cap H_2 = SU(3) \times SU(2) \times U(1) \times U(1) \times U(1)$

- Example VEV pattern: $\langle \chi_1 \rangle \propto Q_1 = \text{diag}(2, 2, 2, 2, 2, -5, -5)$ and $\langle \chi_2 \rangle \propto Q_1' = \text{diag}(3, 3, 3, -4, -4, -4, 3)$.

- Hence, $SU(5) \cap SU(4) = SU(3)$ and $SU(5) \cap SU(3) = SU(2)$.

- Leftover diagonal generators: $T_1 = \text{diag}(2/3, 2/3, 2/3, -1, -1, 0, 0)$, $T_2 = \text{diag}(0, 0, 0, 0, 0, 1, -1)$ from H_1 and $T_1' = \text{diag}(2/3, 2/3, 2/3, 0, 0, 0, -2)$, $T_2' = \text{diag}(0, 0, 0, 1, 1, -2, 0)$ from H_2.

- Preserved Abelian generators: $q_1 = -T_1 - 2T_2 = -T_1' + T_2' = \text{diag}(-2/3, -2/3, -2/3, 1, 1, -2, 2)$, $q_2 = 4Q_1 + 7T_1 - 6T_2 = 2Q_1' + 10T_1' + 9T_2' = \text{diag}(38/3, 38/3, 38/3, 1, 1, -26, -14)$ and $q_3 = -3Q_1 + 12T_1 + 12T_2 = 3/2Q_1' - 3/8T_1' - 15'T_2 = \text{diag}(2, 2, 2, -18, -18, 27, 3)$.

- Preserved symmetry on intersection: $H_1 \cap H_2 = SU(3) \times SU(2) \times U(1)_{q_1} \times U(1)_{q_2} \times U(1)_{q_3}$. The $SU(3)$, $SU(2)$ and $U(1)_{q_1}$ subgroups are fully localized to the domain-wall intersection. The $U(1)_{q_2}$ and $U(1)_{q_3}$ subgroups are semi-delocalized and their photons can propagate along both walls.

D.5.3 Case 3: $H_1 \cap H_2 = SU(3) \times SU(2) \times SU(2) \times U(1) \times U(1)$

- Example VEV pattern: $\langle\chi_1\rangle \propto Q_1 = \text{diag}(2,2,2,2,2,-5,-5)$ and $\langle\chi_2\rangle \propto Q_1' = \text{diag}(-4,-4,-4,3,3,3,3)$.

- Hence, $SU(5) \cap SU(3) = SU(3)$, $SU(5) \cap SU(4) = SU(2)_1$ and $SU(2) \cap SU(4) = SU(2)_2$.

- Leftover diagonal generators: $T_1 = \text{diag}(2/3, 2/3, 2/3, -1, -1, 0, 0)$ from H_1 and $T_1' = \text{diag}(0,0,0,1,1,-1,-1)$ from H_2.

- Preserved Abelian generators: $q_1 = Q_1 + 3T_1 = -Q_1' + 2T_1' = \text{diag}(4,4,4,-1,-1,-5,-5)$ and $q_2 = 3Q_1 - T_1 = -4/3Q_1' + 11T_1' = \text{diag}(16/3, 16/3, 16/3, 7, 7, -15, -15)$.

- Preserved symmetry on intersection: $H_1 \cap H_2 = SU(3) \times SU(2)_1 \times SU(2)_2 \times U(1)_{q_1} \times U(1)_{q_2}$. Only the $SU(2)_1$ subgroup is fully localized to the domain-wall intersection. The $SU(3)$ subgroup is semi-delocalized and its gauge bosons can propagate along the H_2-respecting wall. The $SU(2)_2$ subgroup is semi-delocalized and its gauge bosons can propagate along the H_1-respecting wall. The $U(1)_{q_2}$ and $U(1)_{q_3}$ subgroups are semi-delocalized and their photons can propagate along both walls.

D.6 $H_1 = SU(4) \times SU(3) \times U(1)$ and $H_2 = SU(4)' \times SU(3)' \times U(1)'$

D.6.1 Case 1: $H_1 \cap H_2 = SU(4) \times SU(3) \times U(1)$

- Example VEV pattern: $\langle\chi_1\rangle \propto Q_1 = \text{diag}(3,3,3,3,-4,-4,-4)$ and $\langle\chi_2\rangle \propto Q_1' = \text{diag}(3,3,3,3,-4,-4,-4)$.

- Hence, $SU(4) \cap SU(4)' = SU(4)$ and $SU(3) \cap SU(3)' = SU(3)$.

- Leftover diagonal generators: None

- Preserved Abelian generators: $q_1 = Q_1 = Q_1' =$ $\mathrm{diag}(3, 3, 3, 3, -4, -4, -4)$

- Preserved symmetry on intersection: $H_1 \cap H_2 = SU(4) \times SU(3) \times U(1)_{q_1}$. All the factor gauge groups are semi-delocalized and free to propagate along both walls.

D.6.2 Case 2: $H_1 \cap H_2 = SU(3) \times SU(2) \times U(1) \times U(1) \times U(1)$

- Example VEV pattern: $\langle \chi_1 \rangle \propto Q_1 = \mathrm{diag}(3, 3, 3, -4, -4, -4, 3)$ and $\langle \chi_2 \rangle \propto Q_1' = \mathrm{diag}(3, 3, 3, -4, -4, 3, -4)$.

- Hence, $SU(4) \cap SU(4)' = SU(3)$ and $SU(3) \cap SU(3)' = SU(2)$.

- Leftover diagonal generators: $T_1 = \mathrm{diag}(2/3, 2/3, 2/3, 0, 0, 0, -2)$, $T_2 = \mathrm{diag}(0, 0, 0, 1, 1, -2, 0)$ from H_1 and $T_1' = \mathrm{diag}(2/3, 2/3, 2/3, 0, 0, -2, 0)$, $T_2' = \mathrm{diag}(0, 0, 0, 1, 1, 0, -2)$ from H_2.

- Preserved Abelian generators: $q_1 = -T_1 - T_2 = -T_1' - T_2' =$ $\mathrm{diag}(-2/3, -2/3, -2/3, -1, -1, 2, 2)$, $q_2 = 4Q_1 + T_1 - T_2 = 2Q_1' + 10T_1' - 9T_2' = \mathrm{diag}(38/3, 38/3, 38/3, -17, -17, -14, 10)$, and $q_3 = Q_1 - 2T_1 + 2T_2 = -1/2Q_1' + 29/4T_1' - 6T_2' = \mathrm{diag}(5/3, 5/3, 5/3, -2, -2, -8, 7)$.

- Preserved symmetry on intersection: $H_1 \cap H_2 = SU(3) \times SU(2) \times U(1)_{q_1} \times U(1)_{q_2} \times U(1)_{q_3}$. The $SU(3)$, $SU(2)$ and $U(1)_{q_1}$ subgroups are fully localized to the domain-wall intersection. The $U(1)_{q_2}$ and $U(1)_{q_3}$ subgroups are semi-delocalized and their photons can propagate along both walls.

D.6.3 Case 3: $H_1 \cap H_2 = SU(2) \times SU(2) \times SU(2) \times U(1) \times U(1) \times U(1)$

- Example VEV pattern: $\langle \chi_1 \rangle \propto Q_1 = \mathrm{diag}(3, 3, 3, 3, -4, -4, -4)$ and $\langle \chi_2 \rangle \propto Q_1' = \mathrm{diag}(3, 3, -4, -4, -4, 3, 3)$.

- Hence, $SU(4) \cap SU(4)' = SU(2)_1$, $SU(4) \cap SU(3)' = SU(2)_2$ and $SU(3) \cap SU(4)' = SU(2)_3$.

- Leftover diagonal generators: $T_1 = \mathrm{diag}(1, 1, -1, -1, 0, 0, 0)$, $T_2 = \mathrm{diag}(0, 0, 0, 0, -2, 1, 1)$ from H_1 and $T_1' = \mathrm{diag}(1, 1, 0, 0, 0, -1, -1)$, $T_2' = \mathrm{diag}(0, 0, 1, 1, -2, 0, 0)$ from H_2.

- Preserved Abelian generators: $q_1 = T_1 - T_2 = T_1' - T_2' = \mathrm{diag}(1,1,-1,-1,2,-1,-1)$, $q_2 = Q_1 + 2T_1 + 2T_2 = 1/2(Q_1' + 7T_1' + 6T_2') = \mathrm{diag}(5,5,1,1,-8,-2,-2)$, and $q_3 = 4Q_1 - T_1 - T_2 = -Q_1' + 14T_1' + 9T_2' = \mathrm{diag}(11,11,13,13,-14,-17,-17)$.

- Preserved symmetry on intersection: $H_1 \cap H_2 = SU(2)_1 \times SU(2)_2 \times SU(2)_3 \times U(1)_{q_1} \times U(1)_{q_2} \times U(1)_{q_3}$. The $SU(2)_1$, $SU(2)_2$, $SU(2)_3$ and $U(1)_{q_1}$ subgroups are fully localized to the domain-wall intersection. The $U(1)_{q_2}$ and $U(1)_{q_3}$ subgroups are semi-delocalized and their photons can propagate along both walls.

D.6.4 Case 4: $H_1 \cap H_2 = SU(3) \times SU(3) \times U(1) \times U(1)$

- Example VEV pattern: $\langle \chi_1 \rangle \propto Q_1 = \mathrm{diag}(3,3,3,3,-4,-4,-4)$ and $\langle \chi_2 \rangle \propto Q_1' = \mathrm{diag}(-4,-4,-4,3,3,3,3)$.

- Hence, $SU(3) \cap SU(4)' = SU(3)_1$ and $SU(4) \cap SU(3)' = SU(3)_2$.

- Leftover diagonal generators: $T_1 = \mathrm{diag}(1,1,1,-3,0,0,0)$ from H_1 and $T_1' = \mathrm{diag}(0,0,0,-3,1,1,1)$ from H_2.

- Preserved Abelian generators: $q_1 = 1/4(Q_1 + T_1) = -1/4(Q_1' + T_1') = \mathrm{diag}(1,1,1,0,-1,-1,-1)$ and $q_2 = 1/2(Q_1 - T_1) = -1/4(Q_1' + 5T_1') = \mathrm{diag}(1,1,1,3,-2,-2,-2)$.

- Preserved symmetry on intersection: $H_1 \cap H_2 = SU(3)_1 \times SU(3)_2 \times U(1)_{q_1} \times U(1)_{q_2}$. The $SU(3)_1$ subgroup is semi-delocalized and its gauge bosons are able to propagate along the H_1-respecting wall. The $SU(3)_2$ subgroup is semi-delocalized and its gauge bosons are able to propagate along the H_2-respecting wall. The $U(1)_{q_1}$ and $U(1)_{q_2}$ subgroups are semi-delocalized and their photons can propagate along both walls.